Development of immunogenic, distributable, and equitable SARS-CoV-2 vaccines

by

Muhammad Sohaib Khan

BS in Biology, Bridgewater College, 2019

Submitted to the Graduate Faculty of the

School of Public Health in partial fulfillment

of the requirements for the degree of

Doctor of Philosophy

University of Pittsburgh

2023

UNIVERSITY OF PITTSBURGH

SCHOOL OF PUBLIC HEALTH

This dissertation was presented

by

Muhammad Sohaib Khan

It was defended on

July 6, 2023

and approved by

Committee Member: **Simon Barratt-Boyes**, Ph.D., Professor, Infectious Diseases and Microbiology, School of Public Health, University of Pittsburgh

Committee Member: **Tullia C. Bruno**, Ph.D., Assistant Professor, Department of Immunology, School of Medicine, University of Pittsburgh

Committee Member: **Amy L. Hartman**, Ph.D., Associate Professor, Infectious Diseases and Microbiology and Center for Vaccine Research, School of Public Health, University of Pittsburgh

Dissertation Advisor: Andrea Gambotto, M.D., Associate Professor, Department of Surgery, School of Medicine, University of Pittsburgh

Development of immunogenic, distributable, and equitable SARS-CoV-2 vaccines

Muhammad Sohaib Khan, PhD

University of Pittsburgh, 2023

The COVID-19 pandemic underscores the critical need for effective vaccines against SARS-CoV-2. This thesis investigates diverse aspects of SARS-CoV-2 vaccine development, emphasizing immunogenicity and innovative strategies. The study comprises multiple chapters, each providing valuable insights into vaccine design and optimization. We initially demonstrated that a single subcutaneous or intranasal immunization with an adenovirus-based SARS-CoV-2 vaccine induces robust humoral and cellular immune responses in mice. This research validates the efficacy of adenovirus-based vaccines for SARS-CoV-2. Next, we investigated next-generation SARS-CoV-2 vaccine approaches incorporating proteins outside of spike using an adenovirus-vectored vaccine expressing the S1-N fusion protein. By incorporating multiple antigenic targets, this research aims to broaden the immune response, exploring its propensity for increasing cellular immunity, the potential for eliciting protective immune responses, and compatibility with protein subunit boosters. After outlining the immunogenic approach of SARS-CoV-2 S1 subunit protein vaccines, I next worked to evaluate a trivalent variant-specific SARS-CoV-2 S1 subunit protein vaccine in BALB/c mice in Chapter 4. This research demonstrates that the trivalent vaccine induces broad humoral immune responses, enhancing the potential for comprehensive protection against SARS-CoV-2 variants. Furthermore, we worked to evaluate the S1 protein subunit vaccine approaches as a booster in aged mice in Chapter 5. The study reveals that the booster vaccination elicits robust humoral immune responses, offering insights into enhancing immune responses in older populations. Chapter 6 investigates the immunogenicity of

a tetravalent SARS-CoV-2 S1 subunit protein vaccine in SIV-infected rhesus macaque controllers. The research demonstrates the vaccine's ability to elicit robust humoral and cellular immune responses in a more advanced animal model and in animals with preexisting viral infection. Finally, I explored the development of chimeric spike protein vaccines for both SARS-CoV-2 and MERS. This research contributes to the expansion of vaccine strategies against related coronaviruses.

Overall, this thesis provides important insights into SARS-CoV-2 vaccine development, and innovative strategies. The findings advance our understanding of vaccine immunogenicity, broaden the scope of protection, and address the unique challenges posed by aging and immunocompromised populations. This research contributes to global efforts in combating the COVID-19 pandemic, informing strategies to prevent future outbreaks of emerging pathogens.

Table of Contents

List of Figures

Acknowledgments

This dissertation is dedicated to my parents, grandparents, and my entire family lineage.

Thank you for your enduring generational sacrifices starting in Chakiwara and Garden West in Karachi, Pakistan which has allowed me to pursue opportunities I could never have dreamed of.

My journey to becoming a scientist has been anything but straightforward. I do not have a story in which I can say I have wanted to be a scientist since I was a child. Truthfully, my childhood and high school years were primarily spent pursuing athletics, specifically American football, instead of focusing on academics. Indeed, it was football which led me, and allowed me, to attend Bridgewater College, in Bridgewater, VA, for my bachelor studies. I specifically remember being told in high school that I would not last in college and would become a college dropout. Safe to say, that has not materialized.

I would like to first thank the person who started me on my journey to become a scientist, Dr. Stephen F. Baron, Harry G M Jopson Professor of Biology at Bridgewater College. It was with Dr. Baron that I learned my foundational knowledge in microbiology, and passion for science, working on the bacterium Streptomyces.

Second, I would like to thank my Ph.D. mentor Dr. Andrea Gambotto, for his investment and belief in my potential as a scientist. Thank you for guiding me through this process, for your patience in my learning from scratch these scientific techniques, and for the installment of my scientific values. I'd also like to recognize the lab members and collaborators who have worked

alongside me these past three years. Specifically, I'd like to thank Tom Kenniston for managing the lab during these high-stress years and for his comradery and support as my desk neighbor.

Thirdly, I would like to thank my committee members, Dr. Simon Barratt-Boyes, Dr. Tullia Bruno, and Dr. Amy Hartman. Thank you for your critical insights, feedback, and overall support of my dissertation journey. Your insights have been vital in shaping this research project and my scientific development.

Fourthly, I would like to thank and recognize my parents for their work to place our family in the position they are in today. As Pakistani immigrants, I saw my parents work hard to give my siblings and me a better future in America. Despite facing challenges, my family's resilience and work ethic taught me important life skills. Seeing my parents sacrifice their free time and energy to provide for us, and my siblings' support and encouragement along the way, inspired me to pursue higher education and work towards my own goals, just as my family worked towards their American dream.

Last, and certainly not least, I would like to thank my better half, my fiancé Madison. I would not have been able to go through this process without her unwavering support, advice, and love. I am excited and so lucky to embark on the next chapter of our lives together, knowing that I have their love and support by my side. I would also like to thank all my friends that have supported and uplifted me during this journey. Your encouragement, motivation, and understanding have been invaluable to me, especially during the most challenging times. I am grateful for the many conversations, laughs, and memories we have shared, which provided much-needed breaks and helped me maintain my sanity. Your belief in me and my abilities has given me the strength to persevere and complete this academic milestone. I am blessed to have such an incredible team on my side.

1.0 Introduction

1.1 Historical Vaccine Development

Vaccination continues to be one of the most effective public health interventions to curb infectious diseases and their impact on human, and animal, health [1–4]. From the development of the first smallpox vaccine to the rapid deployment of Coronavirus Disease 2019 (COVID-19) vaccines, the history of vaccines highlights the critical role of scientific discovery in improving public health.

The first vaccine was created in the late 1700s by Edward Jenner, who used the cowpox virus to protect against smallpox [5]. Jenner's observation that milkmaids who had contracted cowpox did not develop smallpox led him to hypothesize that cowpox could be used to prevent smallpox. In 1796, Jenner inoculated an eight-year-old boy with cowpox and later exposed him to smallpox, which the boy did not contract [6]. However, it wasn't until the 20th century that vaccines became a widespread public health intervention.

During the 20th century, the development of vaccines accelerated, leading to the eradication of smallpox, and the curbing of diseases such as polio, measles, mumps, rubella, and pertussis [7,8]. The Salk and Sabin vaccines were instrumental in reducing the incidence of polio from hundreds of thousands of cases to just a few dozen cases a year [9,10].

The Salk vaccine, developed by Jonas Salk at the University of Pittsburgh in the 1950s, was the first polio vaccine to use an inactivated form of the poliovirus [11]. The vaccine was made by growing the virus in cultures of monkey kidney cells, then inactivating it with formalin. The inactivated virus does not cause disease, but still induced an immune response that protected

against live poliovirus infection. The Salk vaccine was first tested in 1952, and by 1955, it was being distributed widely in the United States. The Sabin vaccine, developed by Albert Sabin in the 1960s, used a weakened form of the poliovirus that could replicate in the gut without causing disease [12].

In recent years, vaccines have played a vital role in controlling and preventing outbreaks of emerging and re-emerging infectious diseases, such as influenza, human papillomavirus (HPV), Ebola, and COVID-19. The development of COVID-19 vaccines has been a global effort involving large teams of scientists, public health agencies, governments, and the private sector. The Pfizer-BioNTech, Moderna, and Johnson & Johnson vaccines are highly effective at preventing severe illness and death from COVID-19 and have been administered to millions of people worldwide [13].

Vaccines have also been crucial in preventing and controlling infectious diseases in livestock and companion animals. For example, vaccines for foot-and-mouth disease, brucellosis, and rabies have been instrumental in reducing animal mortality, improving animal health, and preventing significant economic losses due to livestock diseases [14–16].

In conclusion, the history of vaccine development highlights the critical role of vaccines in global health. Vaccines have saved countless lives and prevented the spread of infectious diseases. As new diseases emerge and existing diseases continue to evolve, the development of new vaccines remains a top priority. Scientific discovery and collaboration across multiple sectors will continue to drive the development of new vaccines, improving public health and advancing human and animal welfare. In the following section, I will provide an overview of traditional vaccine platforms.

1.1.1 Whole-Virus

Whole virus vaccines have been used for over a century as a traditional means of vaccination against pathogens. These vaccines work by exposing the immune system to either an inactivated or live attenuated virus, which stimulates an immune response that can fight the virus in the event of future exposure. In this chapter, I will explore the history, development, advantages, and disadvantages of whole virus vaccine platforms, with a focus on the inactivated virus and live attenuated virus vaccines.

Inactivated virus vaccines were first developed in the 19th century, with Louis Pasteur's development of an inactivated rabies vaccine in 1885 [17]. Inactivated virus vaccines are created by treating viruses with chemicals, heat, or radiation to render them non-infectious while retaining their antigenic properties [18]. The immune system is then exposed to the inactivated virus, which stimulates humoral and cellular immune responses that can neutralize or control the live virus in the future exposures [19].

Inactivated virus vaccines have advantages over live attenuated virus vaccines. Inactivated virus vaccines cannot cause disease because the virus is not viable, making them safe for use in immunocompromised individuals [20]. Additionally, inactivated virus vaccines are stable and can be easily transported and stored, making them more accessible in resource-limited settings [21]. However, inactivated virus vaccines typically require multiple doses to achieve optimal protection, and they may not provide as robust and long-lasting an immune response as live attenuated virus vaccines [22].

Examples of successful inactivated virus vaccines include the polio vaccine, the hepatitis A vaccine, and the flu vaccine [23]. The polio vaccine was first developed in the 1950s and has nearly eradicated the disease worldwide [24]. The hepatitis A vaccine, which was introduced in the 1990s,

has significantly reduced the incidence of hepatitis A infections [25]. The flu vaccine, which is updated annually to account for new strains of influenza, has been successful in reducing the spread and severity of flu infections [26].

Live attenuated virus vaccines are created by weakening the virus in the laboratory, typically through serial passage in cell culture or animal model, so it is less able to cause disease in humans while still retaining its antigenic properties [27]. Live attenuated virus vaccines can provide a more robust and long-lasting immune response than inactivated virus vaccines, as they more closely mimic a natural infection. Examples of live attenuated virus vaccines include the measles, mumps, and rubella (MMR) vaccine, the varicella (chickenpox) vaccine, and the rotavirus vaccine [28–31].

Live attenuated virus vaccines have specific advantages over inactivated virus vaccines. They can provide longer-lasting immunity with a single dose, most likely due to the ability to stimulate a variety pattern recognition receptors (PRRs) specialized to the target pathogen, making them more convenient for patients and healthcare providers [32]. Additionally, live attenuated virus vaccines can confer broader protection against different strains of a virus, as they mimic natural infection, and can stimulate the immune system to produce a wider range of antibodies [33]. However, live attenuated virus vaccines can be more difficult to manufacture, as they require specialized laboratory techniques, and they may not be safe for use in immunocompromised individuals due to their live virus nature [27]. There is also the risk that live attenuated vaccines may revert to a more virulent form, causing disease in vaccinated individuals, and possibly being transmitted to others. Indeed, in rare cases individuals who received the oral polio vaccine may shed the weakened poliovirus in their feces; possibly spreading it to other individuals [34].

The MMR vaccine, which is a live attenuated virus vaccine, was first introduced in 1971 and has significantly reduced the incidence of measles, mumps, and rubella [35]. The varicella vaccine, which is another live attenuated virus vaccine, was introduced in 1995 and has reduced the incidence of chickenpox and its complications [36]. The rotavirus vaccine, which is also a live attenuated virus vaccine, has been successful in reducing the incidence of severe diarrhea and dehydration caused by rotavirus in infants [37].

Whole virus vaccines have been an important tool in the prevention of infectious diseases caused by viruses. Inactivated virus vaccines and live attenuated virus vaccines are two of the most used vaccine platforms, each with its advantages and disadvantages. Due to the limitations of whole virus vaccines, modern-day vaccine approaches are moving towards more specific vaccines that target specific antigenic proteins of the virus rather than the whole virus. This approach allows for a targeted immune response, maximizing neutralizing antibody production, and reducing the risk of unwanted side effects. Examples of these approaches are protein subunit and viral-vectored vaccines, which can be produced in a safer manner and to a higher yield than traditional platforms.

1.1.2 Protein Subunit

Protein subunit vaccines have emerged as a highly effective, distributable, and scalable vaccine platform [38,39]. These vaccines are made up of purified proteins from the pathogen of interest, which are used to elicit an immune response. Compared to traditional whole virus vaccines, protein subunit vaccines offer advantages, including increased safety and the ability to target specific components of the pathogen.

The development of protein subunit vaccines dates back to the 1970s when researchers first began exploring the use of recombinant DNA technology for vaccine production. This technology

5

allowed the use of laboratory techniques to isolate, manipulate, combine, and create DNA segments for the production of recombinant DNA and recombinant proteins. The production of protein subunit vaccines is a multi-step process including the identification of a target antigen, the synthesis of recombinant protein, and the purification of the recombinant protein. The first step is to identify the target antigen. Typically, target antigens for a pathogen consist of an antigen that is responsible for virus-host cell binding and/or a target of neutralizing antibodies [38,39].

Protein subunit vaccines can be produced using a variety of expression systems, including bacteria, yeast, and mammalian cells. The choice of expression system depends on various factors, such as the specific vaccine target, the desired level of protein complexity and modification, and the intended use of the vaccine.

Bacterial expression systems, such as E. coli, are commonly used for the production of simple protein subunit vaccines [40]. Bacteria can be grown quickly and efficiently in large quantities, making it a cost-effective option [41]. Moreover, bacterial expression systems offer easy manipulation, high expression rates, and a large number of host strains to choose from. However, bacterial systems may not be suitable for complex or post-translationally modified proteins [19,40–42]. Bacteria may also produce endotoxins and other contaminants that require extensive purification steps to remove [43].

Yeast expression systems, such as Saccharomyces cerevisiae, are also commonly used for protein subunit vaccine production [41]. Yeast can produce complex proteins with proper folding and post-translational modifications, making it a popular choice for vaccine production [43]. Moreover, yeast expression systems can offer high yields of recombinant protein and may be easier to manipulate than mammalian cell systems. However, the complexity of post-translational modifications and the potential for variability in glycosylation patterns require extensive

characterization and optimization, which can make yeast expression systems more challenging to work with leading to avoidance of the production of glycosylated proteins within yeast [40,43,44].

Mammalian cell expression systems, such as Chinese hamster ovary (CHO) cells and human embryonic kidney (HEK)293 cells, are often used for the production of complex protein subunit vaccines [42,45,46]. These systems offer the advantage of producing highly complex and properly folded proteins with post-translational modifications, making them an attractive choice for certain protein subunit vaccines, particularly those requiring glycosylation or other modifications [42,45,46]. Mammalian cell systems may be easier to scale up than bacterial or yeast systems, as they can use suspension cell culture and bioreactors, which allow for larger production volumes and resulting protein yield. Moreover, stable transfection techniques can be used for long-term expression, ensuring consistent production and section of the desired protein at high amounts. However, mammalian cell expression systems can be more challenging to work with due to their higher cost, longer production times, and lower expression rates than bacterial or yeast systems.

After the recombinant protein has been produced, it must be purified and formulated into a vaccine. The purification process is necessary to isolate and remove contaminants, such as host cell proteins, nucleic acids, and endotoxins, that can cause adverse reactions in patients. Additionally, purification can help ensure the quality, potency, and safety of the final vaccine product.

Protein subunit vaccines are typically purified using a combination of chromatography techniques. The exact purification strategy depends on the specific vaccine and the expression system used. For example, vaccines produced in bacterial systems may require a different purification strategy than those produced in mammalian cells. Some commonly used chromatography techniques include ion exchange chromatography, size exclusion

chromatography, hydrophobic interaction chromatography, and affinity chromatography [47–50]. Each of these techniques can isolate and separate different components of the protein subunit vaccine, allowing for the removal of contaminants and the purification of the target protein. The final product may then be subjected to additional quality control tests to ensure its purity, potency, and safety. Overall, the purification of protein subunit vaccines is a critical step in the production process that helps ensure the quality, potency, and safety of the final vaccine product. The use of a combination of chromatography techniques and other purification methods can effectively remove impurities and contaminants from the vaccine, resulting in a highly purified and safe vaccine product.

One of the earliest examples of a protein subunit vaccine is the hepatitis B vaccine, which was approved for use in the United States in 1986 [51]. This vaccine is made up of a single protein from the hepatitis B virus, which is produced using recombinant DNA technology in yeast cells [52]. The hepatitis B vaccine has been highly effective at preventing new infections and is now included as part of routine childhood immunization schedules in many countries [53,54].

Since the development of the hepatitis B vaccine, many other protein subunit vaccines have been developed and deployed around the world. These include vaccines for diseases such as human papillomavirus (HPV), pertussis, and pneumococcal disease, among others.

The HPV vaccine is a protein subunit vaccine that protects against multiple strains of the HPV virus, which can cause cervical cancer, as well as other types of cancer and genital warts [55]. The vaccine is made up of virus-like particles (VLPs) that mimic the structure of the HPV virus but do not contain any viral DNA. These VLPs are made using recombinant DNA technology, in which genes encoding the structural proteins of the virus are inserted into yeast or insect cells for production [56]. The HPV vaccine is highly effective at preventing new infections and associated

diseases. Studies have shown that the vaccine is up to 99% effective at preventing cervical precancers and genital warts caused by the HPV strains included in the vaccine [55,57,58,58–61]. Additionally, since the introduction of the HPV vaccine, there has been a significant decrease in the number of new cases of HPV-related cancers and genital warts [62,63].

Pertussis, also known as whooping cough, is a respiratory illness caused by the bacteria Bordetella pertussis [64]. The disease can be particularly severe in infants and young children and can lead to complications such as pneumonia, seizures, and death [64]. The pertussis vaccine is a protein subunit vaccine that contains purified components of the B. pertussis bacteria, including the pertussis toxin and other virulence factors [65,66]. The pertussis vaccine was first introduced in the 1940s and has gone through several iterations over the years [67]. In the 1990s, new protein subunit pertussis vaccines were developed, which contained only purified components of the B. pertussis bacteria [65,66,68]. These vaccines were less reactogenic than the earlier whole-cell pertussis vaccines and were found to be highly effective at preventing pertussis [68]. Currently, the pertussis vaccine is often given in combination with other vaccines, such as diphtheria and tetanus vaccines, in a single injection known as the DTaP vaccine [69].

One of the main advantages protein subunit vaccines offer over traditional whole virus vaccines is safety. Because these vaccines do not contain live or inactivated viruses, they are generally well-tolerated and have a lower risk of side effects. This is particularly important for vulnerable populations, such as young children, pregnant women, and immunocompromised individuals. Another advantage of protein subunit vaccines is their ability to target specific components of the pathogen. By focusing on key proteins or fragments, these vaccines can elicit a more targeted and effective immune response. This can result in higher levels of protection against the pathogen and may also reduce the risk of vaccine-associated side effects.

Despite these advantages, there are also some disadvantages associated with protein subunit vaccines. One of the main disadvantages is that they may require multiple doses to achieve full immunity [70–72]. This is because the purified proteins or fragments used in these vaccines may not elicit as strong of an immune response as whole virus vaccines.

Additionally, these vaccines may require adjuvants, which are substances that help to boost the immune response [73,74]. Adjuvants can increase the cost and complexity of the vaccine production process. However, ongoing research and development in this area are likely to lead to new and improved vaccine options in the future.

In conclusion, protein subunit vaccines have played an important role in the prevention of infectious diseases. These vaccines offer several advantages over traditional whole virus vaccines, including increased safety and the ability to target specific components of the pathogen. While there are some challenges associated with the production and deployment of protein subunit vaccines, ongoing research and development in this area are likely to lead to new and improved vaccine options in the future.

1.1.3 Viral Vectored

Viral vector vaccines are promising vaccine platform that utilizes a weakened or modified virus to deliver antigens from the target pathogen to the immune system. By using a viral vector, the vaccine can generate a stronger (increased antibody secretion and cell-mediated response), durable, and more specific immune response than traditional subunit or inactivated vaccines. This approach has been particularly successful in the development of vaccines against viruses such as Ebola and COVID-19.

The development of viral vector vaccines begins with the selection of an appropriate viral vector. Viruses such as adenoviruses, poxviruses, and vesicular stomatitis virus (VSV) are commonly used as vectors due to their ability to infect a wide range of host cells, their capacity for genetic modification, and their ability to induce strong immune responses [75]. The target antigen is then inserted into the viral vector genome using recombinant DNA technology [76]. There are advantages to using viral vectors as a vaccine platform. Firstly, viral vectors have a high capacity to accommodate foreign genetic material, allowing for the delivery of large or complex antigens that may be difficult to produce using other vaccine platforms [75,77,78]. Secondly, viral vectors are highly immunogenic, which means they can activate a strong and durable immune response [75,77,78]. Thirdly, viral vectors can be engineered to target specific cells or tissues, which can improve vaccine efficacy and reduce side effects [75,77,78]. Fourthly, a key advantage of viral vector vaccines is their ability to mimic the natural infection process, which enhances the body's immune response [75,77,78].

The most used viral vectors for vaccine development are adenoviruses, which are common viruses that cause non-severe respiratory and gastrointestinal infections in humans [76,79]. Adenoviral vectors are modified to remove genes that cause disease, or immune dysregulation, and replace them with genetic material encoding the antigen of interest. When the modified adenoviral vector infects cells, the genetic material is taken up by the cells, and the antigen is produced, triggering a strong immune response.

Other viral vectors used for vaccine development include VSV, measles virus, and modified vaccinia virus Ankara (MVA) [75]. Each viral vector has its advantages and limitations, and the choice of viral vector depends on the specific antigen and the intended use of the vaccine. The viral vector vaccine is produced by growing the modified virus in cell culture and purifying

11

the virus particles [80–83]. The purified virus is then used as the vaccine, which is administered to patients via injection or intranasal administration. Once inside the body, the virus infects host cells and presents the target antigen to immune cells, triggering an immune response. Multiple factors can affect the production of viral vectors, including the choice of host cells, the efficiency of the transfection process, and the purification process. Host cells for viral vector production can be mammalian or insect cells, and each has its advantages and disadvantages. Mammalian cells, such as HEK293 or CHO cells, are often used to produce viral vectors because they can produce high yields of virus particles and can perform post-translational modifications to the viral vector proteins, which can improve vaccine efficacy [45]. The purification process for viral vectors involves multiple steps, including filtration, ultracentrifugation, and chromatography [80–83]. Each step helps to remove contaminants and impurities from the viral vector preparation, ensuring the purity and potency of the final vaccine product. Quality control tests are also performed on the viral vector vaccine to ensure that it meets regulatory standards for safety, efficacy, and purity.

In the case of Ebola, viral vector vaccines were developed using a chimpanzee adenovirus (ChAd) vector, VSV, adenovirus serotype 26 (Ad.26), and MVA expressing the Ebola virus glycoprotein [84]. All vaccines demonstrated immunogenicity in phase 1 trials, inducing both humoral and cellular immune responses in vaccinated individuals [84,85]. In a subsequent phase 3 trial, the vaccine VSV-based vaccine was found to be highly effective, with a 97.5% efficacy rate in individuals vaccinated [86,87]. This vaccine was approved by the European Medicines Agency in 2019, becoming the first vaccine against Ebola to receive regulatory approval [86,88–92]. The two-dose Ad.26 and MVA-based Ebola vaccines received approval from the European Union in July 2020, although a phase 3 trial has yet to be concluded [93–98].

For influenza, viral vector vaccines have been developed using different vectors, including adenovirus, VSV, and MVA [99–111]. These vaccines typically express the hemagglutinin (HA) protein from the influenza virus, which is the primary target of influenza-specific antibodies [99–111]. In preclinical studies, these vaccines have demonstrated efficacy against multiple strains of the influenza virus and have shown the ability to induce long-lasting immune responses [99–111]. Clinical trials have also shown that these vaccines are safe and immunogenic, although further research is needed to fully evaluate their efficacy [112–114].

Despite their effectiveness in inducing a robust immune response, viral vector vaccines have disadvantages. One of the main disadvantages is the potential for pre-existing immunity to the viral vector used in the vaccine [115–120]. Since most individuals have been exposed to natural viral infections or prior vaccination, they may have developed immunity to the vector. This pre-existing immunity can lead to a reduced immune response to the vaccine antigen and limit the efficacy of the vaccine [115–120]. Another disadvantage of viral vector vaccines is the potential for vector-mediated adverse events. For instance, the adenovirus vector used in the COVID-19 vaccine has been associated with rare cases of blood clots, leading to the suspension of the vaccine in some countries [121–126].

Furthermore, the manufacturing process for viral vector vaccines can be complex and time-consuming, which can lead to delays in the production and distribution of the vaccine [76]. This delay can be detrimental, especially during disease outbreaks when a rapid response is required to prevent further spread.

Viral vector vaccines have become an essential tool in the fight against infectious diseases. The use of viral vectors to deliver vaccine antigens has proven to be effective in inducing robust immune responses against a wide range of pathogens, such as Ebola, influenza, and COVID-19.

However, the manufacturing process for these vaccines can be complex and time-consuming. The distribution of these vaccines can also be challenging due to the need for cold chain storage. Additionally, pre-existing immunity to the viral vector, and the potential for vector-mediated adverse events, are significant disadvantages of this platform. Despite these challenges, viral vector vaccines remain a critical tool in the fight against infectious diseases and will continue to play a vital role in future vaccination programs.

1.2 Next-Generation Vaccine Development

Traditional vaccine approaches outlined in the previous sections have been highly effective tools in the fight against infectious diseases. However, their limitations have necessitated the development of next-generation approaches. The slow and laborious development nature of whole-virus vaccines, along with their limited broad-spectrum immunity, have made them less than ideal for rapidly evolving, and emerging, respiratory viruses. While traditional protein subunit vaccines were a landmark improvement in historical vaccine development, there has been a need to develop more immunogenic approaches for greater induction of neutralizing antibodies and increased immunity longevity. In terms of viral vector vaccine development, preexisting immunity to the viral vector, along with safety concerns, has severely hampered clinical translation.

To address these limitations and challenges in traditional vaccine approaches, a new era of next-generation vaccine development has emerged. Next-generation vaccines aim to improve immunogenicity, specificity, safety, speed of vaccine development, and the ability to provide long-lasting immunity to a broad spectrum of pathogens. These novel vaccine platforms include

messenger RNA (mRNA) vaccines, structured-based protein design, and alternative vaccine administration routes.

mRNA vaccines represent a new frontier in vaccine technology that utilizes synthetic nucleic acid molecules to encode and express viral proteins in the host cell. mRNA vaccines have been successful in the development of vaccines for COVID-19, with the advantage of rapid design and production, enhanced immunogenicity, and the ability to induce potent and long-lasting immune responses. However, challenges such as storage and distribution at low temperatures along with waning immunity, necessitating multiple doses may hinder their widespread use.

Structure-based protein design is another emerging technology that combines advances in cryo-electron microscopy (cryoEM) and deep learning algorithms to design stable and highly immunogenic viral proteins that can induce strong immune responses. This technology has shown promising results in the development of vaccines against influenza, respiratory syncytial virus (RSV), and COVID-19; with the potential to provide better coverage against antigenically diverse strains and reduce the risk of vaccine escape mutants.

Alternative vaccine administration routes, such as intranasal and intradermal, are also being explored as potential alternatives to traditional intramuscular injection. Intranasal administration routes have the advantage of inducing strong mucosal immunity, which is particularly important for respiratory pathogens that enter through the nasal cavity. Additionally, intranasal and intradermal vaccine administration may provide needle-free and painless delivery, improve vaccine coverage, and increase vaccine accessibility in low-resource settings. Intradermal vaccination through microneedle array (MNA) has the additional advantages of inducing greater immunity than the traditional intramuscular injection, along with increased vaccine stability at

room temperature and potential self-application by the vaccinee without the need for trained medical personnel.

Overall, next-generation vaccine development represents a promising direction in the fight against infectious diseases, with the potential to provide more effective and accessible vaccines for a wide range of pathogens. The following subchapters will discuss in detail the advances in mRNA vaccines, structure-based protein design, and alternative vaccine administration routes, along with their current status, challenges, and prospects.

1.2.1 mRNA

mRNA vaccines have garnered significant attention as a promising next-generation class of vaccines. They are developed using genetic material, specifically messenger RNA (mRNA), which encodes the instructions to produce a viral protein [127]. The mRNA is delivered to host cells, where it is translated to produce the viral protein [127]. This protein is recognized as foreign by the immune system, which in turn triggers an immune response. This protein serves as an antigen that stimulates the immune system to produce a response, including the production of neutralizing antibodies [128]. In the event of future exposure to the actual pathogen, the immune system is primed to quickly recognize and neutralize the pathogen.

mRNA vaccines represent a novel approach to vaccination. Unlike traditional vaccines that rely on the use of attenuated or inactivated pathogens or recombinant proteins, mRNA vaccines use genetic material in the form of messenger RNA to produce an immune response. mRNA vaccines work by instructing cells to produce a fragment of the virus, such as the spike protein of SARS-CoV-2, which triggers an immune response in the body [128]. The development of mRNA technology has a rich history dating back decades. In the 1990s, researchers first began to explore

the potential of mRNA as a therapeutic agent, but progress was slow due to technical challenges such as rapid degradation of mRNA in the body and inefficient delivery to target cells [129,130]. In the early 2000s, advances in RNA chemistry and nanotechnology helped to overcome these hurdles, leading to the development of more stable and efficient mRNA molecules [131]. Researchers began to explore the use of mRNA as a vaccine platform, as it offered advantages over traditional vaccine technologies such as live attenuated or inactivated pathogens. In 2005, researchers at the University of Pennsylvania published a seminal study demonstrating the feasibility of using mRNA to induce immune responses against infectious diseases [132]. Since then, the field of mRNA-based vaccines has advanced rapidly, with companies including Moderna and BioNTech developing mRNA-based vaccines for a range of infectious diseases. The success of the mRNA-based COVID-19 vaccines from Moderna and BioNTech represents a major milestone in the field, demonstrating the potential of mRNA technology to rapidly respond to emerging infectious diseases and provide a new platform for the development of next-generation vaccines [133–135].

The manufacturing of mRNA vaccines involves numerous critical steps, starting from the design of the mRNA sequence, through to its production, purification, and formulation. The entire process is complex and involves specialized equipment, skilled personnel, and rigorous quality control measures. The process is also relatively cost-intensive compared to other vaccine platforms. Once the mRNA sequence has been designed, it is synthesized in the laboratory using an RNA polymerase from a DNA template [129,136]. This involves the stepwise addition of nucleotides to the growing mRNA chain, guided by the mRNA sequence yielding a single-stranded mRNA molecule that is ready for downstream processing. The synthesized mRNA is typically contaminated with residual reagents, nucleotides, and other impurities that can interfere with its function or elicit an immune response. To remove these contaminants, the mRNA is subjected to

rounds of purification using high-performance liquid chromatography (HPLC) [129]. This process separates the mRNA from other impurities based on its size, charge, and hydrophobicity. The resulting purified mRNA is then ready for formulation which is the process of packaging the mRNA into a lipid nanoparticle (LNP) carrier that will protect it from degradation and facilitate its delivery into cells. LNPs are composed of a mixture of lipids and cholesterol that self-assemble into a spherical particle around the mRNA [129,131]. This provides a protective shell that can shield the mRNA from the harsh extracellular environment and allow it to be taken up by cells through endocytosis [131]. The formulation process involves mixing the mRNA with the LNP components, sonication to form the particles, and purification to remove excess lipids and other impurities. Once the mRNA vaccine has been formulated it is filled into vials and then subjected to quality control tests for the antigen content, mRNA concentration, particle size, and sterility. Manufacturing of mRNA vaccines is a complex process that involves multiple critical steps, including mRNA synthesis, purification, formulation, and filling. The process requires specialized equipment, skilled personnel, and rigorous quality control measures to ensure that the final product is safe, effective, and of high quality. Despite the challenges, mRNA vaccines have emerged as a promising new platform for the development of vaccines against a wide range of infectious diseases and other conditions.

mRNA vaccines offer multiple advantages over traditional vaccine platforms, with their most significant advantage being their rapid development timeline. mRNA vaccines can be designed and synthesized quickly, allowing for a timelier response to emerging pathogens [127]. Additionally, mRNA vaccines are highly adaptable and can be easily modified to target new variants of a virus. This was particularly important in the case of COVID-19, where mRNA vaccines were developed and authorized for emergency use within a year of the emergence of

SARS-CoV-2 [127]. mRNA vaccines are highly effective, with both the Pfizer-BioNTech and Moderna vaccines demonstrating efficacy rates of over 90% in clinical trials, although the waning immunity over time has been a concern [137,138]. The success of the mRNA-based COVID-19 vaccines from Moderna and BioNTech represents a major milestone in the field, demonstrating the potential of mRNA technology to rapidly respond to emerging infectious diseases and provide a new platform for the development of next-generation vaccines. Influenza has also been one of the primary targets for mRNA vaccine research due to the high variability of the virus and the need for annual vaccine updates [139,140]. Clinical trials have shown promising preliminary results for mRNA-based influenza vaccines, with some studies demonstrating improved protection compared to traditional influenza vaccines [139,141].

Along with COVID-19 and influenza viruses, mRNA vaccines targeting flaviviruses are currently being developed. Flaviviruses are a group of viruses that are responsible for many diseases in humans, including dengue fever, Zika virus, and yellow fever. One of the major challenges in developing a vaccine for flaviviruses is the fact that they are highly variable and can rapidly mutate, making it difficult to produce a vaccine that is effective against all strains. Despite these challenges, significant progress has been made in the development of mRNA vaccines for flaviviruses. Zika virus mRNA vaccines have shown the potential in producing strong and protective immune responses in preclinical studies [142,143]. The same has been shown for dengue virus mRNA vaccines [144,145]. While the development of mRNA vaccines for flaviviruses is still in its early stages, the promising results from these studies suggest that they may become an important tool in the fight against these diseases. Further research is needed to determine the safety and efficacy of these vaccines in humans, but the early results suggest that they could play an important role in the prevention of flavivirus infections.

In conclusion, mRNA vaccines have emerged as a promising solution for infectious diseases due to their high efficacy rates and rapid development timelines. While still relatively new, mRNA vaccines have shown great potential in clinical trials and have been successfully deployed against COVID-19. Research on mRNA vaccines against other pathogens, such as flaviviruses, has also shown promising results, with preclinical studies demonstrating robust immune responses. The ability to rapidly develop and produce mRNA vaccines, without the need for live pathogens, makes this platform a valuable tool in the fight against infectious diseases. As with any vaccine platform, challenges remain, such as the need for extreme cold chain storage and the potential side effects of immunization. However, the benefits of mRNA vaccines suggest that they will continue to play an important role in future vaccination programs.

1.2.2 Structure-Based Protein Design

The use of structure-based protein design (SBPD) has led to the development of highly effective vaccines against the respiratory syncytial virus (RSV) and the severe acute respiratory syndrome coronavirus 2 (SARS-CoV-2), the causative agent of COVID-19. SBPD is a rapidly advancing field that has revolutionized the development of new vaccines utilizing the three-dimensional structure of proteins to design novel vaccine antigens that are optimized for immunogenicity and efficacy [146]. This process involves the use of high-resolution imaging techniques such as cryo-electron microscopy (cryoEM) to determine the structure of the target protein. Once the protein structure has been elucidated, computational modeling and experimental tools can be used to design mutations that stabilize the protein in its most immunogenic structural conformation [146].

One notable application of SBPD is the development of vaccines for RSV, a leading cause of severe lower respiratory tract infection in infants and young children [147–150]. It is a major cause of illness in young children and can be particularly dangerous in premature babies and children with underlying medical conditions [147–150]. Despite efforts over several decades, the development of a vaccine against RSV has been challenging due to the virus's complex structure and the difficulty in inducing an effective immune response against it [147]. The RSV fusion (F) protein is the primary target for RSV vaccines, and the protein undergoes a structural transition from a pre-fusion to a post-fusion conformation during the virus-host cell fusion process [151]. In the 1960s, a formalin-inactivated RSV vaccine was developed and tested in clinical trials, but it led to severe disease upon natural infection in infants, resulting in two deaths and the hospitalization of many others [152]. Later, a live attenuated RSV vaccine was developed and tested in clinical trials but also resulted in severe respiratory disease in some recipients [153]. These setbacks led to a long hiatus in RSV vaccine development, and the need for a safe and effective RSV vaccine remained unmet.

Recent advances in SBPD have enabled the development of a new generation of RSV vaccines. The key to success in these efforts has been the use of cryo-EM to visualize the structure of the RSV F protein, which is responsible for viral entry into host cells [154]. Cryo-EM allows researchers to study the protein in its native state, which is critical for understanding its structure and function. Using cryo-EM, researchers have been able to identify key structural elements of the RSV F protein that are necessary for stabilizing the protein in its prefusion conformation [155]. By presenting RSV F protein in the prefusion context, it allowed for the induction of an immune response that is effectively able to neutralize RSV through replicating the F structure before virus-host cell binding and fusion. By introducing specific mutations into the protein sequence, researchers have been able to stabilize the F protein in its prefusion conformation, leading to the

21

development of highly effective RSV vaccines [155,156]. Clinical trials of these new RSV vaccines have shown promising results. In a phase III clinical trial, a prefusion-stabilized RSV F protein nanoparticle protein subunit vaccine (RSVpreF) was found to have an efficacy of 85.7% in preventing more severe disease primary endpoint of lower respiratory tract illness (LRTI-RSV) defined by analysis of three or more RSV-associated symptoms in healthy older adults [157,158]. The vaccine was also found to be safe and well-tolerated, with no vaccine-related serious adverse events reported [159–161]. Recently, in a phase 3 trial in pregnant women, RSVpreF was found to have a vaccine efficacy of 81.8% in infants within 90 days of birth against medically attended LRTI-RSV [162]. These results are encouraging and suggest that SBPD-based RSV vaccines have the potential to address an unmet medical need and improve public health outcomes.

In addition to its successful application in RSV vaccine development, SBPD has also been applied in the development of vaccines against coronaviruses, including Middle East respiratory syndrome coronavirus (MERS-CoV) and SARS-CoV-2.

In the case of MERS-CoV, initial attempts to develop a vaccine were hindered by the lack of knowledge about the virus's structure and immunogenicity. However, with the discovery of the spike (S) protein as the primary target for neutralizing antibodies, researchers were able to utilize SBPD to engineer stabilized versions of the protein that could elicit a strong immune response [163]. Specifically, a trimeric version of the S protein was developed by introducing proline mutations that locked the protein into the prefusion conformation, which is more stable and more closely resembles the structure of the protein on the virus surface [163]. This trimeric protein, known as MERS-CoV-2p, was found to elicit strong neutralizing antibody responses in animal studies and has advanced to phase I clinical trials [163].

The lessons learned from the development of MERS-CoV vaccines were instrumental in the rapid development of SARS-CoV-2 vaccines utilizing SBPD. The SARS-CoV-2 S protein shares significant structural similarities with the MERS-CoV S protein, and early studies on SARS-CoV-2 demonstrated the importance of stabilizing the protein in the prefusion conformation to elicit strong neutralizing antibody responses [164]. Utilizing cryo-EM, researchers were able to determine the structure of the SARS-CoV-2 S protein in the prefusion conformation, providing a blueprint for SBPD efforts [164]. The Pfizer-BioNTech and Moderna mRNA vaccines for SARS-CoV-2 also utilize SBPD by incorporating 2 proline mutations, based on the MERS vaccines trials, that stabilize the prefusion conformation of the S protein and demonstrated high efficacy rates in clinical trials [133,134,137,138]. Additionally, further stabilized proteins with increased proline substitutions and increased spike protein secretion, known as HexaPro and HexaPro-Fc, were found to elicit strong neutralizing antibody responses in animal studies and are currently in phase I clinical trials [165,166].

Deep learning approaches have revolutionized the field of protein structure prediction, offering a promising avenue for accelerating SBPD-based vaccine design by potentially circumventing the time needed to resolve protein structures through cryo-EM. One such example is Rosetta Fold, a software suite that employs a combination of computational algorithms and experimental data to predict protein structures with previously unseen high levels of accuracy [167]. In the context of vaccine design, Rosetta Fold can be used to model protein structures and identify potential antigenic epitopes for the design of novel vaccines. Similarly, Alpha Fold, a deep learning-based protein structure prediction tool has also shown promising results. Alpha Fold's approach leverages a neural network to predict the distance between pairs of amino acids in a protein sequence, allowing it to accurately predict protein structure with a high degree of accuracy

[168]. By employing these deep learning-based tools in conjunction with experimental data, researchers can rapidly and accurately design novel vaccines with a high likelihood of success.

Deep learning-based approaches for vaccine design are an emerging field with promising potential. Despite being in its infancy, preliminary and preclinical studies have demonstrated the ability of these approaches to design multi-epitope vaccines [169–174]. Deep learning-based approaches have the potential to accelerate SBPD-based vaccine design and facilitate the development of effective vaccines against various infectious diseases. However, more research is required to optimize these approaches for vaccine design and to ensure their safety and efficacy in human clinical trials. As such, the field of deep learning-based approaches for vaccine design is an exciting area of research with the potential to revolutionize the development of vaccines against infectious diseases.

1.2.3 Alternative Administration Strategies

Traditionally, vaccines have been administered through intramuscular injections. However, in recent years, alternative routes of vaccine administration have gained significant attention due to their potential benefits such as ease of administration, improved patient compliance, and enhanced immune response. Intranasal and intradermal vaccine administration are two such alternative strategies that have shown promising results in preclinical and clinical studies. Intranasal vaccination involves delivering the vaccine directly into the nasal cavity, while intradermal vaccination involves delivering the vaccine into the dermal layer of the skin. These alternative routes of vaccine administration have shown potential for inducing strong and long-lasting immune responses, making them attractive options for the development of novel vaccines against a variety of infectious diseases. In this section, we will explore the current state of research

on intranasal and intradermal vaccination and discuss their potential as alternative vaccine administration strategies.

1.2.3.1 Intranasal

Intranasal vaccination is a promising alternative to traditional parenteral routes for vaccine administration. It offers advantages, including the ability to induce mucosal immune responses that can prevent infection at the site of pathogen entry, such as the respiratory tracts which are particularly important for highly variable respiratory pathogens [175,176]. Additionally, intranasal vaccines have the potential to provide broader protection against both homologous and heterologous strains of a pathogen, as well as offer a more convenient and painless method of vaccination [177].

Intranasal vaccine administration offers multiple advantages over traditional injection-based approaches. The nasal cavity is an attractive site for vaccination due to its abundant supply of antigen-presenting cells (APCs), such as dendritic cells, macrophages, and B cells [178–180]. These APCs are responsible for capturing, processing, and presenting antigens to T cells, which initiate an adaptive immune response. The nasal mucosa contains a rich network of lymphatic vessels, which enables efficient transport of vaccine antigens to draining lymph nodes and induction of antigen-specific immune responses [178–180]. Additionally, the nasal mucosa is enriched in specialized lymphoid tissue, such as nasopharynx-associated lymphoid tissue (NALT), which has been shown to play a critical role in mucosal immune defense [181,182].

Intranasal vaccination also induces the production of secretory immunoglobulin A (sIgA), a class of antibodies that plays a key role in protecting mucosal surfaces from infection. sIgA can neutralize pathogens and prevent their attachment to host cells, thereby limiting the spread of infection [183,183,184]. Moreover, sIgA can bind to pathogens and transport them across mucosal

25

surfaces, leading to their clearance by other components of the immune system [185–187]. In addition to sIgA, intranasal vaccination can stimulate the production of systemic and mucosal memory responses. Memory B and T cells generated by intranasal vaccination can persist for long periods and provide rapid protection upon re-exposure to the pathogen [188].

Despite the advantages of intranasal vaccination, there are also limitations and challenges associated with this route of administration. One potential concern is the lack of systemic T-cell response induced by intranasal vaccination, as studies have found intramuscular vaccination elicited stronger cellular immune responses than intranasal vaccination [177,189]. The potential transport of vaccine from the nasal cavity to the brain is also a safety concern, especially with live virus and viral vector vaccines [190]. Additionally, the amount of antigen that can be delivered by intranasal administration is limited, which may affect the strength and duration of the immune response. Another potential limitation is the variability in the size and shape of the nasal cavity between individuals, which may impact the distribution and uptake of vaccine antigens.

Intranasal vaccines targeting influenza have been studied extensively and have shown promise in preclinical and clinical trials. For instance, a live attenuated influenza vaccine (LAIV) administered intranasally has been licensed for use in the United States and other countries [191]. Studies have demonstrated that LAIV can elicit both systemic and mucosal immune responses, providing long-lasting protection against influenza infection [192–194]. Intranasal LAIV has also been shown to be effective in children and has been approved for use in individuals aged 2-49 years [193,195]. Furthermore, the intranasal administration of LAIV is well-tolerated and associated with fewer side effects than the injectable influenza vaccine [196].

Intranasal vaccines targeting SARS-CoV-2, the virus responsible for COVID-19, have also been investigated. In preclinical studies, intranasal vaccination with multiple different vaccine

platforms, including mRNA, viral vectored vaccines, and protein vaccines, have been shown to induce robust neutralizing antibody responses and T cell responses, as well as prevent viral replication in the lungs of mice infected with SARS-CoV-2 [33,177,182,197,198]. Additionally, intranasal administration of the S protein antigen of SARS-CoV-2 has been shown to induce protective immunity in animal models, suggesting the potential of intranasal vaccines as a viable strategy for preventing COVID-19 [199–202].

Other respiratory pathogens, such as RSV and pneumococcus, have also been targeted with intranasal vaccines, showing high potential in preclinical studies along with safety and immunogenicity in early-phase clinical trials [203–206]. Overall, the intranasal administration of vaccines targeting respiratory pathogens has shown great potential for providing protective immunity and preventing the spread of infectious diseases. While challenges remain for widespread clinical translation, intranasal vaccines remain an attractive tool for inducing mucosal immunity to halt the transmission of respiratory pathogens.

1.2.3.2 Intradermal

Intradermal (ID) vaccination is a novel and emerging vaccination strategy that targets the immune cells located in the skin to induce strong and durable immune responses against the antigen. The skin is the largest organ of the human body, and it contains various immune cells, including Langerhans cells, dermal dendritic cells, and memory T cells, which play a crucial role in triggering the immune response against invading pathogens [207,208]. Compared to traditional intramuscular (IM) vaccination, ID vaccination requires lower doses of vaccine antigens due to the higher density of immune cells in the skin [209–212]. This approach also has the potential to induce both systemic and local immunity, making it an attractive option for vaccines targeting respiratory pathogens, such as influenza and SARS-CoV-2.

One promising approach for ID vaccination is the use of microneedle arrays (MNA), which are minimally invasive devices that painlessly penetrate the skin to deliver vaccines directly to the immune cells in the skin (**Figure 1**). MNAs consist of an array of tiny needles that are only a few hundred micrometers in length and can be made from a variety of materials, such as metals, ceramics, and polymers [213,214]. The manufacturing of MN arrays is achieved using different techniques, including micro-molding, atomic spray drying, and 3D printing [215,216]. Micro-molding involves casting a polymer material into a mold containing microneedle features and then removing the solidified material from the mold [215,216]. Atomic spray drying involves using a nozzle to spray a liquid formulation of the MNA material onto a substrate, where it solidifies into a dry, powdery form [215,216]. 3D printing involves depositing layers of MNA material onto a substrate using a computer-controlled printer [215,216]. These different techniques offer varying levels of precision, scalability, and cost-effectiveness for MN array production.
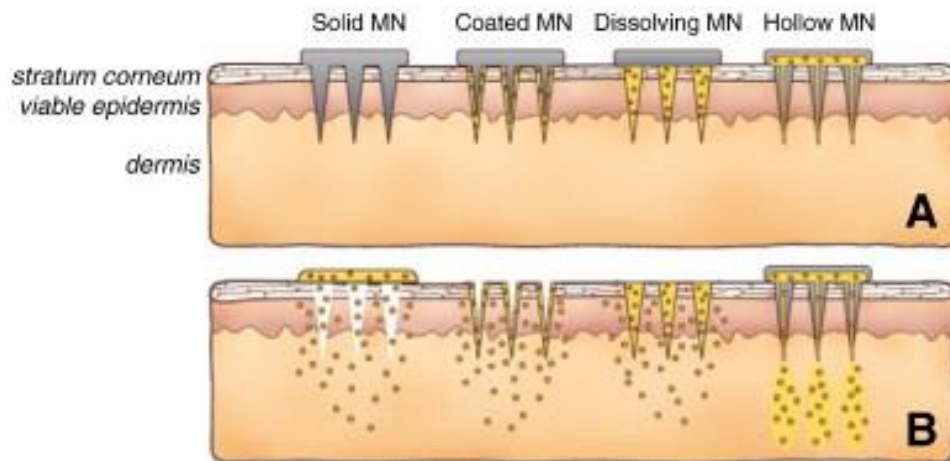
Figure 1: Methods of drug delivery to the skin using microneedles (MN). Microneedles are first applied to the skin (A) and then used for drug delivery (B). Solid microneedles are used as a pretreatment, after which drug can diffuse through residual holes in skin from a topical formulation (solid MN). After insertion of drug-coated microneedles into the skin, the drug coating dissolves off the microneedles in the aqueous environment of the skin

(coated MN). Drug-loaded microneedles are made of water-soluble or biodegradable materials encapsulating drug that is released in the skin upon microneedle dissolution (dissolving MN). Hollow microneedles are used to inject liquid formulations into the skin (hollow MN). 1. Kim, Y.-C., Park, J.-H. & Prausnitz, M. R. Microneedles for drug and vaccine delivery. Advanced Drug Delivery Reviews 64, 1547–1568 (2012). Copyright © 2012 Elsevier B.V. All rights reserved. Use with permission.

Dissolvable microneedle array (DMNA) patches have emerged as an attractive alternative to traditional MNA patches due to their potential advantages of controlled antigen release (**Figure 1**). DMNA patches consist of arrays of solid microneedles that are made of biocompatible, water-soluble polymers, such as polyvinylpyrrolidone (PVP), carboxymethyl cellulose, or hyaluronic acid, that can dissolve upon skin insertion (**Figure 1**) [215,217,218]. This means that there is no need for needle removal after application, reducing the risk of needle-stick injuries and biohazardous waste. Additionally, the dissolution of the microneedles in the skin allows for the controlled release of the vaccine, resulting in a more effective and efficient immune response. The use of DMNA patches also eliminates the need for cold chain storage, simplifying the logistics of vaccine distribution and administration, particularly in resource-limited settings [215]. Overall, the development of DMNA patches represents an exciting advancement in the field of microneedle-based vaccine delivery, with the potential to improve vaccine efficacy, safety, and accessibility.

One example of an intradermal vaccine currently in use is the intradermal polio vaccine, which uses a fractional dose of inactivated poliovirus delivered using a needle-free jet injector or a needle and syringe [219,220]. Studies have shown that this approach induces a robust immune response and could help accelerate the eradication of polio in regions where the disease is still endemic [219,220]. Another example is the DMNA patch-based vaccine for the SARS-CoV-2 virus, which is currently in development [217]. The DMNA patch is made using micro-molding technology

and is loaded with a recombinant spike protein antigen [217]. Preclinical studies have shown that the MNA patch elicits strong antibodies against the SARS-CoV-2 virus [217].

The advantages of intradermal vaccination using MNA arrays include their ease of use, painlessness, and the potential for self-administration. MNAs also have the potential to enhance vaccine stability and reduce the need for cold chain storage and transportation. MNAs also can achieve similar, or greater immune responses, than that of traditional IM injection with lower doses, allowing for dose sparing. However, MNA arrays also have some limitations, such as the need for specialized manufacturing and time-extensive micro-molding manufacturing techniques which are not compatible with large-scale pharmaceutical production. DMNA as a means for controlled vaccine release is an attractive tool for increasing the immune response to vaccination while circumventing needle removal and disposal, allowing for self-application by the vaccinee. Although there are some limitations to MNA, including the potential for skin irritation and the need for specialized equipment, intradermal vaccination using MNA holds great promise for the development of effective and convenient vaccine delivery systems for a wide range of infectious diseases.

1.3 Beta Coronaviruses

BetaCoronaviruses are a genus of enveloped, positive-sense RNA viruses that belong to the family Coronaviridae and are known to cause mild to severe respiratory illnesses in humans and animals (**Figure 2**). The first human BetaCoronavirus to cause substantial human morbidity and mortality, Severe Acute Respiratory Syndrome Coronavirus (SARS-CoV), emerged in 2002 and caused a global outbreak of Severe Acute Respiratory Syndrome (SARS) [221,222]. After which

another severe human BetaCoronavirus, the Middle East Respiratory Syndrome Coronavirus (MERS-CoV), emerged in 2012 and caused subsequent outbreaks in the Middle East and South Korea [221,223]. The recent emergence of SARS-CoV-2 in late 2019, causing the COVID-19 pandemic, has highlighted the importance of understanding the virology and pathogenesis of BetaCoronaviruses.

BetaCoronaviruses are spherical viruses with a diameter of approximately 80-160 nm. They have a helical nucleocapsid that contains a single-stranded, positive-sense RNA genome of approximately 27-32 kilobases [221]. The genome contains several open reading frames (ORFs) that encode structural and non-structural proteins [221]. The structural proteins include the spike (S), envelope (E), membrane (M), and nucleocapsid (N) proteins, while the non-structural proteins are involved in viral RNA replication and transcription [221].
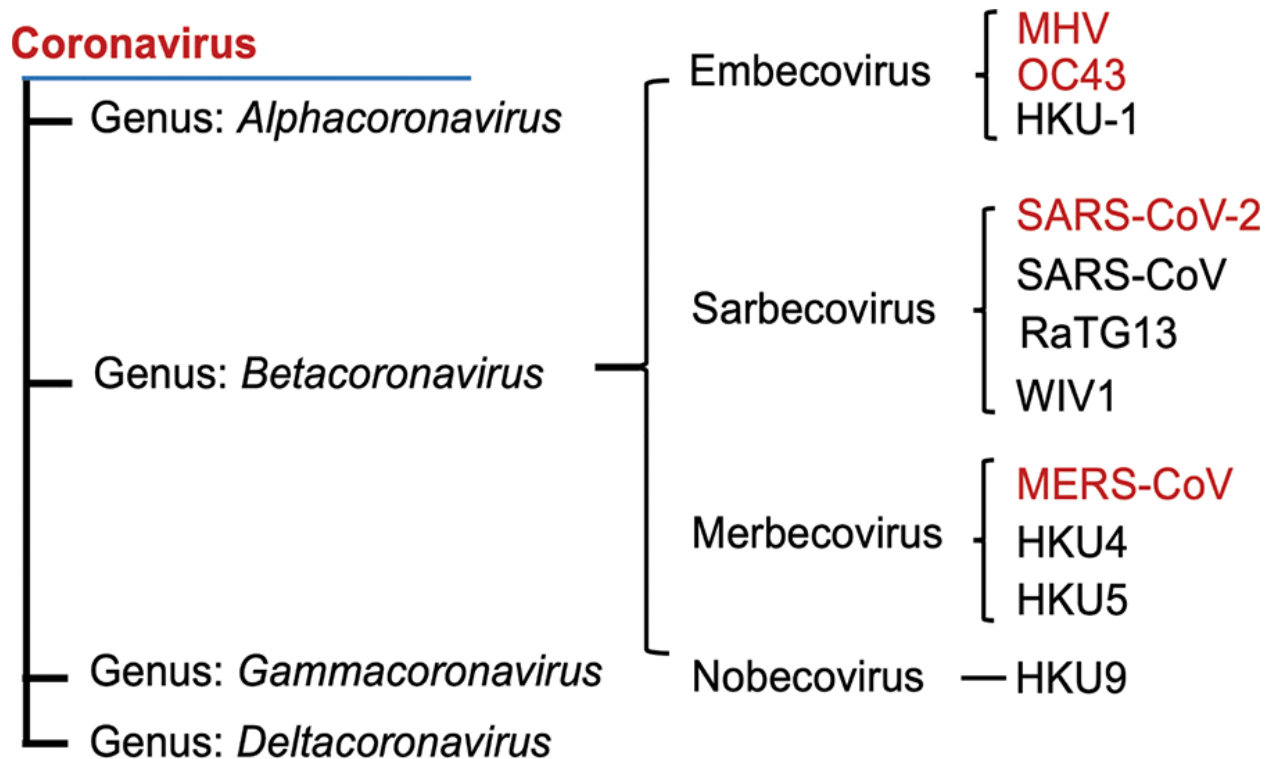
Figure 2: The Coronavirus family. Phylogenetic tree of betacoronaviruses and their subgenera. Nguyen, L. C. et al. SARS-CoV-2 Diverges from Other Betacoronaviruses in Only Partially Activating the IRE1α/XBP1 Endoplasmic Reticulum Stress Pathway in Human Lung-Derived Cells. mBio 13, e02415-22 (2022). Creative Commons Attribution 4.0 International license. https://creativecommons.org/licenses/by/4.0/

SARS-CoV-2 is a Betacoronavirus that is closely related to SARS-CoV (**Figure 2**). The virus has a genome length of approximately 29.9 kb and encodes for 4 structural proteins, including the spike (S), envelope (E), membrane (M), and nucleocapsid (N) proteins [221]. The S protein mediates viral entry by binding to the human receptor, angiotensin-converting enzyme 2 (ACE2) [221]. The virus also utilizes the host proteases, such as furin and transmembrane protease, serine 2 (TMPRSS2), for S protein priming, which enhances viral infectivity. SARS-CoV-2 has a higher transmission rate compared to SARS-CoV and can cause severe respiratory illness, leading to high mortality rates, especially in elderly and immunocompromised individuals [221].

MERS-CoV is also a Betacoronavirus that has a genome length of approximately 30 kb and encodes for 4 structural proteins, including the spike (S), envelope (E), membrane (M), and nucleocapsid (N) proteins [221,223]. The S protein of MERS-CoV binds to the human receptor, dipeptidyl peptidase 4 (DPP4), which is expressed on the surface of human cells [221,223]. The virus also utilizes the host protease, furin, for S protein priming, similar to SARS-CoV-2. MERS-CoV causes severe respiratory illness, leading to high mortality rates, especially in individuals with underlying medical conditions [221,223].

SARS-CoV-2 and MERS-CoV share multiple similarities, including their Betacoronavirus classification, genome organization, and utilization of furin cleavage site for S protein priming (**Figure 2**) [221,223]. However, they differ in their primary human receptor. While SARS-CoV-2 utilizes ACE2 for entry, MERS-CoV utilizes DPP4 (**Figure 3**) [221,223]. This difference in receptor utilization likely contributes to the differences in their clinical presentation and disease severity. Additionally, while both viruses can cause severe respiratory illness, the mortality rate of MERS-CoV is higher compared to SARS-CoV-2 [221,223].
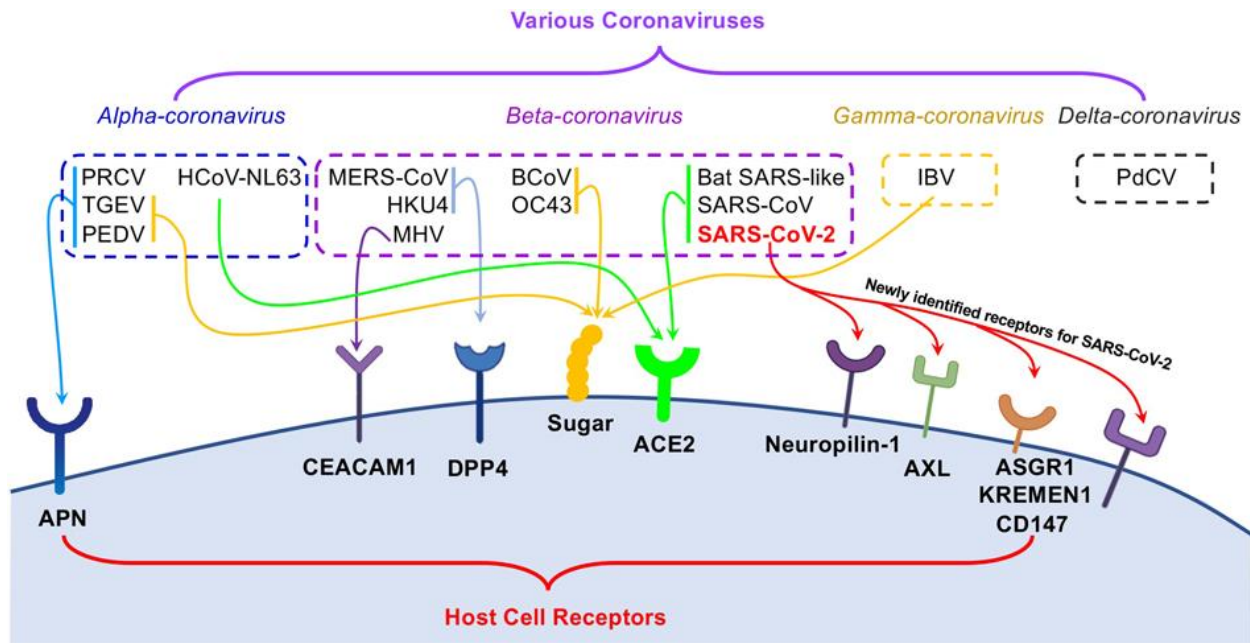
Figure 3: Different coronaviruses use a variety of receptors for viral attachment and entry. In the upper panel, various coronaviruses from four major genera, alpha-, beta-, gamma-, and delta-coronavirus, are in the dashed line boxes. In the lower panel, distinct receptors on the surface of host cell mediates the viral entry of the specific coronavirus. Coronaviruses: PRCV porcine respiratory coronavirus, TGEV porcine transmissible gastroenteritis coronavirus, PEDV porcine epidemic diarrhea coronavirus, MERS-CoV Middle East respiratory syndrome coronavirus, MHV mouse hepatitis coronavirus, BCoV bovine coronavirus, IBV avian infectious bronchitis coronavirus, PdCV porcine delta-coronavirus. Host cell receptors: APN aminopeptidase N, CEACAM1 carcinoembryonic antigen-related cell adhesion molecule 1, DPP4 dipeptidyl peptidase 4, ACE2 angiotensin-converting enzyme 2, ASGPR asialoglycoprotein receptor. Zhang, Q. et al. Molecular mechanism of interaction between SARS-CoV-2 and host cells and interventional therapy. Sig Transduct Target Ther 6, 1–19 (2021). Creative Commons Attribution 4.0 International license. https://creativecommons.org/licenses/by/4.0/.

In conclusion, BetaCoronaviruses have caused significant public health concerns over the last two decades, with the emergence of SARS-CoV-2 and MERS. These viruses share many similarities in their genomic organization, structural proteins, and receptor binding mechanisms, which have allowed them to cross to be causes of significant mortality and morbidity in humans.

The rapid global spread of SARS-CoV-2 highlights the urgent need for the effective and timely development of vaccines to control and prevent future outbreaks. In the following subsections, we will discuss the virology, pathogenesis, and current approaches to combating SARS-CoV-2 and MERS, to gain a deeper understanding of the similarities and differences between these two viruses, and to identify potential strategies for future prevention.

1.3.1 SARS-CoV-2

SARS-CoV-2 emerged in Wuhan, China in late 2019 and is the cause of the global, ongoing, COVID-19 pandemic. The COVID-19 pandemic has caused over 762 million confirmed cases and over 6.8 million deaths worldwide, as of April 2023[224]. The genome of SARS-CoV-2 is a single-stranded, positive sense RNA genome approximately 30 kilobases in length[221,222]. The genome consists of ORFs encoding for non-structural proteins involved in RNA replication while the structural proteins of SARS-CoV-2 include the S, E, M, and N proteins (Figure 4)[221,222]. The spike protein has been the focus of currently approved COVID-19 vaccines, and of various COVID-19 vaccines in development, due to its role in viral infection of host cells[225].
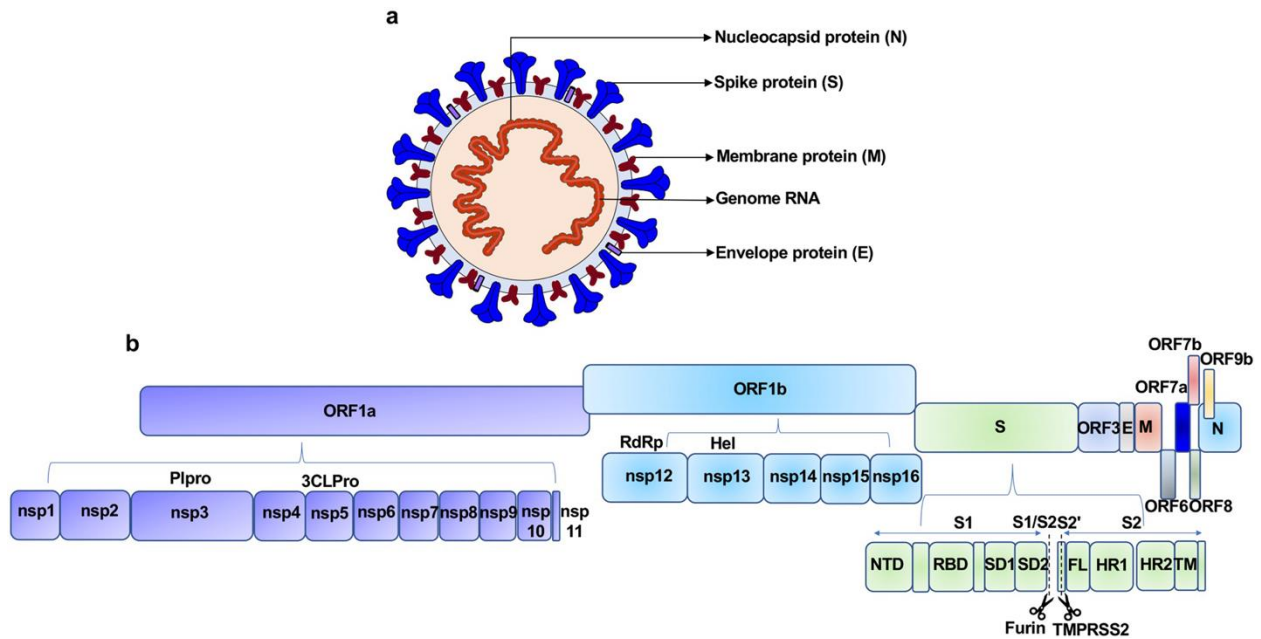
Figure 4: Schematic diagrams of the SARS-CoV-2 virus particle and genome. (A) Four structural proteins of SARS-CoV-2 include Spike protein (S), Membrane protein (M), Nucleocaspid protein (N), and Envelope protein (E). (B) The genome includes ORF1a-ORF1b-S-ORF3-E-M-ORF6-ORF7 (7a and 7b)-ORF8-ORF9b-N in order. Sixteen nonstructural proteins (nsp1–11, 12–16) are encoded by ORF1a and ORF1b, respectively, and six accessory proteins were delineated. Plpro papain like protease, 3CLPro 3C-like proteinase, RdRp RNA-dependent RNA polymerase, Hel Helicase, S encodes NTD N-terminal domain, RBD receptor-binding domain, SD1 subdomain 1, SD2 subdomain 2, FL fusion loop, HR1 heptad repeat 1, HR2 heptad repeat 2, TM transmembrane domain. Dotted line indicates S1/S2 and S2′ site cleavage by Furin and TMPRSS2. Zhang, Q. et al. Molecular mechanism of interaction between SARS-CoV-2 and host cells and interventional therapy. Sig Transduct Target Ther 6, 1–19 (2021). Creative Commons Attribution 4.0 International license. https://creativecommons.org/licenses/by/4.0/.

The S protein of SARS-CoV-2 is a type 1 trimeric transmembrane glycoprotein that is composed of two subunits, S1 and S2, which allow for viral attachment to the host cell receptor and fusion to the host cellular membrane (**Figure 4**) [225,226]. The S1 subunit contains the receptor-binding domain (RBD) that engages with the host cell receptor angiotensin-converting enzyme 2 (ACE2), while the S2 subunit mediates membrane fusion (**Figure 4**) [164,227]. The S protein is heavily

glycosylated, with approximately 22 N-linked glycosylation sites per protomer, which helps shield it from host immune surveillance [228,229]. The S protein undergoes conformational changes upon host cell binding, leading to cleavage by host proteases, including furin, at a specific site between the S1 and S2 subunits, which is thought to increase the efficiency of viral entry into host cells (**Figure 4**) [230,231]. It has been demonstrated that antibodies targeting the S protein can block the binding of SARS-CoV-2 to the cell receptor, allowing the S protein to be a focal target of vaccine development [232–236]. Of particular interest is the investigation of including more conserved regions of SARS-CoV-2, such as the N protein, in vaccine strategies to combat emerging variants. The primary function of the SARS-CoV-2 N protein is to package the viral genome, replication, and transcription [237]. The N protein is a phosphoprotein that binds to the viral RNA genome and forms the ribonucleoprotein (RNP) complex, which is the basic unit of viral replication [238–240]. The N protein has a modular structure, with two main domains: the N-terminal RNA-binding domain (NTD) and the C-terminal dimerization domain (CTD) [238–240]. The NTD is responsible for RNA binding and is highly positively charged, while the CTD mediates N protein dimerization, which is necessary for RNP formation [238–240]. The N protein is more conserved than the S protein, with 90% amino acid homology, and also accumulates fewer mutations over time [241,242]. The N protein also contains key T cell epitopes for SARS-CoV-2 immunity [243–245]. The E and M proteins of SARS-CoV-2 interact together to make up the viral membrane and are not focal targets of vaccines in development [246,247].

SARS-CoV-2 pathogenesis involves a complex interplay of viral and host factors that can determine the severity and clinical outcomes of COVID-19. The virus primarily infects respiratory epithelial cells lining the upper and lower respiratory tract through binding human ACE2 receptors [226,232]. The virus then starts to replicate and form new virions, using host-cell machinery, leading

to cell death and tissue damage [248]. The viral replication process induces an inflammatory immune response from the host which can lead to greater tissue damage and the potential of a cytokine storm [248]. The severity of COVID-19 is highly influenced by age of the infected and the presence of comorbidities such as hypertension, cardiovascular disease, diabetes, and obesity [248]. Severe cases of COVID-19 are usually the result of systemic hyper inflammation, caused by cytokine storm, leading to acute respiratory distress syndrome (ARDS) and multi-organ dysfunction [248]. Imbalance in the coagulation system is also seen in severe COVID-19, associated with low platelet counts and immunothrombosis [248].

Although approved COVID-19 vaccines have been effective in reducing mortality and morbidity caused by SARS-CoV-2 infection, the emergence of new variants that can evade the preexisting immunity to SARS-CoV-2 has raised concerns about their long-term efficacy. Furthermore, the uneven distribution of vaccines worldwide has resulted in many low to middle-income countries being left without access to variant-specific vaccines that are better suited for the evolving SARS-CoV-2 variant landscape [13,249,250]. This highlights the need for the development of vaccines that can provide broad protection against a range of SARS-CoV-2 variants, as well as the importance of the equitable distribution of vaccines to mitigate the risk of further virus evolution and spread [1,13,249,250]. Since its emergence in late 2019, SARS-CoV-2 has continuously evolved, at a higher-than-expected rate, giving rise to multiple variants with multiple genetic mutations and various phenotypic properties, including increased transmissibility, virulence, and immune escape [250,251]. The emergence of these variants has raised concerns about the efficacy of current vaccines and the potential for future outbreaks.

In conclusion, SARS-CoV-2 is a highly infectious virus that has resulted in one of, if not the worst, pandemics in modern human history. The virus uses the S protein to bind to host cells

via the ACE2 receptor and replicates leading to cell death. Hallmarks of severe COVID-19 are systemic inflammation, cytokine storm, and coagulation imbalances disease which is associated with the presence of one or more comorbidities in infected persons. Ongoing research efforts are aiming to characterize the long-term effects of SARS-CoV-2 infection along with formulating vaccines that may better fight immune evasive viral variants.

1.3.2 MERS

Middle East Respiratory Syndrome (MERS) is a coronavirus that was first identified in Saudia Arabia in 2012 [252]. As of March 2023, there have been 2,604 laboratory-confirmed cases of MERS-CoV infection, with 936 deaths reported to the World Health Organization and a mortality rate of around 36% [252]. The majority of cases have occurred in the Middle East, but cases have also been reported in other regions, including Europe and Asia [253]. Like SARS-CoV-2, MERS-CoV is a single-stranded, positive sense RNA virus, but its genome is slightly larger at approximately 30.1 kilobases [221,223,253]. MERS-CoV has a similar genome structure to SARS-CoV-2, with ORFs encoding non-structural proteins involved in RNA replication and structural proteins including the spike (S), envelope (E), membrane (M), and nucleocapsid (N) proteins [221,223,253]. The S protein of MERS-CoV is a trimeric transmembrane glycoprotein that mediates viral entry into host cells by binding to the host cell receptor dipeptidyl peptidase 4 (DPP4) [221,223,253]. Similar to the S protein of SARS-CoV-2, the S protein of MERS-CoV has been the focus of vaccine development due to its role in viral entry into host cells. MERS-CoV is primarily transmitted from dromedary camels to humans, although human-to-human transmission has also been reported in healthcare settings [253]. The MERS-CoV S protein has a shorter receptor binding domain (RBD) than that of SARS-CoV-2, which may contribute to its lower transmissibility [254]. The MERS-CoV

spike protein is highly glycosylated, which may play a role in immune evasion with the S protein of MERS being slightly more glycosylated than the S protein of SARS-CoV-2 with approximately 23 N-linked glycosylation sites per protomer, assisting in masking immunogenic protein epitopes from host humoral immune responses [228,229,255]. Additionally, MERS S has a region of high glycan density that leads to the formation of oligomannose-type glycan clusters, not seen in SARS CoV [255]. Mutations in the MERS-CoV spike protein have been shown to alter its receptor binding specificity, suggesting that it has the potential to adapt to new host species or increase transmissibility in humans [256]. Other MERS structural proteins, such as N, E, and M proteins, serve a similar role and function as they do in SARS-CoV-2 such as assisting in viral replication and making up the viral membrane [257,258].

As mentioned above, MERS has a much greater mortality rate (approximately 35-36%) than COVID-19 (approximately 5.6% in July 2020) [259]. Studies have found MERS-CoV-2 was closely related to bat-associated coronaviruses and is considered to be derived from bats, such as SARS. It has also been established that dromedary camels serve as an intermediate host of MERS-CoV and can be transmitted from camels to humans [260]. MERS is primarily a respiratory virus, and its pathogenesis is similar to other coronaviruses such as SARS-CoV-2. The virus enters the body through the inhalation of respiratory droplets containing the virus or through contact with contaminated surfaces [260]. Once inside the body, MERS primarily targets the respiratory tract, specifically the lower respiratory tract. The virus infects the epithelial cells lining the airways and causes inflammation, leading to symptoms such as fever, cough, and shortness of breath [260]. In severe cases, MERS can cause pneumonia, ARDS, and kidney failure. Comparative analysis of SARS-CoV-2 and MERS infection in young and aged cynomolgus macaques uncovered differences in viral infection and subsequent pathogenesis [261]. SARS-CoV-2 antigens were

detected in the nasal mucosae but not detected for SARS-CoV or MERS infection possibly explaining the increased transmission of SARS-CoV-2 by increased nasal tropism in a study by Rockx et al [261]. Additionally, MERS-CoV-2 primarily infects type II pneumocytes in cynomolgus macaques with both SARS-CoV and SARS-CoV-2 also infecting type I pneumocytes [261]. This finding may explain why hyaline membrane formulation is a hallmark of SARS and COVID-19 but not frequently reported for MERS [261].

Vaccine development for MERS has been ongoing since the virus was first identified in 2012 but has been hampered by a lack of financial commitment to advance effective vaccines [262]. Multiple vaccine candidates have been developed, including viral vector vaccines, DNA vaccines, mRNA, and protein subunit vaccines [20,263–265]. Most of these vaccines target the S protein of MERS, which is the main target of neutralizing antibodies. There have been promising results early-phase clinical trial results for MERS viral vector vaccines using ChAd and MVA vectors with these being the most advanced vaccine candidates to date [266–270]. However, there is currently no licensed vaccine for MERS, and more research is needed to develop effective vaccines that can provide long-term protection against the virus.

1.4 The Landscape of COVID-19 Vaccine Development

The landscape of COVID-19 vaccine development has been rapidly evolving since the onset of the pandemic. As of March 30, 2023, there are over 382 COVID-19 vaccines in development with 183 in clinical development and 199 in pre-clinical development [271]. As of March 4, 2023, there have been 50 vaccines approved by at least one country and made available for use outside of clinical trials [272]. There are currently 11 vaccines that have been granted

Emergency Use Listing (EUL) by the World Health Organization (WHO) for use in preventing COVID-19. These vaccines include Pfizer-BioNTech, Moderna, Johnson & Johnson, AstraZeneca, Sinopharm, Sinovac, Covishield, Bharat Biotech's Covaxin, and the protein subunit vaccines Novavax and CoronaVac.

The Pfizer-BioNTech vaccine is a mRNA vaccine that requires two doses and has shown an efficacy rate of 95% in clinical trials [137]. Moderna's mRNA vaccine also requires two doses and has shown an efficacy rate of 94.1% [138]. Johnson & Johnson's vaccine, which uses a viral vector, requires a single dose and has shown an efficacy rate of 72% in the US and 66% globally [273,274]. The AstraZeneca vaccine, which also uses a viral vector, requires two doses and has shown an efficacy rate of 70% on average [275]. Sinopharm and Sinovac, both of which are inactivated virus vaccines, have been approved for emergency use in several countries [276,277]. Covishield, a version of the AstraZeneca vaccine produced in India, has also been approved for emergency use [278]. Bharat Biotech's Covaxin, an inactivated virus vaccine, has been approved for emergency use in India [279]. Novavax, a protein subunit vaccine, has shown an efficacy rate of 89.3% in clinical trials and has been approved for emergency use in multiple countries [280].

Assessing the preclinical efficacy and safety of these vaccines requires multiple approaches. Animal models have been used to evaluate immune responses and protection against the virus, for investigation of candidate vaccines before use in humans. Humoral immunity, to produce virus-specific antibodies, is also a key factor in vaccine efficacy, and studies have been conducted to measure the levels and durability of these antibodies highlighting their importance in preventing viral infection. Cellular immunity, which includes T-cell responses, is important for controlling viral infection, and these responses have been studied in clinical trials as well. Finally, challenge studies, in which vaccinated animals are deliberately exposed to the virus to test

protection, have been conducted to further evaluate vaccine efficacy. These methods are crucial in determining the effectiveness of the vaccines against the virus, as well as any potential adverse effects.

1.4.1 Animal Models

The use of animal models has been crucial in the rapid development and employment of vaccines against COVID-19, providing valuable insights into vaccine immunogenicity before testing in humans. In COVID-19 vaccine development, two of the most used animal models are mice and non-human primates (NHPs). Alternative models such as hamsters and ferrets also provide valuable information through modeling transmission of the virus, with a range of age-dependent clinical outcomes from mild sublethal disease in younger aged models and severe to lethal disease in older aged models.

Mice represent a convenient animal model for vaccine investigation due to their small size, ease of handling, and availability of genetic strains with specific immunological differences. BALB/c and C57BL/6 mice strains are the most commonly used for vaccine investigation due to their high responsiveness to immunization along with commonality throughout scientific literature, leading to a wealth of immunological data for these strains. BALB/c mice have been known to produce a Th2-biased immune response with high levels of antibody production, specifically IgG1 production [281–283]. C57BL/6 mice are known to produce a Th1-biased immune response with high levels of cellular immunity and higher levels of IgG2a antibody response [281–283]. It has been observed that wild-type SARS-CoV-2 does not efficiently infect mice due to the low binding affinity of the viral spike protein to the mouse ACE2 receptor [284]. Therefore, researchers have used alternative methods to study SARS-CoV-2 infection and evaluate vaccine

candidates' protection against disease in mice. One approach has been to use a mouse-adapted strain of SARS-CoV-2, which has been genetically modified to enhance its binding affinity to the mouse ACE2 receptor [285]. Another approach has been to use transgenic mice that express the human ACE2 receptor, which allows for more efficient infection and replication of the virus [286]. Additionally, recent studies have shown that some SARS-CoV-2 variants with mutations in the spike protein, such as the N501Y mutation, are able to infect mice without the need for additional modifications [287–289]. These alternative methods have allowed for the evaluation of vaccine candidates and the study of SARS-CoV-2 pathogenesis in mice.

NHPs are commonly used as preclinical models to evaluate the safety and efficacy of vaccines and therapeutics for infectious diseases, including SARS-CoV-2 [290–293]. NHPs are a valuable model due to their genetic similarity to humans and their susceptibility to SARS-CoV-2 infection [294,295]. Rhesus macaques are an advantageous NHP model because of their availability and large body size, allowing for easier blood collection and tissue sampling. Other nonhuman primate species, such as African green monkeys and cynomolgus macaques, have also been used [294–296]. Multiple studies have demonstrated the utility of RMs as a preclinical model for SARS-CoV-2 vaccine development [294,295]. For example, macaques have been used to evaluate the immunogenicity and the correlates of protection, as well as the protective efficacy of various vaccine platforms, including viral vector-based vaccines, mRNA vaccines, and protein subunit vaccines.[133,292,293,297–300] Moreover, the use of NHP models can provide critical insights into the mechanisms of vaccine-induced immunity, including the kinetics, specificity, and durability of the immune responses.

1.4.2 Humoral Immunity

Assessing humoral immunity is a crucial aspect of COVID-19 vaccine development as antibody responses can prevent infection. IgG and IgA antibodies have been determined to be key players in preventing SARS-CoV-2 infection and are routinely measured to assess humoral responses to vaccines. IgG is the most abundant immunoglobulin in sera and is involved in long-term protection against infection and disease [301]. IgG facilitates protection through multiple mechanisms such as IgG-mediated binding of the pathogen, agglutination, opsonization, and allowing recognition by other phagocytic immune cells [301]. IgG also activates the complement system allowing for antibody-dependent cell-mediated cytotoxicity (ADCC) [301]. IgA antibodies are the most abundant immunoglobulin in the mucosae and are involved in mucosal defense against infection [301]. IgA can bind pathogens and lead to agglutination, opsonization, and ADCC for mucosal clearance of pathogens, such as IgG [301].

Th bias is an important consideration in assessing humoral immunity to candidate vaccines and is primarily done by measuring the titers of IgG subclasses, IgG1 and IgG2a. IgG1 is associated with a Th2 bias, which is characterized by the production of cytokines that promote antibody production and humoral immunity [282]. In contrast, IgG2a is associated with a Th1 bias, which is characterized by the production of cytokines that promote cell-mediated immunity [282]. Understanding the Th bias induced by a vaccine is critical, as it can influence the type of immune response generated and therefore the efficacy of the vaccine. Th2 bias can be associated with vaccine-associated enhanced respiratory disease (VAERD), a phenomenon observed in some animal models and during SARS-CoV vaccine trials [302,303]. Therefore, it is important to strive for the balanced induction of Th1 and Th2 responses. In the context of vaccines, protein subunit

vaccines tend to skew towards a Th2 bias and therefore must be assessed with immune modulating approaches in humans, such use of an adjuvant, to skew towards a balanced Th1 Th2 response [304].

Neutralizing antibodies are another important aspect of humoral immunity that can protect against viral infections by preventing viral entry into host cells. These antibodies bind to the viral spike protein and block its interaction with the host receptor. The assessment of neutralizing antibodies is typically done using live virus neutralization assays or pseudotype neutralization assays. In the live virus neutralization assay, the ability of antibodies to neutralize the virus is measured by incubating the virus with the antibodies and then assessing viral replication. In the pseudotype neutralization assay, a pseudovirus that expresses the viral spike protein is used instead of the live virus. The ability of the antibodies to neutralize the pseudovirus is measured by assessing its ability to enter host cells. As a conventional pseudo-neutralizing test, measurement of a competitive immunoassay for quantifying inhibition of the spike-ACE2 interaction can be used as a surrogate for traditional virus-based plaque reduction neutralizing assay and reported in a high level of concordance and correlation (>96%) [305,306].

Correlates of protection are measurable immunological parameters that can predict protection against disease. The level of neutralizing antibodies is currently the most widely accepted correlate of protection against COVID-19 [307–310]. In general, high levels of neutralizing antibodies indicate a high likelihood of protection against infection or disease. The level of IgG antibodies against the S protein has also been shown to be a correlate of protection, with higher titers of IgG antibodies indicating greater protection against COVID-19 [307–310]. However, it is important to note that the protective threshold for neutralizing antibodies and IgG antibodies has not been definitively established and may vary between individuals and populations. The

assessment of humoral immunity is an important part of vaccine development and evaluation, as it helps to determine the efficacy and potential protection provided by a vaccine.

1.4.3 Cellular Immunity

Assessing cellular immunity is another crucial aspect of COVID-19 vaccine development playing a significant role in controlling viral infections by eliminating infected cells and secreting inflammatory cytokines. T cell response have been shown to play a critical role in COVID-19 immunity and protection [243,311–317]. Cellular responses to COVID-19 have also been shown to be important for induction of long-term immunity [318]. The T cell response mainly consists of $CD4^+$ and $CD8^+$ T cells, with $CD4^+$ T cells provide help to B cells to generate antibody responses, and $CD8^+$ T cells involved in directly killing infected cells.

Assessing the activation of T cells can be done by measuring the levels of cytokines produced in response to a viral antigen (i.e., peptide stimulation) by T cells, such as interferon-gamma (IFN-γ), interleukin-2 (IL-2), and tumor necrosis factor-alpha (TNF-α). These cytokines are produced by activated T cells and are critical for controlling viral infections. Flow cytometry can be used to measure activation, proliferation, phenotype, and memory status of T cells through characterization of CD markers and cytokines. Correlates of protection for cellular immunity are not well established for COVID-19. However, it has been shown that the presence of SARS-CoV-2-specific T cells in convalescent individuals correlates with protection against reinfection [317]. In the context of long covid and in populations that are at high risk of SARS-CoV-2 morbidity and mortality, T cell responses have been shown to play an important role [311,312,319–321]. These studies suggest that the assessment of cellular immunity is important for understanding the immune

response to COVID-19 vaccines and may provide additional levels of protection beyond neutralizing antibodies.

1.5 Specific Aims

SPECIFIC AIMS: Worldwide vaccine equity continues to be a major hurdle for resolving the Coronavirus Disease 2019 (COVID-19) pandemic, with many low to middle income countries struggling to obtain and distribute currently approved vaccines. Protein subunit vaccine formulations using recombinant DNA technology (RDT) are ideal for worldwide distribution due to their relative stability at room temperature, low price per dose, and excellent safety profile. RDT has made it possible to take immunogenic viral protein sequences, and, by use of a plasmid, transfect these sequences into cells to allow those cells to produce the subunit vaccine. Using RDT, we can express the SARS-CoV-2 S1 subunit of the spike protein. The S1 subunit includes the receptor binding domain (RBD) which has become the focal antigen in all candidate and approved COVID-19 vaccine formulations, as it is responsible for binding the virus to cells and is a main target of neutralizing antibodies. These neutralizing antibodies target the trimeric, class I fusion protein spike, and block infection of susceptible cells. Due to being able to block infection, neutralizing antibodies have been hypothesized to be a correlate of protection against COVID-19 infection and severe disease. A current issue with SARS-CoV-2 protein subunit vaccine formulations is the lack of induction of neutralizing antibodies. I aim to investigate novel techniques to improve SARS-CoV-2 protein subunit vaccine formulation through characterization of the impact of the native trimeric antigen structure, inclusion of integrated adjuvant peptide, investigation of immunostimulatory vaccination routes, and deconstruction of the S1 subunit to

identify the roles of each portion of the antigen. I will also investigate the creation of a chimeric spike protein using the SARS-CoV-2 RBD in a Middle Eastern Respiratory Syndrome (MERS) S1 scaffold. MERS is a Betacoronavirus, such as SARS-CoV-2, that is more neutralization sensitive, yielding high microneutralization titers post vaccination. Using the MERS S1 as a scaffold to present SARS-CoV-2 RBD may overcome the lack of SARS-CoV-2 neutralizing antibodies. My central hypothesis is that COVID-19 protein subunit vaccine neutralizing antibody induction can be increased through inclusion of a foldon domain and an adjuvant peptide, while being further improved through harnessing a neutralization-sensitive MERS S1 scaffold.

Aim 1: Identification of optimal SARS-CoV-2 protein subunit vaccine antigen formulation to overcome lack of neutralizing antibody induction.

1a. Elucidate differences between a monomeric subunit antigen and native trimeric subunit antigens through inclusion or exclusion of T4 fibritin foldon domain and determine the impact of integrated adjuvant TLR4 agonist peptide RS09.

1b. Investigate impact of vaccine administration routes on induction of humoral and cellular immune response by comparing intramuscular, intranasal, and intradermal vaccine administration of each antigen.

1c. Deconstruct S1 subunit of SARS-CoV-2 spike protein to identify antigen portions that maximize IgG and neutralizing antibody production.

Aim 2: Development of chimeric spike protein including SARS-CoV-2 RBD in MERS S1 scaffold.

2a. Create chimeric spike proteins that have RBD of SARS-CoV-2 in MERS S1 scaffold with optimized subunit antigen formulation.

2b. Test immunogenicity of chimeric spike proteins in BALB/c mice through quantification of SARS-CoV-2 S1 specific endpoint IgG antibody titer, neutralizing and cross-neutralizing antibody titers, and cell mediated response.

2.0 A Single Subcutaneous or Intranasal Immunization with Adenovirus-based SARS-CoV-2 Vaccine Induces Robust Humoral and Cellular Immune Responses In Mice

Text from this chapter has been modified from the publication: Kim, E., Weisel F.J., Balmert, S.C., **Khan, M.S.**, Huang, S., Erdo, G., Kenniston, T.W., Carey, C.D., Joachim, S.M., Conter, L.J., Weisel, N.M., Okba, N.M.A., Haagmans, B.L., Percivalle, E., Cassaniti, I., Baldanti, F., Korkmaz, E., Shlomchik, M.J., Falo, L.D., Gambotto, A#. A single subcutaneous or intranasal immunization with adenovirus-based SARS-CoV-2 vaccine induces robust humoral and cellular immune responses in mice. *European Journal of Immunology* 51, 1774–1784 (2021). # corresponding author. PMID: 33772778

2.1 Introduction

Outbreaks caused by coronaviruses represent an unprecedented global health challenge. Previous coronavirus outbreaks, Severe Acute Respiratory Syndrome (SARS) and Middle East Respiratory Syndrome (MERS), have been a cause of substantial morbidity and mortality [322–324]. The ongoing COVID-19 outbreak, caused by Severe Acute Respiratory Syndrome Coronavirus 2 (SARS-CoV-2), constitutes a major threat to public health and global eco-nomic growth [325–328]. COVID-19, which first emerged in late 2019, was declared a global pandemic by the World Health Organization on March 11, 2020, and has claimed approximately 2.7 million lives as of March 15, 2021. Despite public health concerns presented by coronaviruses, progress in the development of therapeutics and vaccines for coronaviruses has been slow until recently.

To prevent the spread of COVID-19, safe and effective vaccines that induce potent and long-lasting virus-specific immune responses are needed [217,329–332]. Betacoronaviruses (Beta-CoVs), such as SARS-CoV-2, are enveloped, positive-sense, ssRNA viruses [247,333]. BetaCoVs encode the envelope, nucleocapsid, membrane, and spike (S) proteins [334,335]. Among these components, the spike protein has received considerable attention due to its proven role in the virus infection process [336]. The S protein of the viral envelope comprises two subunits, S1 and S2, that function in viral attachment to the host cell receptor and in fusion to the cells, respectively [336,337]. For instance, the S protein on the envelope of SARS-CoV-2 binds to the cell receptor angiotensin converting enzyme 2 (ACE2) and facilitates viral entry [337,338]. Importantly, it has been demonstrated with the two preceding Beta-CoVs (SARS-CoV and MERS-CoV) that antibodies targeting the S protein can block the binding of these viruses to the cell receptor, rendering the S protein an attractive target for vaccine development to elicit virus-specific neutralizing antibody responses, and in turn, protective immunity against coronaviruses [339]. Indeed, vaccine candidates based on the viral S protein have been previously developed for SARS-CoV and MERS-CoV, establishing the immunogenicity of the S protein of Beta-CoVs [340–342]. Furthermore, our previous efforts on the development of vaccines against MERS-CoV and SARS-CoV have shown that vaccine candidates targeting the S1 subunit are capable of generating efficacious neutralizing antibody responses [343,344]. More recently, we have also presented that skin-targeted S1 subunit protein vaccines induce antigen-specific antibody responses against MERS-CoV and SARS-CoV-2 [217]. As such, the literature suggests that the S1 subunit is an important target for vaccine candidates against coronaviruses.

Remarkable progress in the fields of molecular biology and biotechnology has enabled production of novel vaccines to combat infectious diseases [345–347]. Recombinant DNA technology

has proven a viable approach due to its versatility, cost-effectiveness, and logistic advantages [348–351]. Genetic immunization based on recombinant DNA or mRNA vaccines, where the intracellular delivery of nucleic acids enables the synthesis of a rationally selected antigen of pathogens to elicit virus-specific protective immunity, has been investigated toward combatting infectious diseases [127,331,345,352–356].

Engineered viral vectors have been an attractive alternative to nonviral transgene expression [357–359]. Adenovirus (Ad)-vectored vaccines encoding a target antigen gene have been increasingly used for their demonstrated capacity to induce both humoral and cellular immune responses [360–363]. The promising immunogenicity of Ad vaccines has been shown in several animal models and there are a number of Ad-based vaccine candidates against a myriad of pathogens currently being evaluated in clinical trials [106,364–366]. Interestingly, our previous studies have demonstrated that Ad-vectored vaccines expressing SARS-CoV-S1 and MERS-CoV-S1 antigens generate potent and efficacious antibody responses, making recombinant Ad-based vaccines an appealing candidate against emerging coronaviruses diseases [343,344]. Importantly, several Ad-based SARS-CoV-2 vaccine candidates have recently emerged with promising results in large clinical trials [367–370], prompting the approval of a number of Ad-based SARS-CoV-2 vaccines for emergency use. In addition to the prevailing Ad serotype (Ad5), Ad26 and a chimpanzee adenovirus have been used for development of SARS-CoV-2 vaccines to overcome pre-existing Ad immunity [367–370]. Interestingly, recent clinical studies have demonstrated the promising immunogenicity of intramuscularly delivered Ad5-vectored COVID-19 vaccines encoding the gene for the full S protein [367,368]. Despite the unprecedented progress with Ad-based SARS-CoV-2 vaccines, there is still an important need for development of alternative Ad-based vaccine candidates for COVID-19 and other infectious diseases, as well as for investigation of the different

administration routes with new adenoviral vaccine candidates to enable sustainable global immunization programs.

Here, we describe the development of an Ad-vectored SARS-CoV-2 vaccine candidate for COVID-19 immunization. Based on our experience with Ad-based vaccines for prior BetaCoVs (SARS-CoV and MERS-CoV) [217,344], we designed and constructed a recombinant type 5 Ad vector encoding the gene for theSARS-CoV-2-S1 subunit antigen (Ad5.SARS-CoV-2-S1). We evaluated the immunogenicity of the developed Ad vaccine in BALB/c mice through S.C. injection or I.N. delivery to test its ability to induce antigen-specific humoral and cellular immune responses and investigated virus-specific neutralization activity of the generated antibodies. Our study demonstrates the rational design and development of an Ad-based SARS-CoV-2 vaccine that is capable of eliciting robust and durable SARS-CoV-2-specific immune responses in mice, supporting the further development of recombinant adenovirus vaccines against COVID-19 and other emerging infectious diseases.

2.2 Results

2.2.1 Adenoviral SARS-CoV-2-S1 Vaccine

To produce E1/E3 deleted, replication-deficient, human type 5 adenovirus expressing SARS-CoV-2-S1 protein, we generated pAd/SARS-CoV-2-S1 by subcloning the codon-optimized SARS-CoV-2-S1 gene into the shuttle vector, pAd (GenBank U62024) at SalI & NotI sites. Next, Ad5.SARS-CoV-2-S1 (Ad5.S1) was created by loxP homologous recombination (**Fig. 5**). To detect SARS-CoV-2-S1 expression driven by the generated Ad candidate, the serum-free

supernatants from A549 cells infected with Ad5.S1 were characterized by SDS-PAGE and Western blot analysis. The recombinant SARS-CoV-2-S1 proteins (both positive control and Ad5.S1-infected cells) were recognized by the polyclonal antibody at the expected glycosylated monomer molecular weights of about 110 kDa, while no expression was detected in the mock-infected cells (**Fig. 5B**).
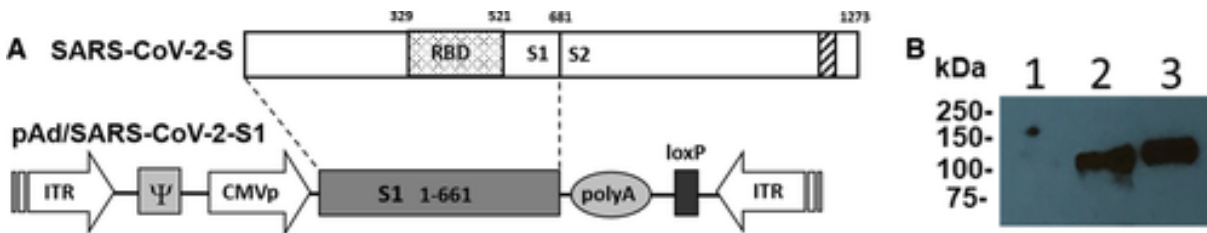
Figure 5: Adenoviral-vectored SARS-CoV-2-S1 vaccine. A shuttle vector carrying the codon-optimized SARS-CoV-2-S1 gene encoding N-terminal 1–661 was designed as shown in the diagram. The vector was used to generate recombinant type 5 replication-deficient adenoviruses (Ad5) by homologous recombination with the adenoviral genomic DNA. ITR, inverted terminal repeat; RBD, receptor binding domain. (B) Detection of the SARS-CoV-2-S1 protein by western blot with the supernatant of A549 cells infected with Ad5.SARS-CoV-2.S1 (Ad5.S1) (10 MOI) using antispike protein of SARS-CoV rabbit polyclonal antibody (lane 2). Mock (AdΨ5)-infected cells were treated the same and used as a negative control (lane 1). As a positive control, 100 ng of recombinant SARS-CoV-2-S1 (Sino biological, 1–685 amino acids with ten histidine tag) was loaded (lane 3). The supernatants were resolved on SDS-10% polyacrylamide gel after being boiled in 2% SDS sample buffer with β-ME.

2.2.2 SARS-CoV-2-S1-Specific Antibody Endpoint Titers

To evaluate the immunogenicity of the constructed Ad5.SARS-CoV-2-S1 vaccine, we first determined antigen-specific IgG, IgG1, and IgG2a antibody endpoint titers in the sera of vaccinated mice (either via I.N. delivery or S.C. injection) and control mice (PBS or AdΨ5 immunized groups). Serum samples, collected from all mice before immunization (Week 0) and

subsequent weeks after vaccination, were serially diluted to determine SARS-CoV-2-S1-specific IgG, IgG1, and IgG2a endpoint titers for each immunization group using ELISA (**Fig. 6**). Results suggest that both I.N. and S.C. immunization induced significantly increased S1-specific IgG, IgG1, and IgG2a endpoint titers as early as 2 weeks after a single vaccination with Ad5.SARS-CoV-2-S1 compared to unimmunized groups (**Fig. 6A-C**, $p < 0.05$, Kruskal–Wallis test, followed by Dunn's multiple comparisons) and the elicited IgG, IgG1, and IgG2a antibody responses remained significantly higher with respect to control groups through week 24 (maximum length of the study to date) (**Fig. 6**). Together, these results indicate that a single immunization with Ad5.SARS-CoV-2-S1 via either S.C. delivery or I.N. administration is capable of generating robust and long-lived S1-specific antibody responses, and the choice of the route of vaccine administration (S.C. or I.N.) had no significant effect on the generated antibody endpoint titers.
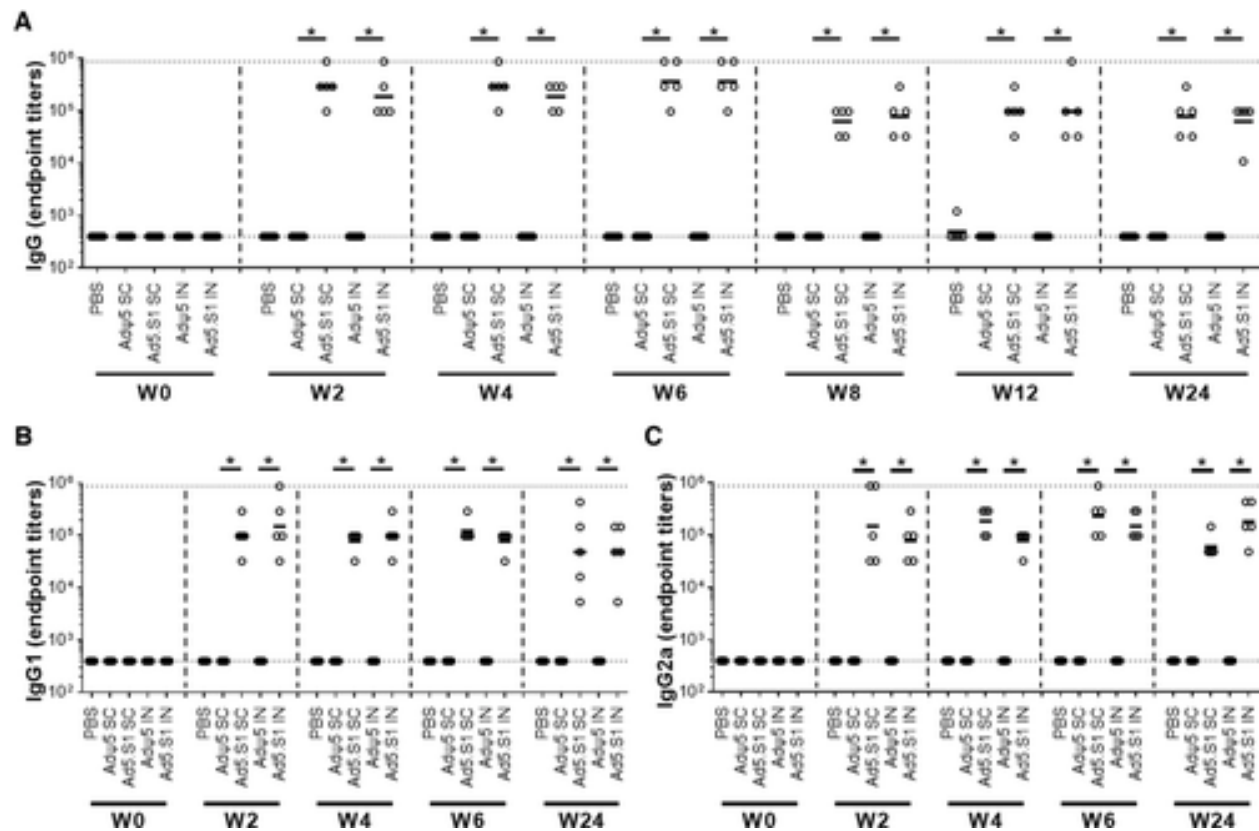
Figure 6: Antigen-specific antibody responses in mice immunized with adenoviral vectored SARS-CoV-2-S1 vaccine. BALB/c mice were immunized S.C. or I.N. with 1.5×10^{10} vp of Ad5.SARS-CoV-2-S1 (Ad5.S1) or AdΨ5, while mice were immunized subcutaneously with PBS as a negative control. On weeks 0, 2, 4, 6, 8, 12, and 24 after vaccination, the sera from mice were collected, diluted, and SARS-CoV-2-S1-specific antibodies were quantified by ELISA to determine the (A) IgG (weeks 0, 2, 4, 6, 8, 12, and 24), (B) IgG1 (weeks 0, 2, 4, 6, and 24), and (C) IgG2a (weeks 0, 2, 4, 6, and 24) endpoint titers. Horizontal lines indicate geometric mean antibody titers. Significance was determined by Kruskal–Wallis test, followed by Dunn's multiple comparisons (*$p < 0.05$). Representative data are from one of two independent experiments (n = 5 mice per group for each experiment).

2.2.3 Antigen-Specific B-Cell Responses

To support the generation of long-lasting antibody responses against SARS-CoV-2 with our Ad-based vaccine, we performed studies to investigate vaccination-induced GC reactions. GC

reactions are highly associated with generation of long-lived, high affinity antibody forming cells (AFC) and, hence, long-term humoral immunity. Mice were immunized with Ad5.SARS-CoV-2-S1, and S1-specific GC reactions and antibody-secreting plasma cells in the BM were measured through flow cytometry and ELISpot, respectively. I.N. and S.C. vaccination resulted in significant S1-specific GC reactions in cervical and axillary LNs of immunized mice, respectively, (**Fig. 7A-D**). As expected, neither S.C. vaccination with Ad5.SARS-CoV-2-S1, nor any of the control immunization groups induced GC reactions in cervical LNs (**Fig. 7A**), whereas I.N. vaccination with Ad5.SARS-CoV-2-S1 produced S1-specific B cells with GC phenotype in cervical LNs in eight out of ten mice, with Ig isotype switch to IgG1 and IgG2a (**Fig. 7A and B**). Nine out of ten mice vaccinated by S.C. injection of Ad.SARS-CoV-2-S1 displayed S1-specific GC B cells in axillary LNs, with induced class switch to IgG1 and IgG2a (**Fig. 7C and D**), whereas I.N. immunization with Ad.SARS-CoV-2-S1 did not result in GC reactions in axillary LNs (**Fig. 7C**). Preliminary results from ELISpot analysis showed that both I.N. and S.C. vaccination produced S1-specific antibody-producing plasma cells in the BM of immunized mice. Collectively, these results show that S.C. and I.N. immunization with Ad5-SARS-CoV-2-S1 are capable of forming significant antigen-specific GC reactions in draining LNs, which yielded detectable antigen-specific plasma cells in the BM of immunized mice, thereby suggesting that our Ad5.SARS-CoV-2-S1 vaccine has the potential to generate durable humoral immune effector cells, such as long-lived plasma cells.
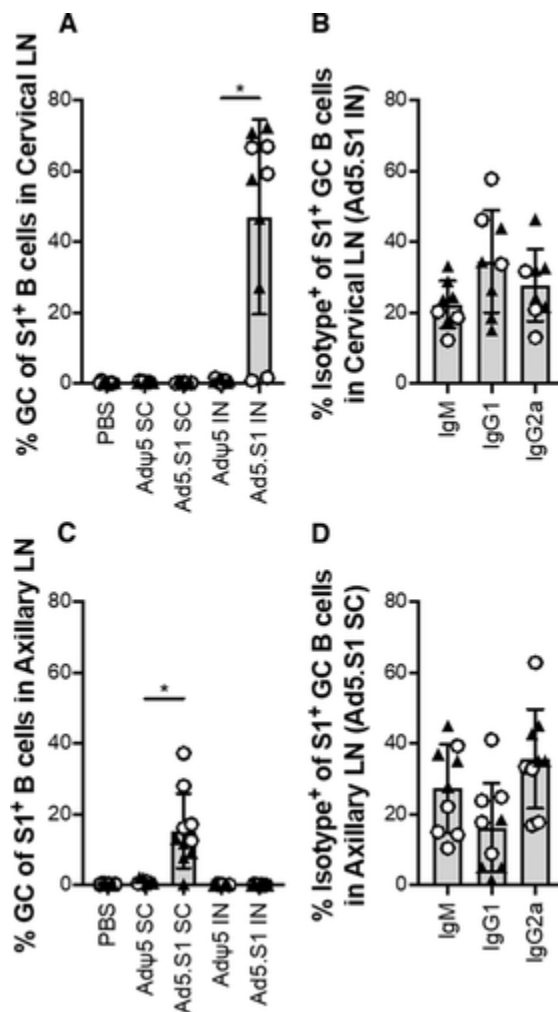
Figure 7: Antigen-specific humoral responses in mice immunized with Ad5.SARS-CoV-2-S1. Formation of GC reactions and Ig isotype switching in draining LNs. BALB/c mice were vaccinated S.C. or I.N. with 1.5×10^{10} vp of Ad5.SARS-CoV-2-S1 (Ad5.S1) or AdΨ5, while mice were immunized S.C. with PBS as a negative control. Cervical and axillary LNs were harvested 14 days after I.N. and S.C. vaccination and single-cell suspensions of LNs were stained and analyzed by flow cytometry to determine the frequencies of S1-specific GC-B cells and their IgM, IgG1, and IgG2a isotype distribution. (A) S1-specific GC B cells in cervical LNs. (B) IgM, IgG1, and IgG2a isotype distribution of S1-specific B cells in cervical LNs. (C) S1-specific GC B cells in axillary LNs. (D) %GC of S1+ B cells in A and C were calculated as %CD95+ CD38− of live CD19+ S1+, and frequencies of isotype-specific GC B-cell subsets in B and D were calculated as %Isotype+ of live CD19+ S1+ CD95+ CD83− cells. Results are mean ± SD. Groups were compared by one-way Welch's ANOVA, followed by Dunnett's T3 multiple comparisons, and significant

differences are indicated by *$p < 0.05$. Data are from two independent experiments (n = 5 mice per group for each experiment) that are indicated by circles or triangles.

2.2.4 Antigen-Specific Cellular Immune Responses

To evaluate antigen-specific cellular immune responses induced by a single immunization of BALB/c mice with Ad5.SARS-CoV-2-S1, we investigated S1-specific cellular immunity in mice after vaccination by quantifying antigen-specific IFN-γ^+ CD8$^+$ and CD4$^+$ T-cell responses through intracellular cytokine staining (ICS) and flow cytometry. Results suggest that both I.N. and S.C. immunization elicited significantly enhanced systemic S1-specific CD8$^+$ and CD4$^+$ T-cell immunity compared to control groups. (**Fig. 8**, $p < 0.05$, one-way Welch's ANOVA, followed by Dunnett's T3 multiple comparisons). Interestingly, S.C. vaccination induced significantly increased systemic S1-specific IFN-γ^+ CD8$^+$ T-cell responses compared to I.N. immunization. (**Fig. 8**, $p < 0.05$, one-way Welch's ANOVA, followed by Dunnett's T3 multiple comparisons). Taken together, these findings indicate that a single vaccination with Ad5.SARS-CoV-2-S1 via either S.C. delivery or I.N. administration is capable of generating robust systemic S1-specific cellular immune responses, and the choice of the route of vaccine administration (S.C. or I.N.) has a significant effect on the Ad5.SARS-CoV-2-S1 vaccine-induced CD8$^+$ T-cell responses.
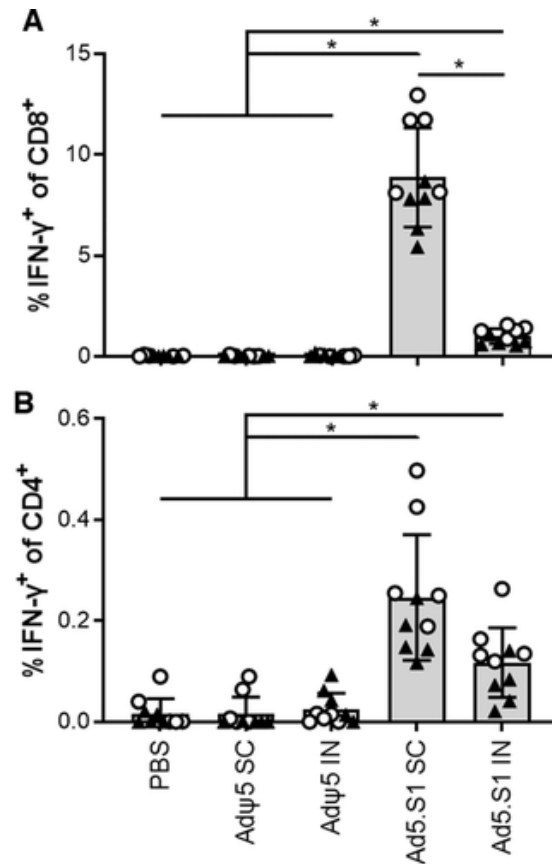
Figure 8: Antigen-specific cellular responses in mice immunized with Ad5.SARS-CoV-2-S1. BALB/c mice were immunized S.C. or I.N. with 1.5×10^{10} vp of Ad5.SARS-CoV-2-S1 (Ad5.S1) or AdΨ5, or subcutaneously with PBS as a negative control. Twelve days after vaccination, splenocytes were isolated and stimulated with SARS-CoV-2 S1 PepTivator, followed by intracellular cytokine staining (ICS) and flow cytometry to identify SARS-CoV-2 S1-specific T cells. Frequencies of SARS-CoV-2 S1-specific (A) CD8+ IFN-γ+ and (B) CD4+ IFN-γ+ T cells, presented after subtracting background responses detected in corresponding unstimulated splenocyte samples. Results are mean ± SD. Groups were compared by one-way Welch's ANOVA, followed by Dunnett's T3 multiple comparisons, and significant differences are indicated by *$p < 0.05$. Data are from two independent experiments (n = 5 mice per group for each experiment) that are indicated by circles or triangles.

2.2.5 SARS-CoV-2 Neutralizing Antibody Titers

To evaluate the functional quality of vaccine-generated antigen-specific antibodies, we used a microneutralization assay (NT_{90}) to test the ability of sera from immunized mice to neutralize the infectivity of SARS-CoV-2. Sera, collected from all mice 8 and 12 weeks after vaccination, were tested for the presence of SARS-CoV-2-specific neutralizing antibodies, and the results are shown in **Fig. 9**. As expected, there were no detected neutralizing antibody responses in the sera of mice immunized with PBS or Adψ5 control groups, while SARS-CoV-2-neutralizating antibodies were detected in mice immunized by either I.N. delivery or S.C. injection of Ad5.SARS-CoV-2-S1 both 8 and 12 weeks after vaccination. The resulting SARS-CoV-2-neutralizing activity on weeks 8 and 12 after I.N. and S.C. immunization was statistically significant **(Fig. 9**, $p < 0.05$, Kruskal–Wallis test, followed by Dunn's multiple comparisons) compared to PBS control, with no significant differences with respect to each other.
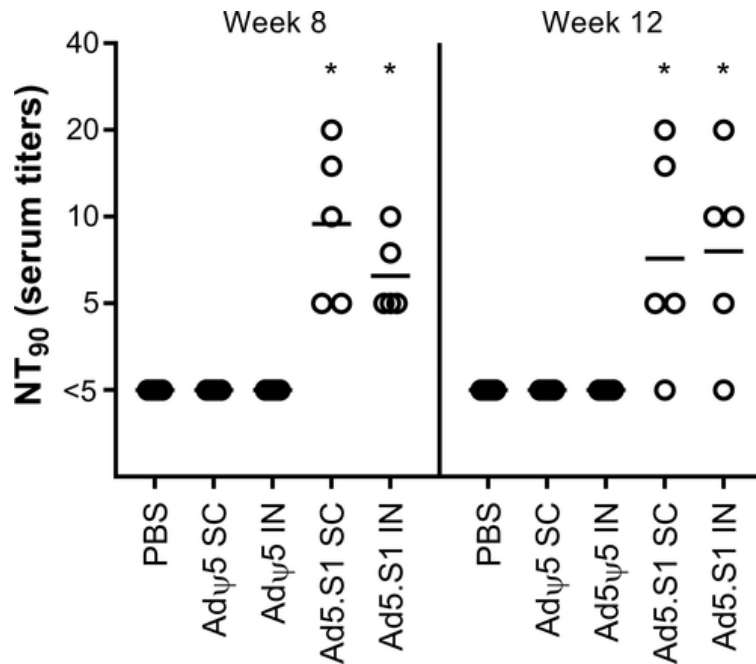
Figure 9: Neutralizing antibody responses in mice immunized with Ad5.SARS-CoV-2 S1. BALB/c mice were immunized S.C. or I.N. with 1.5×10^{10} vp of Ad5.SARS-CoV-2-S1 (Ad5.S1) or AdΨ5, while mice were immunized subcutaneously with PBS as a negative control. Neutralizing antibodies in serum of mice 8 or 12 weeks after immunization were measured using a microneutralization assay (NT_{90}) with SARS-CoV-2. Serum titers that resulted in a 90% reduction in cytopathic effect compared to the virus control were reported. Horizontal lines represent geometric mean neutralizing antibody titers. Groups were compared by Kruskal–Wallis test at each time point, followed by Dunn's multiple comparisons. Significant differences relative to the PBS control are indicated by *$p <$ 0.05. The minimal titer tested was 5, and undetectable titers (those with NT_{90} serum titers < 5) were assigned a value of 2.5. Data are from a single experiment (n = 5 mice per group).

2.3 Materials and Methods

2.3.1 Construction of Recombinant Adenoviral Vectors

The coding sequence for SARS-CoV-2-S1 amino acids 1 to 661 of full length from BetaCoV/Wuhan/IPBCAMS-WH-05/2020 (GISAID accession id. EPI_ISL_403928) flanked with SalI & NotI was codon-optimized using the UpGene algorithm for optimal expression in mammalian cells [371] and synthesized (GenScript). pAd/SARS-CoV-2-S1 was then created by subcloning the codon-optimized SARS-CoV-2-S1 gene into the shuttle vector, pAdlox (GenBank U62024), at SalI/NotI sites. Subsequently, replication-deficient human recombinant serotype 5 adenovirus vector (Ad5.SARS-CoV-2-S1) was generated by loxP homologous recombination and purified [343,372,373].

2.3.2 SDS-PAGE and Western Blot

To evaluate the infectivity of the constructed recombinant adenoviruses, A549 (human lung adenocarcinoma epithelial cell line) cells were transduced with a MOI of 10 of Ad5.SARS-CoV-2-S1. At 6 h after infection, cells were washed three times with PBS, and then incubated with serum-free media for 48 h. The supernatants of A549 cells transduced with Ad5.SARS-CoV-2-S1 were subjected to SDS-PAGE and Western blot. Briefly, after the supernatants were boiled in Laemmli sample buffer containing 2% SDS with beta-mercaptoethanol (β-ME), the proteins were separated by Tris-Glycine SDS-PAGE gels and transferred to nitrocellulose membrane. After blocking for 1 h at room temperature (RT) with 5% nonfat milk in PBS-T, rabbit anti-SARS-CoV spike polyclonal antibody (1:3000) (Sino Biological) was added and incubated overnight at 4°C

as primary antibody, and HRP-conjugated goat anti-rabbit IgG (1:10 000) (Jackson immunoresearch) was added and incubated at RT for 2 h as secondary antibody. After washing three times with PBS, the signals were visualized using ECL Western blot substrate reagents and Amersham Hyperfilm (GE Healthcare). Mock (AdΨ5)-infected A549 cells and 100 ng of recombinant SARS-CoV-2-S1 (Sino biological, 1–685 amino acids with ten histidine tag) were used as negative and positive controls, respectively.

2.3.3 Animals and Immunization

BALB/cJ mice (n = 5 animals per group in each independent experiment unless otherwise noted) were vaccinated by either S.C. injection or I.N. delivery of 1.5×10^{10} viral particles (vp) of AdΨ5 (a null Ad5 vector control) or, Ad5.SARS-CoV-2-S1, or by S.C. injection of PBS as a negative control. Mice were bled from retro-orbital vein at weeks 0, 2, 4, 6, 8, 12, and 24 after immunization, and the obtained serum samples were diluted and used to evaluate S1-specific antibodies by ELISA. Serum samples obtained on weeks 8 and 12 after vaccination were also used for microneutralization (NT) assay. Mice were maintained under specific pathogen-free conditions at the University of Pittsburgh, and all experiments were conducted in accordance with animal use guidelines and protocols approved by the University of Pittsburgh's Institutional Animal Care and Use (IACUC) Committee.

2.3.4 ELISA

Sera from all mice were collected prior to immunization (week 0) and every two weeks (weeks 2, 4, 6) after immunization and evaluated for SARS-CoV-2-S1-specific IgG, IgG1, and

IgG2a antibodies using ELISA [217]. Further, sera from all mice collected at weeks 8, 12, and 24 after immunization were tested for SARS-CoV-2-S1-specific IgG antibodies using ELISA for long-term humoral responses. Sera collected at week 24 after vaccination were also tested for SARS-CoV-2-S1-specific IgG1 and IgG2a antibodies using ELISA. Briefly, ELISA plates were coated with 200 ng of recombinant SARS-CoV-2-S1 protein (Sino Biological) per well overnight at 4°C in carbonate coating buffer (pH 9.5) and then blocked with PBS-T and 2% BSA for 1 h. Mouse sera were diluted in PBS-T with 1% BSA and incubated for 72 h. After the plates were washed, anti-mouse IgG-HRP (1:2000, SantaCruz) or anti-mouse IgM-HRP (1:5000, Jackson Immunoresearch) were added to each well and incubated for 1 h. The plates were washed three times, developed with 3,3'5,5'-tetramethylbenzidine, and the reaction was stopped. Next, absorbance was determined at 450 nm using a plate reader. For IgG1 and IgG2a ELISAs, mouse sera were diluted in PBS-T with 1% BSA and incubated for 72 h. After the plates were washed, biotin-conjugated IgG1 and IgG2a (1:1000, eBioscience) and streptavidin alkaline phosphatase (1:500, PharMingen) were added to each well and incubated for 1 h. The plates were washed three times and developed with para-nitrophenylphosphate, and the reaction was stopped and absorbance at 405 nm was determined using a plate reader.

2.3.5 Flow Cytometry Analysis for Humoral Immune Responses

In order to address the humoral immune response, mice were sacrificed 14 days after vaccination and single cell suspensions of draining LNs were analyzed by flow cytometry, adhering to the recently published guidelines [374]. We biotinylated SARS-CoV-2-S1 protein, which allowed us to use it as "bait" in flow cytometric analysis to identify antigen-specific B cells, formation of GC reactions, and immunoglobulin isotype switching in draining LNs. Lymph nodes

were disrupted by crushing them between frosted glass slides in staining buffer (SB; PBS/2%FCS/ 2 mM EDTA). Single cell suspensions were subjected to viability staining using Zombie NIR fixable viability dye [FVD] (BioLegend) for 15 min on ice and then incubated with anti-CD16/CD32 Abs in SB for 5 min on ice to block Fc receptors. Cells were then stained in SB with antibodies against CD19-BV786 (clone 1D3), CD38-Al594 (clone 90), CD95-PE-Cy7 (clone Jo2), IgM-Al680 (clone B7-6), IgG1-V450 (clone A-85), IgG2a-Al488 (goat polyclonal; Southern Biotech), and biotinylated-SARS-CoV-2-S1. Cells were washed and stained with Streptavidin PE (PROzyme) for 15 min and then washed and fixed with 1% PFA over night at 4°C before data acquisition (0.5-1 $\times$ 10^6 cells per flow stain) on the Cytek^{TM} Aurora Cytometer (Cytek Biosciences). For flow cytometric analysis, SARS-CoV-2-S1-specific GC B cells were defined as live singlets (fixable viability dye^{neg}) and consecutively gated as SARS-CoV-2-S1^{pos}, CD19^{pos}, CD38^{neg}, CD95^{pos} using the software FlowJo Version 10.

2.3.6 ELISpot for Antibody-Secreting Cells

The frequency of SARS-CoV-2-specific antibody producing cells in the BM of mice was determined by ELISpot assay 6 weeks after immunization using our established and previously published methods [375,376]. Briefly, 4-HBX plates were coated as described for ELISA assays, and nonspecific binding was blocked with RPMI media containing 5% FCS. Cells were plated at the indicated density and incubated at 37°C for 5 h. Secondary Ab (anti-mIgG-alkaline phosphatase; Southern Biotech) was detected using 5-bromo-4-chloro-3-indolyl phosphate substrate (BCIP; Southern Biotech) in 0.5% low melting agarose (Fisher Scientific). Spots were counted using a binocular on a dissecting microscope and the detected numbers of IgG anti-SARS-CoV-2-S1

AFCs were calculated per million BM cells. The picture of the ELISpot plate was prepared in Photoshop.

2.3.7 Flow Cytometry Analysis for Cellular Immune Responses

Antigen-specific T-cell responses in the spleen of BALB/c mice immunized as described above were analyzed 12 days after immunization by flow cytometry, adhering to the recently published guidelines [374]. A number of previous studies also investigated systemic cellular immune responses induced by Ad-based vaccines in the spleen of mice at day 12 postimmunization [363,377,378]. Splenocytes isolated from vaccinated and PBS control mice were stimulated with PepTivator SARS-CoV-2-S1 (a pool of S1 MHC class I- and MHC class II-restricted peptides) for 6 h in the presence of protein transport inhibitors (Brefeldin A + Monensin) for the last 4 h. Unstimulated cells were used as negative controls. Cells were stained with antibodies for CD4 (GK1.5, BUV395, BD Biosciences), CD8b (H35-17.2, BUV737, BD Biosciences), and a (FVD, eFluor 780, eBioscience), followed by ICS using a Fix & Perm Cell Permeabilization Kit (Invitrogen) and IFN-γ antibody (XMG1.2, BV421, BD Biosciences). Data were collected and analyzed using a BD LSR II cytometer and FlowJo v10 software (BD Biosciences). Frequencies of IFN-γ^+ cells from unstimulated controls were subtracted from corresponding peptide-stimulated samples, and any negative values set to zero.

2.3.8 SARS-CoV-2 Microneutralization Assay

Neutralizing antibody (NT-Ab) titers against SARS-CoV2 were defined according to the following protocol [379,380]. Briefly, 50 µL of sample from each mouse, in different dilutions, were

added in two wells of a flat bottom tissue culture microtiter plate (COSTAR, Corning Incorporated, NY 14831, USA), mixed with an equal volume of 50 TCID50 of a SARS-CoV2 chinese strain isolated from a symptomatic chinese patient, previously titrated and incubated at 33°C in 5% CO_2. All dilutions were made in Eagle's Minimum Essential Medium with addition of 1% penicillin, streptomycin, and glutamine and 5 γ/mL of trypsin. After 1 h incubation at 33°C 5% CO_2, 3×10^4 VERO E6 cells [VERO C1008 (Vero 76, clone E6, Vero E6); ATCC® CRL-1586™] were added to each well. After 72 hours of incubation at 33°C 5% CO2 wells were stained with Gram's crystal violet solution (Merck KGaA, 64271 Damstadt, Germany) plus 5% formaldehyde 40% m/v (Carlo ErbaSpA, Arese (MI), Italy) for 30 min. Microtiter plates were then washed in running water. Wells were scored to evaluate the degree of cytopathic effect (CPE) compared to the virus control. Blue staining of wells indicated the presence of neutralizing antibodies. Neutralizing titer was the maximum dilution with the reduction of 90% of CPE. A positive titer was equal or greater than 1:5. Sera from mice before vaccine administration were always included in microneutralizaiton (NT) assay as a negative control.

2.3.9 Statistical Analysis

Statistical analyses were performed using GraphPad Prism v9 (San Diego, CA). Antibody endpoint titers and neutralization data were analyzed by Kruskal–Wallis test, followed by Dunn's multiple comparisons. B- and T-cell data were analyzed by one-way Welch's ANOVA, followed by Dunnett's T3 multiple comparisons. Significant differences are indicated by *$p < 0.05$. Comparisons with nonsignificant differences are not indicated.

2.4 Discussion

Sustainable immunization programs against SARS-CoV-2 and other novel coronaviruses require cost-effective, patient-friendly, rapidly scalable, and clinically feasible vaccines that are capable of inducing long-term immunity after a single immunization. To address this continuing demand, our study presents the development of an Ad-based COVID-19 vaccine (Ad5.SARS-CoV-2-S1) and its immunogenicity in mice. Current leading Ad-based SARS-CoV-2 vaccines, Oxford-AstraZeneca, Janssen, CanSinoBio, and Sputnik V COVID-19 vaccines, encode the gene for full-length SARS-CoV-2 spike protein and are administered intramuscularly, whereas our vaccine encodes the gene for SARS-CoV-2-S1 subunit and is being tested for its immunogenicity via I.N and S.C administration. A single immunization of BALB/c mice via either I.N. or S.C. delivery of our Ad5.SARS-CoV-2-S1 vaccine elicited robust S1-specific humoral and cellular immune responses, where I.N. administration represents a minimally invasive option. Further improvements could be achieved with different immunization regimens including homologous or heterologous prime-boost vaccination strategies [381–383]. For instance, intracutaneous vaccination with microneedle arrays, which have been shown to deliver a broad range of recombinant DNA or protein vaccines, with or without adjuvants, could be utilized to achieve different prime-boost immunization strategies [384–387].

In support of long-lasting S1-specific antibody responses, our mechanistic studies suggest that a single vaccination of BALB/c mice via either I.N. administration or S.C. delivery of Ad5.SARS-CoV-2-S1 was capable of forming antigen-specific GC reactions and inducing Ig isotype switches to IgG1 and IgG2a in GCs in the corresponding draining LNs 14 days after vaccination. Further, these Ig-isotype switched GC reactions in draining LNs likely enabled the generation of S1-specific antibody-secreting plasma cell responses in the BM of immunized mice

6 weeks after immunization, as GCs are typically the source of long-lived humoral immune effector cells ensuring sustained antibody production [19,375,388]. These results are promising and support the use of Ad5.SARS-CoV-2-S1 vaccine against COVID-19 to induce antigen-specific GC reactions, leading to the generation of long-lived plasma cells and mutated memory B cells in response to a single vaccination.

We also analyzed S1-specific T-cell responses in the spleen of mice to investigate the capacity of Ad5.SARS-CoV-2-S1 administered by either S.C. or I.N. routes to elicit antigen-specific systemic cellular immune responses. A single vaccination via either I.N. or S.C. delivery of Ad5.SARS-CoV-2-S1 was capable of generating significant systemic cellular immune responses compared to unimmunized control groups. In agreement with a previous report [389], vaccination via S.C. route was more efficient in inducing systemic S1-specific CD8$^+$ T-cell responses compared to I.N. delivery. Our future work will include more comprehensive investigation of these differences to establish the impact of the route of Ad5.SARS-CoV-2-S1 administration on antigen-specific cellular immune responses. In addition, we will study the magnitude, kinetics, and types of S1-specific cellular immune responses in different organs, such as lungs and various draining LNs, to provide additional insight into the quality, breadth, and durability of protective T-cell responses induced by Ad5.SARS-CoV-2-S1 vaccine.

Neutralization assays are pivotal for testing the quality of the immunization-induced antibodies in terms of their ability to reduce the amount of infectious virus titer in culture. Here, we used a microneutralization test (NT_{90}) to evaluate the function of the generated antibodies in the sera of immunized mice and showed that a single immunization using either I.N. delivery or S.C. injection of Ad5.SARS-CoV-S1 vaccine was capable of inducing significant SARS-CoV-2-neutralizing antibody titers at weeks 8 and 12 after vaccination with respect to control groups. If

needed, it may be possible to further improve neutralizing antibody responses with different prime-boost vaccination strategies. Further, clinical translation of Ad vaccines has been predominantly hampered by pre-existing immunity against the viral capsid, which diminishes vaccine efficacy [390]. Notably, a recent study demonstrated that intramuscular immunization with a recombinant type 5 adenovirus vaccine encoding the gene for the full spike protein could overcome the pre-existing vector immunity [367]. Thus, immunization with Ad-based vaccines could be a feasible alternative to combat emerging infectious respiratory diseases including COVID-19.

BALB/c mice have been widely used to investigate the immunogenicity of different vaccines against coronaviruses [217,274,343,355], thereby representing a reliable model for the immunogenicity testing of Ad5.SARS-CoV-2-S1. The rational design and construction of our Ad5.SARS-CoV-2-S1 vaccine resulted in promising immune responses in BALB/c mice; however, it will still be important to test the immunogenicity of Ad5.SARS-CoV-2-S1 in different mouse strains and especially in larger animal models to extrapolate these responses to human studies. Our future studies will include animal challenge models with more detailed T- and B-cell studies. Two recent studies have investigated viral replication and clearance after challenge in rhesus macaque and guinea pig models and demonstrated promising results [300,355]. We are currently working on the development and validation of a transgenic hACE2 mouse model to perform protection studies in the future.

In sum, our Ad-based vaccine induces significant antigen-specific humoral and cellular immune responses against SARS-CoV-2. These results suggest that Ad-based vaccines have the potential to be versatile candidates for the induction of virus-specific protective immune responses against COVID-19 and other emerging infectious diseases.

2.5 Acknowledgements

3.0 Adenovirus-Vectored SARS-CoV-2 Vaccine Expressing S1-N Fusion Protein

Text from this chapter has been modified from the publication: **Khan, M. S.**, Kim E., McPherson, A., Weisel, F.J., Huang, S., Kenniston, T.W., Percivalle, E., Cassaniti, I., Baldanti, F., Meisel, M., Gambotto, A#. Adenovirus-vectored SARS-CoV-2 vaccine expressing S1-N fusion protein. *Antibody Therapeutics* **5**, 177–191 (2022). # corresponding author. PMID: 35967905

3.1 Introduction

The ongoing COVID-19 pandemic, caused by severe acute respiratory syndrome coronavirus 2 (SARS-CoV-2), continues to have a large impact on public health across the globe [326,327,391]. COVID-19 first emerged in 2019, was declared a global pandemic by the World Health Organization on 11 March 2020, and has since claimed approximately 5.6 million lives as of 24 January 2022. Vaccination continues to be one of the most effective public health interventions to curb infectious diseases and their impact on human, and animal, health [1–4]. Currently approved COVID-19 vaccines have been a key tool in fighting this pandemic; however, they have been hampered by worldwide distribution inequalities that have left many low to middle income countries without access [134,249,392–395]. With many countries now distributing a COVID-19 booster to those already vaccinated, global vaccine inequality is at risk of increasing further [396–399]. Global vaccine inequality has, and will continue to, lead to new SARS-CoV-2 variants that may be able to escape natural and vaccine acquired immunity [251,400–402]. To this effect, new COVID-19 vaccines

are needed, which are better suited for worldwide vaccination and incorporate strategies to target more conserved regions of SARS-CoV-2, to combat new viral variants.

Beta coronaviruses (BetaCoVs), such as SARS-CoV-2, are enveloped, positive sense, ssRNA viruses [247,333]. BetaCoVs encode the envelope, nucleocapsid (N), membrane, and spike (S) proteins [334,335]. The spike protein has been the focus of currently approved COVID-19 vaccines, and of various COVID-19 vaccines in development, due to its role in viral infection of host cells [336]. The S protein composed of two subunits, S1 and S2, that allow for viral attachment to the host cell receptor and in fusion to the host cellular membrane [336,338]. It has been demonstrated that antibodies targeting the S protein can block the binding of SARS-CoV-2 to the cell receptor, allowing the S protein to be a focal target of vaccine development [236,307,309,339,403]. Our previously published reports on vaccines against not only SARS-CoV-2, but also SARS-CoV-1 and MERS, have shown the ability of S1 subunit targeting vaccines to generate neutralizing antibody response [189,217,343,344]. Our previous efforts have established the immunogenicity of S1-based BetaCoVs vaccines through both Adenoviral (Ad)-vectored vaccines and subunit recombinant protein vaccines. Most recently, we have described an Ad-vectored SARS-CoV-2 vaccine expressing S1 alone generating a robust immune response in BALB/cJ mice [189]. We have also presented skin-targeted S1 subunit protein vaccines that induce antigen-specific antibody responses against MERS-CoV and SARS-CoV-2 [217].

Of particular interest is the investigation of including more conserved regions of SARS-CoV-2, such as the N protein, in vaccine strategies to combat emerging variants. The primary function of the SARS-CoV-2 N protein is to package the viral genome [237].The N protein is more conserved than the S protein, with 90% amino acid homology, and also accumulates fewer mutations over time [241,242]. The N protein also contains key T-cell epitopes for SARS-CoV-2

immunity [243–245]. The literature suggests potential for an S1- and N-based COVID-19 vaccine that incorporates the neutralizing antibody response to S1 with the conserved T-cell response to N. One concern with including other SARS-CoV-2 proteins, outside of S, is that it will reduce the S-specific antibody response and reduce the neutralizing antibody response against SARS-CoV-2. This manuscript thoroughly investigates the impact of including N, as a S1N fusion antigen, on S1-specific antibody response, S1-specific IgG isotype switch, and neutralization response against live SARS-CoV-2, adding crucial information for next-generation SARS-CoV-2 vaccines.

Adenovirus (Ad)-vectored vaccines have been investigated thoroughly due to their ability to induce a balanced humoral and cellular immune response [360–362]. Our previous studies using Ad-vectored vaccines expressing SARS-CoV-2-S1, SARS-CoV-1-S1, and MERS-S1 have illustrated the potential for Ad-based vaccines against coronavirus diseases. Indeed, there have been a number of Ad-based SARS-CoV-2 (including Ad5, Ad26, and chimpanzee adenovirus vectors) vaccines that have shown promising results in clinical trials [404]. The Ad5-vectored COVID-19 vaccine, CanSino Convidicea Vaccine (Ad5-nCoV), encoding for the full S protein has also shown promising immunogenicity when delivered intramuscularly and has been approved by multiple countries [367,368,405]. Although there has been remarkable progress of Ad-based COVID-19 vaccines, there is still a need for investigation of novel vaccine strategies, such as including the N protein, or homologous and heterologous prime-boost strategies, which induce sustained immunity against SARS-CoV-2 variants.

Here, we describe the development of multiple Ad-vectored and subunit recombinant protein SARS-CoV-2 vaccine candidates against COVID-19. We designed and constructed a recombinant type 5 Ad vector encoding for a fusion protein S1N subunit antigen (Ad5.SARS-CoV-2-S1N). We evaluated the immunogenicity of a single immunization, along with homologous

and heterologous prime-boost immunization, of this vaccine in BALB/cJ mice through multiple delivery routes including intranasal (I.N.) delivery, subcutaneous (S.C.) injection, and intramuscular (I.M.) injection. We investigated the ability of Ad5.SARS-CoV-2-S1N to induce antigen-specific humoral and cellular immune responses and investigated the virus-specific neutralization activity of the generated antibodies. Our study demonstrates the development of an Ad-based SARS-CoV-2 vaccine, along with heterologous boost using subunit recombinant SARS-CoV-2 vaccine, that can induce robust and durable SARS-CoV-2 specific immune response in mice, which is sustained against Beta (B.1.351) and Gamma (P.1) SARS-CoV-2 variants.

3.2 Results

3.2.1 Adenoviral SARS-CoV-2 S1N Vaccine

To produce E1/E3 deleted replication-deficient human type 5 adenovirus expressing SARS-CoV-2-S1 protein, we generated pAd/SARS-CoV-2-S1N by subcloning the codon-optimized SARS-CoV-2-S1 and wild-type Nucleoprotein gene into the shuttle vector, pAd (GenBank U62024) at SalI and NotI sites. Next, Ad5.SARS-CoV-2-S1N (Ad5.S1N) was created by loxP homologous recombination (**Fig. 10A**). To detect SARS-CoV-2-S1 expression driven by the generated Adenoviral candidate, the serum-free supernatants from A549 cells infected with Ad5.S1N were characterized by SDS-PAGE and western blot analysis. The recombinant SARS-CoV-2-S1N proteins (Ad5.S1N infected cells) were recognized by the polyclonal S1 and N antibody at the expected glycosylated monomer molecular weights of about 150 kDa (**Fig. 10B and C**).

77
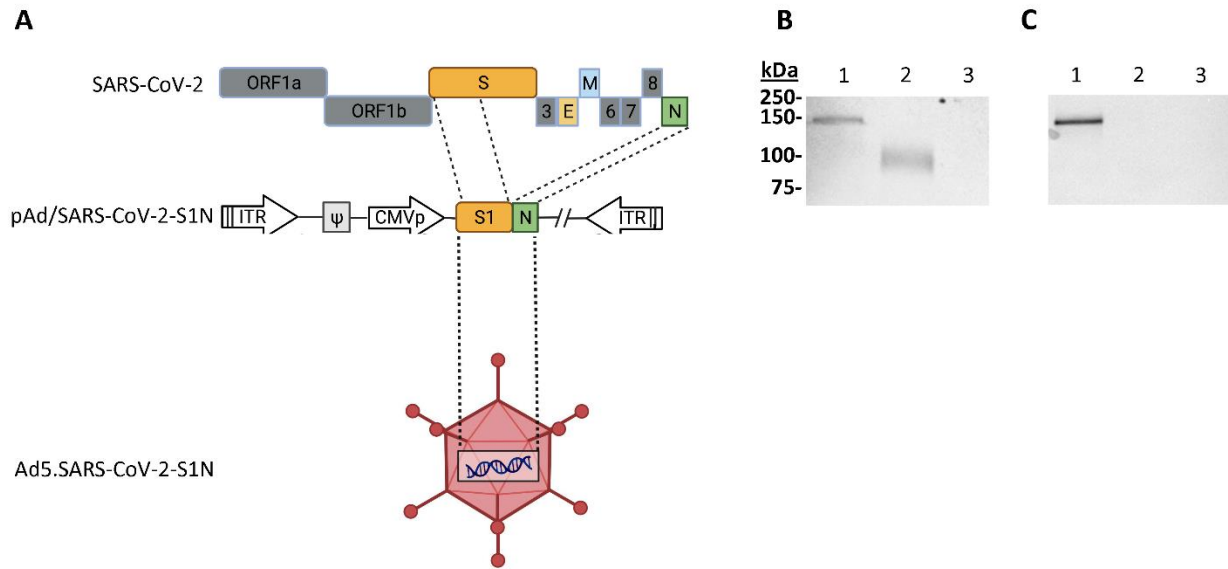
Figure 10: Adenoviral-vectored SARS-CoV-2-S1N vaccine. (A) A shuttle vector carrying the codon-optimized SARS-CoV-2-S1 gene encoding N-terminal 1–661 along with full Nucleoprotein was designed as shown in the diagram. The vector was used to generate recombinant type 5 replication-deficient adenoviruses (Ad5) by homologous recombination with the adenoviral genomic DNA, shown by the BioRender illustration of Ad5.SARS-CoV-2-S1N. ITR, inverted terminal repeat. (B) Detection of the SARS-CoV-2-S1N fusion protein by western blot with the supernatant of A549 cells infected with Ad5.SARS-CoV-2.S1N (Ad5.S1N) using S1 SARS-CoV-2 rabbit polyclonal antibody (lane 1). As a positive control, supernatant of A549 cells infected with Ad5.SARS-CoV-2.S1 (Ad5.S1) was loaded (lane 2). As a negative control, supernatant of A549 cells infected with an empty vector (AdΨ5) was loaded (lane 3). (C) Detection of the SARS-CoV-2-S1N fusion protein by western blot with the supernatant of A549 cells infected with Ad5.SARS-CoV-2.S1N (Ad5.S1N) using N SARS-CoV-2 rabbit polyclonal antibody (lane 1). As a negative control, supernatant of A549 cells infected with Ad5.SARS-CoV-2.S1 (Ad5.S1) was loaded (lane 2). As a negative control, supernatant of A549 cells infected with an empty vector (AdΨ5) was also loaded (lane 3). The supernatants were resolved on SDS-10% polyacrylamide gel after being boiled in 2% SDS sample buffer with β-ME.
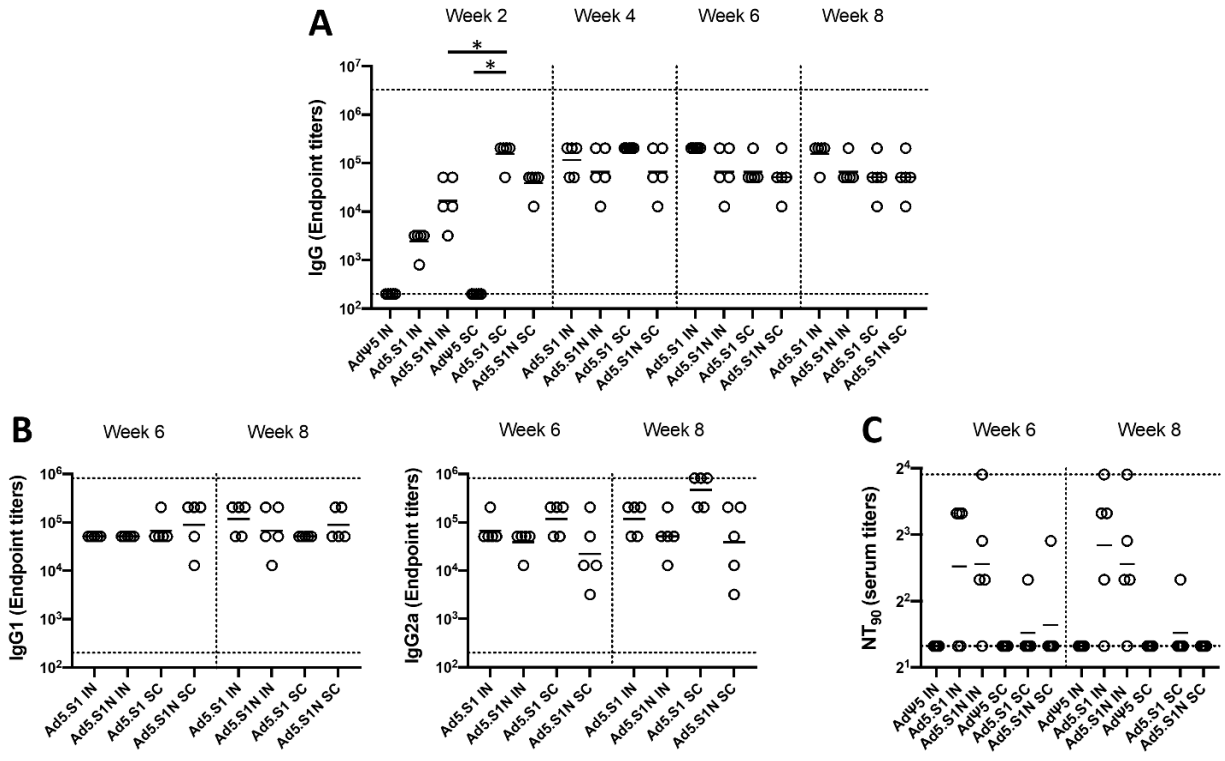
Figure 11: Antigen-specific antibody responses in mice immunized with adenoviral-vectored SARS-CoV-2-S1N vaccine. BALB/c mice ($n = 5$ mice per groups) were immunized intranasally (IN) or subcutaneously (SC) with 5×10^{10} v.p. of Ad5.SARS-CoV-2-S1N (Ad5.S1N), Ad5.SARS-CoV-2-S1 (Ad5.S1), or empty Ad5 vector as negative control (AdΨ5). On weeks 2, 4, 6, and 8 after vaccination, the sera from mice were collected, serially diluted (200×), and tested for the presence of SARS-CoV-2-S1-specific (A) IgG and (B) IgG1 & IgG2 antibody levels at the indicated time points by ELISA. (C) Serum from immunized mice was tested neutralizing antibodies using a plaque reduction neutralization test (PRNT) SARS-CoV-2 strain from Wuhan. Serum titers that resulted in a 90% reduction in SARS-CoV-2 viral plaques (NT90) compared to the virus control are reported at 6 and 8 weeks after immunization, respectively, and bars represent geometric means. No neutralizing antibodies were detected in serum AdΨ5 control group. Significance was determined by Kruskal-Wallis test followed by Dunn's multiple comparisons (*$p < 0.05$). Horizontal solid lines represent geometric mean antibody titers. Horizontal dotted lines represent minimum and maximum dilutions. Results are from a single animal experiment. ($N = 5$ mice per group). ELISA experiments were conducted twice while neutralizing antibody experiments were conducted once.

3.2.2 Single-Shot Immunogenicity of Adenoviral SARS-CoV-2 S1N Vaccine

To evaluate the impact of including the N protein of SARS-CoV-2 in vaccine formulation through a S1N fusion protein, we first compared the immunogenicity of Ad5.SARS-CoV-2-S1N (Ad5.S1N) with our previously published Ad5.SARS-CoV-2-S1 (Ad5.S1), which expresses S1 alone [189]. We determined S1-specific IgG, IgG1, and IgG2a endpoint titers in the sera of vaccinated BALB/cJ mice (either via I.N. delivery or S.C. injection) and control mice (AdΨ5 immunized groups). Serum samples, collected from mice at the timepoints indicated, were serially diluted to determine SARS-CoV-2-S1-specific IgG, IgG1, and IgG2a endpoint titers for each immunization group using ELISA (**Fig. 11**). Results suggest that both Ad5.S1 and Ad5.S1N resulted in comparable S1-specific IgG, IgG1, and IgG2a endpoint titers (**Fig. 11**). S.C. injection of Ad5.S1 and Ad5.S1N resulted in significantly increased S1-specific IgG endpoint titers as early as 2 weeks after a single vaccination, compared to the mock vaccinated group (**Fig. 11**, $p < 0.05$, Kruskal-Wallis test, followed by Dunn's multiple comparisons). I.N. Ad5.S1 and Ad5.S1N SARS-CoV-2-S1-specific IgG endpoint titer increased to comparable levels of S.C. injection by week 3 and were sustained through week 8 (**Fig. 11A**). Both Ad5.S1 and Ad5.S1N, regardless of immunization delivery route, resulted in similar IgG1 and IgG2a endpoint titers indicating a balanced Th1/Th2 response (**Fig. 11B**). To evaluate the functional quality of vaccine-generated antigen-specific antibodies, we used a microneutralization assay (NT_{90}) to test the ability of sera from immunized mice to neutralize the infectivity of SARS-CoV-2. Sera, collected from all mice 6 and 8 weeks after vaccination, were tested for the presence of SARS-CoV-2-specific neutralizing antibodies (**Fig. 11C**). As expected, there was no detected neutralizing antibody response in sera of AdΨ5 immunized mice. Neutralizing antibodies were detected in Ad5.S1 and Ad5.S1N vaccinated mice (for both I.N. and S.C. delivery routes) at week 6. Neutralizing antibody response for I.N. delivery

was greater in magnitude for both Ad5.S1 and Ad5.S1N, when compared to S.C. injection, with S.C. injected mice having low to undetectable neutralizing antibodies by week 8 (**Fig. 11C**).

Next, we evaluated the antigen-specific cellular immune response induced by the single immunization. We investigated S1- and N-specific cellular immunity in mice after vaccination by quantifying IFN-γ^+ CD8$^+$ and CD4$^+$ T-cell responses through intracellular cytokine staining (ICS) and flow cytometry. Results suggest that I.N. delivery of either Ad5.S1 or Ad5.S1N did not induce increased systemic S1-specific or N-specific CD8$^+$ T cell immunity, when compared to I.N. AdΨ5 control groups (**Fig. 12**). However, S.C. vaccination induced increased systemic S1-specific IFN-γ^+ CD8$^+$ T-cell responses for both Ad5.S1 and Ad5.S1N. S.C. vaccination of Ad5.S1 and Ad5.S1N resulted in significantly increased S1-specific IFN-γ^+ CD8$^+$ T-cell response when compared to both I.N. AdΨ5 and S.C. AdΨ5 (**Fig. 12A**, $p < 0.05$, one-way Welch's ANOVA, followed by Dunnett's T3 multiple comparisons). S1-specific IFN-γ^+ CD8$^+$ T-cell response for S.C. vaccinated Ad5.S1N mice were significantly higher than in S.C. vaccinated Ad5.S1 mice (**Fig. 12A**, $p < 0.05$, one-way Welch's ANOVA, followed by Dunnett's T3 multiple comparisons). However, S.C. vaccinated Ad5.S1N mice did not have significantly higher N-specific IFN-γ^+ CD8$^+$ T-cell response when compared to S.C. vaccinated Ad5.S1N (**Fig. 12A**, $p > 0.05$, one-way Welch's ANOVA, followed by Dunnett's T3 multiple comparisons). There was no significant increase in S1-specific or N-specific IFN-γ^+ CD4$^+$ T-cell response in vaccinated groups when compared to controls (**Fig. 12B**, $p > 0.05$, one-way Welch's ANOVA, followed by Dunnett's T3 multiple comparisons). In sum, these finding indicate that a single vaccination with Ad5.S1 or Ad5.S1N, via either S.C. injection or I.N. delivery, results in a robust S1-specific IgG response, with a balanced IgG1/IgG2a ratio. The choice of the route of vaccine administration (S.C. or I.N.) influences both SARS-CoV-2 neutralizing antibodies and S1-specific CD8$^+$ T-cell responses. Most

importantly, inclusion of the N protein, through Ad5.S1N, results in a significantly higher induction of S1-specific CD8$^+$ T-cells when compared to Ad5.S1.
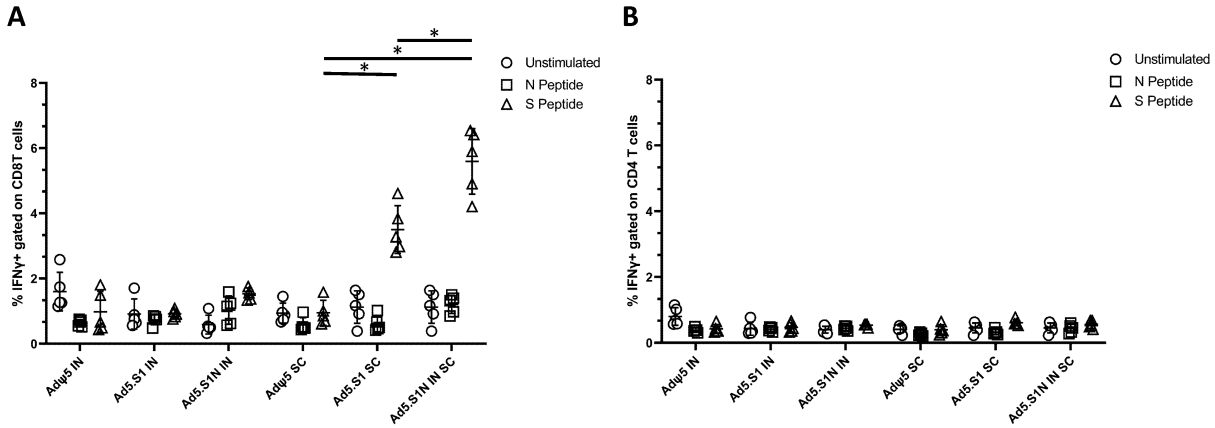
Figure 12: Antigen-specific cellular responses in BALB/c mice immunized with Ad5.SARS-CoV-2-S1 and Ad5.SARS-CoV-2 S1N. BALB/c mice were immunized S.C. or I.N. with 5×10^{10} v.p. of Ad5.SARS-CoV-2-S1 (Ad5.S1), Ad5.SARS-CoV-2-S1N (Ad5.S1N), or AdΨ5. Ten days after vaccination, splenocytes were isolated and stimulated with SARS-CoV-2 S1 and SARS-CoV-2 Nucleoprotein PepTivator, followed by ICS and flow cytometry to identify SARS-CoV-2 S1 and Nucleoprotein-specific T cells (see Supporting Information for complete gating strategy). (A) Frequencies of SARS-CoV-2 S1 and Nucleoprotein-specific CD8+ IFN-γ$^+$. Results are mean ± SD. (B) Frequencies of SARS-CoV-2 S1 and Nucleoprotein-specific CD4$^+$ IFN-γ$^+$. Groups were compared by one-way Welch's ANOVA, followed by Dunnett's T3 multiple comparisons, and significant differences are indicated by *$p <$ 0.05. Unstimulated controls are represented by circles, Nucleoprotein stimulated samples (N peptide) are represented by squares, and S1 peptide stimulated samples (S peptide) are represented by triangles. Results are from a single animal experiment. ($N = 5$ mice per group). This experiment was conducted once.

3.2.3 Immunogenicity of Homologous and Heterologous Prime-Boost Vaccination Strategy

To evaluate the ability to further increase neutralizing antibody and cellular immune response to vaccination with Ad5.S1N, we investigated prime-boost strategies leveraging homologous and heterologous strategies. Prime-boost vaccination strategies have been shown to increase the quantity, durability, and quality of the immune response to vaccination and have been employed for numerous types of vaccines [381,406]. **Figure 13A** outlines the prime-boost vaccination strategies used. Homologous prime-boost of Ad5.S1N using differing vaccination routes (I.N. and S.C.) was done to circumvent Ad5 vector immunity induced by prime immunization, which has been shown to limit the effectiveness of Ad5 vectored vaccines [117,407]. We also evaluated a heterologous prime-boost group that was primed S.C. with Ad5.S1N and boosted with 15 μg of recombinant subunit S1 WT protein. Heterologous prime-boost strategies have been shown to be more immunogenic than homologous prime-boost regimens, necessitating its investigation [406,408–410].
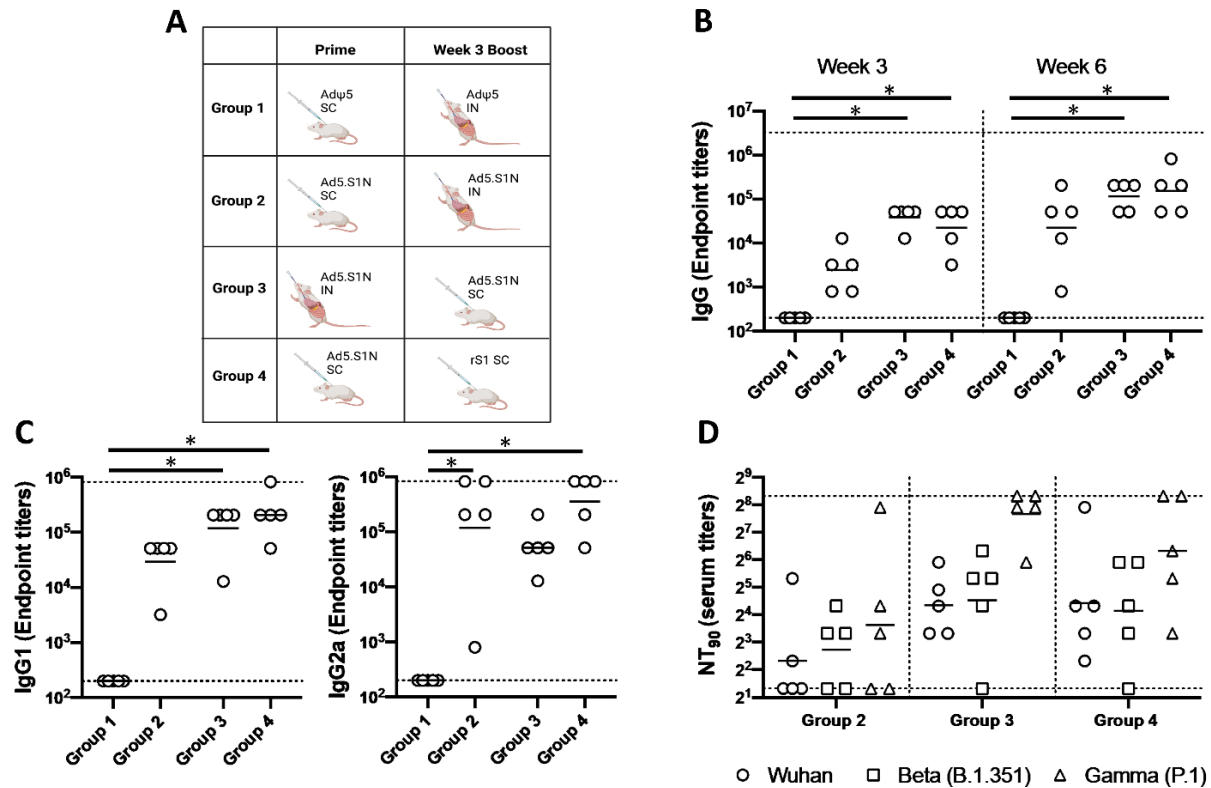
Figure 13: Homologous and heterologous prime-boost vaccination with Ad5.SARS-CoV-2-S1N (Ad5.SIN) using differing vaccination routes along with recombinant S1 protein (rS1). (A) Schematic layout of mice ($N = 5$ mice per group) vaccinations. Group 1 served as control with SC AdΨ5 (1×10^{10} v.p.) prime and IN AdΨ5 (1×10^{10} v.p.) boost. Group 2 primed with SC Ad.S1N (1×10^{10} v.p.) and IN Ad.S1N (1×10^{10} v.p.) boost. Group 3 primed with IN Ad.S1N (1×10^{10} v.p.) and SC Ad.S1N boost (1×10^{10} v.p.). Group 4 primed with SC Ad.S1N (1×10^{10} v.p.) and SC non-adjuvanted rS1 boost (15 µg). On weeks 3 and 6 after vaccination, the sera from mice were collected, serially diluted (200×), and tested for the presence of SARS-CoV-2-S1-specific (B) IgG antibody levels. (C) Week 6 sera were tested for the presence of IgG1 and IgG2 antibody levels. (D) Week 6 serum from immunized mice was tested for neutralizing antibodies using a plaque reduction neutralization test (PRNT) with three different SARS-CoV-2 strains from Wuhan, South Africa (Beta B.1.351), or Brazil (Gamma P.1). Neutralization of Wuhan strain represented by circle, neutralization of Beta B.1.351 represented by square, and neutralization of Gamma P.1 represented by triangle. Serum titers that resulted in a 90% reduction in SARS-CoV-2 viral plaques (NT90) compared to the virus control are reported at 6 weeks after immunization and bars represent geometric means. No neutralizing antibodies were detected in serum PBS control group (not shown). Significance was determined by Kruskal-Wallis

84

test followed by Dunn's multiple comparisons (*$p < 0.05$). Horizontal lines represent geometric mean antibody titers. Horizontal dotted lines represent minimum and maximum dilutions. Results are from a single animal experiment. ($N = 5$ mice per group). ELISA experiments were conducted twice while neutralizing antibody experiments were conducted once.

We determined S1-specific IgG, IgG1, and IgG2a endpoint titers in the sera of prime-boost vaccinated BALB/cJ mice (either via I.N. delivery or S.C. injection) and control mice (AdΨ5 immunized groups). Serum samples, collected from mice at the timepoints indicated, were serially diluted to determine SARS-CoV-2-S1-specific IgG, IgG1, and IgG2a endpoint titers for each immunization group using ELISA (**Figure 13**). Interestingly, I.N. prime and S.C. boost Ad5.S1N (Group 3), along with Ad5.S1N S.C prime and S.C. rS1 boost (Group 4), mice resulted in significantly higher IgG at weeks 3 and 6 when compared to control group (Group 1), while S.C. prime and S.C. boost Ad5.S1N (Group 2) did not (**Figure 13B**, $p < 0.05$, Kruskal-Wallis test, followed by Dunn's multiple comparisons). IgG1 and IgG2a endpoint titers were relatively balanced for experimental groups; however, Group 3 and Group 4 IgG1 endpoint titers were statistically significant when compared to Group 1; while Group 2 and Group 4 IgG2a endpoint titers were statistically significant when compared to Group 1 (**Figure 13C**, $p < 0.05$, Kruskal-Wallis test, followed by Dunn's multiple comparisons). We used a microneutralization assay (NT_{90}) to test the ability of sera from immunized mice to neutralize the infectivity of SARS-CoV-2. The ability of sera to neutralize Beta (B.1.351) and Gamma (P.1) variants was also investigated. Sera, collected from all mice at 6 weeks after prime vaccination, were tested for the presence of SARS-CoV-2-specific neutralizing antibodies (**Figure 13D**). Neutralizing antibodies were detected in Group 2, Group 3, and Group 4, which were sustained, or increased, against Beta and Gamma variants. Group 2 had the lowest neutralizing antibody response when compared to Group

3 and Group 4 (**Figure 13D**). Prime-boost vaccination resulted in approximately 3-fold greater NT_{90} serum titers when compared to single-shot immunization. We then evaluated the antigen-specific cellular immune response induced by homologous and heterologous prime-boost immunization.

We investigated S1-specific and N-specific cellular immunity in Group 1, Group 2, and Group by quantifying IFN-γ^+ CD8$^+$ and CD4$^+$ T-cell responses through ICS and flow cytometry 8 weeks post prime vaccination. Results suggest that route of both prime and boost vaccination has an impact on both systemic S1-specific and N-specific CD8$^+$ T-cell immunity. Although S.C. and I.N. boost of Ad5.S1N resulted in S1-specific CD8$^+$ T-cell immunity, this was not significant when compared to empty vector control (**Figure 14A**, $p > 0.05$, one-way Welch's ANOVA, followed by Dunnett's T3 multiple comparisons). No N-specific CD8$^+$ T-cell immunity was detected for S.C. prime and I.N. boost of Ad5.S1N vaccinated mice. However, I.N. prime and S.C. boost of Ad5.S1N resulted in systemic S1-specific CD8$^+$ T-cell immunity with S1-specific CD8$^+$ IFN-γ^+ amounts being significantly higher when compared to empty vector control (**Figure 14A**, $p < 0.05$, one-way Welch's ANOVA, followed by Dunnett's T3 multiple comparisons). While there was an induction in both S1-specific and N-specific IFN-γ^+ CD4$^+$ T-cell response in I.N. prime and S.C. boost of Ad5.S1N vaccinated groups, it was not statistically significant when compared to controls (**Figure 14B**, $p > 0.05$, one-way Welch's ANOVA, followed by Dunnett's T3 multiple comparisons). Taken together, these findings indicate that prime-boost vaccination with Ad5.S1N results in higher S1-specific IgG, IgG1, IgG2a, and neutralizing response when compared to single immunization alone. The neutralizing ability was robust with I.N. prime and S.C. boost of Ad5.S1N, along with S.C. Ad5.S1N prime and S.C. rS1 boost. Prime-boost vaccination of

Ad5.S1N indicated the choice of vaccine administration order (S.C. or I.N.) impacted S1-specific and N-specific CD8+ T-cell response.
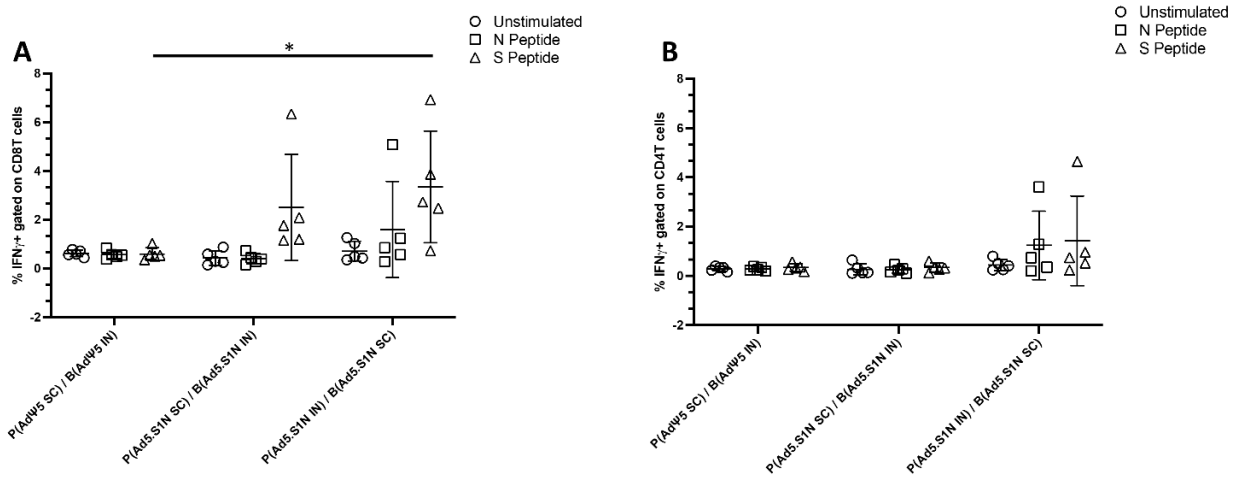
Figure 14: Antigen-specific cellular responses in BALB/c mice heterologous prime-boost immunized with Ad5.SARS-CoV-2 S1N. BALB/c mice were immunized as follows: Group 1 served as control with SC AdΨ5 $(1 \times 10^{10}$ v.p.) prime and IN AdΨ5 $(1 \times 10^{10}$ v.p.) boost. Group 2 prime SC Ad.S1N $(1 \times 10^{10}$ v.p.) and IN Ad.S1N $(1 \times 10^{10}$ v.p.) boost. Group 3 prime IN Ad.S1N $(1 \times 10^{10}$ v.p.) and SC Ad.S1N $(1 \times 10^{10}$ v.p.) boost. Eight weeks after initial vaccination, 5 weeks post boost, splenocytes were isolated and stimulated with SARS-CoV-2 S1 and SARS-CoV-2 Nucleoprotein PepTivator, followed by ICS and flow cytometry to identify SARS-CoV-2 S1 and Nucleoprotein-specific T cells (see Supporting information for complete gating strategy). (A) Frequencies of SARS-CoV-2 S1 and Nucleoprotein-specific CD8+ IFN-γ+. (B) Frequencies of SARS-CoV-2 S1 and Nucleoprotein-specific CD4+ IFN-γ+. Results are mean ± SD. Groups were compared by one-way Welch's ANOVA, followed by Dunnett's T3 multiple comparisons, and significant differences are indicated by *$p < 0.05$. Unstimulated controls are represented by circles, Nucleoprotein stimulated samples (N peptide) are represented by squares, and S1 peptide stimulated samples (S peptide) are represented by triangles. Results are from a single animal experiment. ($N = 5$ mice per group). This experiment was conducted once.

87

3.2.4 Immunogenicity of Heterologous Prime-Boost Vaccination with Ad.S1N and Variant Specific Recombinant S1 Subunit Protein

Due to the robust antibody response to S.C. Ad5.S1N prime and S.C. rS1 boost in **Figure 13**, we aimed to further compare the immunogenicity of recombinant monomeric S1 subunit vaccine formulation. **Figure 15A** outlines the prime-boost vaccination strategies investigated with prime-boost of 15 µg rS1 WT, rS1 B.1.351, a combination of rS1 WT & rS1 B.1.351, and Ad5.S1N. A key advantage of harnessing heterologous prime-boost vaccination, with Ad5-vectored and recombinant subunit vaccines, is circumventing anti-Ad5 vector immunity induced by prime immunization [117,407]. Due to not having to account for Ad5 vector immunity following prime immunization, along with the clinical familiarity with I.M. injection of vaccines, all mice were vaccinated intramuscularly.
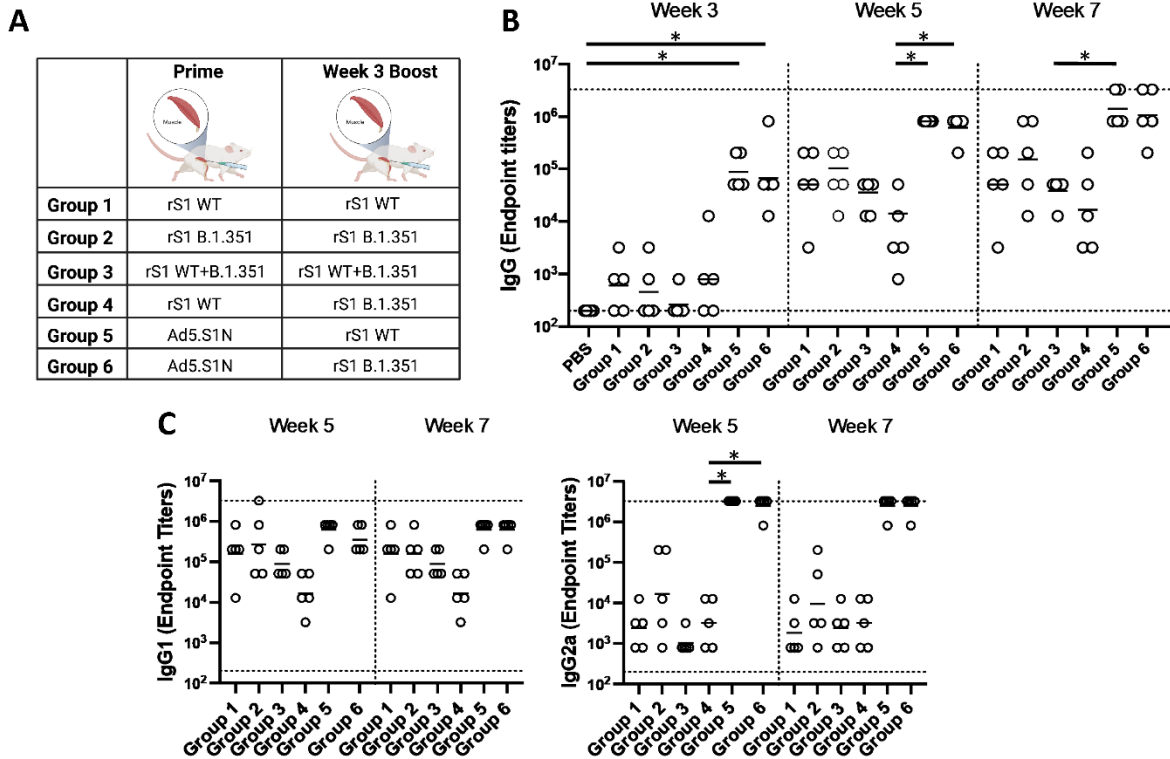
Figure 15: Homologous and heterologous intramuscular prime-boost vaccination with variant-specific recombinant S1 proteins (rS1) and Ad5.SARS-CoV-2-S1N (Ad5.SIN). BALB/c mice ($n = 5$ mice per groups) were immunized and boosted intramuscularly with 15 μg of Wuhan rS1 (rS1 WT), South Africa rS1 (rS1 B.1.351), mixture of Wuhan rS1 and South Africa rS1 (rS1 WT+B.1351), or 1×10^{10} v.p. of Ad5.SARS-CoV-2-S1N (Ad5.S1N), while mice were immunized intramuscularly with PBS as a negative control. (A) Schematic layout of mice ($N = 5$ mice per group) vaccinations. Group 1 prime and homologous boost 15 μg rS1 WT. Group 2 prime and homologous boost 15 μg rS1 B.1.351. Group 3 prime and homologous boost 15 μg rS1 WT+B.1.351. Group 4 prime 15 μg rS1 WT and heterologous boost 15 μg rS1 B.1.351. Group 5 prime 1×10^{10} v.p. Ad5.S1N and heterologous boost 15 μg rS1 WT. Group 6 prime 1×10^{10} v.p. Ad5.S1N and heterologous boost 15 μg rS1 B.1.351. Antigen-specific antibody responses in mice immunized. On weeks 3,5, and 7 after vaccination, the sera from mice were collected, serially diluted (200×), and tested for the presence of SARS-CoV-2-S1-specific (B) IgG and (C) IgG1 and IgG2a antibody levels at the indicated time points by ELISA. Significance was determined by Kruskal-Wallis test followed by Dunn's multiple comparisons (*$p < 0.05$). Horizontal lines represent geometric mean antibody titers. Horizontal dotted lines represent minimum and maximum dilutions. Results are from a single animal experiment. ($N = 5$ mice per group). ELISA experiments were conducted twice while neutralizing antibody experiments were conducted once.

Serum samples, collected from mice at the timepoints indicated, were used to determine S1-specific IgG, IgG1, and IgG2a endpoint titers for each immunization group using ELISA (**Figure 15A**). Heterologous Ad5.S1N prime with either WT rS1 or B.1.351 rS1 boost (Group 5 and Group 6) resulted in statistically different IgG at week 3 when compared to PBS vaccinated group (**Figure 15B**, $p < 0.05$, Kruskal-Wallis test, followed by Dunn's multiple comparisons). Groups vaccinated with rS1 protein, both WT and B.1.351 (Group 1 through Group 4), regardless of heterologous or homologous prime-boost, resulted in lower IgG endpoint titers that were not statistically different from control group at week 3 and, in some cases, significantly lower than Group 5 and Group 6 at week 5 and week 7 (**Figure 15B**, $p < 0.05$, Kruskal-Wallis test, followed by Dunn's multiple comparisons). Interestingly, mice vaccinated with monomeric rS1 proteins (Group 1 through Group 4) showed a skew towards to a IgG1 dominant response rather than the balanced IgG1 and IgG2a response in Ad5.S1N primed groups (Group 5 and Group 6) (**Figure 15C**). To evaluate the functional quality of vaccine-generated antigen-specific antibodies, we used a microneutralization assay (NT_{90}) to test the ability of sera from immunized mice to neutralize the infectivity of SARS-CoV-2. The ability of sera to neutralize Beta (B.1.351) and Gamma (P.1) variants was also investigated. Sera, collected from all mice at 7 weeks after prime vaccination, were tested for the presence of SARS-CoV-2-specific neutralizing antibodies (**Figure 16**). Neutralizing antibodies were detected against WT, Beta, and Gamma, albeit relatively low, for monomeric rS1 vaccinated groups (Group 1 through Group 4) (**Figure 16**). However, Ad5.S1N prime & rS1 WT boost (Group 5) and Ad5.S1N prime & rS1 B.1.351 boost (Group 6) resulted in the greatest amount of neutralizing capacity, which was not diminished against Beta (B.1.351) or Gamma (P.1). Due to the robust humoral response elicited by Group 5 and Group 6, along with the importance of long-lasting humoral response for protection against SARS-CoV-2 infection,

mice were bled monthly, and on week 29 Group 1, Group 2, Group 5, and Group 6 were sacrificed

to investigate the long-lived S1-specfic and N-specific antibody-forming cells in the bone marrow

(**Figure 17**) [411–414]. As expected, PBS vaccinated mice did not induce any S1-specfiic or N-specific

antibody-producing plasma cells in the bone marrow (**Figure 17**). Group 1, Group 2, Group 5, and

Group 6 had S1-specific IgG secreting spots, with Group 5 and Group 6 having significantly higher

number of spots than PBS vaccinated mice (**Figure 17A**, $p < 0.05$, Kruskal-Wallis test, followed

by Dunn's multiple comparisons). Indeed, only Group 5 and Group 6 had N-specific IgG secreting

spots with a significant difference from PBS, Group 1, and Group 2 mice (**Figure 17**B, $p < 0.05$,

Kruskal-Wallis test, followed by Dunn's multiple comparisons).
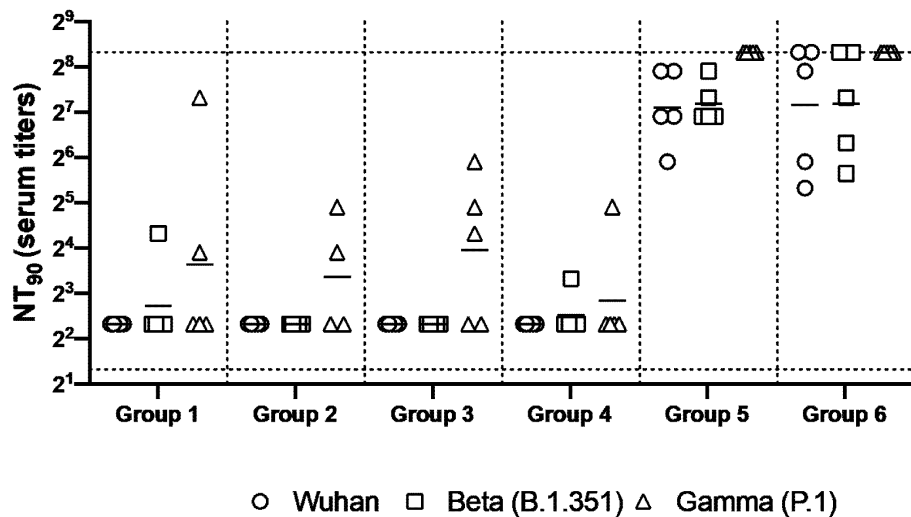
Figure 16: Neutralizing antibody responses in mice 7 weeks post heterologous prime-boost immunization.
Group 1 prime and homologous boost 45 μg rS1 WT. Group 2 prime and homologous boost 15 μg rS1 B.1.351. Group

3 prime and homologous boost 15 μg rS1 WT+B.1.351. Group 4 prime 15 μg rS1 WT and heterologous boost 15 μg

rS1 B.1.351. Group 5 prime 1×10^{10} v.p. Ad5.S1N and heterologous boost 15 μg rS1 WT. Group 6 prime 1×10^{10}

v.p. Ad5.S1N and heterologous boost 15 μg rS1 B.1.351. Serum from immunized mice was tested for neutralizing

antibodies using a plaque reduction neutralization test (PRNT) with three different SARS-CoV-2 strains from Wuhan, South Africa (Beta B.1.351), or Brazil (Gamma P.1). Neutralization of Wuhan strain represented by circle, neutralization of Beta B.1.351 represented by square, and neutralization of Gamma P.1 represented by triangle. Serum titers that resulted in a 90% reduction in SARS-CoV-2 viral plaques (NT90) compared to the virus control are reported 7 weeks post initial vaccination, and bars represent geometric means ($N = 5$ mice per group). Results are from a single animal experiment. No neutralizing antibodies were detected in serum PBS control group (not shown). This experiment was conducted once.
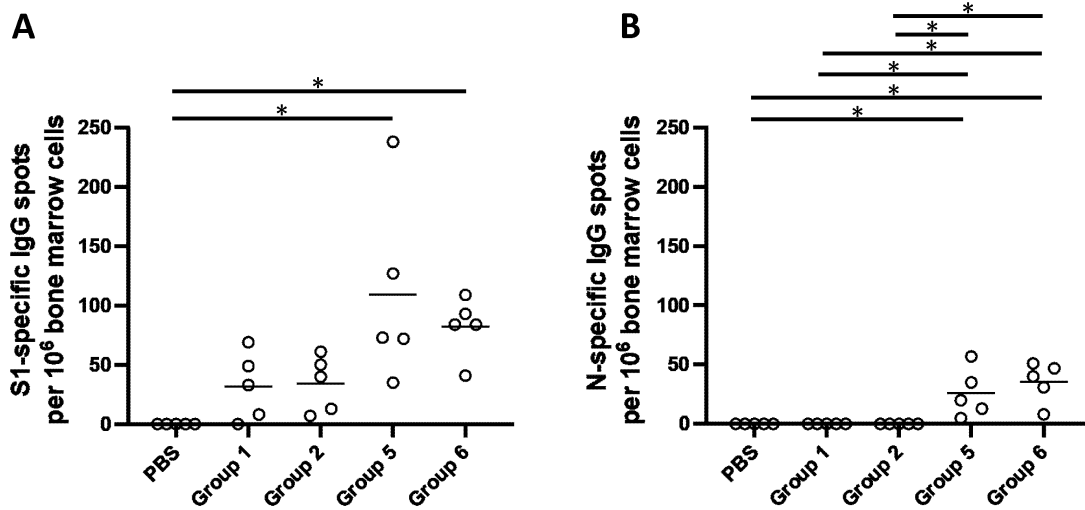
Figure 17: Analysis of long-term persistent antibody forming responses in the bone marrow of immunized mice. Mice were immunized as follows: Group 1 prime and homologous boost 15 µg rS1 WT. Group 2 prime and homologous boost 15 µg rS1 B.1.351. Group 5 prime 1×10^{10} v.p. Ad5.S1N and heterologous boost 15 µg rS1 WT. Group 6 prime 1×10^{10} v.p. Ad5.S1N and heterologous boost 15 µg rS1 B.1.351. Mice injected with PBS only served as negative controls. 29 weeks after immunization, S1-specific and N-specific antibody-forming cells in the bone marrow of mice were analyzed using ELISpot. (A) Quantification of SARS-CoV-2 S1-specific antibody forming cells in the bone marrow of immunized mice. (B) Quantification of SARS-CoV-2 N-specific antibody forming cells in the bone marrow of immunized mice. Data are from a single experiment ($n = 5$ per group). This experiment was conducted once.

3.3 Materials and Methods

3.3.1 Construction of Recombinant Adenoviral Vectors

The coding sequence for SARS-CoV-2-S1 amino acids 1 to 661 of full-length from BetaCoV/Wuhan/IPBCAMS-WH-05/2020 (GISAID accession id. EPI_ISL_403928) flanked with SalI & BamH I-6H-Not I was codon-optimized using the UpGene algorithm for optimal expression in mammalian cells and synthesized (GenScript) ref. 2020 EBioM [371]. pAd/SARS-CoV-2-S1 was then created by subcloning the codon-optimized SARS-CoV-2-S1 gene into the shuttle vector, pAdlox (GenBank U62024), at Sal I/Not I sites. The coding sequence of N (GenBank NC_045512) having Sac I & Sal I in 5' end and Not I & Apa I in 3' end was synthesized and cloned in Sac I/ApaI sites in pCMV-3Tag-4A generated in pCMV3/SARS-CoV-2-N (GenScript). For the construction of pAd/SARS-CoV-2-S1N, BamH I-6H-Not I of pAd/SARS-CoV-2-S1 was replace with Nucleoprotein gene digested with BamH I & Not I after amplified with NP-S (5'-GACGGATCCATGTCTGATAATGGACCCC-3') & T7 (5'-TAATACGACTCACTATAGGG-3') primers from pCMV3/SARS-CoV-2-NP. Subsequently, replication-deficient human recombinant serotype 5 adenovirus vector (Ad5.SARS-CoV-2-S1N) was generated by loxP homologous recombination and purified [343,371,372].

3.3.2 Construction of Recombinant Protein Expressing Vectors

The coding sequence for SARS-CoV-2-S1 amino acids 1 to 661 of full-length from BetaCoV/Wuhan/IPBCAMS-WH-05/2020 (GISAID accession id. EPI_ISL_ 403928) having C-terminal tag known as 'C-tag', composed of the four amino acids (aa), glutamic acid – proline –

glutamic acid – alanine (E-P-E-A) flanked with SalI & NotI was codon-optimized using the UpGene algorithm for optimal expression in mammalian cells and synthesized (GenScript) [371]. The construct also contained a Kozak sequence (GCC ACC) at the 5′ end. For B.1.351 variant, SARS-CoV-2-S1 mutated (Del144; K417N; E484K; N501Y; A570D; D614G) was synthesized based on above codon-optimized SARS-CoV-2-S1 from Wuhan. pAd/SARS-CoV-2-S1WU and pAd/SARS-CoV-2-SAS1SA were then created by subcloning the codon-optimized SARS-CoV-2-S1 inserts into the shuttle vector, pAdlox (GenBank U62024), at SalI/NotI sites. The plasmid constructs were confirmed by DNA sequencing.

3.3.3 Transient Production of Recombinant Proteins in expi293 Cells

pAd/SARS-CoV-2-S1WU and pAd/SARS-CoV-2-SAS1SA were amplified and purified using ZymoPURE II plasmid maxiprep kit (Zymo Research). For Expi293 cell transfection, we used ExpiFectamie^{TM} 293 Transfection Kit (ThermoFisher) and followed the manufacturer's instructions. Cells were seeded 3.0×10^6 cells/ml one day before transfection and grown to 4.5-5.5×10^6 cells/ml. 1µg of DNA and ExpiFectamine mixtures per 1ml culture were combined and incubated for 15 min before adding into 3.0×10^6 cells/ml culture. At 20h post-transfection, enhancer mixture was added, and culture was shifted to 32°C. The supernatants were harvested 5 days post transfection and clarified by centrifugation to remove cells, filtration through 0.8µm, 0.45µm, and 0.22µm filters and either subjected to further purification or stored at 4°C before purification.

3.3.4 Purification of Recombinant Proteins

The recombinant proteins named rS1WT (Wuhan) and rS1 B.1.351 were purified using a CaptureSelect[TM] C-tagXL Affinity Matrix prepacked column (ThermoFisher) and followed the manufacturer's guidelines [415]. Briefly, The C-tagXL column was conditioned with 10 column volumes (CV) of equilibrate/wash buffer (20 mM Tris, pH 7.4) before sample application. Supernatant was adjusted to 20 mM Tris with 200 mM Tris (pH 7.4) before being loaded onto a 5-mL prepacked column per the manufacturer's instructions at 5ml/min rate. The column was then washed by alternating with 10 CV of equilibrate/wash buffer, 10 CV of strong wash buffer (20 mM Tris, 1 M NaCl, 0.05% Tween-20, pH 7.4), and 5 CV of equilibrate/wash buffer. The recombinant proteins were eluted from the column by using elution buffer (20 mM Tris, 2 M $MgCl_2$, pH 7.4). The eluted solution was concentrated and desalted with preservative buffer (PBS) in an Amicon Ultra centrifugal filter devices with a 50,000 molecular weight cutoff (Millipore). The concentrations of the purified recombinant proteins were determined by the Bradford assay using bovine serum albumin (BSA) as a protein standard, aliquoted, and stored at −80°C until use.

3.3.5 SDS-PAGE and Western Blot

To evaluate the infectivity of the constructed recombinant adenoviruses, A549 (human lung adenocarcinoma epithelial cell line) cells were transduced with a multiplicity of infection of 7.5 (MOI = 7.5) of Ad5.SARS-CoV-2-S1N, Ad5.SARS-CoV-2-S1, and empty vector control (AdΨ5). At 48 hours after infection, cell supernatant was collected. The supernatants of A549 cells transduced with Ad5.SARS-CoV-2-S1N, Ad5.SARS-CoV-2-S1, and AdΨ5 were subjected to sodium dodecyl sulfate polyacrylamide gel electrophoresis (SDS-PAGE) and Western blot.

95

Briefly, after the supernatants were boiled in Laemmli sample buffer containing 2% SDS with beta- mercaptoethanol (β-ME), the proteins were separated by Tris-Glycine SDS-PAGE gels and transferred to nitrocellulose membrane. After blocking for 1 hour at room temperature (RT) with 5% non-fat milk in TBS-T, rabbit anti-SARS-CoV spike polyclonal antibody (1:3000) (Sino Biological), or rabbit anti-SARS-CoV nucleoprotein (1:3,000) (Sino Biological) was added and incubated overnight at 4°C as primary antibody, and horseradish peroxidase (HRP)-conjugated goat anti-rabbit IgG (1:10000) (Jackson immunoresearch) was added and incubated at RT for 1 hours as secondary antibody. After washing, the signals were visualized using ECL Western blot substrate reagents and iBright 1500 (Thermo Fisher). The full image of the original western blot used for Fig. 1B and Fig. 1C is available in Supplementary Figure 3.

3.3.6 Animals and Immunization

For single immunization experiment, BALB/cJ mice (n = 5 animals per group in each independent experiment) were vaccinated by either I.N. delivery or S.C. injection of 5×10^{10} viral particles (v.p.) of AdΨ5 (a null Ad5 vector negative control), Ad5.SARS-CoV-2-S1, or by Ad5.SARS-CoV-2-S1N. Mice were bled from retro-orbital vein at weeks 0, 2, 4, 6, and 8 after immunization, and the obtained serum samples were diluted and used to evaluate S1-specific antibodies by enzyme-linked immunosorbent assay (ELISA). Serum samples obtained on Week 8 and 12 after vaccination were also used for microneutralization (NT) assay. For homologous and heterologous prime-boost immunization experiment, BALB/cJ mice (n = 5 animals per group in each independent experiment) were prime or boosted by either I.N. delivery or S.C. injection of 1×10^{10} viral particles (v.p.) of AdΨ5 (a null Ad5 vector negative control), Ad5.SARS-CoV-2-S1N, or by 15µg of non-adjuvanted subunit recombinant wild type S1 monomeric protein. Mice were

bled from retro-orbital vein at weeks 3 and 6 after immunization, and the obtained serum samples were diluted and used to evaluate S1-specific antibodies by enzyme-linked immunosorbent assay (ELISA). Serum samples obtained on Week 6 after vaccination were also used for microneutralization (NT) assay. For heterologous prime-boost immunization experiment, BALB/cJ mice (n = 5 animals per group in each independent) were prime or boosted intramuscularly with 15µg of rS1 WT and/or rS1 B.1.351, or by Ad5.SARS-CoV-2-S1N. Mice were bled from retro-orbital vein at weeks 3, 5 , and 6 after immunization, and the obtained serum samples were diluted and used to evaluate S1-specific antibodies by enzyme-linked immunosorbent assay (ELISA). Serum samples obtained on Week 6 after vaccination were also used for microneutralization (NT) assay. Mice were maintained under specific pathogen-free conditions at the University of Pittsburgh, and all experiments were conducted in accordance with animal use guidelines and protocols approved by the University of Pittsburgh's Institutional Animal Care and Use (IACUC) Committee.

3.3.7 ELISA

Sera from all mice were collected prior to immunization (week 0) and at weeks indicated after immunization and evaluated for SARS-CoV-2-S1-specific IgG, IgG1, and IgG2a antibodies using ELISA [189]. Briefly, ELISA plates were coated with 200 ng of recombinant SARS-CoV-2-S1 protein (Sino Biological) per well overnight at 4°C in carbonate coating buffer (pH 9.5) and then blocked with PBS-T and 2% bovine serum albumin (BSA) for one hour. Mouse sera were serially diluted in PBS-T with 1% BSA and incubated overnight. After the plates were washed, anti-mouse IgG-horseradish peroxidase (HRP) (1:10000, SantaCruz) was added to each well and incubated for one hour. The plates were washed three times, developed with 3,3'5,5'-

tetramethylbenzidine, and the reaction was stopped. Next, absorbance was determined at 450 nm using a plate reader. For IgG1 and IgG2a ELISAs, mouse sera were diluted in PBS-T with 1% BSA and incubated overnight. After the plates were washed, biotin-conjugated IgG1 and IgG2a (1:1000, eBioscience) and biotin horseradish peroxidase (Av-HRP) (1:50000, Vector Laboratories) were added to each well and incubated for 1 hour. The plates were washed three times and developed with 3,3'5,5'-tetramethylbenzidine, the reaction was stopped, and absorbance at 450nm was determined using a plate reader.

3.3.8 Flow Cytometry and Analysis for Cellular Immune Responses

Antigen-specific T-cell responses in the spleen of BALB/cJ mice immunized as described above were analyzed after immunization by flow cytometry, adhering to the recently published guidelines [81]. Briefly, spleens were mashed and underwent erythrocyte lysis using the Mouse Erythrocyte Lysing Kit (R&D Systems, WL2000), remaining cells were used for cellular immune response analysis. Isolated splenocytes from vaccinated and PBS control mice were stimulated with PepTivator SARS-CoV-2-S1 (a pool of S1 MHC class I– and MHC class II– restricted peptides) or SARS-CoV-2-N (a pool of N MHC class I– and MHC class II– restricted peptides) overnight in the presence of protein transport inhibitors (Golgi Stop) for the last 4 hours. Unstimulated cells were used as negative controls. Phorbol myristate acetate (PMA) and ionomycin stimulated cells served as positive controls. Cell were washed with FACS buffer (PBS, 2 % FCS), incubated with Fc Block (BD Biosciences, 553142) for 5 min at 4 °C, and stained with surface marker antibody (Ab) stain for 20 min at 4 °C. Surface Abs were used as follows: anti-CD45 (30-F11, BV480, BD Biosciences), anti-TCRb (Alexa Fluor® 700, BD Biosciences), anti-CD4 (GK1.5, BUV650, Biolegend), anti-CD8a (53-6.7, BUV570, Biolegend). For dead cell

exclusion, cells were stained with Zombie NIR Fixable Viability dye (BioLegend) for 10 min at 4 °C and washed in FACS buffer. Intracellular cytokine staining (ICS) was performed on surface Ab-stained cells by first fixing and permeabilizing cells using the FoxP3 Transcription Factor Staining Buffer kit (eBioscience, 00-5523-00) following manufacturer's instructions. Intracellular staining with anti-IFN-γ Ab (XMG1.2, BV605, Biolegend) for 30 min at 4 °C was performed. Samples were run on an Aurora (Cytek) flow cytometer and analyzed with FlowJo v10 software (BD Biosciences). Live, antigen-specific, IFN-γ producing CD8+ and CD4+ T cells were identified according to the gating strategy in Supplementary Figure 1. Results for positive and negative controls are also available in Supplementary Figure 2.

3.3.9 SARS-CoV-2 Microneutralization Assay

Neutralizing antibody (NT-Ab) titers against SARS-CoV2 were defined according to the following protocol [379,380]. Briefly, 50 µl of sample from each mouse, in different dilutions, were added in two wells of a flat bottom tissue culture microtiter plate (COSTAR, Corning Incorporated, NY 14831, USA), mixed with an equal volume of 100 TCID50 of a SARS-CoV2 wildtype, Beta, or Gamma variant isolated from symptomatic patients, previously titrated and incubated at 33°C in 5% CO2. All dilutions were made in EMEM (Eagle's Minimum Essential Medium) with addition of 1% penicillin, streptomycin and glutamine and 5 γ/mL of trypsin. After 1 hour incubation at 33°C 5%CO2, 3×10^4 VERO E6 cells [VERO C1008 (Vero 76, clone E6, Vero E6); ATCC® CRL-1586TM] were added to each well. After 72 hours of incubation at 33°C 5% CO2 wells were stained with Gram's crystal violet solution (Merck KGaA, 64271 Damstadt, Germany) plus 5% formaldehyde 40% m/v (Carlo ErbaSpA, Arese (MI), Italy) for 30 min. Microtiter plates were then washed in running water. Wells were scored to evaluate the degree of cytopathic effect

(CPE) compared to the virus control. Blue staining of wells indicated the presence of neutralizing antibodies. Neutralizing titer was the maximum dilution with the reduction of 90% of CPE. A positive titer was equal or greater than 1:5. Sera from mice before vaccine administration were always included in microneutralization (NT) assay as a negative control.

3.3.10 ELISpot for Antibody Forming Cells

The frequency of SARS-CoV-2-specific antibody producing cells in the bone marrow of mice was determined by ELISpot assay 29 weeks after immunization using our established and previously published methods [375,376]. Briefly, 4-HBX plates were coated as described for ELISA assays, and non-specific binding was blocked with RPMI media containing 5% FCS. dilution series of cells of each individual bone marrow sample were plated in triplicates and incubated at 37 °C for 5 hours. Secondary Ab (anti-mIgG-alkaline phosphatase; Southern Biotech) was detected using 5-bromo-4-chloro-3- indolyl phosphate substrate (BCIP; Southern Biotech) in 0.5% low melting agarose (Fisher Scientific). Spots were counted using a binocular on a dissecting microscope and the detected numbers of IgG anti-SARS-CoV-2-S1 and anti-SARS-CoV-2-N antibody forming cells were calculated per million bone marrow cells.

3.3.11 Statistical Analysis

Statistical analyses were performed using GraphPad Prism v9 (San Diego, CA). Antibody endpoint titers and neutralization data were analyzed by Kruskal-Wallis test, followed by Dunn's multiple comparisons, T-cell data were analyzed by one-way Welch's ANOVA, followed by

Dunnett's T3 multiple comparisons. Significant differences are indicated by * $p < 0.05$. Comparisons with non-significant differences are not indicated.

3.4 Discussion

More immunization programs against SARS-CoV-2 are urgently needed to battle global vaccine inequity and new viral variants. Our study presents the development, and analysis in mice, of an Ad-based COVID vaccine incorporating novel antigen design (Ad5.SARS-CoV-2-S1N). Currently approved Ad-based SARS-CoV-2 vaccines, such as Oxford-AstraZenca, Janssen, CansinoBio, and Sputnik V COVID-19 vaccines, encode for full-length SARS-CoV-2 spike protein and are administered intramuscularly. Our vaccine encodes the gene for SARS-CoV-2-S1 subunit and SARS-CoV-2 N protein through a S1N fusion protein delivered in multiple administration routes (S.C., I.N., and I.M.). This study also investigates novel prime-boost immunization strategies leveraging subunit recombinant proteins that are relatively thermostable [38,46,416]. Further improvements could be achieved harnessing intracutaneous vaccination with microneedle arrays, which have been shown to deliver a wide range of recombinant DNA or protein vaccines [217,384–386].

Our studies suggest that a single vaccination of BALB/cJ mice via either I.N. or S.C. delivery of 5×10^{10} v.p. Ad5.SARS-CoV-2-S1N was capable of inducing antigen-specific IgG, Ig isotype switch, and a moderate neutralizing antibody response. We also show that Ad5.SARS-CoV-2-S1N shows a similar S1-specific antibody response, and neutralizing response, to Ad5.SARS-CoV-2-S1. We believe this is important as a concern with including proteins outside of the SARS-CoV-2 S protein is that it will decrease the antibody response against S. We show

that this is not the case and that inclusion of N, through S1N fusion antigen, does not reduce S1-specific antibody responses. S.C. delivery of Ad5.SAR-CoV-2-S1N induced a significantly increased S1-specific T cell response, when compared to S.C. delivery of AdΨ5 and S.C. delivery of Ad5.SARS-CoV-2-S1. We hypothesize that this increased S1-specific T-cell response to Ad5.SARS-CoV-2-S1N may be due to the inclusion of N-derived T-cell epitopes, in the fusion protein, aiding in processing and presentation of S1 by MHC molecules, especially for presentation to CD8 T cells; however, this needs to be further elucidated through mechanistic studies [317,417]. We also illustrate that this immunogenicity can be improved by homologous prime-boost strategies, using either S.C. or I.N. delivery. Particularly immunogenicity can further be improved through heterologous prime-boost, with traditional I.M. injection, using subunit recombinant S1 protein. Priming with low dose $(1 \times 10^{10}$ v.p.) of Ad5.S1N and boosting with either WT recombinant rS1 or B.1.351 recombinant rS1 induced a robust neutralizing response, which was sustained against immune evasive variants, and a long-lived antibody-forming cell response in the bone marrow 29 weeks post vaccination. Interestingly, boosting with B.1.351 recombinant rS1 did not increase the neutralizing response to SARS-CoV-2 Beta variant virus when compared to boosting with WT recombinant rS1. The results are promising and support the use of a heterologous prime-boost immunization routine using Ad5.S1N and subunit recombinant S1 protein to induce antigen-specific humoral and cellular responses, leading to generation of long-lived plasma cells, and a potent CD8^{+} T-cell response. For the subunit recombinant S1 protein anti- gens, it is important to note that these are non-adjuvanted monomeric S1 proteins, which may explain the relatively poor neutralization breadth seen after prime-boost vaccination in **Figure 16** for Groups 1–4. Our results suggest that monomeric non-adjuvanted subunit recombinant S1 protein can serve as an immunostimulatory booster and induces a robust neutralizing response to

SARS-CoV-2 variants. We believe that this also emphasizes the potential for currently approved protein subunit vaccines that incorporate adjuvants or nanoparticle design, such as NVX-coV2373. This is critical information as COVID-19 booster demand is rapidly increasing across the globe. A booster platform using recombinant S1 protein would be thermostable, easy to manufacture, and affordable; lending it to be a preferred method to achieve global COVID-19 vaccine equity.

An important limitation regarding our findings concerning intranasal vaccination of Ad5.SARS-CoV-2-S1N is that we did not investigate key mucosal immunity aspects, such as IgA production. Indeed, mucosal immunity plays an important role in preventing SARS-CoV-2 infection [418]. Our future studies will not only investigate mucosal IgA and IgM production post intranasal administration but also mechanistically investigate the kinetics of intranasal immunization through isolation of tissues in closer proximity to the nasal cavity. Particularly, the lack of induction of CD4$^+$ and CD8$^+$ T-cell response to intranasal vaccination could be attributed to isolating splenocytes, rather than mucosa-associated lymph node tissue (MALT) or conducting bronchoalveolar lavage (BAL). In our future studies, we will isolate MALT and lung tissue post intranasal vaccination to investigate the localized cellular immune response post intranasal immunization. Our future studies will also include conducting BAL on intranasally immunized mice to better investigate local immunity.

We believe that the increasing CD8$^+$ T-cell response through including the N protein in vaccine formulation will not only help by introducing more conserved regions of SARS-CoV-2 to the immune system, potentially allowing for resistance against emerging variants, but will also assist in viral clearance. This is particularly important in the context of long COVID and in populations that are at high risk of SARS-CoV-2 morbidity and mortality where the T-cell response has been shown to play an important role [311,312,319–321]. While previous clinical translation

of Ad vaccines has been hampered by pre-existing immunity against the Ad viral capsid, CanSino Convidicea Vaccine (Ad5-nCoV), encoding for the full S protein, was able to overcome pre-existing vector immunity while using intramuscular immunization [367,368]. Immunization with Ad-based vaccines, such as Ad5.S1N, could be an important tool to combat COVID-19 global vaccine inequality and the emergence of immune evasive SARS-CoV-2 variants. These finding concerning the immunogenicity of the S1N fusion antigen also adds knowledge to general COVID-19 vaccine approaches as S1N can be expressed through other vaccine vectors, such a mRNA or DNA technologies.

BALB/cJ mice have historically been used to investigate numerous different coronavirus vaccines and represent a reliable model for testing of immunogenicity of Ad5.SARS-CoV-2-S1N [217,274,343]. However, it is difficult to extrapolate our results in BALB/cJ mice to potential immunogenicity in humans. Particularly, our findings on the potency of S1- and N-specific T-cell response to Ad5.SARS-CoV-2-S1N vaccination may not directly translate to responses in humans due to the differences in human leukocyte antigen (HLA) and mouse major histocompatibility complex (MHC). The difference in HLA and MHC may explain the lack of N-specific T-cell response after vaccination, as N-derived epitopes may be less able to bind to mouse MHC than S1-derived epitopes. The lack of CD4 T-cell responses may also be explained by the model organism, BALB/cJ mice, which have been shown to have an abrogated CD4 T-cell response when compared to C57BL/6 mice [283]. To this effect, future studies will use more translatable animal models such as hACE2 mice and rhesus macaques. Our future studies will also include animal challenge models with live SARS-CoV-2 virus to investigate protection against infection and death. Along with these studies, we will also harvest axillary and cervical lymph nodes to investigate the specific kinetics and location of T-cell immunity post intramuscular vaccination.

Taken together, this study illustrates the potential of Ad5.SARS-CoV-2-S1N as it induces significant antigen-specific humoral and cellular immune responses against SARS-CoV-2. Particularly, heterologous prime-boost vaccine with low dose Ad5.SARS-CoV-2-S1N along with subunit recombinant S1 protein have the potential to induce a very effective virus-specific immune response against COVID-19 and emerging SARS-CoV-2 variants.

3.5 Acknowledgements

4.0 Trivalent Variant-Specific SARS-CoV-2 S1 Subunit Protein Vaccination Induces Broad Humoral Immune Responses in BALB/c Mice

Text from this chapter has been modified from the publication: **Khan, M. S.**, Kim, E., Huang, S., Kenniston, T. W. & Gambotto, A#. Trivalent SARS-CoV-2 S1 Subunit Protein Vaccination Induces Broad Humoral Responses in BALB/c Mice. *Vaccines* **11**, 314 (2023). # corresponding author. PMID: 36851191

4.1 Introduction

The current COVID-19 pandemic, caused by severe acute respiratory syndrome coronavirus 2 (SARS-CoV-2), continues to have a significant impact on human and animal health globally [327,400,419]. The COVID-19 pandemic has over 637 million cases, 6.5 million deaths, with 12.9 billion COVID-19 vaccine doses administered across the human population, as of 29 November 2022 [224]. Approved COVID-19 vaccines have been a vital tool in reducing mortality and morbidity caused by SARS-CoV-2 infection. However, emerging immune-evasive SARS-CoV-2 variants, fueled by worldwide COVID-19 vaccine distribution inequalities, have left many low to middle income countries without access to variant-specific vaccines better suited for the evolving SARS-CoV-2 variant landscape [1,13,249,250]. Particularly, Delta (B.1.617.2), Omicron (BA.1), and Omicron sub lineages (BA.2, BA.4, BA.5, etc.) have shown to have the greatest resistance to vaccine-induced and infection-acquired immunity, leading to significant COVID-19 infection waves [250,251,420–422].

The spike (S) protein of SARS-CoV-2 has been the main target of currently approved COVID-19 vaccines and of most COVID-19 vaccines in development [336]. The S protein mediates virus binding and infection of susceptible cells through interaction with host receptor angiotensin-converting enzyme 2 (ACE2) [338]. The S protein is composed of two subunits, the S1 subunit which contains the receptor binding domain (RBD) that binds to ACE2, and the S2 subunit that allows for cell fusion and viral entry [227,423]. It has been well established that antibodies targeting the S protein, and the RBD within the S1 subunit, are able to block the binding of SARS-CoV-2 to the cell receptor and prevent infection of susceptible cells [236,307,339,403,424]. Protein subunit vaccine approaches against COVID-19 are highly favorable for worldwide equitable distribution due to their low cost per dose, relative thermostability, and excellent safety profile [38,46,416,425]. Our previously published reports on vaccines against SARS-CoV-1, Middle-East respiratory syndrome coronavirus (MERS-CoV), and SARS-CoV-2 have demonstrated the ability of S1 subunit targeting vaccines to generate neutralizing antibody responses against Beta coronaviruses [217,343,344,426,427].

Of particular interest is the investigation of novel COVID-19 vaccines, which may be able to induce broader antibody responses against multiple variants through multivalent vaccine immunization. A multivalent vaccine is a traditional approach used to increase antigen coverage against ever-changing pathogens such as COVID-19 [428–430]. However, it is necessary to investigate whether increasing valency of COVID-19 vaccines decreases the overall potency of the immune response or abrogates the per-variant host-antibody response. Indeed, a bivalent COVID-19 vaccine approach, through the mRNA platform, has been shown to have increased immunogenicity when compared to the monovalent approach in humans [431]. Trivalent vaccine approaches have been shown to increase immunogenicity of various vaccines, especially in the context of influenza

[432–436]. Preclinical trivalent COVID-19 vaccines have also been shown to have increased immunogenicity when compared to monovalent approaches; however, these studies did not incorporate SARS-CoV-2 Omicron BA.1 variant of concern (VOC), an important piece of information explored by our study [434,435].

Here, we compared the immunogenicity of wild-type Wuhan spike S1 (WU-S1RS09cg), Delta variant-specific spike S1 (Delta S1-RS09cg), and Omicron variant-specific spike S1 (OM S1-RS09cg) subunit protein vaccines delivered either as a monovalent antigen or a combination of the three in trivalent antigen form (Wu/Delta/OM S1-RS09cg). We found that while monovalent vaccination resulted in substantial humoral response against S, a trivalent approach induced a broader humoral response with more coverage against antigenically distinct variants particularly in the context of monovalent Omicron-specific S1. The trivalent approach of Wu/Delta/OM S1-RS09cg showed increased ACE2 binding inhibition, and increased S1 IgG endpoint titer at early timepoints, against Wuhan and Delta S than monovalent OM S1-RS09cg. Our studies demonstrate the utility of protein subunit vaccines against COVID-19 and contribute insights into the impact of variant-specific COVID-19 vaccine approaches on the immune response in the context of the current SARS-CoV-2 variant landscape.

4.2 Results

4.2.1 Design and Expression of Recombinant Proteins

Recombinant proteins of SARS-CoV-2-S1, pAd/S1 Wu, pAd/S1 Delta, pAd/S1 Omicron (BA.1) were generated by subcloning the codon-optimized SARS-CoV-2-S1 gene having C-tag

into the shuttle vector, pAd (GenBank U62024) at SalI and NotI sites (**Fig. 18**). To determine

SARS-CoV-2-S1 expression and purity post C-tagXL affinity matrix purification, proteins were

separated by 10% SDS-PAGE and assessed by silver staining (**Fig. 18B**). The purified recombinant

proteins WU S1-RS09cg (lane 1), Delta S1-RS09cg (lane 2), and Omicron S1-RS09cg (lane 3)

were visualized at their expected glycosylated monomeric molecular weights of about 110 kDa

under the denaturing reduced conditions. The proteins were also recognized by a polyclonal anti-

spike SARS-CoV-2 antibody through western blot (**Fig. 18C**).
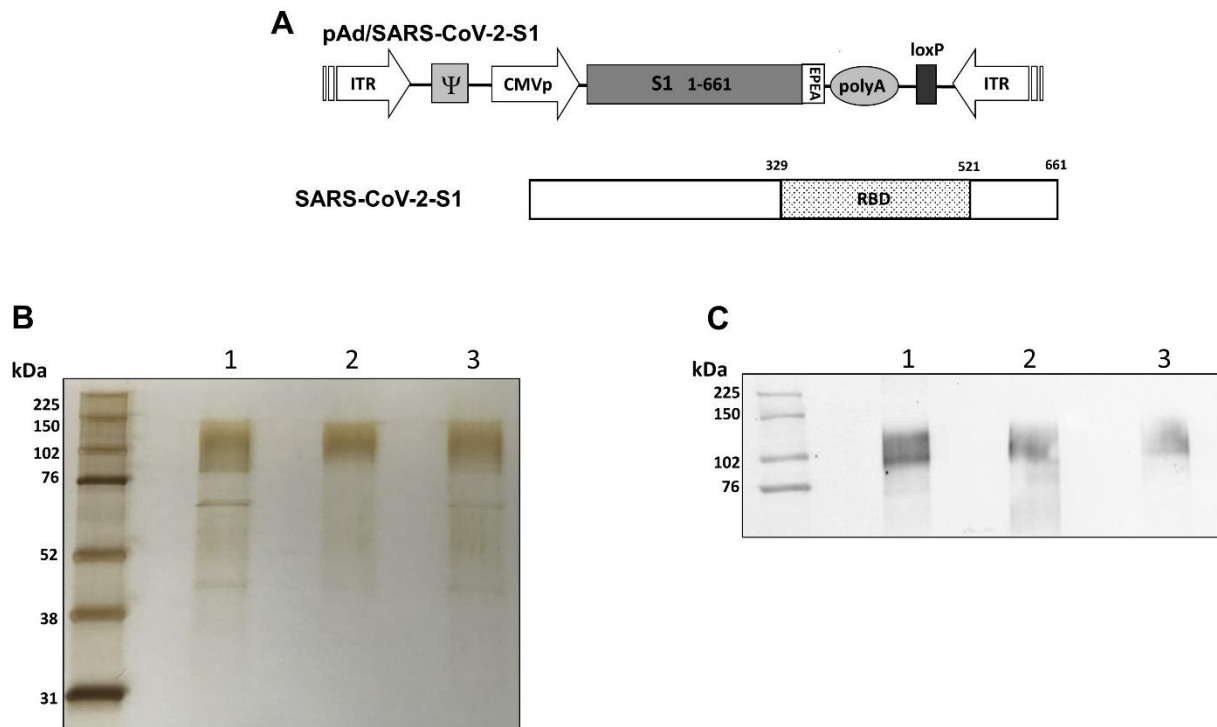
Figure 18: Construction of recombinant SARS-CoV-2-S1 protein expressing plasmid. (A) Shuttle vector carrying

the codon-optimized wild-type (Wuhan), Delta variant, and Omicron variant (BA.1) SARS-CoV-2-S1 gene encoding

N-terminal 1-661 with c-tag (EPEA) was designed as shown in the diagram. ITR: inverted terminal repeat; RBD:

receptor binding domain. (B) Silver-stained reducing SDS-PAGE gel of purified Expi293 cell derived Wuhan (WU)

S1-RS09cg (Lane 1), Delta S1-RS09cg (Lane 2), and Omicron (OM) S1-RS09cg (Lane 3). (C) Detection of the SARS-

CoV-2-S1 proteins by western blot with purified proteins using anti S SARS-CoV-2 polyclonal antibody; Wuhan (WU) S1-RS09cg (Lane 1), Delta S1-RS09cg (Lane 2), and Omicron (OM) S1-RS09cg (Lane 3).

4.2.2 Protein Subunit SARS-CoV-2 S1 Vaccines Induce Robust and Cross-Variant Binding IgG Responses

To assess the magnitude of the antibody response and the long-term persistence of immunogenicity, we first determined Wuhan, Delta, and Omicron (BA.1) specific IgG antibody endpoint titers (EPT) in the sera of vaccinated mice. Mice were prime and boosted on week 3 with either 45 µg of WU S1-RS09cg, Delta S1-RS09cg, OM S1-RS09cg, or a trivalent cocktail of the three antigens (15 µg WU S1-RS09cg, 15 µg Delta S1-RS09cg, 15 µg OM S1-RS09cg) in a single immunization. We collected serum samples from all mice prior to immunization, which were used set the endpoint titer cutoff for all antibody ELISA's [437]. Serum samples collected on weeks 3, 5, 7, 9, 12, 16, and 20 after prime immunization were serially diluted to determine SARS-CoV-2-S1-specific IgG titers against Wuhan S1 (**Fig. 19**), Delta S1 (**Fig. 20**), and Omicron BA.1 (**Fig. 21**) for each immunization group using ELISA.

Figure 19: Wuhan S1-specific IgG antibody responses in mice after prime-boost immunization in BALB/c mice.
BALB/c mice (n = 5 mice per groups) were immunized intramuscularly with 45 μg of either WU S1-RS09cg, Delta S1-RS09cg, OM S1-RS09cg or trivalent WU/Delta/OM S1-RS09cg and received a homologous booster at week 3. On weeks 3, 5, 7, 9, 12, 16, and 20 sera from mice were collected, serially diluted (200×), and tested for the presence of Wuhan SARS-CoV-2-S1-specific IgG antibody levels by ELISA. Significance was determined by Kruskal-Wallis test followed by Dunn's multiple comparisons (* $p < 0.05$). Horizontal solid lines represent geometric mean antibody titers. Serum collected on week 0, prior to immunization, were used to set the ELISA endpoint titer cutoff.

Delta S1 IgG

Figure 20: Delta S1-specific IgG antibody responses in mice after prime-boost immunization in BALB/c mice.

BALB/c mice (n = 5 mice per groups) were immunized intramuscularly with 45 µg of either WU S1-RS09cg, Delta S1-RS09cg, OM S1-RS09cg or trivalent WU/Delta/OM S1-RS09cg and received a homologous booster at week 3. On weeks 3, 5, 7, 9, 12, 16, and 20 sera from mice were collected, serially diluted (200×), and tested for the presence of Delta variant SARS-CoV-2-S1-specific IgG antibody levels by ELISA. Significance was determined by Kruskal-Wallis test followed by Dunn's multiple comparisons (* $p < 0.05$). Horizontal solid lines represent geometric mean antibody titers. Serum collected on week 0, prior to immunization, were used to set the ELISA endpoint titer cutoff.

BA.1 S1 IgG
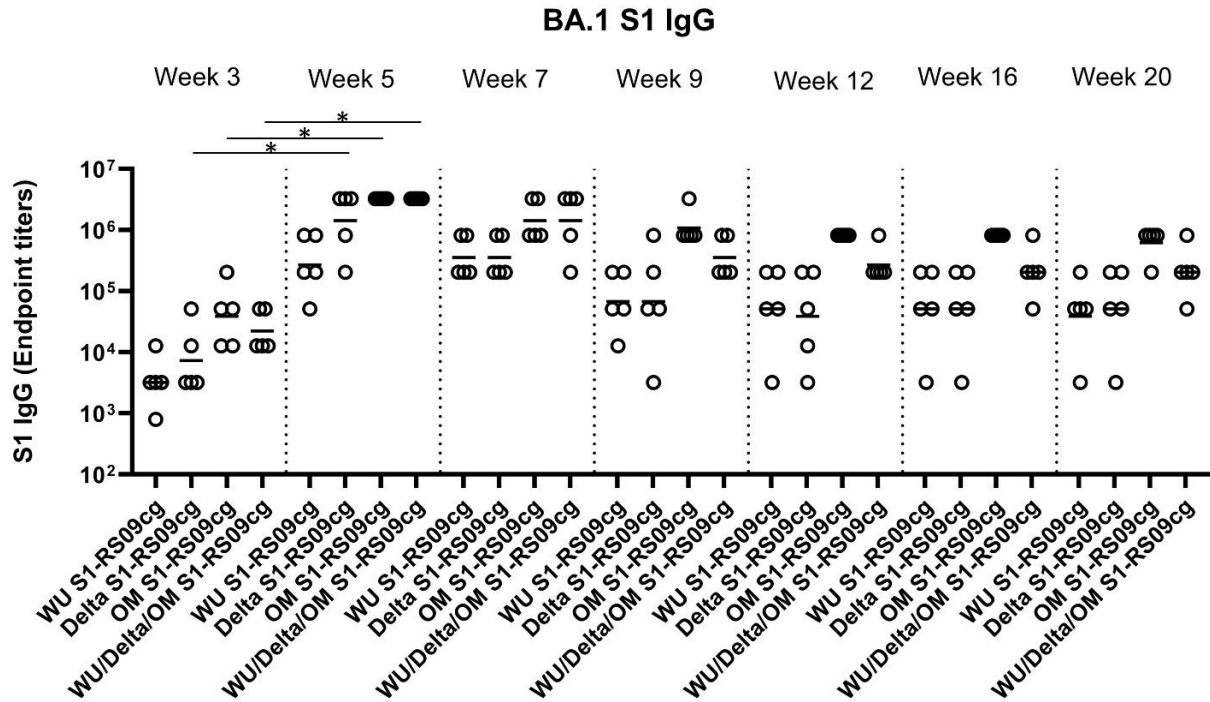
Figure 21: Omicron (BA.1) S1-specific IgG antibody responses in mice after prime-boost immunization in BALB/c mice. BALB/c mice (n = 5 mice per groups) were immunized intramuscularly with 45 μg of either WU S1-RS09cg, Delta S1-RS09cg, OM S1-RS09cg or trivalent WU/Delta/OM S1-RS09cg and received a homologous booster at week 3. On weeks 3, 5, 7, 9, 12, 16, and 20 sera from mice were collected, serially diluted (200×), and tested for the presence of Omicron (BA.1) SARS-CoV-2-S1-specific IgG antibody levels by ELISA. Significance was determined by Kruskal-Wallis test followed by Dunn's multiple comparisons (* $p < 0.05$). Horizontal solid lines represent geometric mean antibody titers. Serum collected on week 0, prior to immunization, were used to set the ELISA endpoint titer cutoff.

Against Wuhan S1, all vaccinated groups had significantly higher geometric mean Wuhan S1 IgG EPT at week 5 when compared to week 3, illustrating the superior immunogenicity conferred by boost immunization (**Fig. 19**, $p < 0.05$, Kruskal-Wallis test, followed by Dunn's multiple comparisons). Interestingly, WU S1-RS09cg vaccinated mice achieved lower geometric mean Wuhan S1 IgG EPT by week 9 when compared to the other immunization groups (Figure

113

2). Indeed, trivalent WU/Delta/OM S1-RS09cg had increased Wuhan S1 IgG EPT when compared to monovalent OM S1-RS09cg at weeks 3, 5, and 7 (**Fig. 19**). However, as waning of the immune response occurred, the trivalent WU/Delta/OM S1-RS09cg vaccinated mice reached similar geometric mean Wuhan S1 IgG EPT as monovalent OM S1-RS09cg vaccinated mice at week 9 with waning continuing to occur through week 20 (**Fig. 19**).

Against Delta S1, Delta S1-RS09cg and Wu/Delta/OM S1-RS09cg vaccinated mice had the highest geometric mean Delta IgG EPT at week 3 (**Fig. 20**). Only OM S1-RS09cg and WU/Delta/OM S1-RS09cg vaccinated mice achieved significantly higher geometric mean Delta S1 IgG EPT at week 5 when compared to week 3 (**Fig. 20**, $p < 0.05$, Kruskal-Wallis test, followed by Dunn's multiple comparisons). However, at week 5 OM S1-RS09cg vaccinated mice and Wu/Delta/OM S1-RS09cg vaccinated mice had the greatest geometric mean Delta IgG EPT (**Fig. 20**). Interestingly, OM S1-RS09cg vaccinated mice and Wu/Delta/OM S1-RS09cg vaccinated mice Delta S1 IgG antibody response waned less from week 5 through week 20 than the other immunization groups (**Fig. 20**).

Against Omicron S1, Delta S1-RS09cg, OM S1-RS09cg, and Wu/Delta/OM S1-RS09cg vaccinated mice had significantly increased Omicron S1 IgG EPT at week 5 when compared to week 3 (**Fig. 21**, $p < 0.05$, Kruskal-Wallis test, followed by Dunn's multiple comparisons). Both OM S1-RS09cg and trivalent Wu/Delta/OM S1-RS09cg vaccinated mice achieved the highest geometric mean Omicron S1 IgG EPT by week 3 and through week 20 (**Fig. 21**). A difference between OM-S1RS09cg and Wu/Delta/OM S1-RS09cg geometric mean Omicron S1 IgG EPT occurred at week 9, with OM-S1RS09cg vaccinated mice having modestly higher EPT than trivalent vaccinated mice through week 20 (**Fig. 21**).

To assess whether the IgG antibody response was Th1- or Th2-specific, serum samples were collected at week 5 and serially diluted to determine Wuhan and BA.1-specific S1, IgG1 (indicating a Th2 bias) and IgG2a (indicating a Th1 bias) endpoint titers for each immunization group (**Fig. 22A–D**). Interestingly, against Wuhan S1 all vaccinated mice groups achieved similar IgG1 and IgG2a geometric mean S1 IgG1 and IgG2a EPT, with no significant differences between groups (**Fig. 22A, B**). Differences between vaccine groups were illuminated against BA.1 S1 (**Fig. 22C, D**). Both OM-S1RS09cg and trivalent WU/Delta/OM S1-RS09cg vaccinated mice had the greatest geometric mean Omicron-S1 IgG1 EPT than WU S1-RS09cg and Delta S1-RS09cg vaccinated mice (**Fig. 22C, D**). OM S1-RS09cg vaccinated mice achieved the highest BA.1 S1 IgG2a geometric mean EPT (**Fig. 22C, D**). As expected for unadjuvanted protein subunit vaccine in BALB/c mouse, all vaccinated groups had a trend to a IgG1 dominant IgG response, indicating a Th2 bias.
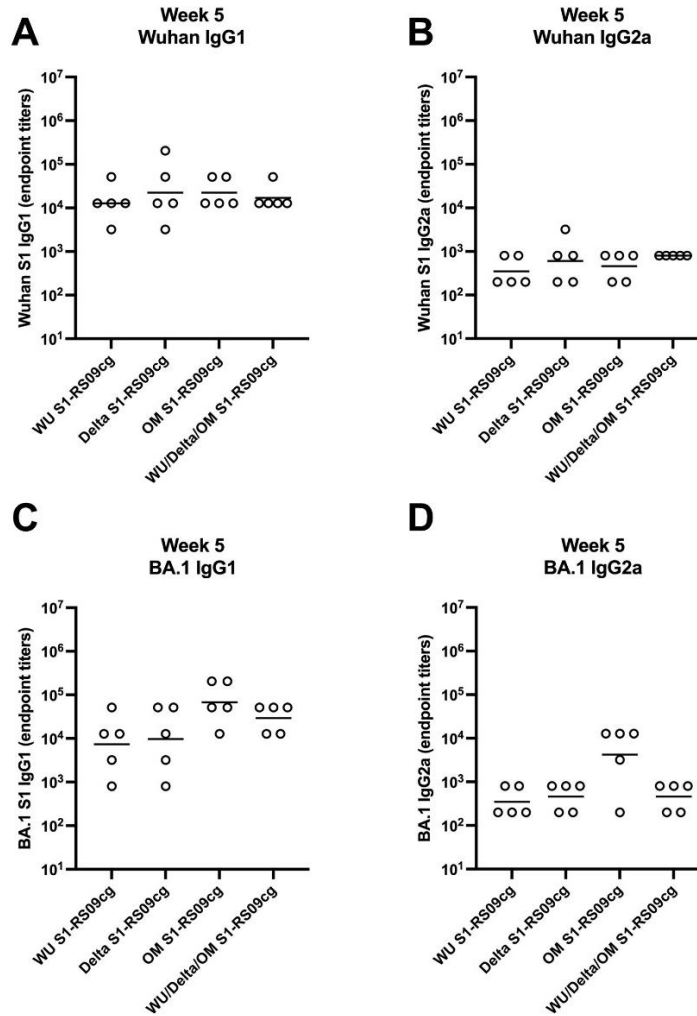
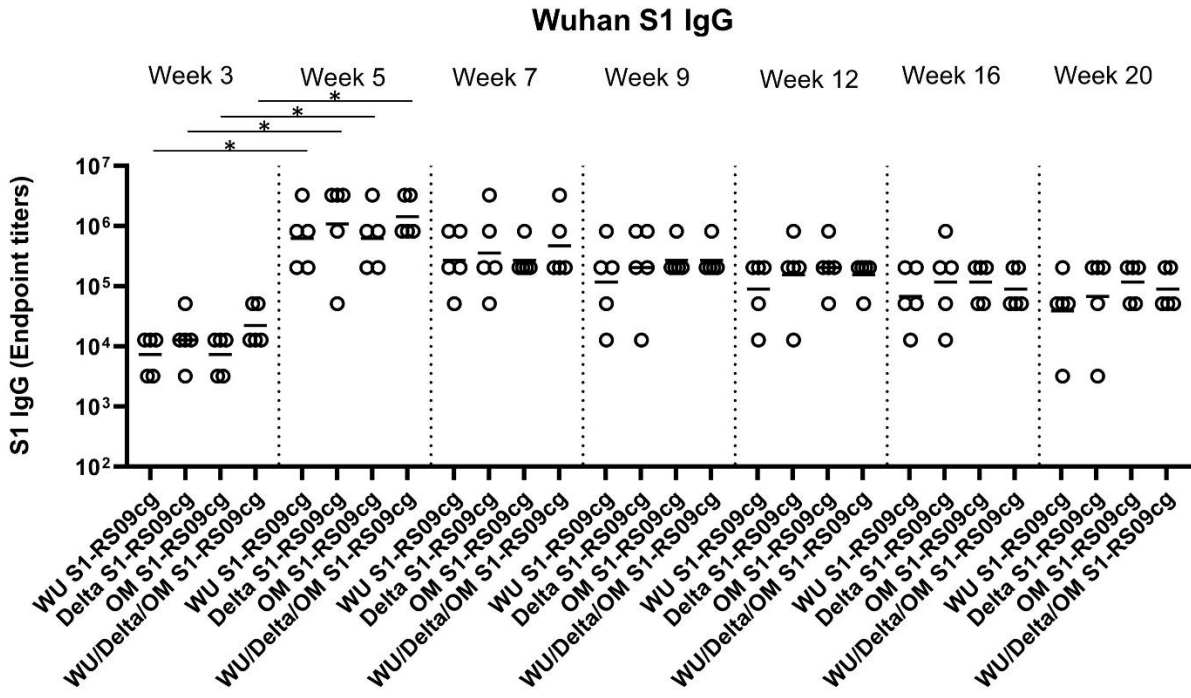**Figure 22: Wuhan and Omicron (BA.1)-specific IgG1 and IgG2a antibody responses in mice after prime-boost immunization in BALB/c mice.** BALB/c mice (n = 5 mice per groups) were immunized intramuscularly with 45 μg of either WU S1-RS09cg, Delta S1-RS09cg, OM S1-RS09cg or trivalent WU/Delta/OM S1-RS09cg and received a homologous booster at week 3. On weeks 3, 5, 7, 9, 12, 16, and 20 sera from mice were collected, serially diluted (200×), and tested for the presence of Wuhan and Omicron (BA.1) SARS-CoV-2-S1-specific IgG1 and IgG2a antibody levels by ELISA. Significance was determined by Kruskal-Wallis test followed by Dunn's multiple comparisons (* $p < 0.05$). Horizontal solid lines represent geometric mean antibody titers. Serum collected on week 0, prior to immunizat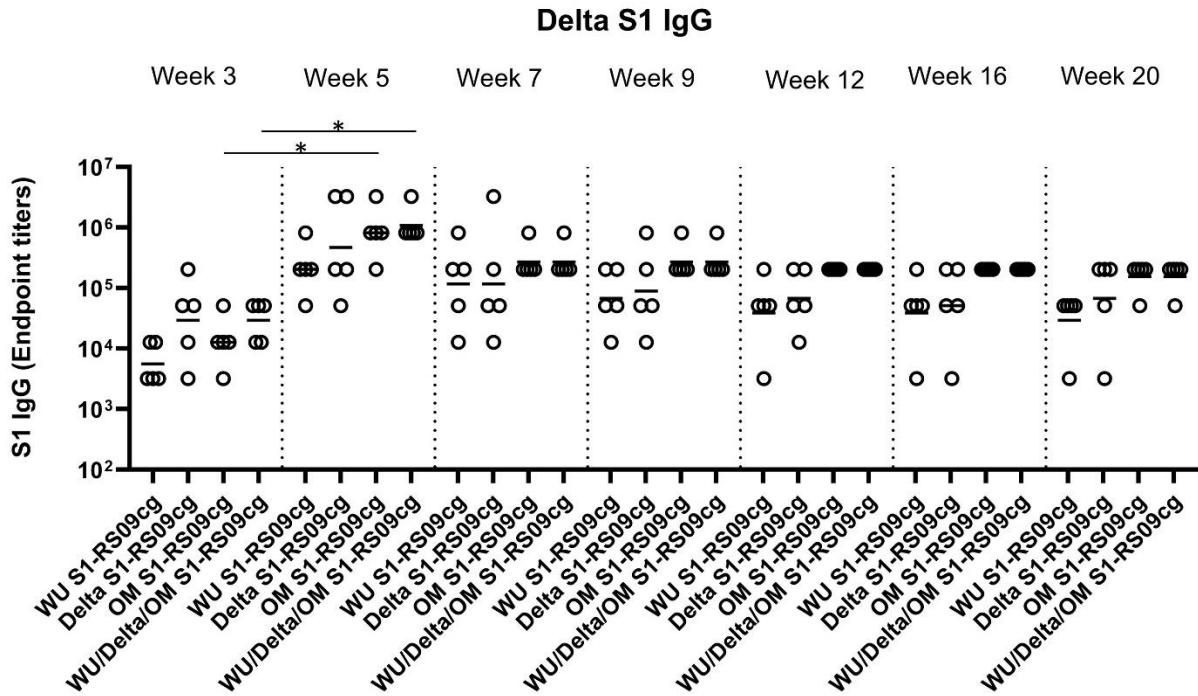ion, were used to set the ELISA endpoint titer cutoff. (A) Week 5 Wuhan S1 IgG1; (B) Week 5 Wuhan S1 IgG2a; (C) Week 5 BA,1 S1 IgG1; (D) Week 5 BA.1 S1 IgG2a.

These results suggest that Wuhan S1-RS09cg, Delta S1-RS09cg, OM-S1RS09cg, and trivalent WU/Delta/OM S1-RS09cg all stimulated a robust IgG binding antibody response in BALB/c mice against Wuhan S1, Delta S1, and Omicron (BA.1) S1.

4.2.3 ACE2 Binding Inhibition

Competitive immunoassays for quantifying inhibition of the spike-ACE2 interaction have been shown to correlate well with live-virus neutralizing tests and serve as a convenient multiplex method to determine the neutralizing capacity of vaccinated sera [305,306,438,439]. To investigate the neutralizing capabilities of antibodies induced by vaccination we used the Meso Scale Discovery (MSD) V-PLEX SARS-CoV-2 (ACE2) Kit. This measures the inhibition of binding between angiotensin converting enzyme-2 (ACE2) and trimeric spike protein of SARS CoV-2 variants. We used kit Panel 25 including Wuhan S and spikes from immune evasive variants; BA.1, BA.2, AY.4 (Delta lineage), BA.3, BA.1 + R346K mutation, BA.1 + L52R mutation, B.1.1.7 (Alpha), B.1.351 (Beta), and B.1.1640.2. Sera from vaccinated animals were examined at week 5 and week 7, the peak of the IgG antibody responses (**Figs. 19-21**). **Fig. 23A, B** depict the median ACE2-binding percent inhibition of each vaccinated mice group sera at week 5 and week 7, respectively. **Fig. 23C–F** depict each vaccination group ACE2-binding percent inhibition individually; WU-S1RS09cg vaccinated mice (**Fig. 23C**), Delta S1-RS09cg vaccinated mice (**Fig. 23D**), OM-S1RS09cg vaccinated mice (**Fig. 23E**), and trivalent WU/Delta/OM S1-RS09cg vaccinated mice (**Fig. 23E**). Antibodies blocking ACE2 and trimeric S binding were detected in all vaccination groups. Interestingly, WU S1-RS09cg vaccinated mice achieved the lowest median ACE2-binding inhibition against Wuhan S, AY.4 (Delta), B.1.1.7, B.1.351, and B.1.640.2 at weeks 5 and 7 when compared to other vaccination groups **Fig. 23A, B**). Delta S1-RS09cg vaccinated mice had a robust

ACE2-binding inhibition response against WU S, AY.4 (Delta), B.1.1.7, B.1.351, and B.1.640.2; with a diminished response against Omicron (BA.1) and Omicron sub lineages (**Fig. 23A, B**). OM-S1RS09cg vaccinated mice had moderate to high median ACE2 binding inhibition against all S tested, with robust inhibition of ACE2 binding of Omicron and Omicron sub lineages, when compared to other vaccination groups at weeks 5 and 7 (**Fig. 23A, B**). Trivalent WU/Delta/OM S1-RS09cg, when compared to the monovalent counterparts, had increased coverage of median ACE-2 binding inhibition against all variants tested (**Fig. 23A, B**). Notably, when comparing OM S1-RS09cg vaccinated mice to trivalent WU/Delta/OM S1-RS09cg vaccinated mice, trivalent vaccinated mice had greater median ACE2-binding percent inhibition against WU S, BA.2, AY.4 (Delta), BA.1 + R346K, B.1.1.7, B.1.351, and B.1.640.2 (**Fig. 23A, B**).
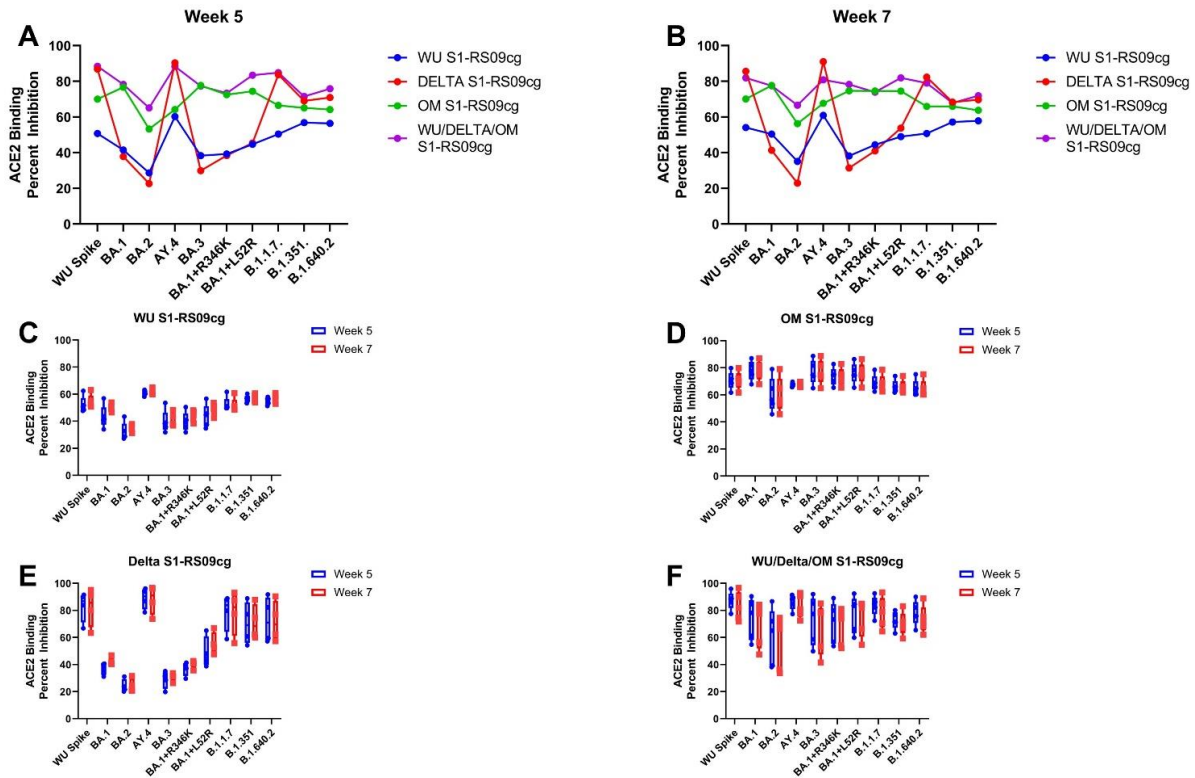
Figure 23: Percent ACE2 binding inhibition of neutralizing antibodies against SARS-CoV-2 variant elicited by monovalent and trivalent immunization in BALB/c mice. Antibodies in sera capable of neutralizing the interaction between SARS-CoV-2 Wuhan, BA.1, BA.2, AY.4 (Delta lineage), BA.3, BA.1 + R346K mutation, BA.1 + L52R mutation, B.1.1.7 (Alpha), B.1.351 (Beta), and B.1.1640.2. variant spike and ACE2 were examined in all animals at week 5 and week 7. (A) Per immunization group median ACE2 binding percent inhibition of WU S1-RS09cg vaccinated mice (blue dots), Delta S1-RS09cg vaccinated mice (red dots), OM S1-RS09cg vaccinated mice (green dots), and OM S1-RS09cg vaccinated mice (purple dots) at week 5 against each SARS-CoV-2 variant. (B) Per immunization group median ACE2 binding percent inhibition of WU S1-RS09cg vaccinated mice (blue dots), Delta S1-RS09cg vaccinated mice (red dots), OM S1-RS09cg vaccinated mice (green dots), and OM S1-RS09cg vaccinated mice (purple dots) at week 7 against each SARS-CoV-2 variant. Figure 23C–F depict each vaccination group individual mice ACE2-binding percent inhibition against all variants at week 5 (blue box and whisker plot) and week 7 (red box and whisker plot). Figure 23C WU S1-RS09cg elicited antibodies percent ACE2 binding inhibition. Figure 23D Delta S1-RS09cg elicited antibodies percent ACE2 binding inhibition. Figure 23E OM S1-RS09cg elicited antibodies percent ACE2 binding inhibition. Figure 23F WU/Delta/OM S1-RS09cg elicited antibodies percent ACE2

binding inhibition. Box and whisker plots represent the median and upper and lower quartile (box) with min and max (whiskers).

To combine the data on Wuhan, Delta, and Omicron (BA.1) S binding IgG EPT and ACE2-percent binding inhibition we plotted the respective mean values at week 5 against each other (**Fig. 24A–C**). In the context of Wuhan S, Delta S1-RS09cg and trivalent WU/Delta/OM S1-RS09cg vaccinated mice grouped together with the highest mean S1 IgG EPT and mean ACE2 binding inhibition (**Fig. 24A**). Against Delta S, Delta S1-RS09cg and trivalent WU/Delta/OM S1-RS09cg vaccinated mice group together with the highest mean S1 IgG EPT and mean ACE2 binding inhibition (**Fig. 24B**). For BA.1 S, OM S1-RS09cg and trivalent WU/Delta/OM S1-RS09cg vaccinated mice grouped together with the highest mean S1 IgG EPT and mean ACE2 binding inhibition (**Fig. 24C**).
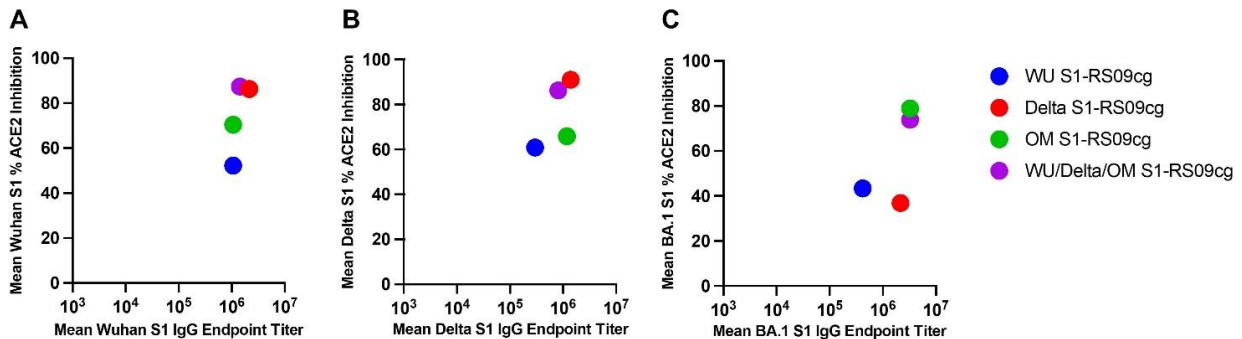
Figure 24: Variant-specific binding IgG and ACE2-percent binding inhibition in BALB/c mice. Wuhan, Delta, and Omicron (BA.1) S binding IgG mean EPT and mean ACE2-percent binding inhibition per variant plotted against the respective mean values at week 5. (A) Wuhan Week 5 binding IgG and ACE2-percent binding inhibition; (B) Delta Week 5 binding IgG and ACE2-percent binding inhibition; (C) BA.1 Week 5 binding IgG and ACE2 percent binding inhibition.

120

Taken together, a prime and boost of non-adjuvanted recombinant S1 protein subunit vaccine induced a robust humoral antibody response against SARS-CoV-2 in BALB/c mice. Particularly, trivalent WU/Delta/OM vaccinated mice induced a broad and cross-reactive neutralizing antibodies against SARS-CoV-2 variants with increased breadth when compared to monovalent WU S1-RS09cg, Delta S1-RS09cg, and OM S1-RS09cg vaccinated mice.

4.3 Materials and Methods

4.3.1 Construction of Recombinant Protein Expressing Vectors

The coding sequence for SARS-CoV-2-S1 amino acids 1 to 661; having C-terminal tag known as 'C-tag', composed of the four amino acids (aa), glutamic acid-proline-glutamic acid-alanine (E-P-E-A) flanked with Sal I & Not I was codon-optimized using UpGene algorithm for optimal expression in mammalian cells [217,371]. The construct also contained a Kozak sequence (GCCACC) at the 5′ end. The plasmid, pAd/SARS-CoV-2-S1 was then created by subcloning the codon-optimized SARS-CoV-2-S1 inserts into the shuttle vector, pAdlox (GenBank U62024), at Sal I/Not I sites. The plasmid constructs were confirmed by DNA sequencing.

4.3.2 Transient Production in expi293 Cells

pAd/S1RS09cg proteins were amplified and purified using ZymoPURE II plasmid maxiprep kit (Zymo Research). For Expi293 cell transfection, we used ExpiFectamieTM 293 Transfection Kit (ThermoFisher, Waltham, MA, USA) and followed the manufacturer's

instructions. Cells were seeded 3.0×106 cells/mL one day before transfection and grown to 4.5–5.5 $\times$ 106 cells/mL. 1 µg of DNA and ExpiFectamine mixtures per 1 mL culture were combined and incubated for 15 min before adding into 3.0×106 cells/mL culture. At 20 h post-transfection, enhancer mixture was added, and culture was shifted to 32 °C. The supernatants were harvested 5 days post transfection and clarified by centrifugation to remove cells, filtration through 0.8 µm, 0.45 µm, and 0.22 µm filters and either subjected to further purification or stored at 4 °C before purification.

4.3.3 Purification of Recombinant Proteins

The recombinant proteins were purified using a CaptureSelect™ C-tagXL Affinity Matrix prepacked column (ThermoFisher) and followed the manufacturer's guideline [415]. Briefly, The C-tagXL column was conditioned with 10 column volumes (CV) of equilibrate/wash buffer (20 mM Tris, pH 7.4) before sample application. Supernatant was adjusted to 20 mM Tris with 200 mM Tris (pH 7.4) before being loaded onto a 5-mL prepacked column per the manufacturer's instructions at 5 mL/min rate. The column was then washed by alternating with 10 CV of equilibrate/wash buffer, 10 CV of strong wash buffer (20 mM Tris, 1 M NaCl, 0.05% Tween-20, pH 7.4), and 5 CV of equilibrate/wash buffer. The recombinant proteins were eluted from the column by using elution buffer (20 mM Tris, 2 M $MgCl_2$, pH 7.4). The eluted solution was concentrated and desalted with preservative buffer (PBS) in an Amicon Ultra centrifugal filter devices with a 50,000 molecular weight cutoff (Millipore). The concentrations of the purified recombinant proteins were determined by the Bradford assay using bovine serum albumin (BSA) as a protein standard, aliquoted, and stored at $-80°C$ until use.

4.3.4 SDS-PAGE, Silver Staining, and Western Blot

The purified proteins were subjected to sodium dodecyl sulfate polyacrylamide gel electrophoresis (SDS-PAGE), Silver Staining, and Western blot. Briefly, after the supernatants were boiled in Laemmli sample buffer containing 2% SDS with beta- mercaptoethanol (β-ME), the proteins were separated by Tris-Glycine SDS-PAGE gels and transferred to nitrocellulose membrane. After blocking for 1 h at room temperature (RT) with 5% non-fat milk in TBS-T, rabbit anti-SARS-CoV spike polyclonal antibody (1:3000) (Sino Biological), or rabbit anti-SARS-CoV nucleoprotein (1:3000) (Sino Biological) was added and incubated overnight at 4 °C as primary antibody, and horseradish peroxidase (HRP)-conjugated goat anti-rabbit IgG (1:10,000) (Jackson immuno research) was added and incubated at RT for 1 hs as secondary antibody. After washing, the signals were visualized using ECL Western blot substrate reagents and iBright 1500 (Thermo Fisher).

4.3.5 Animals and Immunization

At week 0 female BALB/c mice (n = 5 animals per group) were bled from retro-orbital vein and primed with 45 µg of either WU S1-RS09cg, Delta S1-RS09cg, OM S1-RS09cg, or trivalent WU/Delta/OM S1-RS09cg. Mice were bled on week 3 and received a homologous booster of 45 µg. Mice were bled on week 5, 7, 9, 12, 16, and 20. Mice were maintained under specific pathogen-free conditions at the University of Pittsburgh, and all experiments were conducted in accordance with animal use guidelines and protocols approved by the University of Pittsburgh's Institutional Animal Care and Use (IACUC) Committee.

4.3.6 ELISA

Sera from all mice were collected prior to immunization (week 0) and at weeks indicated after immunization and evaluated for SARS-CoV-2-S1-specific IgG, IgG1, and IgG2a antibodies using ELISA [217]. Briefly, ELISA plates were coated with 200 ng of recombinant SARS-CoV-2-S1 protein per well overnight at 4 °C in carbonate coating buffer (pH 9.5) and then blocked with PBS-T and 2% bovine serum albumin (BSA) for one hour. For ELISA coating antigens, Wuhan S1 was purchased from Sino Biological, Delta S1cg was produced by our lab, and Omicron S1-RS09cg was used to elucidate Omicron (BA.1) specific response. Mouse sera were serially diluted in PBS-T with 1% BSA and incubated overnight. After the plates were washed, anti-mouse IgG-horseradish peroxidase (HRP) (1:10,000, SantaCruz, Dallas, Texas, USA) was added to each well and incubated for 60 min. The plates were washed three times, developed with 3,3′5,5′-tetramethylbenzidine, and the reaction was stopped. Next, absorbance was determined at 450 nm using a plate reader. For IgG1 and IgG2a ELISAs, mouse sera were diluted in PBS-T with 1% BSA and incubated overnight. After the plates were washed, biotin-conjugated IgG1 and IgG2a (1:1000, eBioscience, San Diego, CA, USA) and biotin horseradish peroxidase (Av-HRP) (1:50,000, Vector Laboratories, Newark, CA, USA) were added to each well and incubated for 1 h. The plates were washed three times and developed with 3,3′5,5′-tetramethylbenzidine, the reaction was stopped, and absorbance at 450 nm was determined using a plate reader. ELISA data graphed is relative to preimmunization sera, using week 0 sera as the standardized cutoff.

4.3.7 ACE2 Blocking Assay

Antibodies blocking the binding of SARS-CoV-2 spike including Wuhan and spikes from immune evasive variants; BA.1, BA.2, AY.4 (Delta lineage), BA.3, BA.1 + R346K mutation, BA.1 + L452R mutation, B.1.1.7 (Alpha), B.1.351 (Beta), and B.1.1640.2 to ACE2 were detected with a V-PLEX SARS-CoV-2 Panel (ACE2) Kit (Meso Scale Discovery (MSD) according to the manufacturer's instructions. The assay plate was blocked for 30 min and washed. Serum samples were diluted (1:20) and 25 µL were transferred to each well. The plate was then incubated at room temperature for 60 min with shaking at 700 rpm, followed by the addition of SULFO-TAG conjugated ACE2, and continued incubation with shaking for 60 min. The plate was washed, 150 µL MSD GOLD Read Buffer B was added to each well, and the plate was read using the QuickPlex SQ 120 Imager. Electrochemiluminescent values (ECL) were generated for each sample. Results were calculated as % inhibition compared to the negative control for the ACE2 inhibition assay, and % inhibition is calculated as follows: % neutralization = $100 \times (1 - (\text{sample signal/negative control signal}))$.

4.3.8 Statistical Analysis

Statistical analyses were performed using GraphPad Prism v9 (San Diego, CA, USA). Antibody endpoint titers and neutralization data were analyzed by Kruskal-Wallis test, followed by Dunn's multiple comparisons. Significant differences are indicated by * $p < 0.05$. Comparisons with non-significant differences are not indicated.

4.4 Discussion

As SARS-CoV-2 variants continue to emerge more vaccination platforms against SARS-CoV-2, which induce a broader immune response covering multiple variants, will be necessary [250,251,420,422,438,440]. Further, as COVID-19 booster doses are distributed, it will be critical to ensure that global vaccine equity is met [396,399]. Protein subunit vaccines are ideal for worldwide distribution due to their excellent safety, low cost, scalability, and thermostability [38,42,46]. Protein subunit vaccine platforms can be further improved through use of alternative vaccine delivery methods such as intranasal or intradermal vaccination, with microneedle arrays [217,441]. The versatility of protein subunit vaccines lends to their utility for mass distribution and vaccination.

In this study, we demonstrate the robust antibody response elicited by our unadjuvanted S1 protein subunit vaccine in BALB/c mice. Wuhan S1-RS09cg, Delta S1-RS09cg, OM-S1RS09cg, and trivalent WU/Delta/OM S1-RS09cg vaccinated mice all elicited a robust IgG binding antibody response against Wuhan S1, Delta S1, and Omicron (BA.1) S1. Particularly, trivalent WU/Delta/OM S1-RS09cg vaccinated mice mounted cross-reactive ACE2 binding inhibiting antibodies against SARS-CoV-2 variants with increased breadth when compared to monovalent WU S1-RS09cg, Delta S1-RS09cg, and OM S1-RS09cg vaccinated mice. We believe that this gives credence to investigating SARS-CoV-2 vaccines that are multivalent to expand variant specific immune responses. Our data also suggests that increasing valency of SARS-CoV-2 vaccines may not reduce magnitude of the individual variant immune response, a key added piece of information for development of next-generation SARS-CoV-2 vaccines. A particularly unexpected result of our study is the low immunogenicity of our WU S1-RS09cg vaccine against Wuhan S1, and other VOCs, when compared to Delta and OM S1-RS09cg. Indeed, Delta and Omicron (BA.1) mutations in S have been shown to increase pathogenicity and S fusogenicity,

126

along with increased ACE2 binding to S, when compared to wild-type Wuhan SARS-CoV-2 [440,442–445]. We hypothesize that this increased ACE2 binding by Delta and Omicron S may explain the increased immunogenicity exhibited by Delta and OM S1-RS09cg when compared to Wuhan S1-RS09cg, however, this will need to be explored further. Furthermore, Omicron BA.1 spike G446S mutation has been shown to potentiate antiviral T-cell recognition which may further explain the increased immunogenicity demonstrated by our OM S1-RS09cg and trivalent vaccine candidates [446].

The IgG isotype of the induced IgG antibodies skew to be IgG1 dominant, indicating a Th2-type bias. Indeed, BALB/c mice are the prototypical Th2-type mouse strain which necessitates the investigation of this protein subunit vaccine in additional animal models to examine the risk of vaccine-associate enhanced respiratory disease (VAERD) [447]. Our previous research has suggested that a booster of unadjuvanted subunit vaccine after an Adenoviral prime vaccine might avoid Th2-based immune response and the occurrence of VAERD [427]. Indeed, there have been numerous Adenoviral vector vaccine platforms used in the SARS-CoV-2 pandemic and constitute a large population necessitating variant-specific boosting [13,404]. Further so, the Th1- and Th2-type immune response may be further augmented using an adjuvant. In the context of SARS-CoV-2 vaccines there have been numerous adjuvants that have shown beneficial effects on immunogenicity [306,396,399,440]. Interestingly, a AS01-like adjuvanted SARS-CoV-2 subunit vaccine enhanced Th1-type IgG2a isotype and IFN-γ secreting T cell immune responses in BALB/c mice when compared to unadjuvanted control [448].

An important limitation regarding our study is the lack of T-cell immunity investigation and SARS-CoV-2 challenge, which were not performed to assess the protection ability of our vaccine constructs. S-specific binding antibodies were positively correlated with S-specific T-cell

responses indicating induction of T cell immune response by our vaccine constructs [449]. We chose to focus on the induction of antibodies because they are the hypothesized correlate of protection against severe COVID-19 [424]. Furthermore, prior studies have shown the positive correlation and high concordance between binding antibodies and traditional virus-based microneutralization tests [427]. Our past work has also shown the positive correlation between the MSD ACE2 binding inhibition and virus-based microneutralization tests [427]. As a conventional and multiplex test, measurement of competitive immunoassay for quantifying inhibition of the spike-ACE2 interaction can serve as a surrogate for traditional virus-based microneutralization tests with high levels of correlation [305,306,438]. Our future studies will probe the protection ability elicited by our monovalent and trivalent vaccines through challenge studies using BALB/c mice and K18-hACE2 mice. The BALB/c mouse model of SARS-CoV-2 infection only supports infection of SARS-CoV-2 variants that carry the N501Y variant, necessitating the use of hACE2-transgenic mice to evaluate protection efficiency against other variants [450].

Overall, this study illustrates the potential of subunit protein vaccine targeting SARS-CoV-2-S1 as it induces significant induction of humoral immune responses against SARS-CoV-2 even without adjuvant. Particularly, immunizing with trivalent WU/Delta/OM S1-RS09cg increased binding antibodies and ACE2-binding inhibiting antibodies against SARS-CoV-2 variant spikes versus monovalent approaches. Furthermore, combining our protein subunit protein vaccine targeting SARS-CoV-2-S1 with an immunostimulatory adjuvant should provide even higher levels of immunogenicity when compared to the unadjuvanted studies presented here. Our findings support the use of trivalent Wuhan, Delta, and Omicron targeting COVID-19 vaccines to increase variant antigenic coverage.

4.5 Acknowledgements

5.0 SARS-CoV-2 S1 Subunit Booster Vaccination Elicits Robust Humoral Immune Responses in Aged Mice

Text from this chapter has been modified from the publication: Kim, E., **Khan, M.S.**, Ferrari, A., Huang, S., Sammartino, J.C., Percivalle, E., Kenniston, T.W., Cassaniti, I., Baldanti, F., Gambotto, A.#. SARS-CoV-2 S1 Subunit Booster Vaccination Elicits Robust Humoral Immune Responses in Aged Mice. *Microbiology Spectrum*. In Press. # corresponding author.

5.1 Introduction

SARS-CoV-2 was identified as the causative agent of coronavirus disease 2019 (COVID-19) in December 2019, leading to a pandemic of COVID-19. The COVID-19 pandemic has resulted in 761 million confirmed cases, 6.8 million reported deaths, and the administration of 13.2 billion vaccine doses worldwide (until March 21, 2023) [224]. Six vaccines targeting the spike (S) protein SARS-CoV-2 (BNT162b2; AZD1222; Ad26.COV2.S; mRNA-1273; NVX-CoV2373; Ad5-nCoV) have been approved by the World Health Organization (WHO), greatly reducing the rate of severe disease and death [451]. However, the evolution of SARS-CoV-2 has given rise to multiple variants, including SARS-CoV-2 variants of concern (VOCs), such as Alpha (B.1.1.7), Beta (B.1.351), Gamma (P.1), Delta (B.1.617.2), Omicron (B.1.1.529), and the most recent Omicron subvariant (XBB.1.5). These variants are characterized by potential for increased transmissibility, ability to escape neutralizing antibodies, and reduced effectiveness of vaccinations or antibody treatment [452].

It is clear that age is the most significant risk factor for death due to COVID-19 [453–455]. Recent reports suggested that individuals over 65 years old account for 80% of COVID-19 hospitalizations and have a 20-fold higher COVID-19 fatality rate compared to those under 65 years old [456–458]. Among elderly individuals, those aged 80 years or more are at the highest risk of severe COVID-19 [459]. Furthermore, elderly individuals have been found to have poor neutralization, which may be due to lower serum IgG level, lower somatic hypermutation in B cell selection, and lower IL-2-producing CD4$^+$Tcell help compared to younger individuals. All of these factors can be overcome by booster vaccination [460]. These findings are consistent with previous studies showing lower immune responses in aged mice vaccinated with ChAdOx1 nCov-19 compared to younger mice, which was improved by booster dosing [461].

The entry of coronaviruses into host cells is mediated by the interaction between the receptor binding domain (RBD) of the viral S protein and the host receptor angiotensin-converting enzyme 2 (ACE2) through the upper and lower respiratory tracts [337,462]. Neutralizing antibodies against SARS-CoV-2 are effective at blocking this interaction to prevent infection [463,464]. Competitive immunoassay for quantifying inhibition of the spike-ACE2 interaction show a high level of concordance with neutralizing test [305,306]. VOCs have mutations or deletions in the spike protein, with some mutations occurring in the RBD, resulting in the highest resistance to vaccine-induced and infection-acquired immunity. In response to the rapid evolution of SARS-CoV-2 and the global circulation of VOCs, booster injections have been considered to protect against breakthrough infections of new emerging variants. The evaluation of booster immunization has been investigated in mice, non-human primates, and humans [449,461,464–466]. The findings suggested that the level of neutralizing antibodies is correlated with the vaccine efficacy for both mRNA and adenovirus vectored vaccines, and there is likely potential efficacy after boosting [403,467–469]. Of

note, ChAdOx1-mRNA vaccination was safe and enhanced immunogenicity compared to ChAdOx1-ChAdOx1 vaccination, highlighting that heterologous prime-boost regimens may offer immunological advantages to elicit strong and long-lasting protection acquired with currently available adenovirus-based vaccines [470–472]. Overall, a heterologous booster administration has been considered a solution to protect elderly people from breakthrough infections of new emerging variants.

In our previous study, we assessed the immunogenicity of an adenovirus-based vaccine expressing SARS-CoV-2-S1 (Ad5.S1) in mice. We found that a single immunization with Ad5.S1, via subcutaneously (SC) injection or intranasal (IN) delivery, induced robust humoral and cellular immune responses [189]. Here we conducted a follow-up study to assess the long-term persistence of immunogenicity and the booster effect of a subunit vaccine in aged mice. For the subunit vaccine, recombinant protein S1 of SARS-CoV-2 Beta (B.1.351) (rS1Beta) was selected because it showed the greatest breakthrough infections against the Wuhan-based vaccines [473,474] before the COVID-19 waves caused by Omicron variants, which have shown even higher levels of vaccine escape lately. In the present study, we evaluated that mice vaccinated with Ad5.S1 had high titers of anti-S1 antibodies one year after immunization compared to PBS-immunized mice. A booster with the rS1Beta subunit vaccine was effective in stimulating strong, long-lived S1-specific immune responses and inducing significantly high cross-neutralizing antibodies against SARS-CoV-2 variants.

5.2 Results

5.2.1 Construction and Expression of Recombinant Proteins

To produce recombinant proteins of SARS-CoV-2-S1, pAd/S1Beta was generated by subcloning the codon-optimized SARS-CoV-2-S1Beta gene with a C-tag into the shuttle vector, pAd (GenBank U62024) at SalI & NotI sites (**Fig. 25A**). To determine whether rS1Beta proteins were expressed from the plasmid, Expi293 cells were transfected with pAd/S1Beta or pAd as a control. At 5 days after transfection, the supernatants of Expi293 cells were characterized by a sandwich ELISA using monoclonal antibodies pair against SARS-CoV-2 Wuhan (WU) (**Fig. 25B**) and Western blot analysis (**Fig. 25C**). As shown in Figure 1B, the titer of recombinant rS1Beta proteins expressed in Expi293 cells was approximately 7.3 mg/L based on a standard of rS1WU and about 40.0 mg/L based on a standard of rS1Beta, while rS1Beta protein was not detected in the Expi293 cells transfected with control pAd. The rS1Beta protein was separated by a 10% SDS-PAGE and recognized by a polyclonal anti-spike of SARS-CoV-2 antibody at the expected glycosylated monomeric molecular weights of approximately 110 kDa under the denaturing reduced conditions, while no expression was detected in the mock-transfected cells (**Fig. 25C**). The purified rS1Beta protein, using C-tagXL affinity matrix, was determined by silver staining (**Fig. 25D**).
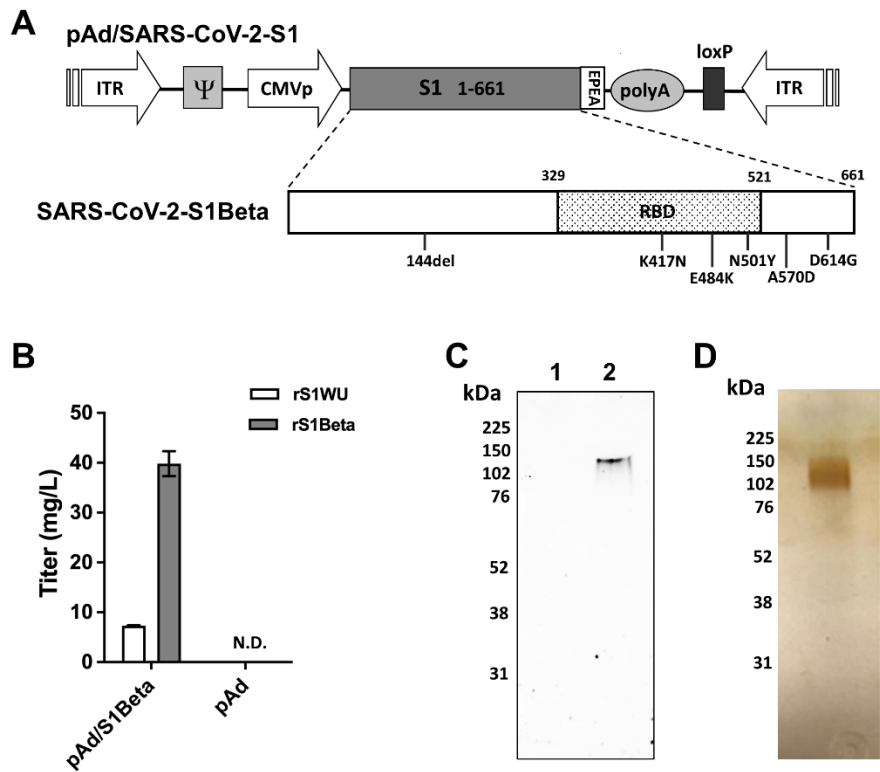
Figure 25: Construction of recombinant SARS-CoV-2-S1Beta protein expressing plasmid. (A) The diagram showed a shuttle vector carrying the codon-optimized SARS-CoV-2-S1 gene of Beta (1.351.1) variants encoding N-terminal 1-661 with C-tag (EPEA). The amino acid changes in the SARS-CoV-2-S1 region of this study are also shown. ITR: inverted terminal repeat; RBD: receptor binding domain. (B) The titer of recombinant SARS-CoV-2-S1 proteins was determined by sandwich ELISA with the supernatant of Expi293 cells transfected with pAd/SARS-CoV-2-S1Beta (pAd/S1Beta) based on the standard of rS1Wuhan (WU) (white box) or rS1Beta (grey box). (C) The detection of the SARS-CoV-2-S1 proteins was done by western blotting with the supernatant of Expi293 cells transfected with pAd/S1Beta using a rabbit anti-spike of SARS-CoV-2 polyclonal antibody (lane 2). As a negative control, mock-transfected cells were treated the same (lane 1). The supernatants were resolved on SDS-10% polyacrylamide gel after being boiled in 2% SDS sample buffer with β-ME. (D) The purified Expi293 cell-derived rS1Beta (300ng) was analysed by silver-stained reducing SDS-PAGE gel.

5.2.2 Rapid Recall of S1-Specific Binding Antibodies After a Booster

In our previous study, we evaluated the immunogenicity of the adenoviral vaccine until week 24 [189]. To assess the long-term persistence of immunogenicity, we first determined antigen-specific IgG antibody endpoint titers in the sera of vaccinated mice (Ad5.S1 immunized groups either via I.N. delivery or S.C. injection) and control mice (PBS or Adψ5 immunized groups) at week 52, one year after prime vaccination (**Fig. 26A**). As shown in **Fig. 26B**, significantly high titers of anti-S1 IgG antibodies were present in Ad5.S1 vaccinated mouse groups (G4, $p = 0.0016$ and G5, $p = 0.0365$) even after one year of vaccination as compared to AdΨ5-vaccinated mouse groups (G2 and G3) or PBS group (G1). To assess the booster effect of the subunit vaccine, we collected serum samples from all mice before booster immunization (W52) and immunized animals with 15 μg of rS1Beta intramuscularly at weeks 52 (60 weeks old) post-prime and collected sera in subsequent weeks until weeks 28 post-boost (**Fig. 26A**). , The endpoint titers of IgG against the S1 subunit of the spike protein (anti-S1) binding antibodies were examined by ELISA (**Fig. 26B**). More binding antibodies were detected significantly in Ad5.S1 vaccinated mouse groups (G4 and G5) compared to AdΨ5-vaccinated mouse groups (G2 and G3) or PBS group (G1) until week 28 ($p < 0.05$) after a booster vaccination. The change of geometric mean titers (GMT) of IgG end point titer in G4 and G5 compared to those at week 0 were the same as 32-fold at week 2 post-boost, and diverged to 55.7-fold and 18.4-fold at week 4 post-boost, respectively. Interestingly, the peak of IgG end point titer showed at week 4 post-boost in G4, while it showed at week 2 post-boost in G5. These recalls were faster after a booster vaccination with rS1Beta subunit vaccine when compared with IgG endpoint titer after prime (week 6 post-prime vs. week 2 or 4 post-boost) [189]. Furthermore, the elicited IgG antibody responses after a booster lasted longer, through week 28 post-boost (maximum length of the study to date), than

135

after a prime, as shown by the comparison with IgG endpoint titers at week 28 post-prime (W28) or post-boost (W80). The GMT of IgG endpoint titers of the mouse group primed SC (G4) was high compared to that of the mouse group primed IN (G5).
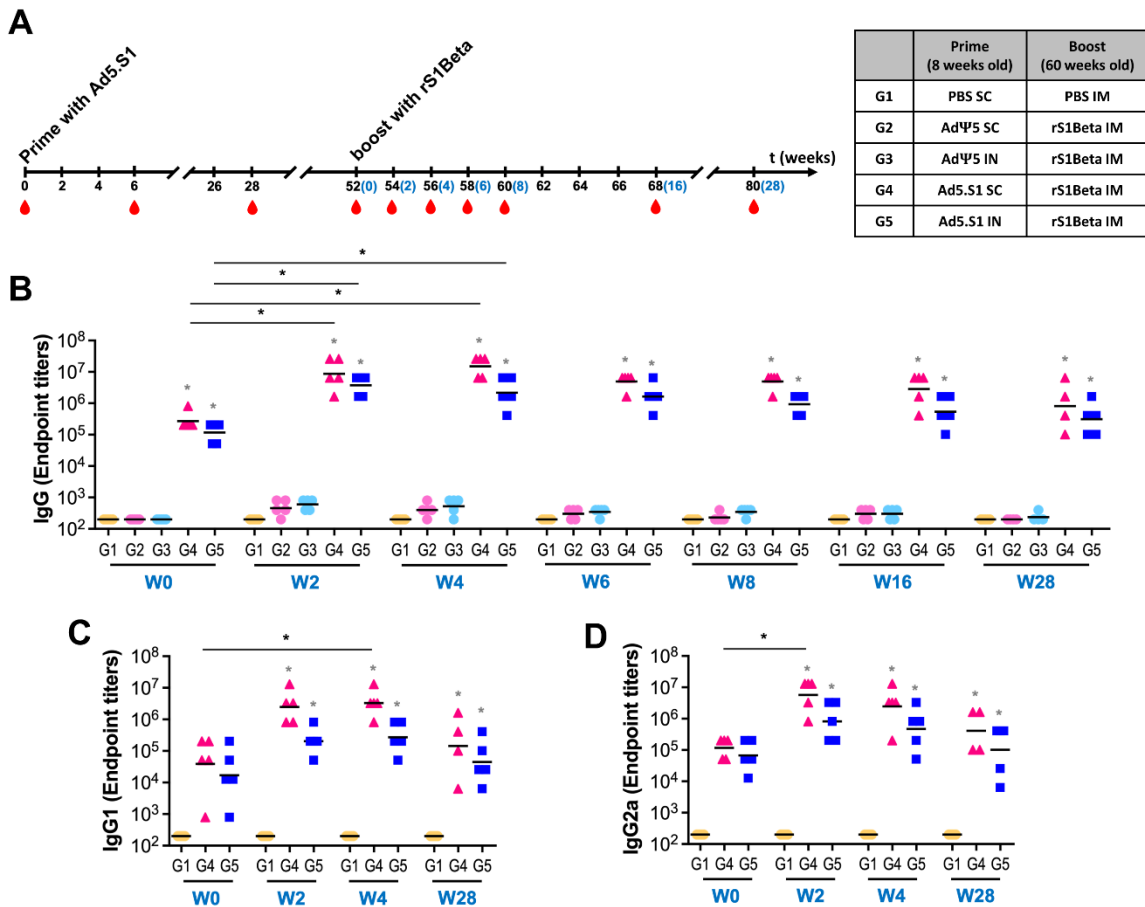
Figure 26: Prime-boost immunization of SARS-CoV-2 adenoviral vaccine-subunit proteins in BALB/c mice.
(**A**) Schedule of immunization and blood sampling for IgG endpoint titration, and explanation of animal groups. BALB/c mice were primed with 1.5×10^{10} vp of adenoviral vaccine (Ad5.S1 or AdΨ5) SC or IN, and with PBS as a negative control at 8 weeks old, and boosted with 15 μg of SARS-CoV-2-S1Beta recombinant proteins intramuscularly at a one-year interval (60 weeks old). The black and blue numbers represent weeks after prime and boost immunization, respectively. The immune responses were assessed at weeks 0, 2, 4, 6, 8, 16, and 28 post-boost (N=5 per group, except G4 at week 80 N=4). Reciprocal serum endpoint dilutions of SARS-CoV-2-S1-specific antibodies

136

were measured by ELISA to determine the **(B)** IgG (at weeks 0, 2, 4, 6, 8, 16, and 28) from G1 (peach circle), G2 (light pink circle), G3 (light blue circle), G4 (pink triangle), and G5 (blue square), **(C)** IgG1 and **(D)** IgG2a (at weeks 0, 2, 4, and 28 post-boost) from G1, G4, and G5. Horizontal lines represent geometric mean antibody endpoint titers (GMT). Significance was determined by Kruskal-Wallis test, followed by Dunn's multiple comparisons ($*p < 0.05$). Grey asterisks in Fig.2 represent statistical differences compared with G1 (PBS group).

Serum samples collected at weeks 0, 2, 4, and 28 post-boost were serially diluted to determine SARS-CoV-2-S1-specific IgG1 and IgG2a endpoint titers for each immunization group, indicating a Th2- or Th1-like response, respectively, using ELISA (**Fig. 26C and D**). The induction of S1-specific IgG1 and IgG2a antibodies was significant and similar in G4 and G5 after a booster shot, indicating a balanced Th1/Th2 response. Although there were no significant differences between S1-specific IgG1 and IgG2a responses at week 0 compared to G1, significantly different IgG1 and IgG2a responses were observed in G4 ($p < 0.001$ at weeks 2 and 4; $p < 0.05$ at week 28) than those in G5 ($p < 0.05$ at weeks 2, 4, and 28) after a booster, when compared with G1. Interestingly, IgG2a (Th1) responses were recalled faster than IgG1 (Th2) in both G4 and G5 (peak at week 2 vs. week 4 post-boost, respectively). The results suggest that a booster immunization with rS1Beta subunit vaccine induced significantly increased S1-specific IgG, IgG1, and IgG2a endpoint titers, which were recalled quickly (**Fig. 26B to D**, $p < 0.05$, Kruskal-Wallis test, followed by Dunn's multiple comparisons). Furthermore, the elicited IgG, IgG1, and IgG2a antibody responses remained significantly high with respect to control groups through week 28 post-boost (maximum length of the study to date) compared to post-prime (**Fig. 26**). Together, these results suggest that a booster could generate robust, balanced, and long-lived S1-specific antibody responses in aged mice primed with Ad5.S1 via either S.C. delivery or I.N. administration one year ago.

5.2.3 Neutralizing Antibody Levels After a Booster

To evaluate the presence of long-term and booster-generated SARS-CoV-2-specific neutralizing antibodies, we used a microneutralization assay (VNT_{90}) to test the ability of sera from immunized mice to neutralize the infectivity of SARS-CoV-2 variants, including Wuhan, Beta (B.1.351), and Delta (B.1.617.2) variants, as shown in **Fig. 27A**. SARS-CoV-2-neutralizating antibodies were detected in Ad5.S1 vaccinated groups (G4 and G5) even after one year of prime vaccination, with no significant differences compared to PBS group (G1). The geometric mean titers (GMT) of VNT_{90} in G4 and G5 were 33.7 and 28.6 against Wuhan, 20.5 and 31.8 against Beta (B.1.351), and 8.7 and 10.8 against Delta at week 0 (at week 52 post-prime), respectively. This result clearly showed low neutralization against the Delta (B.1.617.2) variant compared to other the variants.

After booster vaccination, the SARS-CoV-2 neutralizing activities at weeks 2 and week 4 were statistically significant (**Fig. 27A**, $p < 0.05$, Kruskal-Wallis test, followed by Dunn's multiple comparisons) compared to the control groups, with no significant differences between each other. The fold change of GMT of VNT_{90} against Wuhan, Beta (B.1.351), and Delta (B.1.617.2) in G4 compared to those at week 0 were 14.7-, 19.5-, and 12.4-fold at week 2, and 11.8-, 19.5-, and 15.5-fold at week 4, respectively (**Fig. 27B**). Those from G5 were 11.5-, 4.9-, 6.1-fold at week 2, and 7.6-, 6.3-, 3.6-fold at week 4, respectively. These fold changes of VNT_{90} GMT were statistically significant in G4 against all variants, with no significant differences compared to G5. Interestingly, the highest fold change was against Beta (B.1.351) in G4, while it was against Wuhan in G5. There were no detected neutralizing antibody responses in the sera from mice immunized with AdΨ5-vaccinated groups (G2 and G3) after booster (data not shown).
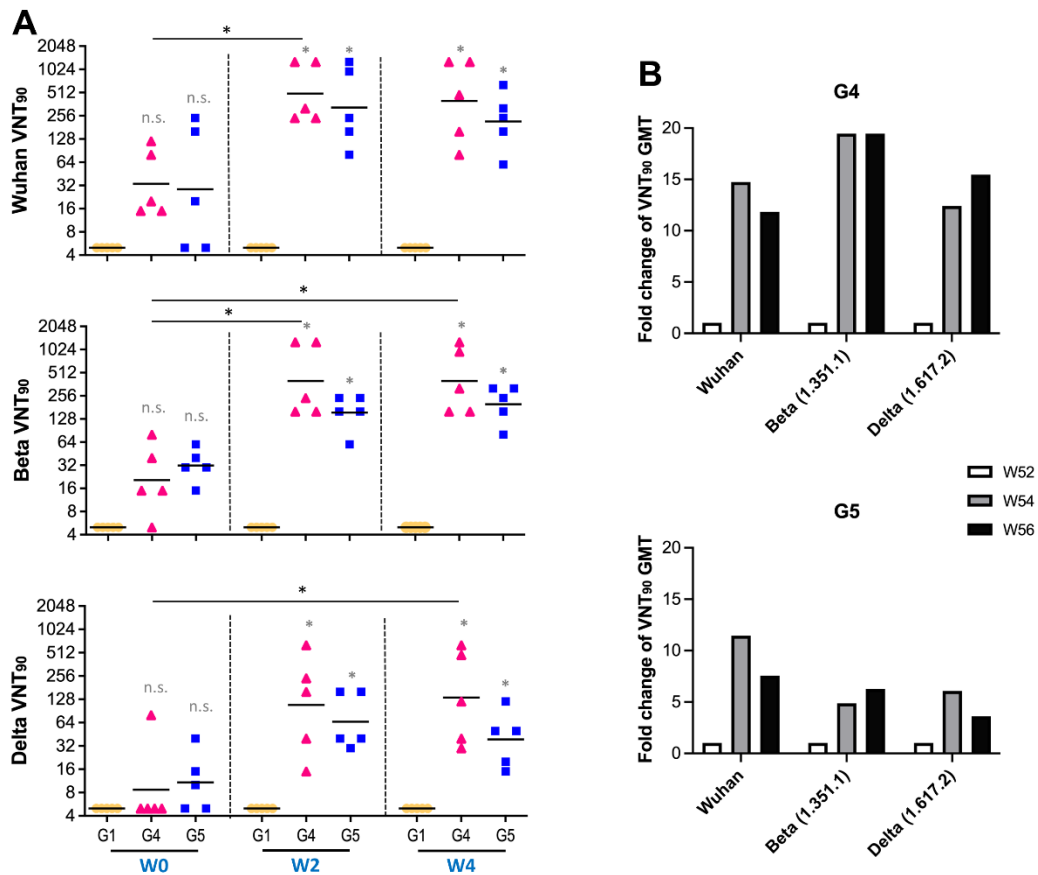
Figure 27: Neutralizing antibody responses in mice after a boost. BALB/c mice (n= 5 mice per group) were prime-immunized SC or IN with $1.5x10^{10}$ vp of Ad5.SARS-CoV-2-S1 (Ad5.S1), with PBS as a negative control at 8 weeks old and boosted with 15 μg of SARS-CoV-2-S1Beta recombinant proteins IM at week 52 post-prime (60 weeks old). (A) Neutralizing antibody titers from G1 (peach circle), G4 (pink triangle), and G5 (blue square) against SARS-CoV-2 Wuhan, Beta (B.1.351), and Delta (B.1.617.2) variants were measured using a VNT_{90} at weeks 0, 2, and 4 post-boost. Serum titers resulting in a 90% reduction in cytopathic effect compared to the virus control were reported. Horizontal lines represent geometric mean neutralizing antibody titers. Groups were compared by Kruskal-Wallis test at each time point, followed by Dunn's multiple comparisons. Significant differences are indicated by asterisks (*$p <$ 0.05). The minimal titer tested was 10, and undetectable titers (those with NT_{90} serum titers < 10) were assigned a value of 5. Grey asterisks represent statistical differences compared with PBS group (G1). (B) Fold change of VNT_{90} GMT against Wuhan, Beta (B.1.351), and Delta (B.1.617.2) in G4 and G5 after a booster (weeks 2 and 4, grey and black box, respectively), relative to those of pre-booster (week 0, white box).

139

To assess the correlations between the levels of S1-binding IgG endpoint titers and neutralizing antibodies, we performed correlation analyses on log-transformed data. We found a positive correlation between S1-binding IgG titers and VNT_{90} in all animals from G1, G4, and G5 at weeks 0, 2, and 4 post-boost (Spearman's correlation coefficients: $r = 0.9177$ (95% CI: 0.8462-0.9567) for Wuhan, $r = 0.9498$ (95% CI: 0.9047-0.9738) for Beta, $r = 0.8875$ (95% CI: 0.7925-0.9404) for Delta). The highest to lowest correlation between S1-binding IgG endpoint titers and neutralizing antibodies were for Beta, Wuhan, and Delta, respectively, with Beta being a subunit vaccine booster variant.

5.2.4 ACE2 Binding Inhibition

Additional tests were conducted to evaluate the ability of serum antibodies to inhibit the binding between ACE2 and the trimeric spike protein of SARS-CoV-2 variants. We used V-PLEX SARS-CoV-2 (ACE2) Kit Panel 18, which included Wuhan, Alpha (B.1.1.7), Beta (B.1.351), Gamma (P.1), Delta (B.1.617.2), Zeta (P.2), Kappa (B.1.617.1), New York (B.1.516.1), India (B.1.617 and B.1.617.3). Antibodies' ability to neutralize the interaction between spike of SARS-CoV-2 variants and ACE2 were examined in all animals from G4 (**Fig. 28A**) and G5 (**Fig. 28B**) at weeks 0, 6, 28, 54, and 80 post-prime at a dilution 1:100. The ACE2 inhibitory activities of the sera from G4 against all variants were on average $13.2\% \pm 6.98$, $13.3\% \pm 6.83$, $94.9\% \pm 6.80$, and $52.9\% \pm 36.47$ at weeks 6, 28, 54, and 80, respectively. Those from G5 were on average $14.7\% \pm 4.82$, $14.7\% \pm 10.87$, $74.1\% \pm 25.38$, and $25.2\% \pm 18.11$, respectively, with $6.4\% \pm 2.65$ at week 0. Overall, the median percent inhibition was lower for all variants compared to Wuhan wild type. Interestingly, the difference for all variants reached statistical significance in both G4 and G5 groups at week 2 post-boost when compared to week 0 (**Fig. 28A and B**). The inhibitions

140

against Wuhan and Alpha (B.1.1.7) spike by vaccine-induced antibodies at week 80 were significantly different compared to week 0 in only G4. The increase and decrease in percent inhibition towards the different variants followed the same trend for both groups. The highest and lowest percent inhibition of neutralizing antibodies compared to Wuhan was observed for Alpha (B.1.1.7) and Delta (B.1.617.2), respectively.
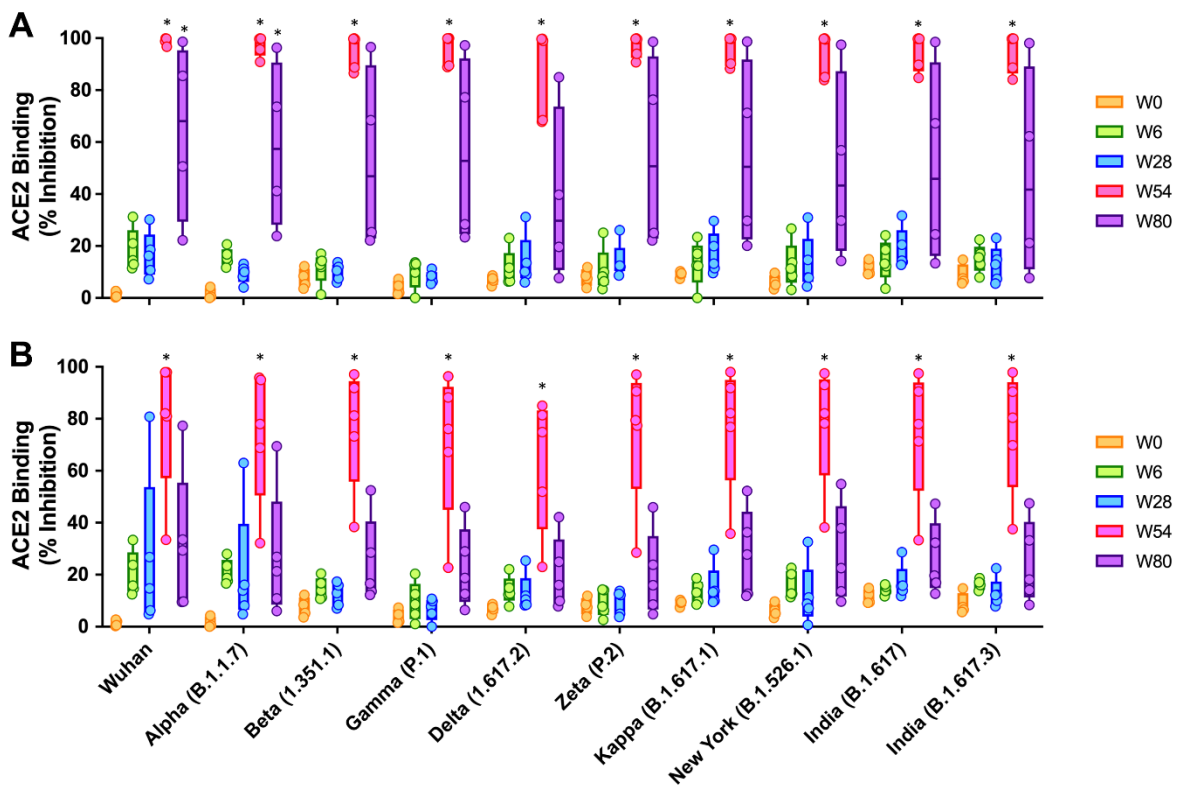
Figure 28: Percent ACE binding inhibition of neutralizing antibodies against SARS-CoV-2 variants. Antibodies in sera capable of neutralizing the interaction between SARS-CoV-2 Wuhan, Alpha (B.1.1.7), Beta (B.1.351), Gamma (P.1), Delta (B.1.617.2), Zeta (P.2), Kappa (B.1.617.1), New York (B.1.516.1), India (B.1.617 and B.1.617.3) variants spike and ACE2 were examined in all animals from G4 (A) and G5 (B) at week 0 (peach), 6 (green), 28 (blue), 54 (pink), and 80 (purple) post-prime. Serum samples were diluted in 1:100 before adding the V-PLEX plates. Box and whisker plots represent the median and upper and lower quartile (box) with min and max (whiskers). There is no

significance difference among all the variants at same time points, neither before nor after a booster. Asterisks represent statistical differences compared with pre-immunized sera.

To further assess the neutralizing capabilities of antibodies after a booster against Omicron (BA.1) and its sub-variants, we used MSD V-PLEX SARS-CoV-2 (ACE2) Kit Panel 25, which includes Wuhan, Omicron (BA.1), Omicron sub-variants (BA.2, BA.3, BA.1+R346K, BA.1+L452R), Delta lineage (AY.4), Alpha (B.1.1.7), Beta (B.1.351), and France (B.1.640.2) (**Fig. 29**). The ACE2-binding inhibitions of sera from G4 and G5 were examined at week 54 (at week 2 post-boost) and compared to preimmunized sera at a 1:100 dilution (**Fig. 29A**). The ACE2-binding inhibitions of antibodies from G4 sera at week 54 were significantly increased when compared to week 0 for all Omicron variants at 1:100 dilution, while antibodies from G5 sera showed very low ACE2-binding inhibition. Only for the spikes of Wuhan, Delta, Alpha, Beta, and France, were they significantly increased when compared to week 0. To further investigate boost-induced neutralizing activities against Omicron variants from G5 sera, mouse sera were diluted to 1:25 (**Fig. 29B**). The ACE2-binding inhibition of G5 week 54 sera was significantly increased when compared to week 0 sera for BA.1+L452R spike at a 1:25 dilution. While not statistically significant when compared to week 0, G5 sera demonstrated moderate ACE2-binding inhibition for BA.1, BA.2, BA.3, and BA.1+R346K spikes. The ACE2 inhibitory activities of G5 week 54 sera against BA.1, BA.2, BA.3, BA.1+R346K, and BA.1+L452R variants were on average $6.4\% \pm 3.38$, $13.1\% \pm 16.29$, $13.5\% \pm 8.81$, $9.7\% \pm 2.18$, and $28.4\% \pm 12.24$, at a 1:100 dilution and $54.5\% \pm 22.15$, $61.1\% \pm 30.66$, $60.2\% \pm 27.51$, $41.3\% \pm 20.13$, and $70.4\% \pm 16.58$, at a 1:25 dilution, respectively.
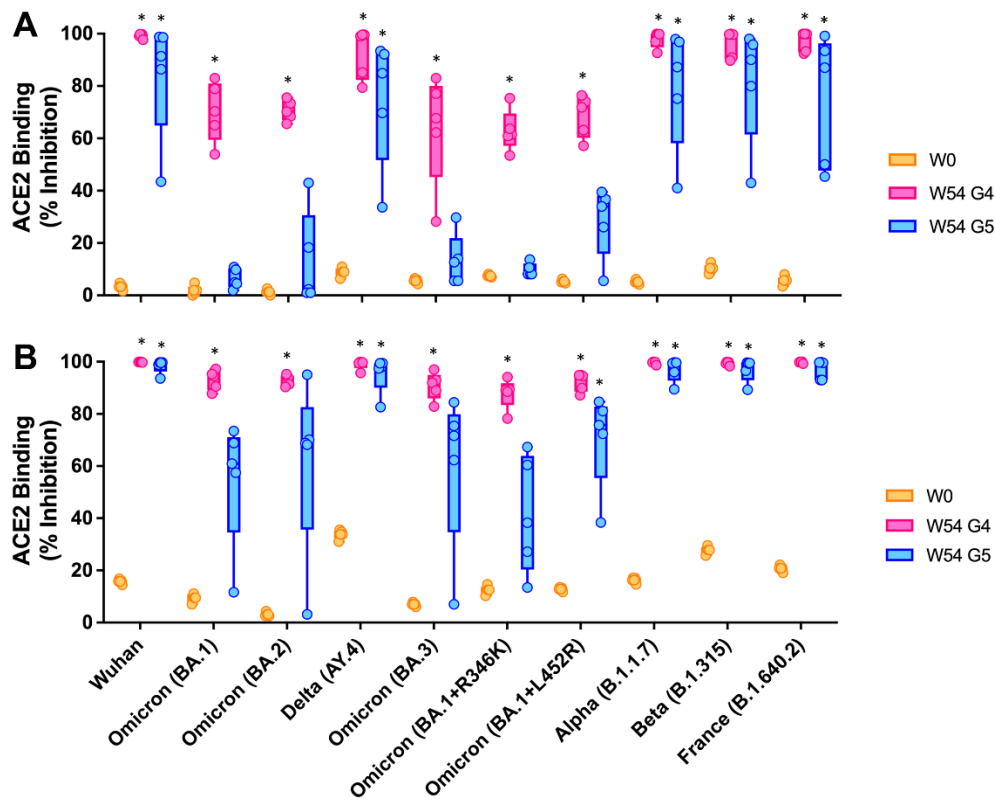
Figure 29: Percent ACE binding inhibition of neutralizing antibodies against SARS-CoV-2 Omicron variants. Antibodies in sera capable of neutralizing the interaction between SARS-CoV-2 Wuhan, Omicron (BA.1), Omicron sub-variants (BA.2, BA.3, BA.1+R346K, BA.1+L452R), Delta lineage (AY.4), Alpha (B.1.1.7), Beta (B.1.351), and France (B.1.640.2) variants spike and ACE2 were examined at week 0 (peach) and weeks 54 from G4 (pink) and from G5 (purple) post-prime. Serum samples were diluted in (A) 1:100 and (B) 1:25 before adding the V-PLEX plates. Box and whisker plots represent the median and upper and lower quartile (box) with min and max (whiskers). Asterisks represent statistical differences compared with pre-immunized sera.

After receiving a booster, ACE2 binding inhibition and VNT_{90} increased significantly against Wuhan, Beta (B.1.351), and Delta (B.1.617.2) compared to the pre-vaccinated sera, with no differences found among the variants. To determine correlations between levels of ACE2 inhibition and levels of neutralizing antibodies, we performed correlation analyses on ACE2

143

inhibition of 1:100 diluted mice sera and log-transformed VNT_{90} data of Wuhan, Alpha (B.1.1.7), and Delta (B.1.617.2). We found a positive correlation between V-PLEX ACE2 inhibition and VNT_{90} in all animals from G1, G4 and G5 at week 2 post-boost (Spearman's correlation coefficients, $r = 0.9025$ (95% CI: 0.8190-0.9486, $p < 0.0001$) (**Fig. 30**). Spearman's correlation coefficients were lower when the analysis was performed with 1:400 diluted mouse sera ($r = 0.7802$ (95%CI: 0.6132-0.8804, $p < 0.0001$). Changes in ACE2-binding inhibition at weeks 6, 28, 54, and 80 post-prime against the Wuhan spike protein were dependent on dilution factor, showing a similar pattern with other variants. Taken together, a single dose of non-adjuvanted recombinant S1 protein subunit vaccine as a booster induced broadly cross-reactive neutralizing antibodies against a wide range of SARS-CoV-2 variants, including Omicron, in aged mice primed with Ad5.S1 SC, and neutralizing antibody titer was correlated with the inhibition of spike-ACE2 binding.
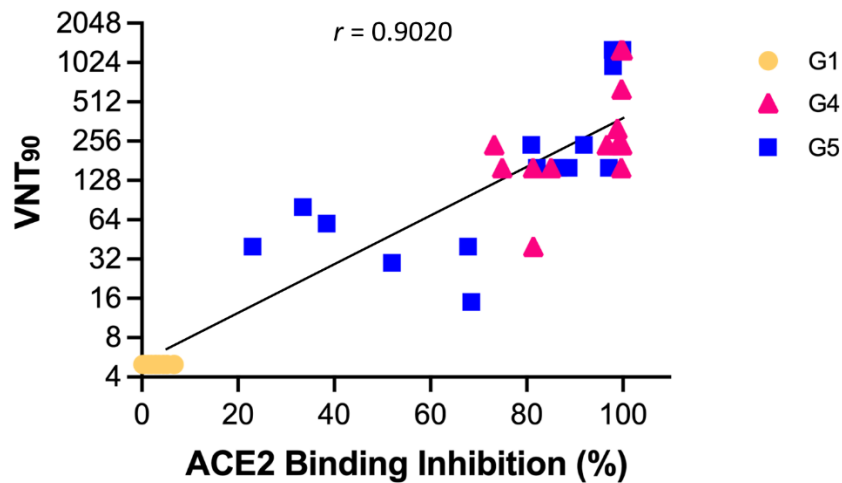
Figure 30: Correlation between the VNT90 and ACE2 binding inhibition. The correlation between VNT_{90} (Log_2) against Wuhan, Beta (B.1.351), and Delta (B.1.617.2) and ACE2 binding inhibition (%) of 1:100 diluted sera from all animals from G1 (peach circle), G4 (pink triangle), and G5 (blue square) at week 2 post-boost is shown. The lines

represent the regression line of all samples. Each symbol represents an individual mouse. Correlation analysis and calculation of Spearman's correlation coefficients were performed using GraphPad Prism v9.

5.3 Materials and Methods

5.3.1 Construction of Recombinant Protein-Expressing Vectors

The coding sequence for SARS-CoV-2-S1 amino acids 1 to 661 [217] was mutated at del144; K417N; E484K; N501Y; A570D; D614G and a C-terminal tag known as 'C-tag', composed of the four amino acids (aa), glutamic acid–proline–glutamic acid–alanine (E-P-E-A) flanked with Sal I & Not I, was added. The sequence was also codon-optimized using the UpGene algorithm for optimal expression in mammalian cells [371] and synthesized by GenScript. The construct also included a Kozak sequence (GCCACC) at the 5′ end. The plasmid pAd/SARS-CoV-2-S1Beta was created by subcloning the codon-optimized SARS-CoV-2-S1Beta inserts into the shuttle vector pAdlox (GenBank U62024) at Sal I/Not I sites. The plasmid constructs were confirmed by DNA sequencing.

5.3.2 Transient Production in epi293 Cells

The pAd/SARS-CoV-2-S1Beta was amplified and purified using ZymoPURE II plasmid maxiprep kit (Zymo Research). For transfection of Expi293 cell, we used ExpiFectamie^{TM} 293 Transfection Kit (ThermoFisher) and followed the manufacturer's instructions. Cells were seeded 3.0×10^6 cells/ml one day before transfection and grown to $4.5{\sim}5.5 \times 10^6$ cells/ml. A mixture of 1µg of DNA and ExpiFectamine per 1ml culture was prepared and incubated for 15 min before

adding it to the culture at a density of 3.0×10^6 cells/ml. At 18-22 h post-transfection, an enhancer mixture was added, and the culture was shifted to 32°C. The supernatants were harvested at 5 days post-transfection and clarified by centrifugation to remove cells, followed by filtration through 0.8μm, 0.45μm, and 0.22μm filters. The supernatants were either subjected to further analysis of SDS-PAGE, western blotting, and purification or stored at 4°C before purification, as previously described [189,217].

5.3.3 Purification of Recombinant Proteins

The recombinant proteins, named rS1Beta, were purified using a CaptureSelect^{TM} C-tagXL Affinity Matrix prepacked column (ThermoFisher), followed the manufacturer's guidelines. Briefly, the C-tagXL column was conditioned with 10 column volumes (CV) of equilibrate/wash buffer (20 mM Tris, pH 7.4) before sample application. The supernatant was adjusted to 20 mM Tris with 200 mM Tris (pH 7.4) before being loaded onto a 5-mL prepacked column per the manufacturer's instructions with 5 ml/min rate. The column was then washed by alternating with 10 CV of equilibrate/wash buffer, 10 CV of strong wash buffer (20 mM Tris, 1 M NaCl, 0.05% Tween-20, pH 7.4), and 5 CV of equilibrate/wash buffer. The recombinant proteins were eluted from the column by using elution buffer (20 mM Tris, 2 M MgCl$_2$, pH 7.4). The eluted solution was concentrated and desalted with preservative buffer (PBS) in an Amicon Ultra centrifugal filter device with a 50,000 molecular weight cutoff (Millipore). The concentration of the purified recombinant proteins was determined by the BCA protein assay kit (Thermo Scientific) using bovine serum albumin (BSA) as a protein standard, separated by reducing SDS-PAGE, and visualized by silver staining.

5.3.4 Animals and Immunization

At week 52 (60 weeks old) post-prime, female BALB/c mice (n = 5 animals per group) primed with adenovirus-based COVID-19 vaccine (Ad5.S1) at 8 weeks old [189] were boosted intramuscularly with 15 µg of rS1Beta in the thigh or PBS as a negative control. Mice were bled from retro-orbital vein at weeks 0, 2, 4, 8, 10, 16, and 28 after booster immunization, and the obtained serum samples were diluted and used to evaluate S1-specific antibodies by enzyme-linked immunosorbent assay (ELISA). Serum samples obtained on weeks 0, 2, and 4 post-boost were also used for VNT assay. Since aged mice develop spontaneous leukemias and other tumors, the dedicated veterinarians oversee the animals' physical and psychological health and ruled out mouse having disease that may influence immune responses. Indeed, one mouse of G4 at W80 was ruled out at week 28 post-boost (88 weeks old), because it was euthanized due to the tumor. Mice were maintained under specific pathogen-free conditions at the University of Pittsburgh, and all experiments were conducted following animal use guidelines and protocols approved by the University of Pittsburgh's Institutional Animal Care and Use (IACUC) Committee.

5.3.5 ELISA

To evaluate the expression of SARS-CoV-2S1Beta recombinant protein, ELISA plates were coated with chimeric MAb 40150-D003 (1:750, Sino Biological) overnight at 4°C in carbonate coating buffer (pH 9.5) and then blocked with PBS containing 0.05% Tween 20 (PBST) and 2% bovine serum albumin (BSA) for one hour. The supernatants of Expi293™ cells transfected with pAd/SARS-CoV-2-S1Beta was diluted 1:40 in PBS-T with 1% BSA and along with standard control protein 40591-V08H (rS1H, Sino Biological) or purified rSARS-CoV-

2S1Beta were incubated overnight at 4°C. After the plates were washed, chimeric MAb 40150-D001 HRP conjugated secondary antibody (1:10000, Sino Biological) was added to each well and incubated for one hour. The plates were then washed three times and developed with 3,3'5,5'-tetramethylbenzidine, and the reaction was stopped with 1M H_2SO_4 and absorbance at 450 nm was determined using an ELISA reader (Molecular Devices SPECTRAmax).

To investigate the immunogenicity of SARS-CoV-2S1Beta recombinant protein, IgG, IgG1, and IgG2a endpoint titers were measured using a laboratory developed ELISA, as previously described [217,217,426].

5.3.6 SARS-CoV-2 Microneutralization Assay

Neutralizing antibody (NT-Ab) titers against SARS-CoV-2 were defined according to the following protocol [379,380]. Briefly, 50 µl of sample from each mouse, starting from 1:10 in a twofold dilution, were added in two wells of a flat bottom tissue culture microtiter plate (COSTAR, Corning Incorporated, NY 14831, USA), mixed with an equal volume of 100 $TCID_{50}$ of a SARS-CoV-2 Wuhan, Beta, or Delta strain isolated from symptomatic patients, previously titrated, and incubated at 33°C in 5% CO_2. All dilutions were made in EMEM (Eagle's Minimum Essential Medium) with the addition of 1% penicillin, streptomycin and glutamine and 5 γ/mL of trypsin. After 1 hour incubation at 33°C 5% CO_2, 3 x 10^4 VERO E6 cells [VERO C1008 (Vero 76, clone E6, Vero E6); ATCC® CRL-1586™] were added to each well. After 72 h of incubation at 33°C 5% CO_2 wells were stained with Gram's crystal violet solution (Merck KGaA, 64271 Damstadt, Germany) plus 5% formaldehyde 40% m/v (Carlo ErbaSpA, Arese (MI), Italy) for 30 min. Microtiter plates were then washed in running water. Wells were scored to evaluate the degree of cytopathic effect (CPE) compared to the virus control. Blue staining of wells indicated the presence

of neutralizing antibodies. Neutralizing titer was the maximum dilution with a reduction of 90% of CPE. A positive titer was equal to or greater than 1:10. The GMT of VNT_{90} endpoint titer was calculated with 5 as a negative shown <10. Sera from mice before vaccine administration were always included in VNT assay as a negative control.

5.3.7 ACE2 Blocking Assay

Antibodies blocking the binding of SARS-CoV-2 spike variants (Alpha (B.1.1.7), Beta (B.1.351), Gamma (P.1), Delta (B.1.617.2), Zeta (P.2), Kappa (B.1.617.1), New York (B.1.516.1), India (B.1.617 and B.1.617.3) to ACE2 were detected with a V-PLEX SARS-CoV-2 Panel 18 (ACE2) Kit (Meso Scale Discovery (MSD)) according to the manufacturer's instructions. For the ACE2-binding inhibitions to Omicron variants, we used MSD V-Plex SARS-CoV-2 ACE2 Kit Panel 25 including Wuhan, Omicron (BA.1), Omicron sub-variants (BA.2, BA.3, BA.1+R346K, BA.1+L452R), Delta lineage (AY.4), Alpha (B.1.1.7), Beta (B.1.351), and France (B.1.640.2). The assay plate was blocked for 30 min and washed. Serum samples were diluted (1:25, 1:100 or 1:400) and 25 µl were transferred to each well. The plate was then incubated at room temperature for 60 min with shaking at 700 rpm, followed by the addition of SULFO-TAG conjugated ACE2, and continued incubation with shaking for 60 min. The plate was washed, 150 µl MSD GOLD Read Buffer B was added to each well, and the plate was read using the QuickPlex SQ 120 Imager. Electrochemiluminescent values (ECL) were generated for each sample. Results were calculated as % inhibition compared to the negative control for the ACE2 inhibition assay, and % inhibition is calculated as follows: % neutralization $= 100 \times (1 - ($sample signal/negative control signal$))$.

5.3.8 Statistical Analysis

Statistical analyses were performed using GraphPad Prism v9 (San Diego, CA). Antibody endpoint titers and neutralization data were analyzed by Kruskal-Wallis test, followed by Dunn's multiple comparisons. Significant differences are indicated by $*$ $p < 0.05$. Comparisons with non-significant differences are not indicated. Correlations between the V-PLEX ACE2 blocking and VNT_{90} or IgG endpoint titers and VNT_{90} were determined using correlation analysis and calculation of Spearman coefficients and 95% confidence interval (95% CI).

5.4 Discussion

We previously reported that a single immunization of BALB/c mice (8 weeks old) via either I.N. or S.C. delivery of our adenovirus-based COVID-19 vaccine (Ad5.S1) elicited robust S1-specific humoral and cellular immune responses in mice. In this study, we demonstrated the long-term persistence of immunogenicity after prime vaccination for up to one year. Additionally, we demonstrate that a booster of non-adjuvanted rS1Beta in aged mice (60 weeks old) primed with Ad5.S1 one year ago induces robust, balanced, and long-lasting IgG antibodies and neutralizing antibodies, that broadly cross-react with SARS-CoV-2 variants and corelate with ACE2-spike interaction inhibition.

There were very low antibody responses in the sera from mice immunized with AdΨ5-vaccinated groups (G2 and G3) after a subunit booster injection at week 52, which might be explained by the age of the mice at the time of single immunization (**Fig. 26A**). Indeed, vaccinated aged mice elicited a lower level of immune responses compared to vaccinated young mice, which

was found to be due to a low frequency of IgG- and IFN-γ-secreting cells in vaccinated aged mice [475]. These results were parallel to previous findings that older individuals have lower immune responses to approved COVID-19 vaccine than younger individuals [458,460,475,476]. Especially, lower serum IgG levels of SARS-CoV-2 in elderly people were due to a lower proportion of peripheral spike-specific memory B cells [460].

We have not compared the immune responses between the young and aged mice using the same immunogens and delivery routes. However, based on our previous experiment with Ad5.S1N-rS1WU or Ad5.S1N-rS1Beta (prime IM-boost IM regimen of 3 weeks interval in 6 weeks old mice), the GMT of IgG endpoint titer at W2 and W4 post-boost was increased 9.2-fold and 16.0-fold, respectively, compared to those at week 0 in both groups [426]. In case of long interval of one year in this manuscript, the change of GMT of IgG endpoint titer in G4 and G5 (Ad5.S1-rS1Beta, prime SC or IN-boost IM regimen of 52 weeks interval in 60 weeks old mice) was 32-fold at week 2 and diverged to 55.7-fold and 18.4-fold at week 4 post-boost, respectively, compared to those at week 0. These abundant and fast recalls might be from memory B cells. This finding could be partially explained by previous research that longer intervals between SARS-CoV-2 infection and vaccination may promote a better humoral immune response in individuals previously infected with SARS-C-V-2 [477]. Additionally, spike-specific memory B cells are more abundant 6 months post-symptomatic onset compared to 1 month [478], and memory B cells against SARS-CoV-2 spike actually increased between 1 month and 8 months after infection [479]. It might be necessary to allow a certain amount of time for antibody somatic mutation, memory B cell clonal turnover, and the development of monoclonal antibodies that are exceptionally resistant to SARS-CoV-2 RBD mutations, including those found in the VOCs [478].

Although there were no significant differences between the groups mice primed with Ad5.S1 SC or IN delivery, the group primed via SC showed long-lasting and higher GMT after a booster injection than the group primed via IN (**Fig. 26A**). These differences could be attributed to more systemic exposure of Ad particles upon SC delivery compared to IN delivery, as well as potentially enhanced innate immune responses by the relatively invasive SC injections. However, it is not guaranteed that SC injection will be better than IN delivery for protection against existing and newly emerging SARS-CoV-2 variants. Various studies have reported that vaccines delivered IN elicited superior mucosal immunity compared to the intramuscular injection and were efficient in protecting against the virus and reducing viral transmission [199,298,480,481]. Moreover, a recent study of adjuvanted S1 subunit vaccines primed-boosted intramuscularly or primed intramuscularly-boosted IN in rhesus macaques reported that the mucosal vaccine demonstrated outstanding protection in both upper and lower respiratory tracts by clearing the input virus more efficiently through higher dimeric IgA and IFN-α in bronchoalveolar lavage (BAL) fluid, although intranasal boosting elicited weaker T cell and lower neutralizing antibody titers [298].

In this study, the high titer of serum S1-binding IgG was investigated for up to 28 weeks after a booster in aged mice that were primed with Ad5.S1 one year ago. Although the limits of IgG duration in mice may not reflect those measured in non-human primates or humans, this result implied that humoral immunity might be long-lasting after a booster, because IgG titers at 28 weeks post-boost in G4 and G5 were approximately 6-fold and 1.7-fold higher than those at 28 weeks post-prime, respectively. Indeed, boosting dramatically enhanced humoral and cell-mediated immune responses in aged mice [476]. Likewise, one of the approved COVID-19 vaccine, Ad26.COV2.S, which is a single-shot regimen vaccine protecting against severe COVID-19, induced durable immune responses detected up to 8 months after vaccination in humans [482]. The

protection of two doses of mRNA BNT162b2 vaccine waned considerably after 6 months in humans. However, infection-acquired immunity boosted with vaccination remained high for more than 1 year after infection [483].

Subunit vaccine booster elicited both high S1-specific IgG1 and IgG2a subclass antibodies in aged mice primed with Ad5.S1, indicating a balanced Th1/Th2 response (**Fig. 26B and C**). In constant subunit vaccine alone induced high IgG1 with lower IgG2a leading to a possibility of vaccine-associated enhanced respiratory disease (VARED) [304]. Indeed, VARED-like pulmonary immunopathology related to Th2-based immune responses was observed in animals vaccinated with whole-inactivated SARS-CoV vaccines [302,303]. In this study, a high level of neutralizing antibodies and the balanced Th1/Th2 immune response were induced, suggesting that a booster of subunit vaccine after an adenoviral prime vaccine might avoid Th2-based immune response and the occurrence of VAERD.

Neutralization assay was frequently used as a correlate of protection following vaccination [403,467–469,484]. Here, we used a microneutralization test (VNT) to evaluate the function of the antibodies generated in the sera of immunized mice. The titer of neutralizing antibodies dramatically increased after a booster and neutralized other variants of Beta and Gamma (**Fig. 27**). Our future studies will include the evaluation of the neutralization effect against the Omicron variant. Notably, a recent study demonstrated that the boosted immune response by mRNA BNT162b2 can neutralize Omicron variant [476]. If needed, it may be possible to further improve neutralizing antibody responses with a booster of Omicron BA.5 rS1 subunit vaccine to overcome emerging SARS-CoV-2 infections. Neutralizing antibodies against SARS-CoV-2 are effective at blocking spike-ACE2 binding to prevent infection [463,464]. As a conventional pseudo-neutralizing test, the measurement of a competitive immunoassay for quantifying the inhibition of the spike-

ACE2 interaction can be used as a surrogate for the traditional virus-based plaque reduction neutralizing assay and has reported a high level of concordance and correlation (>96%) [305,306]. In this study, we assessed animal immune response for blocking spike-ACE2 binding using the V-PLEX neutralization kit and showed that a booster of aged mice primed with Ad5.S1 could induce significant blocking in the binding of ACE2 to spike of a wide range of SARS-CoV-2 variants, including Omicron variants (**Fig. 28 and 29**), which was correlated with VNT_{90} (**Fig. 30**). In addition, our future work will include further investigation in VNT_{90} to the spike of Omicron variants.

Here we have demonstrated the booster effect of the non-adjuvanted subunit vaccine. However, an adjuvanted subunit booster strategy is likely to have a beneficial effect for protection, particularly against distant variants such as Omicron BA.5. In fact, in non-human primates, the AS03-adjuvanted CoV2 preS dTM (B.1.351) induced higher neutralizing antibody titers against the Beta variant compared to the animal group that received the non-adjuvanted vaccine in the mRNA-primed cohort [466]. The AS01-like adjuvanted SARS-CoV-2 subunit vaccine enhanced the Th1 type-IgG2a isotype, neutralizing antibodies, and IFN-γ-secreting T cell immune responses in both young and aged mice [448]. Moreover, the combination of recombinant S protein and adjuvant CoVaccine HT^{TM} induced a balanced IgG subtype antibody response [304].

Two limitations of this study were the absence of T-cell immunity testing a cellular immunity and SARS-CoV-2 challenge to assess the protection efficiency of a booster vaccination. However, various studies have previously reported that T-cell immunity was activated after a booster [298,449,485,486]. Homologous and heterologous boosters in healthcare workers who had received a priming dose of Ad26.COV2.S COVID-19 vaccine resulted in higher levels of T-cell responses than the non-booster group, although T-cell response was significantly larger with

mRNA-based vaccines (91%) than with the homologous booster (72%) [449]. Additionally, a booster dose of mRNA BNT162b2 elicits robust T-cell responses that cross-recognized SARS-CoV-2 Omicron variant in aged mice [476]. Not only mRNA vaccine, but also adenoviral vectors or adjuvanted protein subunit vaccines enhanced cellular immune response in aged mice after a boost [461,487]. Furthermore, S-specific T-cell responses were positively correlated with the presence of S-specific binding antibodies [449], implying the induction of a robust T cell immune response after the rS1beta booster in this study.

As our study does not define protection ability against SARS-CoV-2 variants by the challenge, it needs to be investigated in the future. In a Syrian hamster model of virus transmission, a prime-boost vaccine strategy using subunit vaccine (Spike HexaPro + cationic liposomal adjuvant) showed effective protection against SARS-CoV-2 infection [441], although antibodies for ACE2-inhibition using MSD panel 19 ACE2 competition assay were lower than those from G4 and G5 at week 2 post-boost. Notably, a recent study was performed a protection experiment against SARS-CoV-2 Omicron variant in aged BALB/c mice boosted with mRNA vaccine [476]. This natural mouse model of SARS-CoV-2 infection by assessing viral replication and histopathological changes in the lung does not require genetic modification of mice or viruses. However, this wild mouse animal model only supports infection of SARS-CoV-2 variants that carry the N501Y mutation, including Alpha, Beta, Gamma, and Omicron [450]. Therefore, it is still important to use K18-hACE2 and other hACE2-transgenic mice to investigate the pathogenicity of different SARS-CoV-2 variants [294].

Overall, our study evaluated the effect of a booster in aged mice after priming of adenoviral vaccines as a pre-clinical model of elderly people immunized with the current approved COVID-19 vaccines. Our findings may have implications for further study of using recombinant protein

S1BA.5 subunit vaccine as a booster to enhance cross-neutralizing antibodies against new emerging variants of concern.

5.5 Acknowledgements

6.0 Tetravalent SARS-CoV-2 S1 Subunit Protein Vaccination Elicits Robust Humoral and Cellular Immune Responses in SIV-Infected Rhesus Macaque Controllers

Text from this chapter has been modified from the publication: **Khan, M.S.***, Kim E.*, Le Hingrat, Q., Kleinman, A., Ferrari, A., Sammartino, J.C., Percivalle, E., Xu, C., Huang, S., Kenniston, T.W., Cassaniti, I., Baldanti, F., Pandrea, I., Gambotto, A.#, Apetrei, C#. Tetravalent SARS-CoV-2 S1 Subunit Protein Vaccination Elicits Robust Humoral and Cellular Immune Responses in SIV-Infected Rhesus Macaque Controllers. 2023.03.15.532808 Preprint at https://doi.org/10.1101/2023.03.15.532808 (2023). * co-first author. # co-corresponding author.

6.1 Introduction

The coronavirus disease 2019 (COVID-19) pandemic caused by the severe acute respiratory syndrome coronavirus 2 (SARS-CoV-2) has had an unprecedented impact on global health, economy, and society. The COVID-19 pandemic consisted of over 675 million cases, with 6.5 million deaths, and 13 billion COVID-19 vaccine doses administered across the human population, as of February 3rd 2023 [224]. Although approved COVID-19 vaccines have been effective in reducing mortality and morbidity caused by SARS-CoV-2 infection, the emergence of new variants that are able to evade the immune response has raised concerns about their long-term efficacy. Furthermore, the uneven distribution of vaccines worldwide has resulted in many low to middle income countries being left without access to variant-specific vaccines that are better suited for the evolving SARS-CoV-2 variant landscape. This highlights the need for the development of

vaccines that can provide broad protection against a range of SARS-CoV-2 variants, as well as the importance of equitable distribution of vaccines to mitigate the risk of further virus evolution and spread [1,13,249,250]. Since its emergence in late 2019, SARS-CoV-2 has continuously evolved, at a higher-than-expected rate, giving rise to multiple variants with multiple genetic mutations and various phenotypic properties, including increased transmissibility, virulence, and immune escape [250,251]. The emergence of these variants has raised concerns about the efficacy of current vaccines and the potential for future outbreaks. Therefore, there is a critical need to develop effective vaccines that can provide broad and durable protection against SARS-CoV-2 and its variants. SARS-CoV-2 variants such as B.1.1.7 (Alpha), B.1.351 (Beta), and P.1 (Gamma) have exhibited substantial increases in immune escape from wildtype (WU) vaccine or infection induced immunity [488,489].

The spike (S) protein of SARS-CoV-2 has been the main target of currently approved COVID-19 vaccines and of most COVID-19 vaccines in development [336]. S protein allows for virus binding and infection of susceptible cells through interaction with host receptor angiotensin-converting enzyme 2 (ACE2) [338]. The S1 subunit of the S protein contains the receptor binding domain (RBD) that binds with ACE2, while the S2 subunit allows for cell fusion and viral entry [227,423]. It has been widely acknowledged that antibodies targeting the S protein, particularly those binding to the RBD, are able to block the binding of SARS-CoV-2 to the cell receptor and prevent infection of susceptible cells [236,307,339,403,424]. We have previously demonstrated the immunogenicity of S1 subunit targeting vaccines against various Beta-coronaviruses including SARS-CoV-1, SARS-CoV-2, and MERS [217,343,344,426,427,490].

A focus for next-generation SARS-CoV-2 vaccine design is the investigation of novel vaccines which may be able to induce a broader immune response effective against multiple

158

SARS-CoV-2 variants. A multivalent vaccine is a traditional approach used to increase antigen immunity coverage against multi-variant viruses such as SARS-CoV-2. We have previously demonstrated the immunogenicity of a trivalent protein subunit vaccine in BALB/c mice [490]. Here, we assessed our S1 protein subunit vaccine, at an increased valency to tetravalent, in an advanced animal model more closely related to humans. Nonhuman primates (NHPs) are commonly used as preclinical models to evaluate the safety and efficacy of vaccines and therapeutics for infectious diseases, including SARS-CoV-2 [290–293]. We employed a rhesus macaque (RM) model of controlled simian immunodeficiency virus (SIV) infection to evaluate the immunogenicity of a tetravalent SARS-CoV-2 S1 protein subunit vaccine delivered with AddaVax adjuvant. Controlled SIV infection in RMs mimic a situation of chronic viral infection which can be encountered in humans, which may influence the development of immune responses to vaccination. Indeed, some studies reported lower SARS-CoV-2 antibody responses for people living with HIV [491,492]. Several studies have demonstrated the utility of RMs as a preclinical model for SARS-CoV-2 vaccine development. For example, macaques have been used to evaluate the immunogenicity and the correlates of protection, as well as the protective efficacy of various vaccine platforms, including viral vector-based vaccines, mRNA vaccines, and protein subunit vaccines [133,292,293,297–300]. Moreover, the use of NHP models can provide critical insights into the mechanisms of vaccine-induced immunity, including the kinetics, specificity, and durability of the immune responses.

Here, we evaluated the immunogenicity of a tetravalent SARS-CoV-2 vaccine approach with S1 subunit protein vaccine targeting Wuhan S1, B.1.1.7 (Alpha), B.1.351 (Beta), and P.1 (Gamma). We chose these variants because, at the time of the start of the study, they represented a diverse and relevant set of SARS-CoV-2 strains that were circulating in different regions of the world and had distinct mutations in the spike protein, which is the main target of neutralizing

159

antibodies. We found that vaccination induced robust humoral and cellular immune responses which resulted in antibodies capable of blocking ACE2 binding to 15 different SARS-CoV-2 variants, including multiple Omicron variants. Vaccination also induced antibodies that were able to block SARS-CoV-2 infection of susceptible cells by live wild-type (WU), Beta, and Delta variant viruses. We profiled the lymphocyte response to immunization for 2 months post initial prime vaccination through quantifying the number of T and B cells, investigating markers of T-cell activation, and memory subsets in peripheral blood mononuclear cells (PBMCs) and showed robust immune activation, primarily after boost immunization. We were also able to measure a spike-specific CD4$^+$ T-cell response in the PBMC's of RMs 42 days post-prime immunization, although, no CD8$^+$ T-cell response was found. Our study further demonstrates the immunogenicity of protein subunit vaccines against SARS-CoV-2 targeting the S1 subunit of the spike protein while also contributing insights on approaches to further increase valency of currently approved COVID-19 vaccines.

6.2 Results

6.2.1 Design and Expression of Recombinant Proteins

To produce recombinant proteins of SARS-CoV-2-S1 pAd/S1Wu, pAd/S1Alpha, pAd/S1Beta, and pAd/S1Gamma were generated by subcloning the codon-optimized SARS-CoV-2-S1 gene having C-tag into the shuttle vector, pAd (GenBank U62024) at *Sal* I and *Not* I sites (**Fig. 31A**). Variant-specific mutations for B.1.1.7 (Alpha), B.1.351 (Beta), and P.1 (Gamma) SARS-CoV-2 recombinant S1 proteins are outlined. To determine SARS-CoV-2-S1 expression

160

from each plasmid, Expi293 cells were transfected with pAd/ S1WU, pAd/S1Alpha, pAd/S1Beta, and pAd/S1Gamma or pAd as a control. At 5 days after transfection, the supernatants of Expi293 cells were characterized by Western blot analysis. As shown in **Fig. 31B**, each S1 recombinant proteins were recognized by a polyclonal anti-spike of SARS-CoV-2 Wuhan antibody at the expected glycosylated monomeric molecular weights of about 110 kDa under the denaturing reduced conditions, while no expression was detected in the mock-transfected cells (lane1). The purified rS1WU, rS1Apha, rS1Beta, and rS1Gamma proteins using C-tagXL affinity matrix were determined by silver staining (**Fig. 31C**).
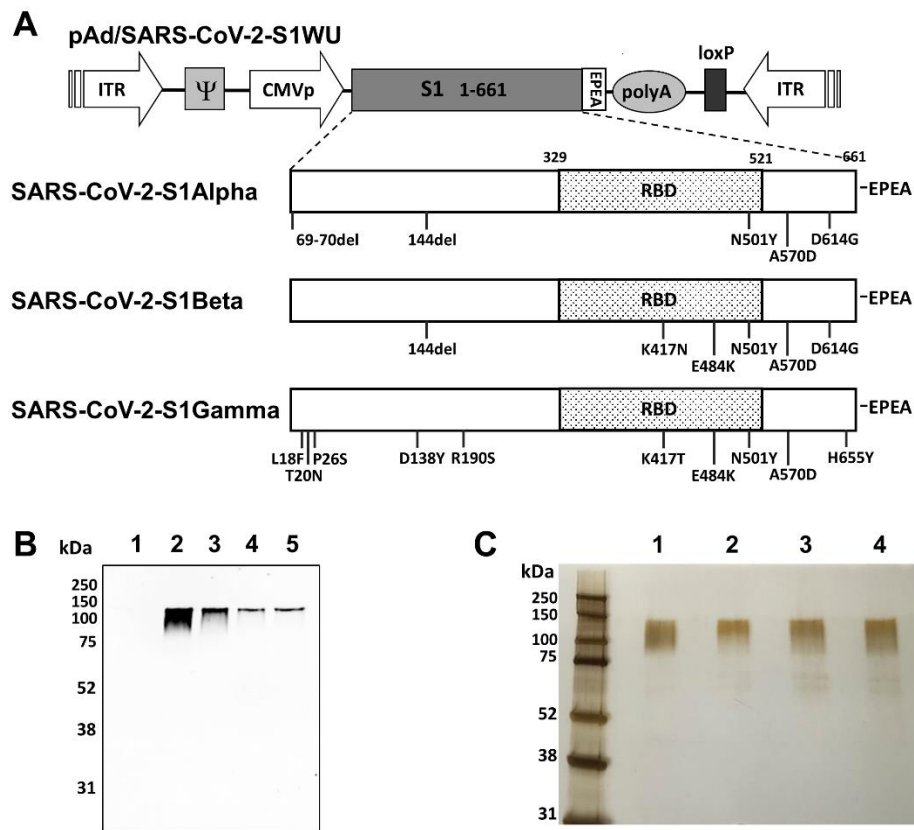
Figure 31: Construction and expression of tetravalent recombinant SARS-CoV-2-S1 proteins. (A) A shuttle vector carrying the codon-optimized four variants of SARS-CoV-2-S1 gene encoding N-terminal 1-661 with c-tag (EPEA) was designated as shown in the diagram. Amino acid changes in the SARS-CoV-2-S1 region of in this study

is shown. ITR: inverted terminal repeat; RBD: receptor binding domain. (B) Detection of the SARS-CoV-2-S1 proteins by western blot with the supernatant of Expi293 cells transfected with pAd/S1WU (lane2), pAd/S1Alpha (lane3), pAd/S1Beta (lane4), and pAd/S1Gamma (lane5), respectively, using rabbit anti spike of SARS-CoV Wuhan polyclonal antibody. As a negative control, mock-transfected cells were treated the same (lane 1). (C) Purified proteins, rS1WU (lane1), rS1Alpha (lane2), rS1Beta (lane3), and rS1Gamma (lane4), isolated by c-tag affinity purification were separated by SDS-PAGE and visualized by silver staining. Molecular weight marker (MW marker) is indicated on the left.

6.2.2 Binding Antibody and Cross-Variant Live Virus Neutralizing Antibody Response

Prior to immunization, RMs were infected with a simian immunodeficiency virus (SIV) that naturally infects African green monkeys (SIVsab) [493]. This virus is completely controlled in RMs [494], in spite of retaining the replicative abilities [495]. At the time of SARS-CoV-2 immunization, the RMs were controlling SIVsab for over a year. Upon prime and boost immunization, SIVsab viral loads remained undetectable suggesting no SIV activation upon vaccination. RMs were primed and boosted on week 3 with 60 µg total of rS1WU, rS1Apha, rS1Beta, and rS1Gamma, 15 µg of each antigen, mixed with 300 µl of AddaVax^{TM}, squalene-based oil in water nano-emulsion adjuvant (**Fig. 32A**). To assess the magnitude of the antibody response we first determined Wuhan IgG antibody endpoint titers (EPT) in the sera of vaccinated RMs with ELISA. Serum samples collected prior to immunization, week 3, week 7, and week 9-11 after immunization were serially diluted to determine SARS-CoV-2-S1-specific IgG titers against Wuhan S1 using ELISA (**Fig. 32B**). RMs had detectable anti-S1 binding antibody response prior to immunization (**Fig 32B**), however, no neutralizing antibody response was found (**Fig. 32C**). S1-specific IgG titers were statistically increased at week 7 and week 9-11 when compared to week 0 (**Fig. 32B,** $p < 0.05$, Kruskal-Wallis test, followed by Dunn's multiple comparisons). To

evaluate the functional quality of vaccine-generate antigen-specific antibodies, we used a microneutralization assay (NT_{90}) to test the ability of sera from immunized RMs to neutralize the infectivity of SARS-CoV-2. Sera, collected from RMs on week 3 (prior to booster immunization) and week 7 (4 weeks post boost) after primary immunization were tested for the presence of SARS-CoV-2-specific neutralizing antibodies with live SARS-CoV-2 Wuhan, Beta, and Delta viruses (**Fig. 32C**). High levels of neutralizing antibodies were detected in sera at week 3 and week 7 against Wuhan, Beta, and Delta SARS-CoV-2 variants (**Fig. 32C**) and showed a similar pattern with IgG endpoint titers in each RM. Furthermore, the geometric mean titers (GMT) of neutralizing antibodies at week 7 against the Wuhan, Beta, and Delta strain were increased with 6.4-, 5.4-, 3.2-fold compared at week 3, respectively, while only neutralizing antibody response against live Wuhan SARS-CoV-2 at week 7 was significantly increased when compared to preimmunized sera (**Fig. 32C**, $p < 0.05$, Kruskal-Wallis test, followed by Dunn's multiple comparisons). Neutralization against highly immune-evasive Beta and Delta SARS-CoV-2 variants of concern (VOC) were found at slightly lower levels than Wuhan at both week 3 and week 7 (**Fig. 32C**). While Beta VOC S1 was included in the tetravalent immunization regimen, Delta VOC was not, highlighting the diverse response induced by tetravalent immunization in RMs.

163
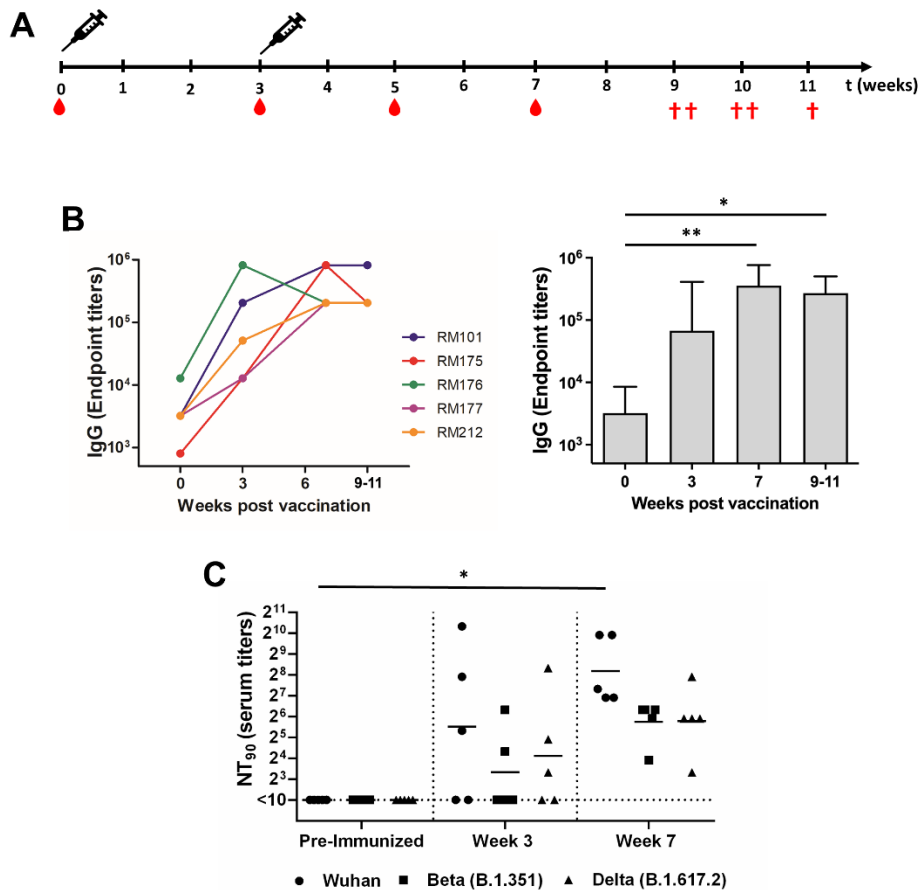
Figure 32: Antigen-specific antibody responses in rhesus macaques immunized with tetravalent SARS-CoV-2 rS1 protein subunit vaccine. (A) Schedule of immunization and blood sampling for IgG end point titration. Rhesus macaques (N=5) were immunized with 60μg of tetravalent rS1 proteins of Wuhan, B.1.1.7 (Alpha), B.1.351 (Beta), and P.1 (Gamma) [15μg of each antigen] mixed with AddaVax adjuvant then administered to RMs arm at week 0 and 3. Syringes indicated the timing of immunization and the red drops denote times at which blood was drawn. The red crosses showed euthanized times of each RM. (B) Sera were diluted and SARS-CoV-2-S1-specific antibodies were quantified by ELISA to determine the IgG endpoint titer. The IgG titers at each time points were showed in each RM. The bars represent geometric mean with geometric SD. (C) Neutralizing antibodies in serum of mice prior to immunization, along with week 3 and week 7 post immunization were measured using a microneutralization assay (NT$_{90}$) with SARS-CoV-2 Wuhan, Beta, and Delta. Serum titers that resulted in 90% reduction in cytopathic effect compared to the virus control were reported. Horizontal lines represent geometric mean titers. Groups were compared

164

by Kruskal-Wallis test at each time point, followed by Dunn's multiple comparisons. Significant differences are indicated by $*p < 0.05$. N = 5 rhesus macaques per group for each experiment.

6.2.3 Potent ACE2 Binding Inhibition Effective Against 15 Different SARS-CoV-2 VOC's Spikes

For further insight into the neutralizing capabilities of antibodies induced by vaccination we used the Meso Scale Discovery (MSD) V-PLEX SARS-CoV-2 (ACE2) Kit to measure the inhibition of binding between angiotensin converting enzyme-2 (ACE2) and trimeric spike protein of SARS CoV-2 variants. Initially, we used kit Panel 18 including Wuhan S and spikes from variants; Alpha (B.1.1.7), Beta (B.1.351), Gamma (P.1), Delta (B.1.617, B.1.617.2), Zeta (P.2), Kappa (B.1.617.1), B.1.526.1, B.1.617, and B.1.617.3 (**Fig. 33**). Sera from vaccinated RMs were examined at week 7, due to that being the peak of measured IgG binding antibody response and compared to preimmunized sera (**Fig. 32A, Fig. 33**). Antibodies blocking ACE2 and trimeric S binding of all variants, by over 90% inhibition, were detected in all 1:10 diluted RM sera at Week 7 (**Fig. 33**). Week 7 sera ACE2 binding inhibition for RMs was significantly increased, when compared to preimmunized sera, for Wuhan, B.1.1.7, B.1.351, P.1, B.1.617.2, P.2, B.1.617.1, B.1.526.1, B.1.617, and B.1.617.3 Spike (**Fig. 33**, $p < 0.05$, Mann-Whitney Test).
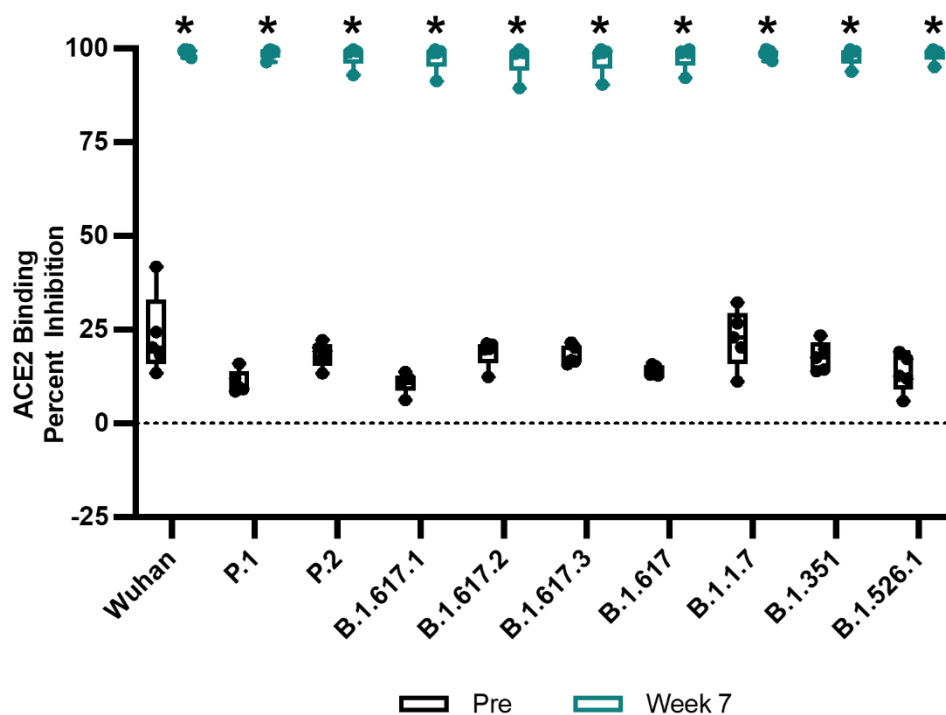
Figure 33: Percent ACE2 binding inhibition of neutralizing antibodies against SARS-CoV-2 variants. Antibodies in sera (diluted 1:10) capable of neutralizing the interaction between SARS-CoV-2 Wuhan, Alpha (B.1.1.7), Beta (B.1.351), Gamma (P.1), Delta (B.1.617.2), Zeta (P.2), Kappa (B.1.617.1), New York (B.1.516.1), India (B.1.617 and B.1.617.3) variants spike and ACE2 were examined in all animals preimmunization and Week 7 post prime immunization with V-PLEX SARS-CoV-2 Panel 18. Groups were compared by Kruskal-Wallis test at each time point, to preimmunized sera control, followed by Dunn's multiple comparisons. Significant differences are indicated by $*p < 0.05$. N = 5 rhesus macaques per group for each experiment.

To assess the neutralizing capabilities of RM vaccine induced antibodies against Omicron (BA.1) VOC, and Omicron sub-variants (BA.2, BA.3, BA.1+R346K, BA.1+L452R) we used MSD V-Plex SARS-CoV-2 ACE2 Kit Panel 25 (**Fig. 34**). Panel 25 includes SARS-CoV-2 Wuhan, BA.1, BA.2, AY.4, BA.3, BA.1+R346K, BA.1+L452, B.1.1.7, B.1.351, and B.1.640.2 trimeric spike. Sera from vaccinated RMs were examined at week 3, week 7, and week 9-11 post vaccination and compared to preimmunized sera at a 1:10 dilution (**Fig. 34A**) and 1:100 dilution

166

(**Fig 34B**). Week 7 and Week 9-11 RM sera ACE2-binding inhibition were significantly increased when compared to preimmunized sera for Wuhan, AY.4 (Delta lineage), BA.1+L452R, B.1.1.7, B.1.351, and B.1.640.2 VOC spikes at 1:10 dilution (**Fig. 34A**, $p < 0.05$, Kruskal-Wallis test, followed by Dunn's multiple comparisons). Week 7 RM sera ACE2-binding inhibition were significantly increased when compared to preimmunized sera for BA.1 VOC spike at 1:10 dilution (**Fig. 34A** $p < 0.05$, Kruskal-Wallis test, followed by Dunn's multiple comparisons).While not statistically significantly increased when compared to preimmunized RM sera; RMs demonstrated moderate ACE2-binding inhibition for BA.2, BA.3, and BA.1+R346K VOC spikes weeks 7 and 9-11 post immunization at 1:10 dilution (**Fig. 34A**, $p > 0.05$, Kruskal-Wallis test, followed by Dunn's multiple comparisons). To further interrogate the vaccine-induced neutralizing capabilities of RMs, we further substantially diluted RM sera to 1:100 (**Fig. 34B**). Week 7 RM 1:100 diluted sera ACE-2 binding inhibition was significantly increased when compared to preimmunized sera for Wuhan, AY.4, B.1.1.7, B.1.351, B.1.640.2 VOC spikes (**Fig. 34B**, $p < 0.05$, Kruskal-Wallis test, followed by Dunn's multiple comparisons). At 1:100 dilution, RM sera did not have ACE-2 binding inhibition above preimmunized sera for BA.1, BA.2, BA.3, BA.1+R346K, BA.1+L452R VOC spikes (**Fig. 34B**). Results suggest the necessity of the booster immunization to induce potent and cross variant recognizing antibodies. Results also suggest that vaccination induced antibodies that are able to potently recognize and block ACE2 binding of a wide range of SARS-CoV-2 variants spikes by week 7 post prime immunization.
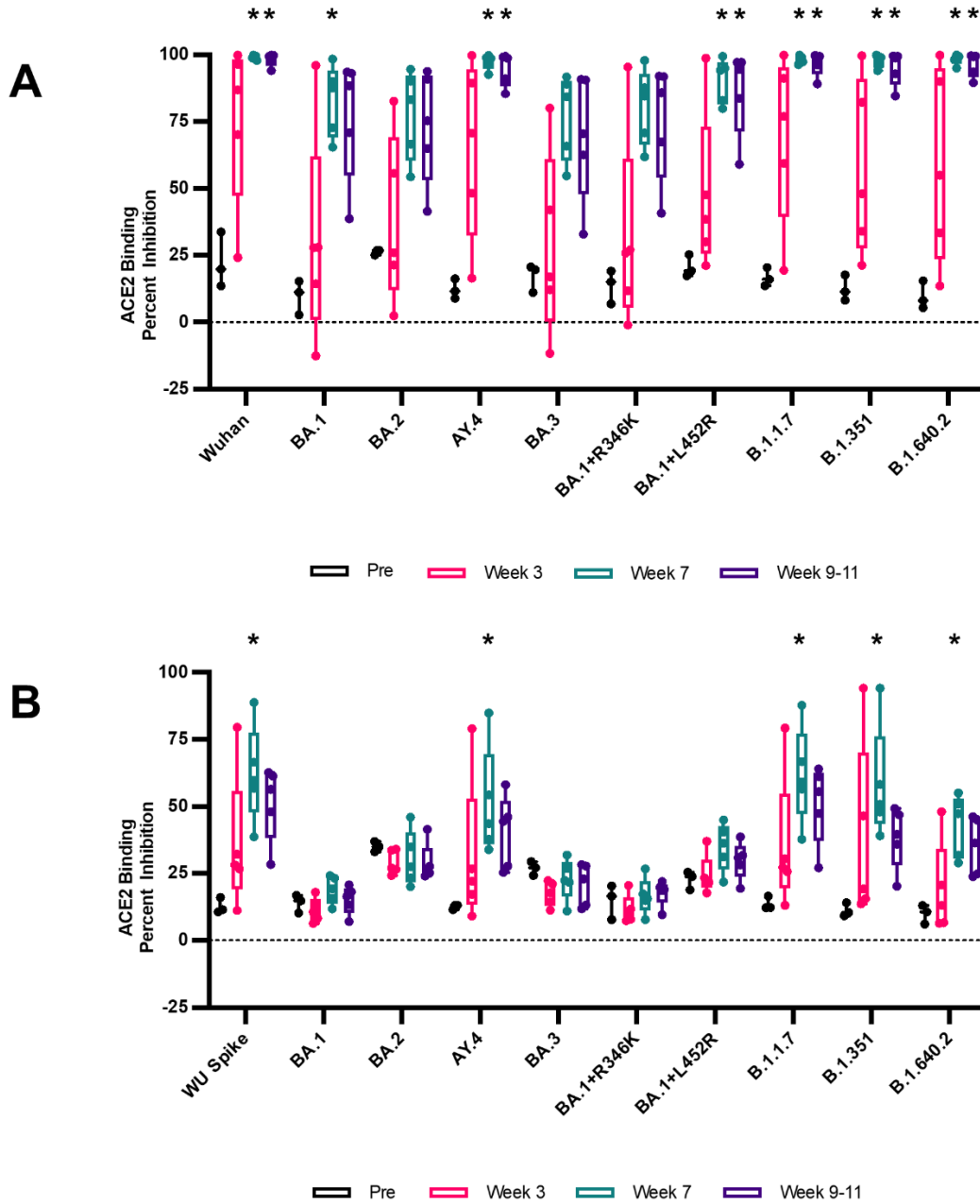
Figure 34: Percent ACE2 binding inhibition of neutralizing antibodies against Omicron SARS-CoV-2 variants.
Antibodies in sera, diluted (A) 1:10 and (B) 1:100 capable of blocking the binding of SARS-CoV-2 spike including Wuhan and spikes from immune evasive variants; BA.1, BA.2, AY.4 (Delta lineage), BA.3, BA.1+R346K mutation, BA.1+L452R mutation, B.1.1.7 (Alpha), B.1.351 (Beta), and B.1.1640.2 to ACE2 were detected with a V-PLEX SARS-CoV-2 Panel 25. Groups were compared by Kruskal-Wallis test at each time point, to preimmunized sera

control, followed by Dunn's multiple comparisons. Significant differences are indicated by $*p < 0.05$. N = 5 rhesus macaques per group for each experiment.

6.2.4 Longitudinal Lymphocyte Dynamics and Cell-Mediate Immune Response to Vaccination Shows Immune Activation Primarily Observed After Boost

To investigate the kinetics and magnitude of immune responses induced by the tetravalent SARS-CoV-2 vaccine, we monitored the peripheral blood mononuclear cells (PBMCs) of vaccinated rhesus macaques over a 60-day period. PBMCs are a mixture of different immune cell types, including T cells and B cells, and are a useful tool for investigating the immune response to vaccination in vivo.

Fig. 5 shows the dynamics of $CD3^+$ T-cells (**Fig. 35A**), $CD4^+$ T-cells (**Fig. 35B**), $CD8^+$ T-cells (**Fig. 35C**), and $CD20^+$ B cell (**Fig. 35D**) counts over 60 days. We observed increases in all T-cell subsets ($CD3^+$, $CD4^+$, and $CD8^+$) and B cells ($CD20^+$) after the prime and especially after the boost, demonstrating clear increases for all subsets, with the $CD8^+$ T cell count showing the greatest increase after boost immunization compared to the other cell types.
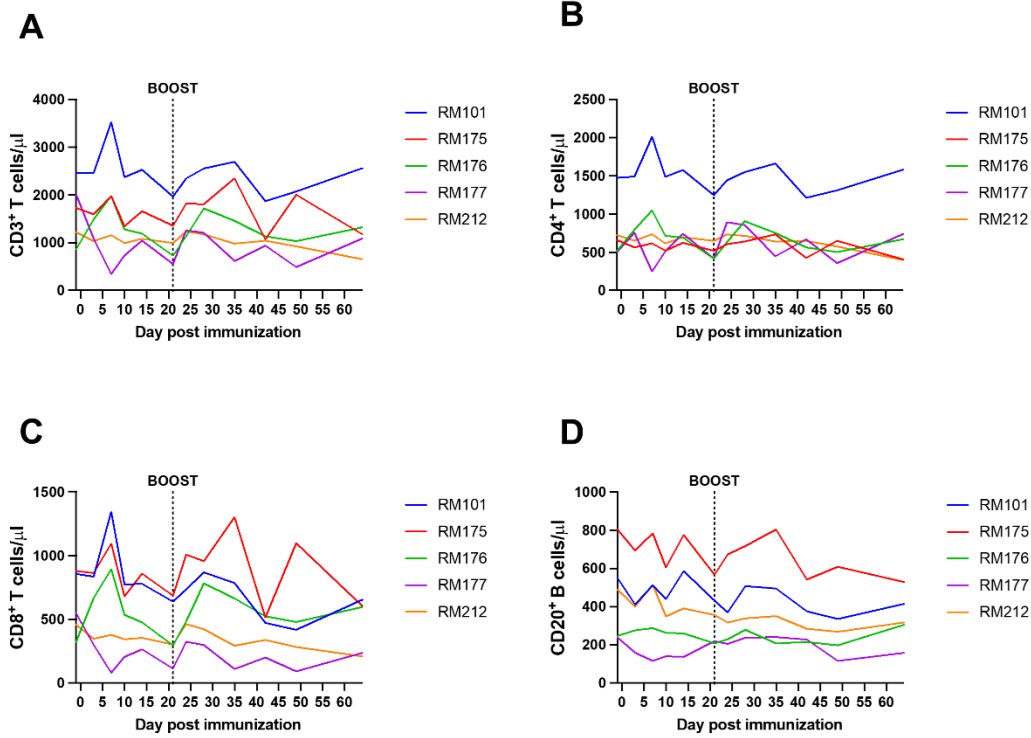
Figure 35: CD3, CD4, CD8, and CD20 cell counts post immunization and boost. Absolute counts of immune cells in whole blood and immunophenotyping of circulating immune cells were determined by flow cytometry. 50 μl of whole blood were added to a TruCount tube (BD Biosciences) containing an antibody mix, allowing to precisely quantify (A) CD45$^+$ cells, (B) CD4$^+$, (C) CD8$^+$ T cells, and (D) CD20$^+$ B cells in blood per μl. PMBC's from RMs were collected and analyzed on Days -1, 3, 7, 10, 14, 21, 24, 28, 31, 35, 42, 49, and 64 days post prime immunization. Individual results for each RM are depicted.

Fig. 36 shows the fraction of activating and proliferating CD4$^+$ and CD8$^+$ T cells. We used the activation markers CD69 and HLDR and CD38, as previously described in the literature [496–498]. We also used Ki-67 as a marker for cell proliferation. CD69$^+$CD4$^+$ T-cell induction was mainly observed in RM177 (**Fig. 36A**). Ki67$^+$CD4$^+$ T cells showed moderate increases in percentage after boost vaccination (**Fig. 36B**). HLA-DR$^+$CD38$^+$CD4$^+$ T-cells showed activation post prime and boost with a return to near baseline by Day 40 (**Fig. 36C**). The fraction of CD69$^+$CD8$^+$ T-cells

170

increased in all RMs post prime and boost, with most starting to return to prevaccination levels at day 60 (**Fig. 36D**). The induction of Ki-67^{+} CD8^{+} T-cells was primarily seen at day 40 postimmunization (**Fig. 36E**), while HLA-DR^{+} CD38^{+} CD8^{+} T-cell activation was mainly seen in RM175 and RM176 at different timepoints (**Fig. 36F**). However, the induction of HLA-DR^{+} CD38^{+} CD8^{+} T cells was not as robust as that of CD69^{+} CD8^{+} T cells and Ki-67^{+} CD8^{+} T cells (**Fig. 36F, Fig. 36D, Fig. 36E**).
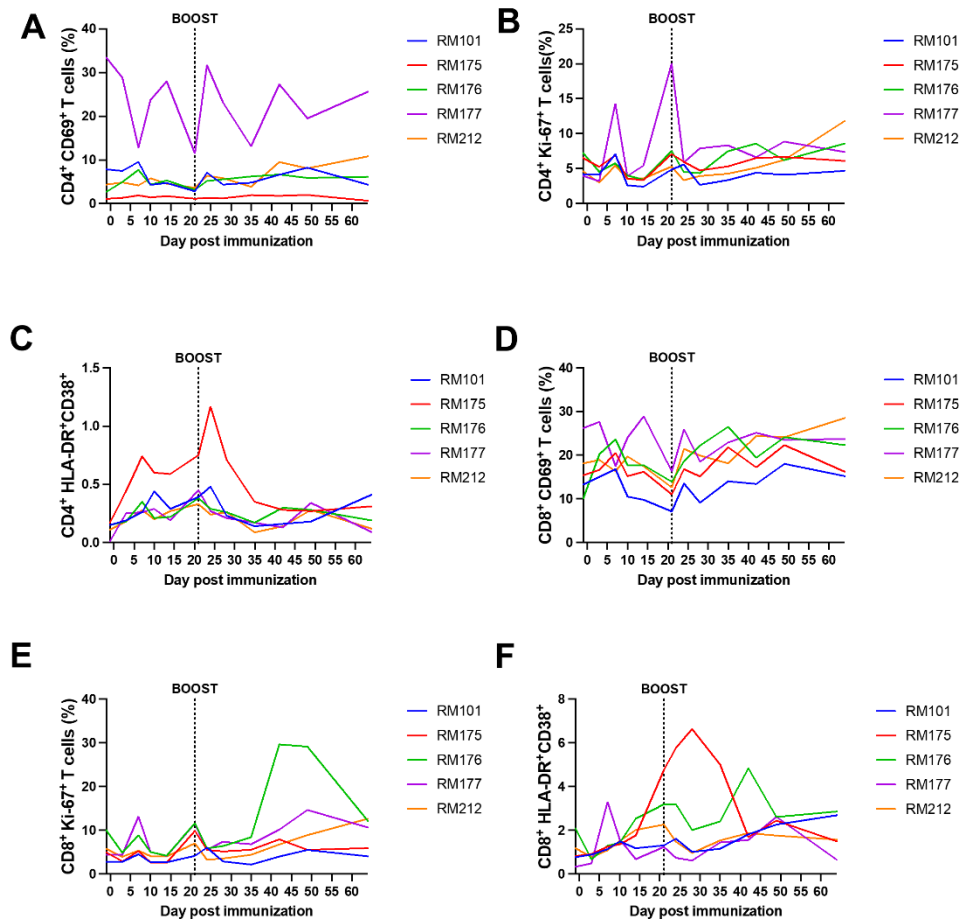
Figure 36: CD4 CD8 T cell activation post immunization and boost. Whole peripheral blood was stained with fluorescently labeled antibodies for CD4^{+}, CD8^{+}, CD69^{+}, Ki-67^{+}, and HLA-DR^{+} to investigate CD4 and CD8 activation induced by vaccination with flow cytometry. (A) Frequencies of CD4^{+} CD69^{+} T cells, (B) Frequencies of CD4^{+} Ki-67^{+} T cells, (C) Frequencies of CD4^{+} HLA-DR^{+} CD38^{+} T cells, (D) Frequencies of CD8^{+} CD69^{+} T cells, €

Frequencies of CD8$^+$ Ki-67$^+$ T cells, and (F) Frequencies of CD8$^+$ HLA-DR$^+$ CD38$^+$ T cells. PMBC's from RMs were collected and analyzed on Days -1, 3, 7, 10, 14, 21, 24, 28, 31, 35, 42, 49, and 64 days post prime immunization. Individual results for each RM are depicted.

Fig. 37 shows the changes in the distribution of T-cell memory subsets over time. We defined naïve, central memory (CM), and effector memory (EM) T cells using CD28$^+$ and CD95$^+$ markers. Naïve T cells are CD28$^+$ CD95^{neg}, CM T-cells are CD28$^+$ CD95$^+$, and EM T cells are CD28^{neg} CD95$^+$. We observed that both CD4$^+$ and CD8$^+$ central memory T cells (**Fig. 37A & 37D**), along with naïve CD4$^+$ naïve CD8$^+$ T cells (**Fig. 37C & 37F**), decreased in abundance after prime and boost, while CD4$^+$ and CD8$^+$ effector memory T cells (**Fig. 37B & 37E**) increased in abundance after prime boost. This finding suggests that the tetravalent S1 protein vaccine induces a shift towards an effector memory phenotype and away from a central memory phenotype, which may be beneficial in generating a rapid and robust response to vaccination.
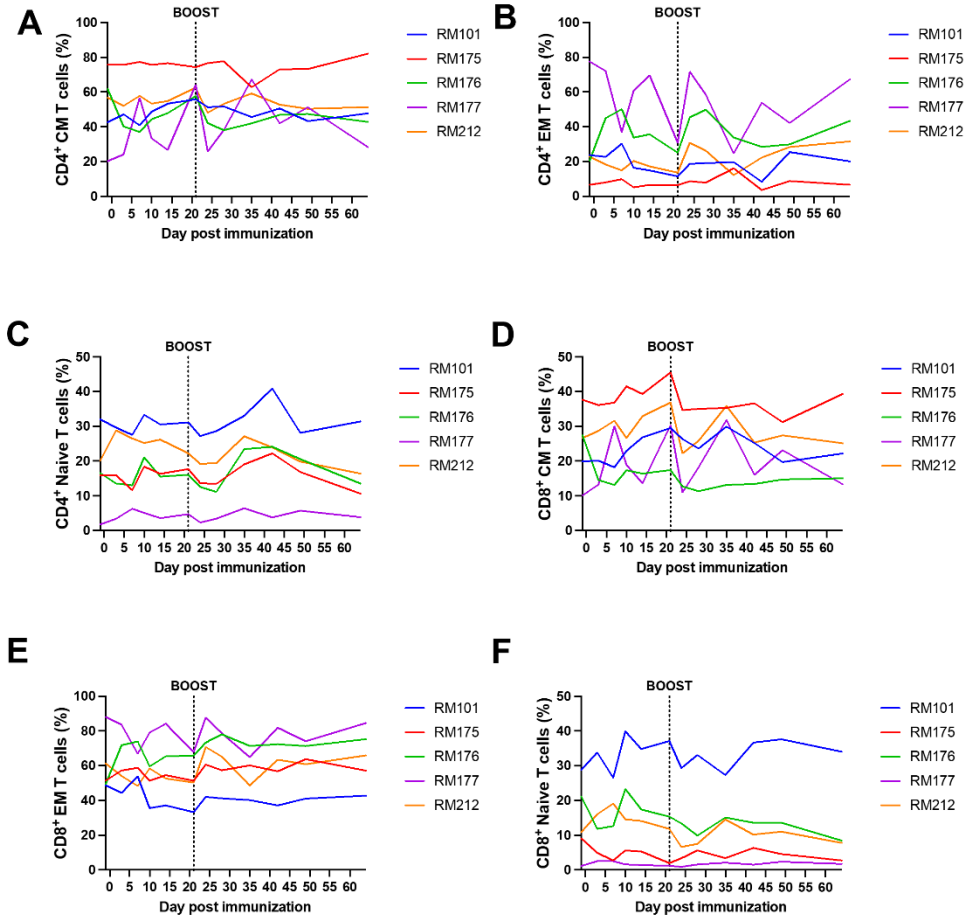
Figure 37: T cell memory subset dynamics and induction post immunization and boost. Whole peripheral blood was stained with fluorescently labeled antibodies for $CD4^+$, $CD8^+$, $CD28^+$ and $CD95^+$. Memory subsets were defined naive, central memory (CM), and effector memory (EM) T cells using $CD28^+$ and $CD95^+$ markers. Naive T cells are $CD28^+CD95-$, CM T cells are $CD28^+CD95^+$, and EM T cells are $CD28-CD95^+$. (A) Frequencies of $CD4^+$ CM T cells, (B) Frequencies of $CD4^+$ EM T cells, (C) Frequencies of $CD4^+$ Naive T cells, (D) Frequencies of $CD8^+$ CM T cells, (E) Frequencies of $CD8^+$ EM T cells, and (F) Frequencies of $CD8^+$ Naïve T cells. PMBC's from RMs were collected and analyzed on Days -1, 3, 7, 10, 14, 21, 24, 28, 31, 35, 42, 49, and 64 days post prime immunization. Individual results for each RM are depicted.

Intracellular cytokine staining was performed to evaluate the spike-specific T-cell responses in $CD4^+$ and $CD8^+$ T cells after stimulation with a spike peptide pool at day 0 and day 42 postvaccination in PBMCs (**Fig. 38**). We tested for interferon-gamma (IFN-γ), interleukin-2

(IL-2), and tumor necrosis factor-alpha (TNF-α) cytokine staining. Only RM212 induced an IFN-γ CD4$^+$ T-cell response, while no such response was observed in the other four RMs (**Fig. 38A**). In **Fig. 38B**, we observed an induction of IL-2 CD4$^+$ T-cell response in RM212 and to a lesser extent in RM101, but not in the other three RMs. **Fig. 38C** shows an induction of TNFα CD4$^+$ T-cell response in RM212, RM176 and, to a minimal extent, in RM101, RM175, and RM177. Notably, we were not able to detect a spike specific CD8$^+$ T-cell response at day 0 or day 42 post vaccination (data not shown). RM212 mounted a robust CD4$^+$ T-cell response for all three cytokines at day 42. These results suggest that there is a variable induction of cytokine responses in CD4$^+$ T cells among different RMs at day 42 postvaccination.
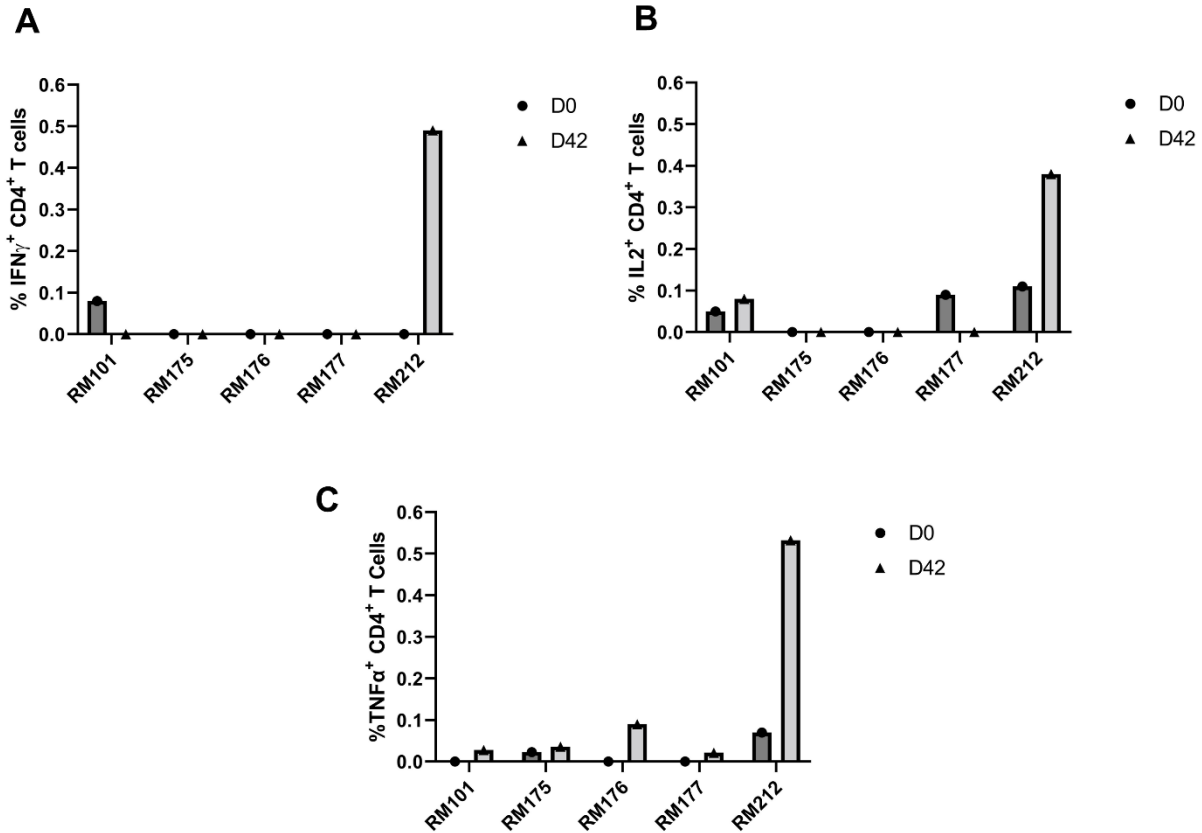
Figure 38: Spike-specific CD4+ T cell responses at Day 0 and Day 42 post immunization in PBMC's. PBMC's collected prior to immunization and on Day 42 post prime immunization were stimulated with PepTivator SARS-CoV-2-S1 (a pool of S1 MHC class I– and MHC class II– restricted peptides), followed by intracellular staining (ICS) and flow cytometry to identify SARS-CoV-2 S1 specific T cells. (A) Frequencies of SARS-CoV-2 S1 CD4$^+$ IFN-γ^+ T cells. Individual results for each RM are depicted. (B) Frequencies of SARS-CoV-2 S1 CD4$^+$ IL-2$^+$ T cells. Individual results for each RM are depicted. (C) Frequencies of SARS-CoV-2 S1 CD4$^+$ TNFα T cells. Individual results for each RM are depicted. Day 0 PBMC responses are indicated by solid circle. Day 42 PBMC responses are indicated by solid triangle.

Overall, the use of PBMC's allowed for the unique assessment of the dynamics of immune activation after vaccination. The results showed a clear increase in T-cell counts and activation after boost immunization, with the CD8$^+$ T-cell counts showing the greatest increase. The use of CD markers allowed for the differentiation of T-cell subsets and their activation status, with the

CD8^{+} T cells expressing either CD69 or Ki-67 CD8^{+} T cells showing the most robust dynamics. Additionally, there was evidence of a functional spike-specific CD4^{+} T-cell response in RMs at day 42 post vaccination, albeit in the context of no CD8^{+} T-cell response. These findings highlight the potential of this vaccine candidate to induce a robust cellular immune response, which is critical for controlling viral infections.

6.3 Materials and Methods

6.3.1 Construction of Recombinant Protein Expressing Vectors

The coding sequence for SARS-CoV-2-S1 amino acids 1 to 661 of full-length from BetaCoV/Wuhan/IPBCAMS-WH-05/2020 (GISAID accession id. EPI_ISL_ 403928) having C-terminal tag known as 'C-tag', composed of the four amino acids (aa), glutamic acid-proline-glutamic acid-alanine (E-P-E-A) flanked with *Sal* I & *Not* I was codon-optimized using the UpGene algorithm for optimal expression in mammalian cells [371] and synthesized (GenScript). The construct also contained a Kozak sequence (GCCACC) at the 5′ end. For Alpha variant (B.1.1.7), SARS-CoV-2-S1 mutated Del69-70; Del144; N501Y; A570D; D614G was synthesized. Also, Beta variant (B.1.351) of SARS-CoV-2-S1 (Del144; K417N; E484K; N501Y; A570D; D614G) and Gamma variant (P.1) of SARS-CoV-2-S1 (L18F; T20N; P26S; D138Y; R190S; K417T; E484K; N501Y; H655Y) were synthesized based on above codon-optimized SARS-CoV-2-S1 Wuhan. pAd/S1WU, pAd/S1Alpha, pAd/S1Beta, and pAd/S1Gamma, were then created by subcloning the four variants of codon-optimized SARS-CoV-2-S1 inserts into the shuttle vector,

pAdlox (GenBank U62024), at *Sal* I/*Not* I sites. The plasmid constructs were confirmed by DNA sequencing.

6.3.2 Transient Production in expi293 Cells

pAd/S1WU, pAd/S1Alpha, pAd/S1Beta, and pAd/S1Gamma, were amplified, and purified using ZymoPURE II plasmid maxiprep kit (Zymo Research). For Expi293 cell transfection, we used ExpiFectamie^{TM} 293 Transfection Kit (ThermoFisher) and followed the manufacturer's instructions. Cells were seeded 3.0×10^6 cells/ml one day before transfection and grown to 4.5-5.5×10^6 cells/ml. 1μg of DNA and ExpiFectamine mixtures per 1ml culture were combined and incubated for 15 min before adding into 3.0×10^6 cells/ml culture. At 20 h post-transfection, enhancer mixture was added, and culture was shifted to 32°C. The supernatants were harvested 5 days post transfection and clarified by centrifugation to remove cells, filtration through 0.8 μm, 0.45 μm, and 0.22 μm filters and either subjected to further purification or stored at 4°C before purification.

6.3.3 SDS-PAGE and Western Blot

To evaluate the expression of S1 from the plasmids, Expi293 cells were transfected with pAd/S1WU, pAd/S1Alpha, pAd/S1Beta, and pAd/S1Gamma, respectively. At 5 days after transfection, 10 μl each supernatant of Expi293 cells was subjected to sodium dodecyl sulfate polyacrylamide gel electrophoresis (SDS-PAGE) and Western blot as previously described [217]. Briefly, after the supernatants were boiled in Laemmli sample buffer containing 2% SDS with beta-mercaptoethanol (β-ME), the proteins were separated by Tris-Glycine SDS-PAGE gels and

transferred to nitrocellulose membrane. After blocking for 1 hour at room temperature (RT) with 5% non-fat milk in PBST, rabbit anti-SARS-CoV Wuhan spike polyclonal antibody (1:3000) (Sino Biological) was added and incubated overnight at 4 °C as primary antibody, and horseradish peroxidase (HRP)-conjugated goat anti-rabbit IgG (1:10000) (Jackson immunoresearch) was added and incubated at RT for 2 hours as secondary antibody. After washing three times with PBST, the signals were visualized on an iBright FL 1500 Imager (ThermoFisher).

6.3.4 Purification of Recombinant Proteins

The recombinant proteins named rS1WU, rS1Alpha, rS1Beta, and rS1Gamma were purified using a CaptureSelect™ C-tagXL Affinity Matrix prepacked column (ThermoFisher) and followed the manufacturer's guidelines. Briefly, The C-tagXL column was conditioned with 10 column volumes (CV) of equilibrate/wash buffer (20 mM Tris, pH 7.4) before sample application. Supernatant was adjusted to 20 mM Tris with 200 mM Tris (pH 7.4) before being loaded onto a 5-mL prepacked column per the manufacturer's instructions at 5 ml/min rate. The column was then washed by alternating with 10 CV of equilibrate/wash buffer, 10 CV of strong wash buffer (20 mM Tris, 1 M NaCl, 0.05% Tween-20, pH 7.4), and 5 CV of equilibrate/wash buffer. The recombinant proteins were eluted from the column by using elution buffer (20 mM Tris, 2 M MgCl$_2$, pH 7.4). The eluted solution was concentrated and desalted with preservative buffer (PBS) in an Amicon Ultra centrifugal filter devices with a 50,000 molecular weight cutoff (Millipore). The concentrations of the purified recombinant proteins were determined by the BCA protein assay kit (ThermoFisher) and separated by reducing SDS-PAGE and visualized by silver staining. The rest proteins were aliquoted and stored at −80°C until use.

6.3.5 ELISA

Sera from all rhesus macaques were collected prior to immunization and on weeks 3 and 7 after immunization. Sera was evaluated for SARS-CoV-2 S1-specific IgG using ELISA. ELISA plates were coated with 200 ng of recombinant SARS-CoV-2-S1 protein (Sino Biological) per well overnight at 4°C in carbonate coating buffer (pH 9.5) and then blocked with PBS-T and 2% bovine serum albumin (BSA) for one hour. Rhesus macaque sera was inactivated at 64°C for 40 minutes, then diluted in PBS-T with 1% BSA and incubated overnight. After the plates were washing, anti-monkey IgG-horseradish peroxidase (HRP) (1:50000, Sigma) were added to each well and incubated for one hour. The plates were washed three times, developed with 3,3'5,5'-tetramethylbenzidine, and the reaction was stopped with 1M H_2SO_4. Next, absorbance was determined at 450nm using a plate reader (Molecular Devices SPECTRAmax).

6.3.6 Animals and Immunizations

At week 0, male RMs (n=5 animals per group) were bled and primed with 60 μg of tetravalent rS1 proteins of Wuhan, B.1.1.7 (Alpha), B.1.351 (Beta), and P.1 (Gamma) [15μg of each antigen]. Total volume of 300 μl of antigen was mixed with 300 μl of AddaVax adjuvant then administered to RMs (600 μl injection volume). RMs were bled on week 3 and received a homologous booster of 60 μg of tetravalent rS1 proteins. RMs were bled on weeks 7. RMs were also bled and serially euthanized after week 9 post-prime vaccination: on day 0 (RM177), 1 (RM175), 6 (RM176), 8 (RM101), and 15 (RM175). PMBC's from RMs were collected and analyzed on Days -1, 3, 7, 10, 14, 21, 24, 28, 31, 35, 42, 49, and 64 days post prime immunization.

RMs were maintained under specific pathogen-free conditions at the University of Pittsburgh, and all experiments were conducted in accordance with animal use guidelines and protocols approved by the University of Pittsburgh's Institutional Animal Care and Use (IACUC) Committee.

6.3.7 SARS-CoV-2 Microneutralization Assay

Neutralizing antibody (NT-Ab) titers against SARS-CoV-2 were defined according to the following protocol [379,380]. Briefly, 50 µl of sample from each mouse, starting from 1:10 in a twofold dilution, were added in two wells of a flat bottom tissue culture microtiter plate (COSTAR, Corning Incorporated, NY 14831, USA), mixed with an equal volume of 100 TCID50 of a SARS-CoV-2 Wuhan, Beta, or Delta strain isolated from symptomatic patients, previously titrated, and incubated at 33°C in 5% CO_2. All dilutions were made in EMEM (Eagle's Minimum Essential Medium) with addition of 1% penicillin, streptomycin and glutamine and 5 γ/mL of trypsin. After 1 hour incubation at 33°C 5% CO_2, 3×10^4 VERO E6 cells [VERO C1008 (Vero 76, clone E6, Vero E6); ATCC® CRL-1586™] were added to each well. After 72 hours of incubation at 33°C 5% CO_2 wells were stained with Gram's crystal violet solution (Merck KGaA, 64271 Damstadt, Germany) plus 5% formaldehyde 40% m/v (Carlo ErbaSpA, Arese (MI), Italy) for 30 min. Microtiter plates were then washed in running water. Wells were scored to evaluate the degree of cytopathic effect (CPE) compared to the virus control. Blue staining of wells indicated the presence of neutralizing antibodies. Neutralizing titer was the maximum dilution with the reduction of 90% of CPE. A positive titer was equal or greater than 1:10. The geometric mean titers (GMT) of NT_{90} end point titer were calculated with 4 as a negative shown <10. Sera from mice before vaccine administration were always included in microneutralizaiton (NT) assay as a negative control.

6.3.8 ACE2 Blocking Assay

Antibodies blocking the binding of SARS-CoV-2 spike variants (Alpha (B.1.1.7), Beta (B.1.351), Gamma (P.1), Delta (B.1.617.2), Zeta (P.2), Kappa (B.1.617.1), New York (B.1.516.1), India (B.1.617 and B.1.617.3)) to ACE2 were detected with a V-PLEX SARS-CoV-2 Panel 18 (ACE2) Kit (Meso Scale Discovery (MSD) according to the manufacturer's instructions. Antibodies blocking the binding of SARS-CoV-2 spike including Wuhan and spikes from immune evasive variants; BA.1, BA.2, AY.4 (Delta lineage), BA.3, BA.1+R346K mutation, BA.1+L452R mutation, B.1.1.7 (Alpha), B.1.351 (Beta), and B.1.1640.2 to ACE2 were detected with a V-PLEX SARS-CoV-2 Panel 25 (ACE2) Kit (Meso Scale Discovery (MSD) according to the manufacturer's instructions. Serum samples were diluted (1:10 and 1:100). The assay plate was blocked for 30 min and washed. Serum samples were diluted (1:10 for P18; 1:10 & 1:100 for P25) and 25 µl were transferred to each well. The plate was then incubated at room temperature for 60 min with shaking at 700 rpm, followed by the addition of SULFO-TAG conjugated ACE2, and continued incubation with shaking for 60 min. The plate was washed, 150 µl MSD GOLD Read Buffer B was added to each well, and the plate was read using the QuickPlex SQ 120 Imager. Electrochemiluminescent values (ECL) were generated for each sample. Results were calculated as % inhibition compared to the negative control for the ACE2 inhibition assay, and % inhibition is calculated as follows: % neutralization $= 100 \times (1 -$ (sample signal/negative control signal).

6.3.9 Flow Cytometry

Absolute counts of immune cells in whole blood and immunophenotyping of circulating immune cells were determined by flow cytometry. First, 50 µl of whole blood were added to a

TruCount tube (BD Biosciences) containing an antibody mix, allowing to precisely quantify CD45$^+$ cell counts in blood, as well as CD4$^+$ and CD8$^+$ T cells, and CD20$^+$ B cells. Whole peripheral blood was stained with fluorescently-labeled antibodies (all purchased from BD Bioscience, San Jose, CA, USA, unless noted otherwise): CD3 (clone SP34-2, V450), CD4 (clone L200, APC), CD8 (clone RPA-T8, PE-CF594), CD28 (clone CD28.2, PE-Cy7), CD38 (clone AT-1, FITC) (Stemcell), CD45 (clone D058-1283, PerCP), CD69 (clone FN50, APC-H7), CD95 (clone DX2, FITC), HLA-DR (clone L243, PE-Cy7), Ki-67 (clone P56, PE). For intracellular staining, cells were fixed and permeabilized with 1X BD Fix/Perm, before being stained for Ki-67. Flow cytometry acquisitions were performed on an LSRFortessa flow cytometer (BD Biosciences), and flow data were analyzed using FlowJo® v10.8.0 (TreeStar, Ashland, OR, USA).

6.3.10 Spike-Specific Intracellular Staining

Antigen-specific T-cell responses in the PBMC's of RMs immunized as described above were analyzed after immunization by flow cytometry, adhering to the recently published guidelines [189,426]. PBMCs collected prior to immunization and on Day 42 post prime immunization were stimulated with PepTivator SARS-CoV-2-S1 (a pool of S1 MHC class I– and MHC class II– restricted peptides) overnight in the presence of protein transport inhibitors (Golgi Stop) for the last 4 hours. Unstimulated cells were used as negative controls. Phorbol myristate acetate (PMA) and ionomycin stimulated cells served as positive controls. Cell were washed with FACS buffer (PBS, 2 % FCS), incubated with Fc Block (BD Biosciences, 553142) for 5 min at 4°C, and stained with surface marker antibody (Ab) stain for 20 min at 4°C. Surface Abs were used as follows: CD3-V450 (SP34-2, V450, BD Biosciences), CD4-APC (L200, APC, BD Biosciences), and CD8ab-PE-CF594 (RPA-T8, PE-CF594, BD Biosciences). For dead cell exclusion, cells were

stained with Zombie NIR Fixable Viability dye (BioLegend) for 10 min at 4°C and washed in FACS buffer. Intracellular cytokine staining (ICS) was performed on surface Ab-stained cells by first fixing and permeabilizing cells using the FoxP3 Transcription Factor Staining Buffer kit (eBioscience, 00-5523-00) following manufacturer's instructions. Intracellular staining with IFNγ-FITC (4S.B3, FITC, BD Biosciences), IL2-PE (MQ1-17H12, PE, BD Biosciences), and TNFa-AF700 (Mab11, AF700, BD Biosciences). Samples were run on an Aurora (Cytek) flow cytometer and flow data were analyzed using FlowJo® v10.8.0 (TreeStar, Ashland, OR, USA).

6.4 Discussion

We evaluated the immunogenicity and efficacy of a tetravalent COVID-19 vaccine candidate based on the spike S1 protein of SARS-CoV-2 in an NHP model of controlled SIV infection. RMs infected with SIVsab from African green monkeys are able to control viral replication and disease progression through maintaining a healthy immune system, unlike HIV-1 in humans [494]. The SIVsab-infected RMs in this study were elite controllers for about a year prior to SARS-CoV-2 immunization.

There were weaker band in western blot of the supernatant after a transient transfection with pAd/S1Alpha, pAd/S1Beta, and pAd/S1Gamma compared with pAd/S1WU **(Fig. 31B)**, which might be explained by the usage of anti-spike of SARS-CoV-2 Wuhan as a primary antibody. Indeed, no big differences were observed in yield pre or post C-tag purification of each recombinant proteins after transient transfection by sandwich ELISA with standard of each purified rS1 proteins.

Our vaccine formulation induced high levels of binding antibodies against the Wuhan strain of SARS-CoV-2, as well as neutralizing antibodies against live B.1.351 (Beta), and B.1.617.2 (Delta) VOC (**Fig. 32**). The sera of vaccinated RMs exhibited potent ACE2-binding inhibition capabilities against a suite of SARS-CoV-2 VOC spikes including Omicron (BA.1) and Omicron subvariants (BA.2, BA.3, BA.1+R246K, and BA.1+L452R) (**Fig. 33 & Fig. 34**). These findings are consistent with previous studies demonstrating the immunogenicity and cross-reactivity of COVID-19 vaccines NHP models [292,293,297–300,499].

Importantly, the vaccine candidate also induced cellular immune responses, including T cell responses, which have been shown to play a critical role in COVID-19 immunity and protection [243,311–317]. We investigated the cellular immune response to the tetravalent SARS-CoV-2 vaccine in vaccinated RMs, using a range of markers to examine T-cell subsets and activation status. The results showed that all T-cell subsets and B cells increased after the prime and especially after the boost, with the CD8$^+$ T-cell count showing the greatest increase after boost immunization compared to other cell types (**Fig. 35**). We demonstrate that the tetravalent S1 subunit protein COVID-19 vaccine candidate induces CD4$^+$ and CD8$^+$ T-cell activation, as indicated by increased expression of CD69, HLA-DR, CD38, and Ki-67 activation and proliferation markers on both T-cell subsets (**Fig. 36**). The distribution of T-cell memory subsets over time was also investigated, revealing a decrease in abundance of both CD4$^+$ and CD8$^+$ central memory T cells, along with CD4$^+$ and CD8$^+$ naive T cells after prime and boost (**Fig. 37**). In contrast, CD4$^+$ and CD8$^+$ effector memory T cells increased in abundance after prime boost, indicating a shift towards an effector memory phenotype and away from a central memory phenotype induced by the tetravalent S1 protein vaccine (**Fig. 37**). Furthermore, intracellular cytokine staining was performed to evaluate the spike-specific responses of CD4$^+$ and CD8$^+$ T

cells after stimulation with a spike peptide pool (**Fig. 38**). Cytokine staining for IFN-γ, IL-2, and TNF-α was tested and a variable induction of cytokine responses by CD4$^+$ T cells among different RMs at day 42 postvaccination was observed (**Fig. 38**). However, no spike-specific response of the CD8$^+$ T cells was detected at day 0 or day 42. It is possible that the spike-specific CD8$^+$ T cells were present, but were not detected by the intracellular staining assay, as this assay may not be sensitive enough to detect low-frequency antigen-specific CD8$^+$ T cells. It is also possible that the undetectable spike-specific CD8$^+$ T-cell response at day 42 post-vaccination was related to the time-point used, which was too late after boost, such as the vaccine-specific T cells had already started to wane in abundance, as shown by Arunachalam et al [500]. Altogether, our study demonstrates that the tetravalent S1 protein vaccine candidate was able to induce a robust SARS-CoV-2-specific immune response in RMs, which is promising for future development and testing of COVID-19 vaccines in humans.

The results of our study have important implications for COVID-19 vaccine development and implementation in humans. The vaccine candidate induced not only humoral immune responses but also cellular immune responses, which have been shown to be important for long-term immunity [318]. The use of RMs as an animal model for studying vaccine efficacy has been widely accepted in the scientific community [133,291,292,501]. Here we have used RM controllers based on the rationale that SIV controllers have a nearly healthy immune system (able to control SIV replication) [494]. We also wanted to assess whether the induction of T-cell activation at the effector sites would result in a burst of SIV replication. Such a boosting of SIV was reported to occur after administration of vectorized vaccines [502]. The use of NHP models has been shown to be highly informative for predicting vaccine efficacy in humans [503,504].

The results showed that the vaccine induced both humoral and cellular immune responses against SARS-CoV-2, including neutralizing antibodies, ACE2 blocking antibodies, and T-cell responses. Furthermore, the vaccine candidate was able to generate Omicron variant binding and ACE2 blocking antibodies without specifically vaccinating with Omicron, suggesting the potential for broad protection against emerging variants [402,421,445,505,506]. This is particularly significant given the emergence of highly diverged SARS-CoV-2 variants, such as Omicron, which have raised concerns about vaccine efficacy and the need for updated vaccines [402,421,505,507]. Another significant feature of the vaccine candidate is its tetravalent composition, which targets the spike proteins of four different SARS-CoV-2 variants. This approach has the potential to provide broad protection against multiple SARS-CoV-2 variants, as well as to minimize the risk of immune escape and emergence of new variants.

Protein subunit vaccines are known for their safety, ease of large-scale production, and distribution, and have been used in other successful vaccine campaigns, such as the hepatitis B vaccine [425,503,508,509]. This makes protein subunit vaccines an ideal candidate for worldwide vaccine equity, particularly for countries that may not have access to the more complex mRNA or viral vector vaccine platforms. Furthermore, the ability to store and transport protein subunit vaccines at a relatively low temperature (-20°C to 4°C) , compared to the ultra-low temperature required for mRNA vaccines, makes their distribution and administration easier in resource-limited settings [71,510]. The protein subunit platform is also amenable to alternative routes of administration, such as intradermal delivery, which has been shown to increase immunogenicity in other vaccine studies [208,217,511,512]. In summary, the tetravalent S1 protein subunit vaccine represents a promising vaccine candidate against SARS-CoV-2, particularly for populations that may not have access to other vaccine platforms and could potentially be further optimized to enhance its immunogenicity.

However, it should be noted that this study has limitations. The sample size was small and we did not perform a SARS-CoV-2 virus challenge in our vaccinated RMs to fully assess vaccine efficacy [293,500]. While our results show promising immune responses to the tetravalent SARS-CoV-2 vaccine in RMs, a virus challenge would have provided further insights into the effectiveness of the vaccine in preventing infection and disease. Additionally, our study did not evaluate the durability of the antibody response generated by the vaccine over a longer period. Studies have shown that antibody responses to SARS-CoV-2 vaccines may wane over time, which highlights the importance of evaluating the longevity of vaccine-induced immunity [413,513–517]. Finally, we did not assess mucosal immunity in our study, which is an important aspect of immune protection against respiratory viruses like SARS-CoV-2. Mucosal immunity may provide an additional layer of protection against infection and transmission, and future studies should investigate the mucosal immune response to the tetravalent SARS-CoV-2 vaccine [135,298,418,518,519].

The tetravalent S1 subunit protein COVID-19 vaccine candidate evaluated in this study contained SARS-CoV-2 S1 antigens from the Wuhan strain, as well as the B.1.1.7 variant, B.1.351 variant, and P.1 variant. Our study demonstrates that this vaccine candidate can induce both humoral and cellular immune responses, as evidenced by increased cell counts in both T and B cells, and the production of neutralizing and cross-reactive antibodies, as well as ACE2 blocking antibodies and T cell responses. It is important to note that the RMs used in this study were infected with SIVsab and controlled the infection for a year prior to immunization. The ability of these animals to control the SIVsab infection, without reactivation of virus upon immunization, while mounting immune responses to the vaccine candidate, further demonstrates the potential of this vaccine candidate to provide robust protection against SARS-CoV-2, even in individuals with pre-existing conditions. Moreover, the tetravalent composition of the vaccine candidate has significant

implications for COVID-19 vaccine development and implementation, with the potential to provide broad protection against multiple SARS-CoV-2 variants and to minimize the risk of immune escape and emergence of new variants.

6.5 Acknowledgements

7.0 Development of Chimeric Spike Protein Vaccines for SARS-CoV-2 and MERS

7.1 Introduction

The recent SARS-CoV-2 outbreak has had a profound impact on human health, underscoring the ongoing pandemic threat posed by Betacoronaviruses. The COVID-19 pandemic, first declared by the World Health Organization on March 11, 2020, has resulted in approximately 6.9 million deaths as of May 15, 2023. Similarly, Middle East Respiratory Syndrome (MERS) is a Betacoronavirus that was first identified in Saudia Arabia in 2012 [252]. As of March 2023, there have been 2,604 laboratory-confirmed cases of MERS-CoV infection, with 936 deaths reported to the World Health Organization and a mortality rate of around 36% [252]. Although most cases have occurred in the Middle East, MERS-CoV has also been reported in other regions, including Europe and Asia [253].

Betacoronaviruses, a genus of enveloped, positive-sense RNA viruses within the Coronaviridae family, are known to cause varying degrees of respiratory illnesses in humans and animals. The first human BetaCoronavirus to cause substantial human morbidity and mortality, Severe Acute Respiratory Syndrome Coronavirus (SARS-CoV), emerged in 2002 and caused a global outbreak of Severe Acute Respiratory Syndrome (SARS) [221,222]. This was followed. By the emergence of the Middle East Respiratory Syndrome Coronavirus (MERS-CoV) in 2012, resulting in subsequent outbreaks in the Middle East and South Korea [221,223]. The recent emergence of SARS-CoV-2 in late 2019, responsible for the COVID-19 pandemic, has further highlighted the urgency of understanding the virology and pathogenesis of BetaCoronaviruses. Developing a vaccine targeting both SARS-CoV-2 and MERS-CoV would significantly enhance protection

189

against the pandemic potential of Betacoronaviruses, potentially inducing broad S1-targeting antibodies and increasing the potency of SARS-CoV-2 protein vaccines.

To effectively prevent the spread of BetaCoronaviruses, it is crucial to develop safe and effective vaccines capable of eliciting potent and durable virus-specific immune responses [217,329–332]. Betacoronaviruses (Beta-CoVs), such as SARS-CoV-2 and MERS, are enveloped, positive-sense, ssRNA viruses [247,333]. BetaCoVs encode the envelope, nucleocapsid, membrane, and spike (S) proteins [334,335]. Among these components, the spike protein has garnered significant attention due to its proven role in the virus infection process [336]. The trimeric class I fusion transmembrane S glycoprotein of the viral envelope is comprised of two subunits, S1 and S2, that function in viral attachment to the host cell receptor and in fusion to the cells, respectively [336,337]. For instance, the S protein on the envelope of SARS-CoV-2 binds to the cell receptor angiotensin-converting enzyme 2 (ACE2) and facilitates viral entry [337,338]. The S protein of MERS-CoV is also a trimeric transmembrane glycoprotein that mediates viral entry into host cells, however, by binding to the host cell receptor dipeptidyl peptidase 4 (DPP4) [221,223,253]. Our previous efforts on the development of vaccines against SARS-CoV, MERS-CoV, and SARS-CoV-2 have shown that vaccine candidates targeting the S1 subunit are capable of generating efficacious neutralizing antibody responses [343,344]. We have also presented that skin-targeted S1 subunit protein vaccines induce antigen-specific antibody responses against MERS-CoV and SARS-CoV-2 [217].

SARS-CoV-2 and MERS-CoV share various similarities, including their Betacoronavirus classification, genome organization, and utilization of furin cleavage site for S protein priming [221,223]. However, they differ in their primary human receptor. While SARS-CoV-2 utilizes ACE2 for entry, MERS-CoV utilizes DPP4 [221,223]. This difference in receptor utilization likely contributes to the differences in their clinical presentation and disease severity. Additionally, while both

viruses can cause severe respiratory illness, the mortality rate of MERS-CoV is higher compared to SARS-CoV-2, with MERS having a mortality rate of approximately 35-36% and COVID-19 approximately 5.6% in July 2020 [221,223,259].

Although approved COVID-19 vaccines demonstrated effectiveness in reducing mortality and morbidity caused by SARS-CoV-2 infection, the emergence of new variants that can evade the preexisting immunity to SARS-CoV-2 has raised concerns about their long-term efficacy. Moreover, the uneven distribution of vaccines worldwide has resulted in many low to middle-income countries being left without access to variant-specific vaccines that are better suited for the evolving SARS-CoV-2 variant landscape [13,249,250]. This situation underscores the need for the development of vaccines that can provide broad protection against a range of SARS-CoV-2 variants, as well as the importance of the equitable distribution of vaccines to mitigate the risk of further virus evolution and spread [1,13,249,250]. Our laboratory has previously described in the literature the robust neutralizing antibody-inducing capabilities of both protein subunit and viral vector MERS and SARS-CoV-2 vaccines expressing S1. MERS, while displaying different disease kinetics and cellular receptors, shares homology in the spike protein with SARS-CoV-2. Notably, MERS S1 vaccines exhibit potent neutralizing capability, while our SARS-CoV-2 S1 vaccine candidates show relatively low neutralizing ability. To address this limitation, we propose a novel approach utilizing the MERS S1 as a scaffold to present the RBD of SARS-CoV-2 which may overcome the deficiency in SARS-CoV-2 neutralizing antibodies. Alternatively, employing the SARS-CoV-2 RBD in a MERS S1 scaffold may induce a broad array of antibodies targeting the hybrid S1, which could potentially protect against a wider range of SARS-CoV-2 variants and MERS. Additionally, there is potential for a hybrid SARS-CoV-2 and MERS S1 to allow for a

multi-Betacoronavirus vaccine, the first of its kind, and may better inform future universal Betacoronavirus vaccine design.

7.2 Results

7.2.1 Design and Expression of Recombinant Proteins

Recombinant proteins of SARS-CoV-2 and MERS S1, pAd/MERS RBD in SARS-CoV-2 S1 (MersRBDS2 Chimera), pAd/SARS-CoV-2 RBD in MERS S1 (SARS2RBDMers Chimera), pAd/SARS-CoV-2 S1 (SARS2 S1), and pAd/MERS S1 were generated by subcloning the codon-optimized S1 gene having C-tag and TLR4 agonist peptide RS09 into the shuttle vector, pAd (GenBank U62024) at SalI and NotI sites. To determine S1 expression and purity post C-tagXL affinity matrix purification, proteins were separated by 10% SDS-PAGE and assessed by western blot and silver staining (**Fig. 39**). The purified recombinant proteins, MERS RBDS2 S1 (lane 1), SARS2RBDMers S1 (lane 2), SARS-CoV-2 S1 (lane 3), and MERS S1 (lane 4) were visualized at their expected glycosylated monomeric molecular weights of about 110 kDa under the denaturing reduced conditions (**Fig. 39A**). The proteins, MERS RBDS2 S1 (lane 1), SARS2RBDMers S1 (lane 2), MERS S1 (lane 3), and SARS-CoV-2 S1 (lane 4) were also recognized by anti-spike SARS-CoV-2 antibodies or anti-spike MERS antibodies through western blot (**Fig 39B**). Mice were prime and boosted on weeks 3 and 6 with either 10 µg of MERS RBDS2 S1, SARS2RBDMers S1, SARS-CoV-2 S1 (WU S1), or MERS S1 (**Fig. 39C and 39D**). Adenovirus vectored MERS targeting vaccines using either an Ad5 human adenovirus

(Ad5.MERS-S1) or chimpanzee adenovirus (ChAd.MERS-S1) were also included as positive

MERS controls at a dose of $1x10^{10}$ v.p. and were only boosted once at week 3.
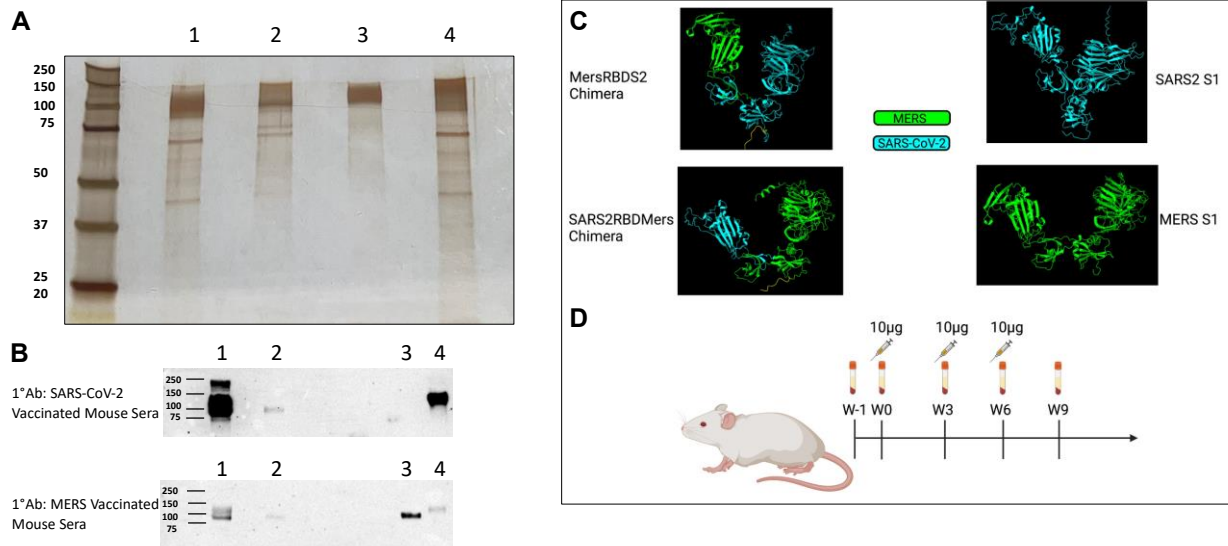
Figure 39: Design and expression of MERS SARS-CoV-2 chimeric S1. (A) Silver-stained reducing SDS-PAGE gel of purified Expi293 cell-derived; MERS RBDS2 S1 (lane 1), SARS2RBDMers S1 (lane 2), SARS-CoV-2 S1 (lane 3), and MERS S1 (lane 4). (B) Detection of the SARS-CoV-2-S1 proteins by western blot with purified proteins using anti-S SARS-CoV-2 polyclonal antibodies (top) and detection of the MERS proteins by western blot with purified proteins using anti-S MERS polyclonal antibodies (bottom); MERS RBDS2 S1 (lane 1), SARS2RBDMers S1 (lane 2), MERS S1 (lane 3), and SARS-CoV-2 S1 (lane 4). (C) AlphaFold V2 protein structure prediction of recombinant proteins with MERS portions in green and SARS-CoV-2 portions in cyan. (D) Diagram of immunization schedule for in-vivo immunogenicity assessment.

7.2.2 SARS-CoV-2 and MERS Binding Antibody Responses

We collected serum samples from all mice before immunization, which were used set the endpoint titer cutoff for all antibody ELISA's [437]. Serum samples collected on weeks 3, 6, and 9

after prime immunization were serially diluted to determine SARS-CoV-2-S1-specific (**Fig. 40**)

and MERS-S1-specific IgG titers (**Fig. 41**) for each immunization group using ELISA.
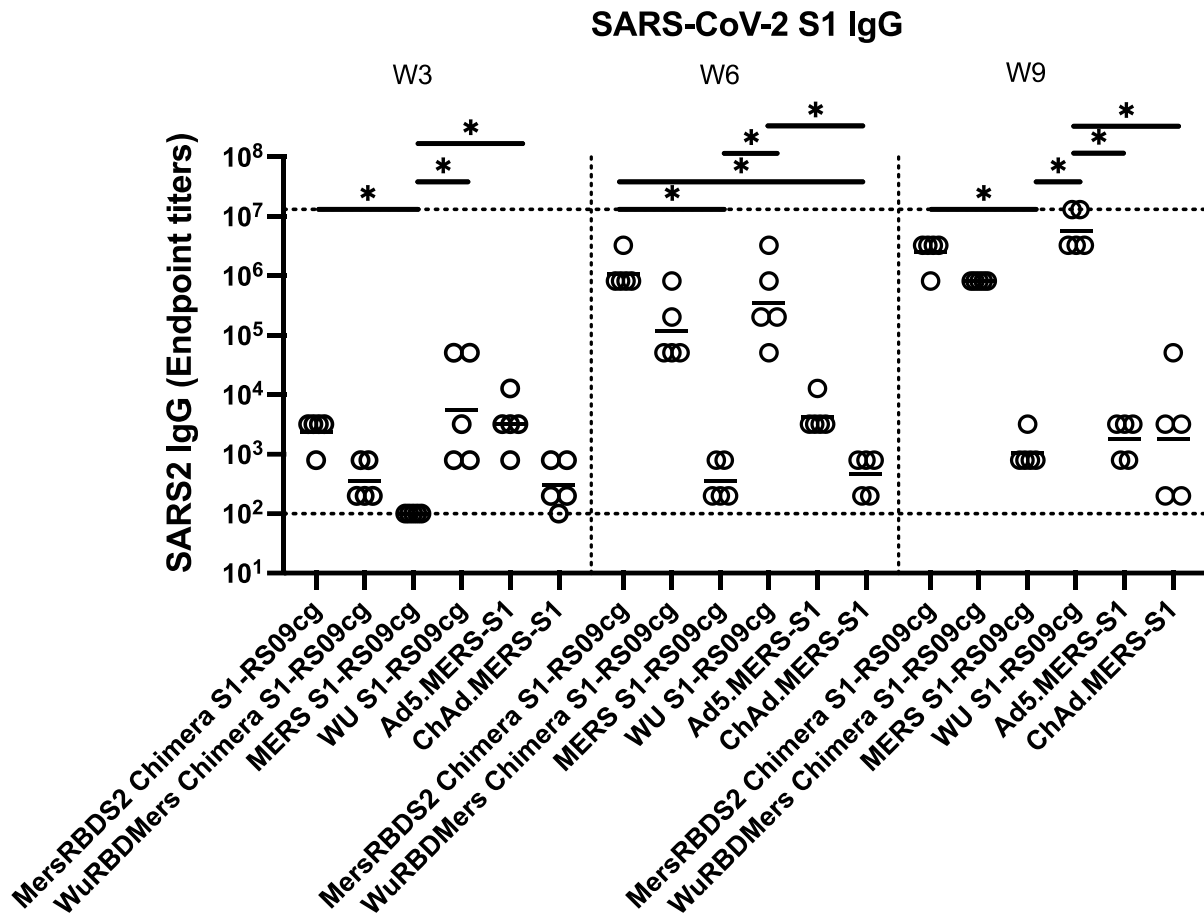
Figure 40: SARS-CoV-2 binding IgG response. BALB/c mice (n = 5 mice per group) were immunized

intramuscularly with 10 μg of either MERS RBDS2 S1, SARS2RBDMers S1, SARS-CoV-2 S1, or MERS S1 and

received a homologous booster at week 3 and week 6. Ad5.MERS-S1 and ChAd.MERS-S1 was given at a dose of

1×10^{10} v.p. and was only boosted once at week 3. On weeks 3, 6, and 9 sera from mice were collected, serially diluted

(200×), and tested for the presence of Wuhan SARS-CoV-2-S1-specific IgG antibody levels by ELISA. Significance

was determined by the Kruskal-Wallis test followed by Dunn's multiple comparisons (* $p < 0.05$). Horizontal solid

lines represent geometric mean antibody titers. Serum collected on week 0, before immunization, was used to set the

ELISA endpoint titer cutoff.

194

Figure 41: MERS IgG binding IgG response. BALB/c mice (n = 5 mice per group) were immunized intramuscularly with 10 µg of either MERS RBDS2 S1, SARS2RBDMers S1, SARS-CoV-2 S1, or MERS S1 and received a homologous booster at week 3 and week 6. Ad5.MERS-S1 and ChAd.MERS-S1 was given at a dose of $1\text{x}10^{10}$ v.p. and was only boosted once at week 3. On weeks 3, 6, and 9 sera from mice were collected, serially diluted (200×), and tested for the presence of MERS-S1-specific IgG antibody levels by ELISA. Significance was determined by the Kruskal-Wallis test followed by Dunn's multiple comparisons (* $p < 0.05$). Horizontal solid lines represent geometric mean antibody titers. Serum collected on week 0, before immunization, was used to set the ELISA endpoint titer cutoff.

Against Wuhan SARS-CoV-2 S1, all solely MERS targeting vaccine antigens (MERS S1-RS09cg, Ad5.MERS-S1, and ChAd.MERS-S1) expectedly elicited the least amount of SARS-CoV-2 IgG antibodies. At week 3; MerRBDS2 S1-RS09cg, WU S1-RS09cg, and Ad5.MERS-S1

had significantly greater geometric mean SARS-CoV-2 IgG EPT than MERS S1-RS09cg (**Fig. 40**, $p < 0.05$, Kruskal-Wallis test, followed by Dunn's multiple comparisons). At week 6; MersRBDS2 S1-RS09cg had significantly greater geometric mean SARS-CoV-2 IgG EPT than MERS S1-RS09cg and ChAd.MERS-S1 (**Fig. 40**, $p < 0.05$, Kruskal-Wallis test, followed by Dunn's multiple comparisons). Similarly, at week 6 WU S1-RS09cg also had significantly greater geometric mean SARS-CoV-2 IgG EPT than MERS S1-RS09cg and ChAd.MERS-S1 (**Fig. 40**, $p < 0.05$, Kruskal-Wallis test, followed by Dunn's multiple comparisons). Following the second homologous booster dose at week 6; at week 9 MersRBDS2 S1-RS09cg and WU S1-RS09cg achieved the highest SARS-CoV-2 IgG EPT (**Fig. 40**). MersRBDS2 S1-RS09cg had significantly greater geometric mean SARS-CoV-2 IgG EPT than MERS S1-RS09cg at week 9 (**Fig. 40**, $p < 0.05$, Kruskal-Wallis test, followed by Dunn's multiple comparisons). Likewise, WU-S1RS09cg had significantly greater geometric mean SARS-CoV-2 IgG EPT than MERS-S1RS09cg, Ad5.MERS-S1, and ChAd.MERS-S1 at week 9 (**Fig. 40**, $p < 0.05$, Kruskal-Wallis test, followed by Dunn's multiple comparisons). At weeks 6 and 9, WuRBDMers S1-RS09cg had the third greatest geometric mean SARS-CoV-2 IgG EPT, following WU S1-RS09cg and MersRBDS2 S1-RS09cg, indicating induction of SARS-CoV-2 immunity, however, was not statistically significantly increased versus MERS constructs (**Fig. 40**, $p > 0.05$, Kruskal-Wallis test, followed by Dunn's multiple comparisons). These results suggest that both SARS-CoV-2 and MERS chimeric constructs, MersRBDS2 S1-RS09cg and WuRBDMers S1-RS09cg, were able to elicit SARS-CoV-2 IgG antibodies with MerRBDS2 Chimera S1-RS09cg being at a greater degree.

Against MERS S1; WuRBDS2 S1-RS09cg, MERS S1-RS09cg, and Ad5.MERS-S1 elicited the highest geometric mean MERS-IgG EPT at weeks 3, 6, and 9 (**Fig. 41**). Specifically at week 3, MERS-S1RS09cg and Ad5.MERS.S1 had significantly greater geometric mean MERS-

IgG EPT than MersRBDS2 S1-RS09cg (**Fig. 41**, $p < 0.05$, Kruskal-Wallis test, followed by Dunn's multiple comparisons). At week 3, Ad5.MERS-S1 also had significantly greater geometric mean MERS-IgG EPT than WU S1-RS09cg (**Fig. 41**, $p < 0.05$, Kruskal-Wallis test, followed by Dunn's multiple comparisons). At week 6, both MERS S1-RS09cg and Ad5.MERS-S1 had significantly greater geometric mean MERS-IgG EPT than MersRBDS2 S1-RS09cg and WU S1-RS09cg (**Fig. 41**, $p < 0.05$, Kruskal-Wallis test, followed by Dunn's multiple comparisons). At week 9, WuRBDMers S1-RS09cg, MERS S1-RS09cg, and Ad5. MERS-S1 achieved similarly high levels of MERS S1 IgG (**Fig. 41**). WuRBDMers S1-RS09cg, MERS S1-RS09cg, and Ad5.MERS-S1 achieved significantly greater geometric mean MERS-IgG EPT than MersRBDS2 S1-RS09cg (**Fig. 41**, $p < 0.05$, Kruskal-Wallis test, followed by Dunn's multiple comparisons). These results suggest that placing the SARS-CoV-2 Wuhan RBD in MERS S1 was able to elicit MERS-specific IgG antibodies to a similar EPT as solely MER S1-RS09cg and Ad5.MERS-S1.

Next, we aimed to investigate the level of IgG binding antibodies that were specific for the SARS-CoV-2 RBD within the S1 protein, to gauge the potential effect of placing the Wuhan RBD into a MERS S1 scaffold, in the case of WuRBDMers S1-RS09cg (**Fig. 42**). Week 6 (left panel) and week 9 (right panel) sera were used to gauge SARS-CoV-2 RBD-specific IgG antibodies using a Delta variant specific RBD-cg recombinant protein. At week 6 and week 9, both WuRBDMers S1-RS09cg and WU S1-RS09cg achieved the greatest geometric mean SARS-CoV-2 Delta RBD-IgG EPT (**Fig. 42**). Notably, WuRBDMersS2 S1-RS09cg had a greater geometric mean SARS-CoV-2 Delta RBD-IgG EPT than WU S1-RS09cg (**Fig. 42**). Specifically, at week 6 both WuRBDMers S1-RS09cg and WU S1-RS09cg had significantly greater geometric mean SARS-CoV-2 Delta RBD-IgG EPT than MersRBDS2 S1-RS09cg and MERS S1-RS09cg (**Fig. 42**, $p < 0.05$, Kruskal-Wallis test, followed by Dunn's multiple comparisons). At week 9, only

WuRBDMers S1-RS09cg had significantly greater geometric mean SARS-CoV-2 Delta RBD-IgG EPT than MersRBDS2 S1-RS09cg and MERS S1-RS09cg (**Fig. 42**, $p < 0.05$, Kruskal-Wallis test, followed by Dunn's multiple comparisons). These data suggest that placing the SARS-CoV-2 RBD in MERS S1 (WuRBDMers S1-RS09cg) was able to effectively increase the RBD-specific IgG EPT when compared to SARS-CoV-2 S1 alone (WU S1-RS09cg).
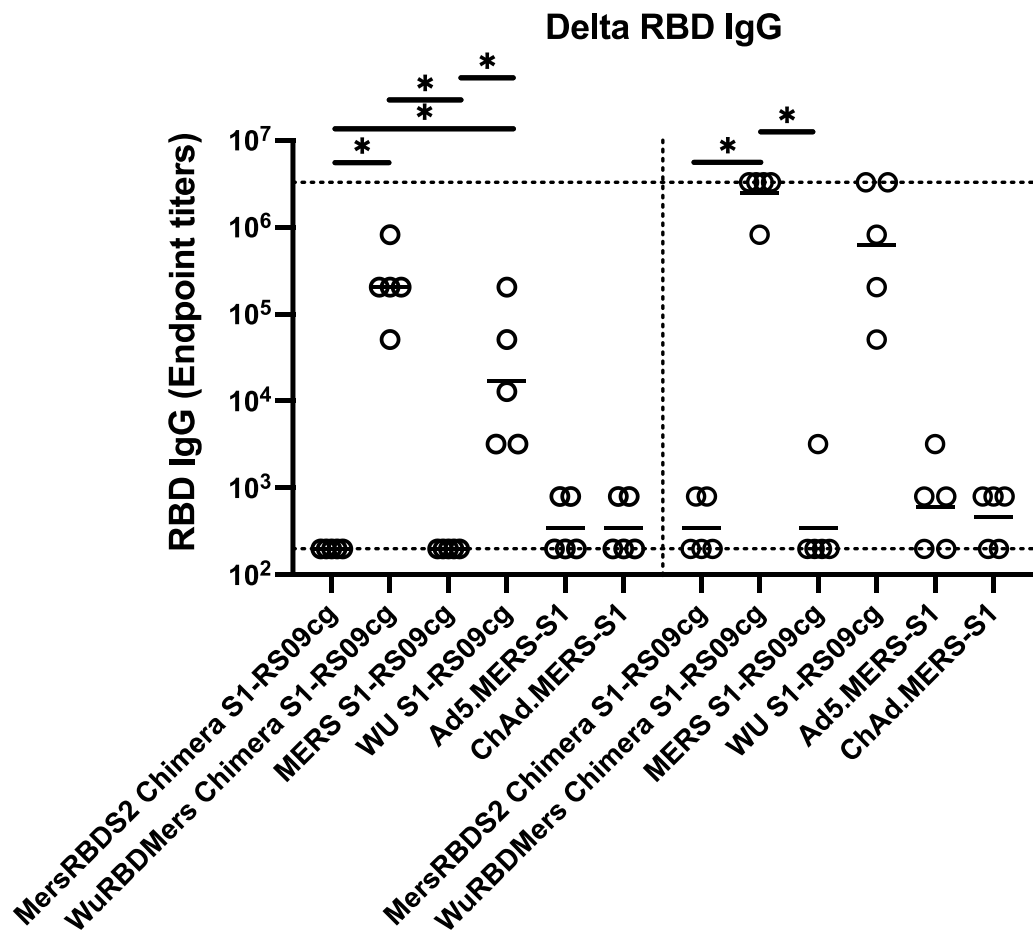
Figure 42: Delta RBD binding IgG response. BALB/c mice (n = 5 mice per group) were immunized intramuscularly with 10 μg of either MERS RBDS2 S1, SARS2RBDMers S1, SARS-CoV-2 S1, or MERS S1 and received a homologous booster at week 3 and week 6. Ad5.MERS-S1 and ChAd.MERS-S1 was given at a dose of 1×10^{10} v.p. and was only boosted once at week 3. On weeks 6 (left panel) and 9 (right panel) sera from mice were collected, serially diluted (200×), and tested for the presence of SARS-CoV-2-RBD-specific IgG antibody levels by ELISA.

Significance was determined by the Kruskal-Wallis test followed by Dunn's multiple comparisons (* $p < 0.05$). Horizontal solid lines represent geometric mean antibody titers. Serum collected on week 0, before immunization, was used to set the ELISA endpoint titer cutoff.

7.2.3 ACE2 Binding Inhibition Induced by Hybrid Betacoronavirus S1

Competitive immunoassays for quantifying inhibition of the spike-ACE2 interaction have been shown to correlate well with live-virus neutralizing tests and serve as a convenient multiplex method to determine the neutralizing capacity of vaccinated sera [305,306,438,439]. To investigate the neutralizing capabilities of antibodies induced by vaccination we used the Meso Scale Discovery (MSD) V-PLEX SARS-CoV-2 (ACE2) Kit. This measures the inhibition of binding between angiotensin-converting enzyme-2 (ACE2) and trimeric spike protein of SARS CoV-2 variants. We used kit Panel 25 including Wuhan S and spikes from immune evasive variants; BA.1, BA.2, AY.4 (Delta lineage), BA.3, BA.1 + R346K mutation, BA.1 + L52R mutation, B.1.1.7 (Alpha), B.1.351 (Beta), and B.1.1640.2. Sera from vaccinated animals were examined at week 6 and week 9, the peak of the IgG antibody responses (**Fig. 41 & 42**). **Fig. 43–46** depict each vaccination group ACE2-binding percent inhibition individually; MersRBDS2 Chimera S1-RS09cg (**Fig. 43**), SARS2RBDMers Chimera S1-RS09cg (**Fig. 44**), SARS-CoV-2 S1 (WU S1-RS09cg) (**Fig. 45**), and MERS S1-RS09cg (**Fig. 46**). Unfortunately, antibodies blocking ACE2 and trimeric S binding were not detected at levels above naïve sera for MersRBDS2 Chimera S1-RS09cg (**Fig. 43**), SARS2RBDMers Chimera S1-RS09cg (**Fig. 44**) and MERS S1-RS09cg (**Fig. 46**). Antibodies blocking ACE2 and trimeric S binding were only detected in WU S1-RS09cg vaccinated mice, with levels above naïve sera against all variant's spikes (**Fig. 45**). Interestingly, antibodies blocking ACE2 and trimeric S binding had the highest median ACE2-binding inhibition against

199

Wuhan S, AY.4 (Delta), B.1.1.7, B.1.351, and B.1.640.2 (**Fig. 45**). Taken together, while a prime and two boosts of MersRBDS2 Chimera S1-RS09cg and SARS2RBDMers Chimera S1-RS09cg elicited cross-reactive IgG binding antibodies against SARS-CoV-2 and MERS, at high levels, these antibodies were not sufficient to block ACE2 and trimeric SARS-CoV-2 S binding.

MersRBDS2 Chimera S1-RS09cg
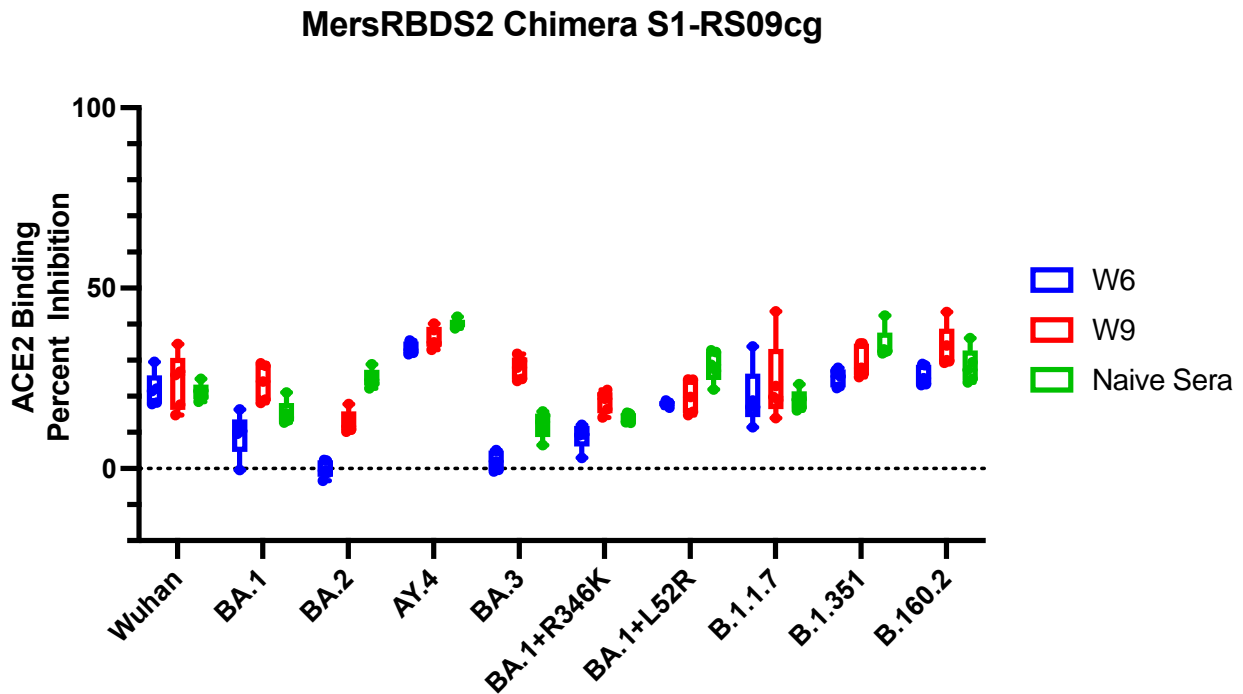
Figure 43: MersRBDS2 chimera S1 ACE2 binding inhibition. Antibodies in sera capable of neutralizing the interaction between SARS-CoV-2 Wuhan, BA.1, BA.2, AY.4 (Delta lineage), BA.3, BA.1 + R346K mutation, BA.1 + L52R mutation, B.1.1.7 (Alpha), B.1.351 (Beta), and B.1.1640.2. variant spike and ACE2 were examined in MersRBDS2 Chimera S1-RS09cg vaccinated animals at week 6 and week 9. ACE2 binding percent inhibition of MersRBDS2 Chimera S1-RS09cg vaccinated at week 6 (blue box and whisker plot) and week 9 (red box and whisker plot) are depicted along with naïve control sera (green box and whisker plot). Box and whisker plots represent the median and upper and lower quartile (box) with min and max (whiskers).

WuRBDMers Chimera S1-RS09cg
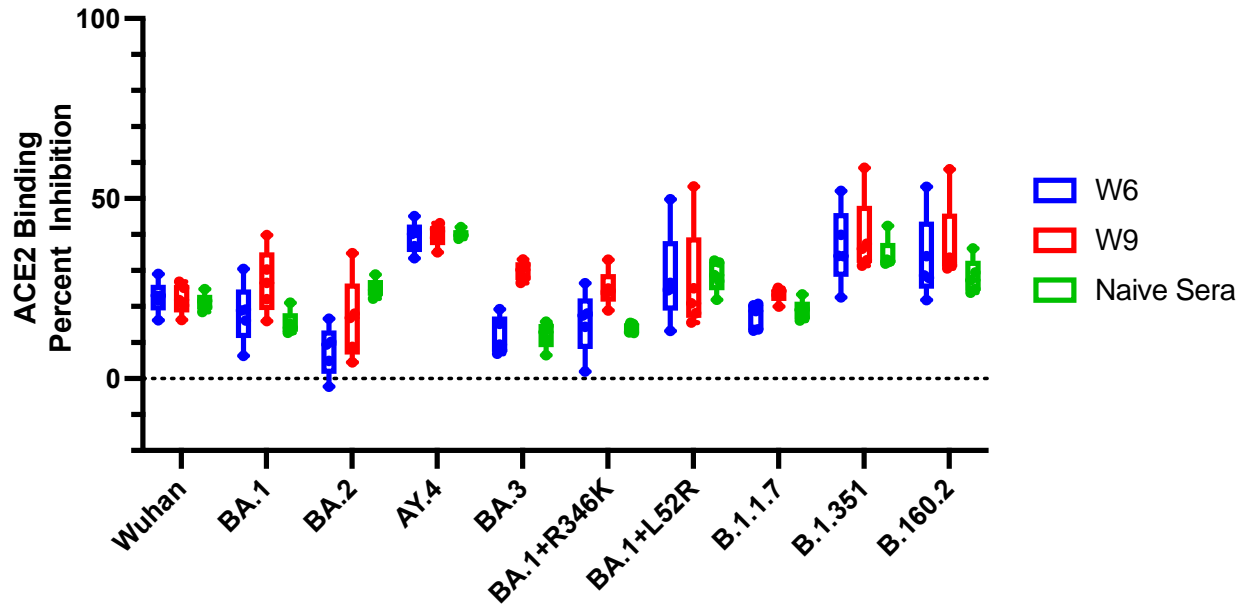
Figure 44: WuRBDMers S1 chimera ACE2 binding inhibition. Antibodies in sera capable of neutralizing the interaction between SARS-CoV-2 Wuhan, BA.1, BA.2, AY.4 (Delta lineage), BA.3, BA.1 + R346K mutation, BA.1 + L52R mutation, B.1.1.7 (Alpha), B.1.351 (Beta), and B.1.1640.2. variant spike and ACE2 were examined in WuRBDMers Chimera S1-RS09cg vaccinated animals at week 6 and week 9. ACE2 binding percent inhibition of sera from WuRBDMers Chimera S1-RS09cg vaccinated mice at week 6 (blue box and whisker plot) and week 9 (red box and whisker plot) are depicted along with naïve control sera (green box and whisker plot). Box and whisker plots represent the median and upper and lower quartile (box) with min and max (whiskers).
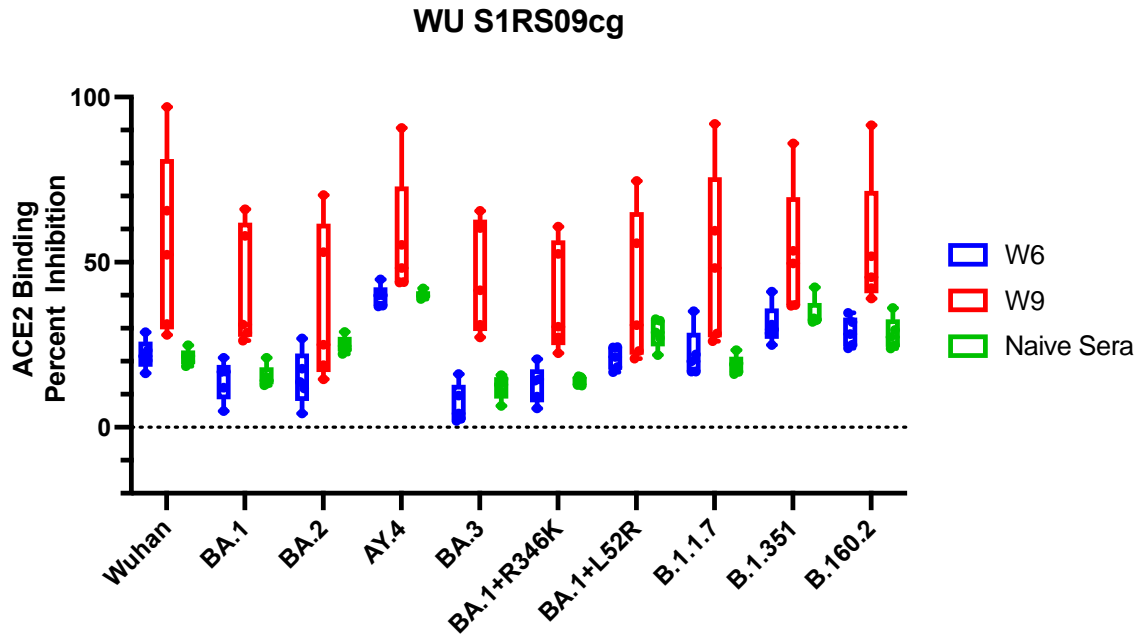
Figure 45: WU S1RS09cg ACE2 binding inhibition. Antibodies in sera capable of neutralizing the interaction between SARS-CoV-2 Wuhan, BA.1, BA.2, AY.4 (Delta lineage), BA.3, BA.1 + R346K mutation, BA.1 + L52R mutation, B.1.1.7 (Alpha), B.1.351 (Beta), and B.1.1640.2. variant spike and ACE2 were examined in WU S1-RS09cg vaccinated animals at week 6 and week 9. ACE2 binding percent inhibition of sera from WU S1-RS09cg vaccinated mice at week 6 (blue box and whisker plot) and week 9 (red box and whisker plot) are depicted along with naïve control sera (green box and whisker plot). Box and whisker plots represent the median and upper and lower quartile (box) with min and max (whiskers).
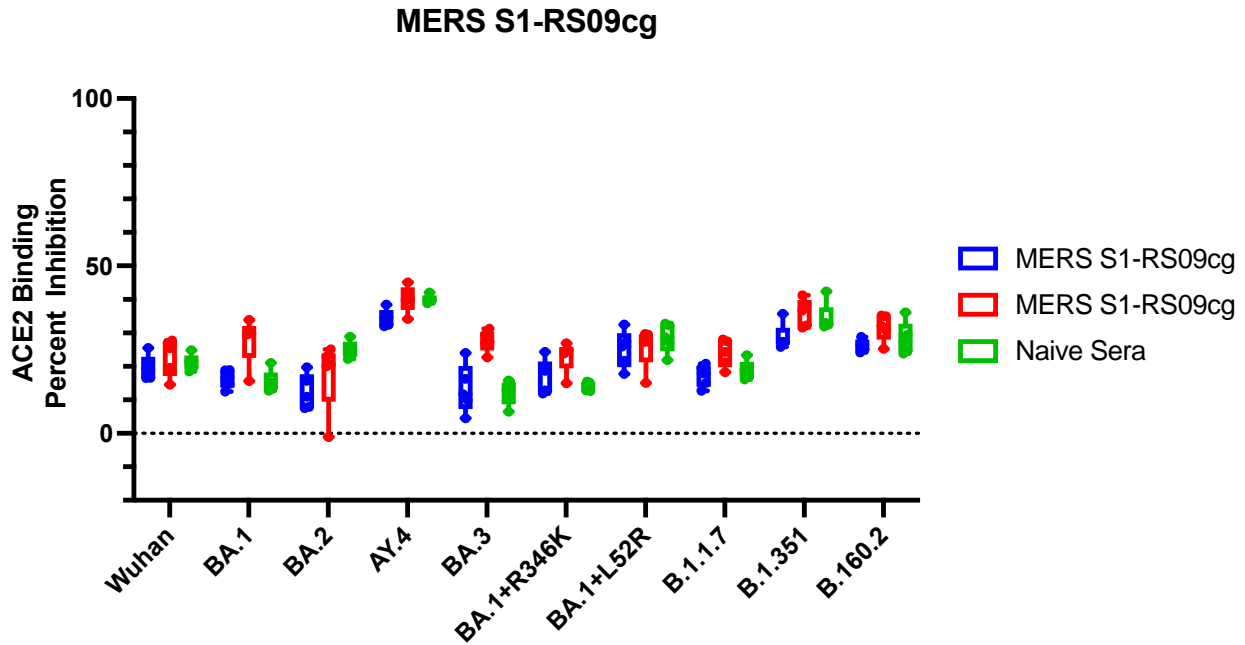
MERS S1-RS09cg

Figure 46: MERS S1-RS09cg ACE2 binding inhibition. Antibodies in sera capable of neutralizing the interaction between SARS-CoV-2 Wuhan, BA.1, BA.2, AY.4 (Delta lineage), BA.3, BA.1 + R346K mutation, BA.1 + L52R mutation, B.1.1.7 (Alpha), B.1.351 (Beta), and B.1.1640.2. variant spike and ACE2 were examined in MERS S1-RS09cg vaccinated animals at week 6 and week 9. ACE2 binding percent inhibition of sera from MERS S1-RS09cg vaccinated mice at week 6 (blue box and whisker plot) and week 9 (red box and whisker plot) are depicted along with naïve control sera (green box and whisker plot). Box and whisker plots represent the median and upper and lower quartile (box) with min and max (whiskers).

7.3 Materials and Methods

7.3.1 Construction of Recombinant Protein Expressing Vectors

The coding sequence for Betacoronavirus S1 amino acids 1 to 661; having C-terminal tag known as 'C-tag', composed of the four amino acids (aa), glutamic acid-proline-glutamic acid-alanine (E-P-E-A) ,along with RS09 peptide, flanked with Sal I & Not I was codon-optimized

using UpGene algorithm for optimal expression in mammalian cells [217,371]. The construct also contained a Kozak sequence (GCCACC) at the 5′ end. The plasmids, pAd/MERS RBD in SARS-CoV-2 S1 (MersRBDS2 Chimera), pAd/SARS-CoV-2 RBD in MERS S1 (SARS2RBDMers Chimera), pAd/SARS-CoV-2 S1 (SARS2 S1), and pAd/MERS S1 were generated by subcloning the codon-optimized S1 gene having C-tag and TLR4 agonist peptide RS09 into the shuttle vector, pAd (GenBank U62024) at SalI and NotI sites. The plasmid constructs were confirmed by DNA sequencing.

7.3.2 Transient Production in expi293 Cells

Recombinant proteins were amplified and purified using ZymoPURE II plasmid maxiprep kit (Zymo Research). For Expi293 cell transfection, we used ExpiFectamieTM 293 Transfection Kit (ThermoFisher, Waltham, MA, USA) and followed the manufacturer's instructions. Cells were seeded 3.0×106 cells/mL one day before transfection and grown to $4.5–5.5 \times 106$ cells/mL. 1 µg of DNA and ExpiFectamine mixtures per 1 mL culture were combined and incubated for 15 min before adding into 3.0×106 cells/mL culture. At 20 h post-transfection, enhancer mixture was added, and culture was shifted to 32 °C. The supernatants were harvested 5 days post transfection and clarified by centrifugation to remove cells, filtration through 0.8 µm, 0.45 µm, and 0.22 µm filters and either subjected to further purification or stored at 4 °C before purification.

7.3.3 Purification of Recombinant Proteins

The recombinant proteins were purified using a CaptureSelect™ C-tagXL Affinity Matrix prepacked column (ThermoFisher) and followed the manufacturer's guideline [415]. Briefly, The C-

tagXL column was conditioned with 10 column volumes (CV) of equilibrate/wash buffer (20 mM Tris, pH 7.4) before sample application. Supernatant was adjusted to 20 mM Tris with 200 mM Tris (pH 7.4) before being loaded onto a 5-mL prepacked column per the manufacturer's instructions at 5 mL/min rate. The column was then washed by alternating with 10 CV of equilibrate/wash buffer, 10 CV of strong wash buffer (20 mM Tris, 1 M NaCl, 0.05% Tween-20, pH 7.4), and 5 CV of equilibrate/wash buffer. The recombinant proteins were eluted from the column by using elution buffer (20 mM Tris, 2 M $MgCl_2$, pH 7.4). The eluted solution was concentrated and desalted with preservative buffer (PBS) in an Amicon Ultra centrifugal filter devices with a 50,000 molecular weight cutoff (Millipore). The concentrations of the purified recombinant proteins were determined by the Bradford assay using bovine serum albumin (BSA) as a protein standard, aliquoted, and stored at $-80°C$ until use.

7.3.4 SDS-PAGE, Silver Staining, and Western Blot

The purified proteins were subjected to sodium dodecyl sulfate polyacrylamide gel electrophoresis (SDS-PAGE), Silver Staining, and Western blot. Briefly, after the supernatants were boiled in Laemmli sample buffer containing 2% SDS with beta- mercaptoethanol (β-ME), the proteins were separated by Tris-Glycine SDS-PAGE gels and transferred to nitrocellulose membrane. After blocking for 1 h at room temperature (RT) with 5% non-fat milk in TBS-T, mouse anti-SARS-CoV spike polyclonal antibodies (1:10,000) (from mice immunized with SARS-CoV-2-S1), or mouse anti-MERS-CoV spike polyclonal antibodies (1:10,000) (from mice immunized with MERS-CoV-2-S1) was added and incubated overnight at 4 °C as primary antibody, and horseradish peroxidase (HRP)-conjugated rat anti-mouse IgG (1:10,000) (Jackson immuno research) was added and incubated at RT for 1 hour as secondary antibody. After washing,

the signals were visualized using ECL Western blot substrate reagents and iBright 1500 (Thermo Fisher).

7.3.5 Animals and Immunization

At week 0 female BALB/c mice (n = 5 animals per group) were bled from retro-orbital vein and primed and boosted on weeks 3 and 6 with either 10 μg of MERS RBDS2 S1, SARS2RBDMers S1, SARS-CoV-2 S1 (WU S1), or MERS S1 . Adenovirus vectored MERS targeting vaccines using either a Ad5 human adenovirus (Ad5.MERS-S1) or chimpanzee adenovirus (ChAd.MERS-S1) were also included as positive MERS controls at a dose of 1×10^{10} v.p. and were only boosted once at week 3. Mice were bled on week 3,6, and 9. Mice were maintained under specific pathogen-free conditions at the University of Pittsburgh, and all experiments were conducted in accordance with animal use guidelines and protocols approved by the University of Pittsburgh's Institutional Animal Care and Use (IACUC) Committee.

7.3.6 ELISA

Sera from all mice were collected prior to immunization (week 0) and at weeks indicated after immunization and evaluated for SARS-CoV-2-S1-specific or MERS-CoV-S1-specific IgG antibodies using ELISA [217]. Briefly, ELISA plates were coated with 200 ng of recombinant SARS-CoV-2-S1RS09cg or MERS-CoV-S1RS09cg protein per well overnight at 4 °C in carbonate coating buffer (pH 9.5) and then blocked with PBS-T and 2% bovine serum albumin (BSA) for one hour. For ELISA coating antigens, WU S1-RS09cg and MERS S1-RS09cg were produced by our lab. Mouse sera were serially diluted in PBS-T with 1% BSA and incubated overnight. After

the plates were washed, anti-mouse IgG-horseradish peroxidase (HRP) (1:10,000, SantaCruz, Dallas, Texas, USA) was added to each well and incubated for 60 min. The plates were washed three times, developed with 3,3′5,5′-tetramethylbenzidine, and the reaction was stopped. Next, absorbance was determined at 450 nm using a plate reader. ELISA data graphed is relative to preimmunization sera, using week 0 sera as the standardized cutoff.

7.3.7 ACE2 Blocking Assay

Antibodies blocking the binding of SARS-CoV-2 spike including Wuhan and spikes from immune evasive variants; BA.1, BA.2, AY.4 (Delta lineage), BA.3, BA.1 + R346K mutation, BA.1 + L452R mutation, B.1.1.7 (Alpha), B.1.351 (Beta), and B.1.1640.2 to ACE2 were detected with a V-PLEX SARS-CoV-2 Panel 25 (ACE2) Kit (Meso Scale Discovery (MSD) according to the manufacturer's instructions. The assay plate was blocked for 30 min and washed. Serum samples were diluted (1:20) and 25 µL were transferred to each well. The plate was then incubated at room temperature for 60 min with shaking at 700 rpm, followed by the addition of SULFO-TAG conjugated ACE2, and continued incubation with shaking for 60 min. The plate was washed, 150 µL MSD GOLD Read Buffer B was added to each well, and the plate was read using the QuickPlex SQ 120 Imager. Electrochemiluminescent values (ECL) were generated for each sample. Results were calculated as % inhibition compared to the negative control for the ACE2 inhibition assay, and % inhibition is calculated as follows: % neutralization $= 100 \times (1 - ($sample signal/negative control signal$))$.

7.3.8 Statistical Analysis

Statistical analyses were performed using GraphPad Prism v9 (San Diego, CA, USA). Antibody endpoint titers and neutralization data were analyzed by Kruskal-Wallis test, followed by Dunn's multiple comparisons. Significant differences are indicated by * $p < 0.05$. Comparisons with non-significant differences are not indicated.

7.4 Discussion

The continued evolution of SARS-CoV-2 throughout the COVID-19 pandemic has enforced the need for next-generation Beta-CoVs vaccines that may induce broader immune responses against multiple variants [250,251,420,422,438,440]. Along with SARS-CoV-2, MERS continues to be a threat to human health, with a large case fatality rate [324]. Additionally, if MERS were to be able to be transmitted from human to human more efficiently it would become a potent threat as the next, high fatality, pandemic. Therefore, there is a need for a next-generation Beta-CoVs vaccine approach that may be able to induce immunity to both SARS-CoV-2 and MERS, potentially increasing the quality and breadth of vaccine-induced antibodies. Protein subunit vaccines are ideal for worldwide distribution due to their excellent safety, low cost, scalability, and thermostability [38,42,46]. Protein subunit vaccine platforms can be further improved through the use of alternative vaccine delivery methods such as intranasal or intradermal vaccination, with microneedle arrays [217,441]. The versatility of protein subunit vaccines lends to their utility for mass distribution and vaccination.

The S protein plays a crucial role in the viral infection process of Beta-CoVs, mediating viral attachment to host cells and entry, making it a favorable target for Beta-CoV vaccines. We have demonstrated that targeting the S1 subunit of the S protein can generate potent antibodies, including neutralizing, responses [189,217,343,344,427]. We have demonstrated the efficacy of S1 protein subunit vaccines in inducing antigen-specific antibody responses against MERS-CoV and SARS-CoV-2 [189,217,343,344]. However, the neutralizing quality of SARS-CoV-2 S1 vaccines was relatively low compared to MERS-CoV S1 vaccines, necessitating a larger dose of SARS-CoV-2 protein subunit vaccine as opposed to MERS-CoV [189,217,343,427]. To investigate this limitation, and potentially enhance neutralizing antibody responses against SARS-CoV-2, we employed a chimeric approach by placing the SARS-CoV-2 RBD in a MERS-CoV S1 scaffold (SARS2RBDMers Chimera S1-RS09cg). We also generated a chimeric S1 with MERS-CoV RBD in a SARS-CoV-2 S1 scaffold (MersRBDS2 Chimera S1-RS09cg). Alternatively, using chimeric SARS-CoV-2 and MERS-CoV S1 could induce a broad array of antibodies, potentially protecting a wider range of SARS-CoV-2 variants and MERS-CoV.

In this study, we successfully designed and expressed the recombinant proteins SARS2RBDMers S1 and MersRBDS2, along with SARS-CoV-2 S1 and MERS S1. We demonstrate the ability to generate vaccine-induced IgG antibodies that can bind to both SARS-CoV-2 and MERS-CoV spikes through the use of SARS-CoV-2 MERS-CoV chimeric S1 antigens. The purified proteins exhibited the expected molecular weights and were recognized by specific antibodies through western blot analysis, confirming their successful expression and purification. Mice were prime and boosted on weeks 3 and 6 with either 10 μg of MERS RBDS2 S1, SARS2RBDMers S1 (WuRBDMers S1), SARS-CoV-2 S1 (WU S1), or MERS S1 (**Fig. 39C and 39D**). Adenovirus vectored MERS targeting vaccines using either an Ad5 human adenovirus

(Ad5.MERS-S1) or chimpanzee adenovirus (ChAd.MERS-S1) were also included as positive MERS controls at a dose of 1×10^{10} v.p. and were only boosted once at week 3.

Serum samples collected from immunized mice were tested for SARS-CoV-2-S1-specific and MERS-S1-specific IgG antibody levels using ELISA at weeks 3, 6, and 9. The solely MERS targeting vaccine antigens elicited the lowest SARS-CoV-2 IgG antibody responses, as expected (**Fig. 40**). MerRBDS2 S1-RS09cg, WuRBDMers S1-RS09cg, and WU S1-RS09cg vaccinated mice all elicited robust IgG binding antibody responses against SARS-CoV-2 S1 (**Fig. 40**). Particularly, WU S1-RS09cg vaccinated mice achieved the greatest geometric mean SARS-CoV-2 IgG EPT, followed by MersRBDS2 Chimera S1-RS09cg then WuRBDS2 Chimera S1-RS09cg (**Fig. 40**). Against MERS-CoV-2-S1; WuRBDMersS2 Chimera S1-RS09cg, MERS S1-RS09cg, and Ad5.MERS-S1 achieved the greatest geometric mean IgG EPT (**Fig. 41**). Notably, ChAd.MERS-S1 was much less immunogenic than its Ad5.MERS-S1 counterpart (**Fig. 41**). Placing the MERS RBD in the SARS-CoV-2 S1 scaffold, MersRBDS2 Chimera S1-RS09cg, was not sufficient in inducing a potent MERS-CoV-S1 IgG response (**Fig. 41**). Next, we assessed SARS-CoV-2 RBD-specific IgG antibody response for insight on the effect of placing the SARS-CoV-2 RBD in a MERS S1 scaffold. Both WuRBDMers Chimera S1-RS09cg and WU S1-RS09cg vaccinated mice showed robust IgG antibody responses against SARS-CoV-2 RBD (**Fig. 42**). WuRBDMers Chimera S1-RS09cg vaccinated mice exhibited the greatest geometric mean RBD-specific IgG EPT, higher than that of WU S1-RS09cg vaccinated mice (**Fig. 42**). These data suggest that WuRBDMers Chimera S1-RS09cg may be an optimal candidate for further refinement due to its ability to induce both SARS-CoV-2 and MERS-CoV S1-specific IgG antibodies. Additionally, WuRBDMers Chimera S1-RS09cg exhibits a greater ability to induce SARS-CoV-2 RBD-specific antibodies than WU S1-RS09cg.

To investigate the neutralizing capabilities of antibodies induced by vaccination we utilized competitive immunoassays to quantify the inhibition of the spike-ACE2 interaction. Such assays have been shown to correlate well with live-virus neutralizing tests and serve as a convenient method to determine the neutralizing capacity of vaccinated sera. We utilized the Meso Scale Discovery (MSD) V-PLEX SARS-CoV-2 (ACE2) Kit, which measures the inhibition of binding between ACE2 and the trimeric spike protein of SARS-CoV-2 variants. We used kit Panel 25 which includes a panel of SARS-CoV-2 variants, including the Wuhan S strain and BA.1, BA.2, AY.4 (Delta lineage), BA.3, BA.1 + R346K mutation, BA.1 + L452R mutation, B.1.1.7 (Alpha), B.1.351 (Beta), and B.1.1640.2 (**Figs. 43-46**). Unfortunately, antibodies blocking ACE2 and trimeric spike (S) binding were not detected at levels above naïve sera for MersRBDS2 Chimera S1-RS09cg, SARS2RBDMers Chimera S1-RS09cg, and MERS S1-RS09cg (**Figs. 43, 44, and 46**). However, antibodies blocking ACE2 and trimeric S binding were detected in mice vaccinated with WU S1-RS09cg, with levels above naïve sera against all variant spikes (**Fig. 45**). Currently, traditional neutralizing tests using live SARS-CoV-2 and MERS-CoV viruses are underway to further elaborate on the discrepancies versus IgG ELISA binding antibody data and ACE2 binding inhibition data as we anticipate this data in the near future, to be published alongside this chapter in an open-access peer-reviewed journal. If live virus neutralizing assays confirm ACE2 binding inhibition data, that the chimeric antigens do not elicit neutralizing antibodies, then this may be explained using mix-match Beta-CoV S1's leading to improper RBD folding or presentation. It has been demonstrated, particularly for SARS-CoV-2, that the RBD is a fluid structure that exhibits multiple "up/open" and "down/closed" confirmations that impact antibody neutralization [164,232,336,520]. It may be that while SARSRBDMers (WuRBDMers) Chimera S1-RS09cg more effectively exposes the RBD, it does so in a "closed" confirmation making the induced antibodies

not effective in blocking ACE2 and trimeric S binding. However, it may also be that the Beta-CoV chimeric antigens may generate antibodies that can neutralize infection of susceptible cells in a manner undetectable through competitive immunoassays which quantify the inhibition of the spike-ACE2 interaction. Therefore, it is necessary to complete traditional live virus neutralization assays to fully assess the ability of induced antibodies to neutralize SARS-CoV-2 or MERS-CoV.

An important limitation regarding our study is the lack of T-cell immunity investigation and SARS-CoV-2 challenge, which were not performed to assess the protection ability of our vaccine constructs. S-specific binding antibodies were positively correlated with S-specific T-cell responses indicating induction of T-cell immune response by our vaccine constructs [449]. We chose to focus on the induction of antibodies because they are the hypothesized correlate of protection against severe COVID-19 [424]. Furthermore, prior studies have shown a positive correlation and high concordance between binding antibodies and traditional virus-based microneutralization tests [427]. Our past work has also shown a positive correlation between the MSD ACE2 binding inhibition and virus-based microneutralization tests [427]. As a conventional and multiplex test, the measurement of a competitive immunoassay for quantifying inhibition of the spike-ACE2 interaction can serve as a surrogate for traditional virus-based microneutralization tests with high levels of correlation [305,306,438].

Overall, this study illustrates the potential of chimeric SARS-CoV-2 and MERS-CoV S1 antigens to induce humoral responses that effectively recognize both Beta-CoVs. Particularly, SARSRBDMers (WuRBDMers) Chimera S1-RS09cg showed potential as a vaccine candidate to elicit immunity against SARS-CoV-2 and MERS-CoV. Antibodies blocking ACE2 and trimeric spike (S) binding were not detected at levels above naïve sera for MersRBDS2 Chimera S1-RS09cg, SARS2RBDMers Chimera S1-RS09cg, and MERS S1-RS09cg through an MSD pseudo-

neutralization assay. Research is currently underway to assess the discrepancies between IgG binding data and ACE2 binding inhibition data using traditional live-virus neutralization assays. Furthermore, future research will also investigate T-cell immunity to immunization, especially in the context of SARSRBDMers (WuRBDMers) Chimera S1-RS09cg.

7.5 Acknowledgements

8.0 Summary, Future Directions, and Public Health Significance

8.1 Summary

These studies contribute greatly toward understanding and developing novel vaccines against Betacoronaviruses. I investigated numerous vaccine strategies against both SARS-CoV-2 and MERS-CoV using protein subunit and adenovirus-vectored vaccine approaches. Chapter 2 validates the approach of using the adenovirus-vectored Ad5.S1 vaccine to induce antigen-specific humoral and cellular immunity. The spike protein of the SARS-CoV-2 virus is identified as an attractive target for vaccine development, as it plays a crucial role in viral attachment and entry into host cells. Previous studies on SARS-CoV and MERS-CoV have shown that vaccines targeting the spike protein can generate protective immune responses. The chapter focuses on the use of recombinant DNA technology and adenoviral vectors as potential approaches for developing vaccines against coronaviruses.

Chapter 2 describes the development of an adenoviral vector-based SARS-CoV-2 vaccine candidate, Ad5.SARS-CoV-2-S1, which encodes the S1 subunit of the spike protein. The immunogenicity of the vaccine candidate is evaluated in mice through subcutaneous injection and intranasal delivery. The results show that a single immunization with Ad5.SARS-CoV-2-S1 induces robust and long-lasting antibody responses specific to the S1 antigen. The route of vaccine administration (subcutaneous or intranasal) does not significantly affect the antibody response, however, does impact the cellular immune response with subcutaneous administration having a greater T-cell response than intranasal. The vaccine also induces antigen-specific germinal center reactions and antibody-secreting plasma cells, suggesting the potential for long-term humoral

immune protection. These findings support the further development of recombinant adenovirus vaccines for COVID-19 and other emerging infectious diseases.

Following the establishment of an Ad5 vectored SARS-CoV-2 vaccine expressing the S1 subunit, I then investigated next-generation vaccine approaches with the inclusion of SARS-CoV-2 structural protein, N. Chapter 3 of the text discusses the development of multiple Adenoviral (Ad)-vectored and subunit recombinant protein SARS-CoV-2 vaccine candidates against COVID-19. It emphasizes the global vaccine inequality and the need for new COVID-19 vaccines that are better suited for worldwide distribution and capable of targeting more conserved regions of the virus to combat emerging variants. The chapter explores the role of the spike protein (S) of SARS-CoV-2 in viral infection and its significance as a target for vaccine development. The inclusion of more conserved regions of the virus, such as the nucleocapsid protein (N), in vaccine strategies is investigated due to its potential to enhance immune responses and provide protection against emerging variants. Previous studies, such as in Chapter 2, using Ad-vectored vaccines expressing S1 subunits of different coronaviruses have shown promising results. The Ad5-vectored COVID-19 vaccine, CanSino Convidicea Vaccine (Ad5-nCoV), is mentioned as an example of an Ad-based vaccine that has demonstrated immunogenicity and received approval in multiple countries. However, the chapter emphasizes the need for further investigation of novel vaccine strategies, such as including the N protein or employing heterologous prime-boost strategies, to achieve sustained immunity against SARS-CoV-2 variants.

Chapter 3 describes the development of an Ad-based SARS-CoV-2 vaccine expressing a fusion protein of S1 and N subunits (Ad5.SARS-CoV-2-S1N). The immunogenicity of this vaccine is evaluated in mice through single immunization and homologous or heterologous prime-boost immunization regimens. Our studies suggest that a single vaccination of BALB/cJ mice via either

I.N. or S.C. delivery of 5×10^{10} v.p. Ad5.SARS-CoV-2-S1N was capable of inducing antigen-specific IgG, Ig isotype switch, and a moderate neutralizing antibody response. We also show that Ad5.SARS-CoV-2-S1N shows a similar S1-specific antibody response, and neutralizing response, to Ad5.SARS-CoV-2-S1. We believe this is important as a concern with including proteins outside of the SARS-CoV-2 S protein is that it will decrease the antibody response against S. We show that this is not the case and that inclusion of N, through S1N fusion antigen, does not reduce S1-specific antibody responses. The results demonstrate that Ad5.SARS-CoV-2-S1N can induce robust and durable SARS-CoV-2-specific immune responses in mice, with an increased T-cell response, specific for S1 and N, than Ad5.SARS-CoV-2-S1. We also illustrate that this immunogenicity can be improved by homologous prime-boost strategies, using either S.C. or I.N. delivery. Particularly immunogenicity can further be improved through heterologous prime-boost, with traditional I.M. injection, using subunit recombinant S1 protein. Priming with a low dose (1 $\times 10^{10}$ v.p.) of Ad5.S1N and boosting with either WT recombinant rS1 or B.1.351 recombinant rS1 induced a robust neutralizing response, which was sustained against immune evasive Beta (B.1.351) and Gamma (P.1) variants of the virus., and a long-lived antibody-forming cell response in the bone marrow 29 weeks post-vaccination.

After our findings showing the use of recombinant protein S1 as an immunogenic boost vaccine candidate, in Chapter 3, I then investigated the effect of variant-specific S1 vaccine approaches, comparing monovalent versus trivalent prime and boost approaches in Chapter 4. I compared the immune responses induced by monovalent vaccination with wild-type Wuhan spike S1 (WU-S1RS09cg), Delta variant-specific spike S1 (Delta S1-RS09cg), and Omicron variant-specific spike S1 (OM S1-RS09cg) proteins to a trivalent vaccine containing all three antigens (Wu/Delta/OM S1-RS09cg).

Chapter 4 results showed that all vaccinated groups had significantly higher IgG endpoint titers against their respective antigens after prime and booster immunization. The trivalent vaccine consistently demonstrated broader antibody responses, greater against heterotypic SARS-CoV-2 variants, compared to the monovalent vaccines. Particularly, trivalent WU/Delta/OM S1-RS09cg vaccinated mice mounted cross-reactive ACE2 binding inhibiting antibodies against SARS-CoV-2 variants with increased breadth when compared to monovalent WU S1-RS09cg, Delta S1-RS09cg, and OM S1-RS09cg vaccinated mice. We believe that this gives credence to investigating SARS-CoV-2 vaccines that are multivalent to expand variant-specific immune responses. Our data also suggest that increasing the valency of SARS-CoV-2 vaccines may not reduce the magnitude of the individual variant immune response, a key added piece of information for the development of next-generation SARS-CoV-2 vaccines. A particularly unexpected result of our study is the low immunogenicity of our WU S1-RS09cg vaccine against Wuhan S1, and other VOCs when compared to Delta and OM S1-RS09cg. Interestingly, the response to the Wuhan-specific S1 antigen waned earlier in the trivalent vaccine group compared to the monovalent Omicron-specific vaccine group. However, the trivalent vaccine showed superior immune responses against the Delta and Omicron variants throughout the study period. We found that the trivalent approach induced a broader humoral response, with increased coverage against antigenically distinct variants, particularly the Omicron variant. The trivalent vaccine also showed increased ACE2 binding inhibition and higher S1 IgG endpoint titers against Wuhan and Delta variants compared to the monovalent Omicron-specific vaccine. As expected for the unadjuvanted protein subunit vaccine in BALB/c mouse, all vaccinated groups had a trend to an IgG1 dominant IgG response, indicating a Th2 bias.

Following the results showing substantial immunity conferred by variant-specific S1 subunit vaccine in Chapter 4, we next aimed to investigate the booster effect of variant S1 subunit vaccine in aged mice that were initially immunized with Ad5.S1 in Chapter 5. The chapter begins by describing the construction and expression of recombinant proteins of SARS-CoV-2-S1, specifically the Beta (B.1.351) variant. The study examines the immunogenicity of the adenoviral vaccine (Ad5.S1) in mice one year after vaccination. The results show that mice vaccinated with Ad5.S1 had high titers of anti-S1 antibodies even after one year. To assess the booster effect, the mice were given a booster immunization with the rS1Beta subunit vaccine, and serum samples were collected at various time points. The analysis reveals that the booster vaccination stimulated strong and long-lived immune responses, leading to significantly high levels of cross-neutralizing antibodies against SARS-CoV-2 variants. The chapter also discusses the recall of S1-specific binding antibodies after the booster. The results demonstrate a rapid recall of binding antibodies, with higher levels detected in Ad5.S1-vaccinated mouse groups compared to control groups. The recall response was faster after the booster vaccination compared to the primary vaccination. Furthermore, the IgG antibody responses after the booster lasted longer, up to week 28 post-boost.

Chapter 5 also investigates the Th1/Th2 response by measuring S1-specific IgG1 and IgG2a antibodies. The induction of these antibodies was significant and balanced in both the Ad5.S1-vaccinated groups after the booster shot. In contrast, the subunit vaccine alone induced high IgG1 with lower IgG2a levels, leading to the possibility of vaccine-associated enhanced respiratory disease (VAERD). In this study, a high level of neutralizing antibodies and a balanced Th1/Th2 immune response were induced, suggesting that a booster of a subunit vaccine after an adenoviral Overall, Chapter 5 evaluated the effect of a booster in aged mice after priming with adenoviral vaccines as a preclinical model of elderly people immunized with the currently

approved COVID-19 vaccines. the prime vaccine might avoid a Th2-biased immune response and the occurrence of VAERD.

We next further evaluated our S1 subunit protein vaccine in a more advanced animal model, rhesus macaques (RMs) with controlled SIV infection, at a tetravalent approach using AddaVax adjuvant. Chapter 6 evaluated the immunogenicity and efficacy of a tetravalent COVID-19 vaccine candidate based on the spike S1 protein of SARS-CoV-2 in a non-human primate (NHP) model of controlled SIV infection. The study used RMs infected with SIVsab, which are known to control viral replication and disease progression, to assess the immune response to the vaccine candidate. The results showed that the vaccine candidate induced high levels of binding antibodies against the Wuhan strain of SARS-CoV-2, as well as neutralizing antibodies against the B.1.351 (Beta) and B.1.617.2 (Delta) variants of concern (VOC). The sera of vaccinated RMs also exhibited potent ACE2-binding inhibition capabilities against a suite of SARS-CoV-2 VOC spikes, including the Omicron variant and its subvariants. These findings were consistent with previous studies in NHP models, demonstrating the immunogenicity and cross-reactivity of COVID-19 vaccines. In addition to humoral immune responses, the vaccine candidate also induced cellular immune responses, including T-cell responses. The study examined T-cell subsets and activation status and found that all T-cell subsets and B cells increased after vaccination, with the CD8$^+$ T-cell count showing the greatest increase. The vaccine candidate was able to induce CD4$^+$ and CD8$^+$ T-cell activation, as indicated by increased expression of activation and proliferation markers. The distribution of T-cell memory subsets over time revealed a decrease in the abundance of central memory T cells and naive T cells, while effector memory T cells increased after vaccination.

The continued evolution of SARS-CoV-2 and the potential threat posed by MERS have highlighted the need for next-generation Beta-CoV vaccines capable of inducing broader immune responses against multiple variants. In Chapter 7, I aimed to enhance the neutralizing antibody responses against SARS-CoV-2 by employing a chimeric approach, combining elements of the S proteins from SARS-CoV-2 and MERS-CoV. I successfully designed and expressed recombinant proteins, including SARS-CoV-2 S1, MERS S1, SARS2RBDMers S1, and MersRBDS2 S1. Mice were prime and boosted on weeks 3 and 6 with either 10 μg of MERS RBDS2 S1, SARS2RBDMers S1 (WuRBDMers S1), SARS-CoV-2 S1 (WU S1), or MERS S1. Adenovirus vectored MERS targeting vaccines using either an Ad5 human adenovirus (Ad5.MERS-S1) or chimpanzee adenovirus (ChAd.MERS-S1) were also included as positive MERS controls at a dose of $1x10^{10}$ v.p. and were only boosted once at week 3. The chimeric SARS-CoV-2 and MERS-CoV antigens, SARS2RBDMers S1 and MersRBDS2 S1, demonstrated the ability to generate vaccine-induced IgG antibodies that could bind to both SARS-CoV-2 and MERS-CoV spikes. Particularly, SARS2RBDMers S1 had robust IgG binding antibodies against SARS-CoV-2 and MERS-CoV S1 like that induced by native S1 counterparts, WU S1-RS09cg and MERS-S1RS09cg. WU S1-RS09cg vaccinated mice achieved the greatest geometric mean SARS-CoV-2 IgG EPT, followed closely by MersRBDS2 Chimera S1-RS09cg, then WuRBDS2 Chimera S1-RS09cg. Against MERS-CoV-2-S1; WuRBDMersS2 Chimera S1-RS09cg, MERS S1-RS09cg, and Ad5.MERS-S1 achieved the greatest geometric mean IgG EPT. Placing the MERS RBD in the SARS-CoV-2 S1 scaffold, MersRBDS2 Chimera S1-RS09cg, was not sufficient in inducing a potent MERS-CoV-S1 IgG response.

Next, we assessed SARS-CoV-2 RBD-specific IgG antibody response for insight into the effect of placing the SARS-CoV-2 RBD in a MERS S1 scaffold. WuRBDMers Chimera S1-

RS09cg vaccinated mice exhibited the greatest geometric mean RBD-specific IgG EPT, higher than that of WU S1-RS09cg vaccinated mice. These data suggest that WuRBDMers Chimera S1-RS09cg may be an optimal candidate for further refinement due to its ability to induce both SARS-CoV-2 and MERS-CoV S1-specific IgG antibodies. Additionally, WuRBDMers Chimera S1-RS09cg exhibits a greater ability to induce SARS-CoV-2 RBD-specific antibodies than WU S1-RS09cg. In terms of neutralizing capabilities, competitive immunoassays were used to measure the inhibition of the SARS-CoV-2 spike-ACE2 interaction, which correlates with live-virus neutralizing tests. Antibodies blocking ACE2 and SARS-CoV-2 trimeric spike binding were detected in mice vaccinated with the SARS-CoV-2 S1-RS09cg antigen, as expected. However, antibodies blocking ACE2 and spike binding were not detected at levels above naïve sera for the chimeric antigens MersRBDS2 S1-RS09cg, SARS2RBDMers S1-RS09cg, and MERS S1-RS09cg. Further investigations using live-virus neutralization assays are planned to provide a more comprehensive understanding of the neutralizing capacity of the induced antibodies.

Overall, Chapter 7 demonstrates the potential of chimeric SARS-CoV-2/MERS-CoV S1 antigens to induce humoral responses capable of recognizing both Beta-CoVs. Particularly, SARSRBDMers (WuRBDMers) Chimera S1-RS09cg showed potential as a vaccine candidate to elicit immunity against SARS-CoV-2 and MERS-CoV. Ongoing research aims to address discrepancies between binding data and ACE2 binding inhibition data and to explore T-cell immunity in the context of the chimeric antigen.

Taken together, this research presents major advancements in Betacoronavirus vaccine research. This is done through the use of novel SARS-CoV-2 antigens (S1N and Chimeric MERS SARS-CoV-2 S1's), establishment of the S1 subunit of Betacoronaviruses as an optimal target for vaccine formulation (as opposed to targeting of the whole S as used predominantly in approved

vaccines worldwide), assessment in a variety of models (young and aged mice along with use of a RM model with latent SIV infection for insights in vaccine response for immunocompromised populations), and assessment of multivalent variant specific vaccine approaches. The use of S1N is an innovative approach for SARS-CoV-2 vaccinology, with the use of S1 and N fusion protein being the first of its kind and has shown promise in stimulating robust S antibody responses, neutralizing antibody responses, and increased T-cell response. Additionally, our work focusing on S1 is a significant advancement especially for the manufacturing of SARS-CoV-2 protein subunit vaccines as S1 is expressed at upwards of 40mg/L in FreeStyle 293-F cells while whole S-2P is expressed at 0.5 mg/L and HexaPro whole S expressed at 10.5 mg/L respectively in FreeStyle 293-F cells [164,165,427]. Furthermore, my work investigating chimeric MERS and SARS-CoV-2 vaccines is also the first of its kind and has demonstrated promising results so far highlighting a potential new frontier in next-generation vaccine design.

8.2 Future Directions

To further advance our understanding of the immune response to SARS-CoV-2 and explore potential strategies for vaccine development, several key areas warrant investigation. Firstly, viral challenge studies of vaccinated animals, to assess the protective efficacy of our candidate vaccines, were not performed in any of the chapters presented. Performing viral challenge studies in either hACE2-mice or wild-type mice, using SARS-CoV-2 variants with the N501Y mutation, would provide valuable insights into the effectiveness of the presented vaccine candidates against emerging viral strains. The N501Y mutation has been associated with increased transmissibility in mice and immune evasion in humans, making it a crucial tool in evaluating our vaccine candidates

in non-ACE2-transgenic mice. Viral challenge studies are a stringent tool for assessing the possible effectiveness of candidate vaccines and would be important information on the vaccine candidates presented here within.

In addition to evaluating systemic immune responses, such as that in the blood (ie: antibodies), it is important to assess mucosal immunity as a potential correlate of protection against infection. Mucosal surfaces, such as the respiratory tract and naval cavity, play a critical role in the initial infection and transmission of SARS-CoV-2. Assessment of mucosal immune responses, including IgA antibody titers and the characterization of mucosal-associated lymphoid tissue (MALT) T cell responses, would provide valuable information on the effectiveness of vaccines in preventing viral entry and replication at the site of infection. Furthermore, investigating the presence and functionality of lung resident T cells would contribute to our understanding of adaptive immune responses and their potential role in viral clearance and long-term protection. Chapters 2 and 3 investigate intranasal approaches to vaccination, however only assess immune responses found in the blood or spleen, and not at mucosal surfaces.

Another important area of research in Chapter 7 is the evaluation of MERS SARS-CoV-2 chimeric proteins in animals with preexisting SARS-CoV-2 immunity. This investigation would shed light on the phenomenon of immune imprinting or original antigenic sin, whereby prior exposure to related viruses influences the immune response to subsequent infections. Assessing the immune response to these chimeric proteins in animals with preexisting SARS-CoV-2 immunity would provide insights into potential antigenic competition, immune enhancement, or cross-reactivity effects. Understanding these interactions is crucial for optimizing vaccine strategies and avoiding potential adverse immune responses in individuals with preexisting immunity which now constitute a major portion of the human population.

Moreover, it is essential to conduct comprehensive studies to investigate T-cell immunity following vaccination and functionality after a large period for recall. While much of the focus has been on antibody responses, T-cell responses play a pivotal role in viral clearance and long-term immune memory. Characterizing the breadth, durability, and functionality of T-cell responses, particularly memory T cells in different organs, would contribute to our understanding of the long-term protective immune response against SARS-CoV-2 and the potential means for increasing the longevity of vaccines. Furthermore, investigating the potential cross-reactivity of T-cell responses between SARS-CoV-2 and other coronaviruses, such as MERS-CoV, could provide insights into the development of cross-protective vaccines that perform better against immune-evasive viral variants of SARS-CoV-2.

In conclusion, future research efforts should aim to address the aforementioned areas of investigation to enhance our understanding of the immune response to SARS-CoV-2 and guide the development of effective vaccines and therapeutics. By performing viral challenge studies with emerging variants, assessing mucosal immunity, investigating the immune imprinting phenomenon, and comprehensively characterizing T-cell responses, we can advance our knowledge and refine strategies for next-generation Betacoronavirus vaccines. These studies will contribute to the development of more robust and broadly protective interventions to mitigate the impact of Betacoronaviruses and potential future coronavirus outbreaks.

8.3 Public Health Significance

The emergence and ongoing threat of SARS-CoV-2 and its associated disease, COVID-19, highlight the significant public health significance of understanding viral infections and

developing effective interventions. SARS-CoV-2 has demonstrated its potential to cause pandemics and public health emergencies, with devastating impacts on global health, economies, and societal well-being. Currently approved COVID-19 vaccines have made a large impact on human health; however, they have been hampered by worldwide distribution inequalities that have left many low to middle-income countries without access [249,327,392–395,521,522]. With many countries now distributing a COVID-19 booster to those already vaccinated, global vaccine inequality is at risk of increasing [396–399]. Therefore, there is a need for a protein subunit vaccine SARS-CoV-2 platform that is safe, easy to mass produce, and easy to distribute worldwide with less stringent cold chain necessities [38,42,46]. Such a vaccine would assist in, not only vaccinating the unvaccinated but also boosting already vaccinated individuals as emerging SARS-CoV-2 variants and waning immunity have decreased protection against infection [251,400,513].

Chapter 2 of this thesis holds significant public health significance by investigating the Ad5.S1 vaccine for SARS-CoV-2. Ad5-based vaccines have been extensively studied and utilized in the development of COVID-19 vaccines. The findings from this chapter can inform the deployment of Ad5-based vaccines, helping to expand the repertoire of available vaccines and enhance population-level immunity against COVID-19. Furthermore, this research contributes to the understanding of viral vector-based vaccine platforms, paving the way for the development of novel vaccine candidates against emerging pathogens in the future. Chapter 5 of this thesis also holds important public health significance by investigating the boosting of aged mice primed with the Ad5.S1 vaccine using the S1 subunit protein vaccine. Aging populations are particularly vulnerable to severe COVID-19 outcomes, and understanding how vaccination strategies can be optimized in older individuals is crucial for public health interventions. By assessing the immunogenicity and efficacy of the S1 subunit vaccine as a booster in aged mice, this research

provides valuable insights into enhancing immune responses in older populations. These findings can inform the development of vaccination strategies tailored to the needs of the elderly, ensuring better protection against SARS-CoV-2 and reducing the burden of severe disease and mortality in this vulnerable population. Implementing effective vaccination approaches for older individuals is vital for public health efforts to control the spread of COVID-19 and protect those at the highest risk of severe illness.

Chapter 3 of this thesis holds significant public health significance by focusing on the inclusion of the N protein of SARS-CoV-2 in vaccines. The N protein plays a crucial role in viral replication and immune responses, and its incorporation into vaccines can enhance the breadth and potency of immune protection against SARS-CoV-2. By investigating the effectiveness of N protein-integrated vaccines, this research addresses the urgent need for robust and comprehensive vaccination strategies to combat the ongoing COVID-19 pandemic. The findings from this chapter can inform the development and optimization of vaccines that offer broad protection against SARS-CoV-2 variants, contributing to global efforts to control the transmission of the virus and reduce the burden of COVID-19 on public health systems.

The investigation of trivalent or tetravalent vaccines in Chapters 4 and Chapter 6 holds significant public health relevance. As SARS-CoV-2 continues to evolve and generate new variants, there is a critical need to develop vaccines that protect against multiple strains of the virus. By assessing the immunogenicity and efficacy of trivalent or tetravalent vaccine formulations, this research addresses the challenge of vaccine strain coverage. Such vaccines have the potential to confer broader protection, minimizing the risk of breakthrough infections and reducing the transmission of SARS-CoV-2 within the population. These findings can guide vaccine development strategies and inform public health policymakers in their decisions on

vaccine formulations and deployment strategies to achieve optimal population-level immunity against SARS-CoV-2.

The investigation of vaccine responses in rhesus macaques (RMs) with SIV infection in Chapter 6 holds particular public health significance by providing insights into vaccine efficacy in immunocompromised individuals. Understanding how vaccines perform in populations with underlying immunodeficiencies, such as people living with HIV or other immunocompromising conditions, is crucial for public health decision-making. The findings from this research can inform the design and evaluation of vaccines that are effective in individuals with compromised immune systems, ensuring equitable access to vaccination and optimal protection for vulnerable populations. Additionally, these insights contribute to our understanding of vaccine responses in general, shedding light on the complex interplay between the immune system, viral infections, and vaccine efficacy.

The development of a MERS SARS-CoV-2 vaccine, as explored in Chapter 7, holds significant public health importance. MERS-CoV has previously caused outbreaks with high mortality rates, and the potential emergence of a hybrid MERS-SARS-CoV-2 virus poses a severe public health threat. Investigating the immunogenicity and efficacy of a MERS SARS-CoV-2 vaccine provides valuable knowledge in combating both MERS-CoV and SARS-CoV-2 infections. By developing a vaccine that targets both viruses, this research contributes to pandemic preparedness and response capabilities, ensuring a proactive approach to mitigating the impact of potential future outbreaks. Furthermore, a MERS SARS-CoV-2 vaccine can potentially reduce the risk of zoonotic transmission and minimize the likelihood of cross-species infections, thereby safeguarding public health and preventing the spillover of deadly coronaviruses into human populations.

Bibliography

1.   Ada, G. Overview of vaccines and vaccination. *Mol Biotechnol* **29**, 255–72 (2005).

2.   Rodrigues, C. M. C. & Plotkin, S. A. Impact of Vaccines; Health, Economic and Social Perspectives. *Front. Microbiol.* **11**, (2020).

3.   Ehreth, J. The global value of vaccination. *Vaccine* **21**, 596–600 (2003).

4.   Schuchat, A. Human Vaccines and Their Importance to Public Health. *Procedia Vaccinol.* **5**, 120–126 (2011).

5.   Riedel, S. Edward Jenner and the history of smallpox and vaccination. *Proc. Bayl. Univ. Med. Cent.* **18**, 21–25 (2005).

6.   Edward Jenner and the Eradication of Smallpox - N J Willis, 1997. https://journals.sagepub.com/doi/abs/10.1177/003693309704200407?journalCode=scma.

7.   Strassburg, M. A. The global eradication of smallpox. *Am. J. Infect. Control* **10**, 53–59 (1982).

8.   Saleh, A., Qamar, S., Tekin, A., Singh, R. & Kashyap, R. Vaccine Development Throughout History. *Cureus* **13**, e16635.

9.   Salk and Sabin: poliomyelitis immunisation | Journal of Neurology, Neurosurgery & Psychiatry. https://jnnp.bmj.com/content/75/11/1552.

10.   Nathanson, N. & Kew, O. M. From Emergence to Eradication: The Epidemiology of Poliomyelitis Deconstructed. *Am. J. Epidemiol.* **172**, 1213–1229 (2010).

11.   Salk, J. E., Bennett, B. L., Lewis, L. J., Ward, E. N. & Youngner, J. S. STUDIES IN HUMAN SUBJECTS ON ACTIVE IMMUNIZATION AGAINST POLIOMYELITIS: 1. A PRELIMINARY REPORT OF EXPERIMENTS IN PROGRESS. *J. Am. Med. Assoc.* **151**, 1081–1098 (1953).

12.   Blume, S. & Geesink, I. A Brief History of Polio Vaccines. *Science* **288**, 1593–1594 (2000).

13.   WHO – COVID19 Vaccine Tracker. https://covid19.trackvaccines.org/agency/who/.

14.   Orsel, K. & Bouma, A. The effect of foot-and-mouth disease (FMD) vaccination on virus transmission and the significance for the field. *Can. Vet. J.* **50**, 1059–1063 (2009).

15.   Frontiers | Evaluation of Brucellosis Vaccines: A Comprehensive Review. https://www.frontiersin.org/articles/10.3389/fvets.2022.925773/full.

16. CDC - Veterinarians: Rabies Vaccination - Rabies. https://www.cdc.gov/rabies/specific_groups/veterinarians/vaccination.html.

17. DA MOTA GOMES, M. Louis Pasteur and Dom Pedro II engaged in rabies vaccine development. *J. Prev. Med. Hyg.* **62**, E231–E236 (2021).

18. Burrell, C. J., Howard, C. R. & Murphy, F. A. Chapter 11 - Vaccines and Vaccination. in *Fenner and White's Medical Virology (Fifth Edition)* (eds. Burrell, C. J., Howard, C. R. & Murphy, F. A.) 155–167 (Academic Press, 2017). doi:10.1016/B978-0-12-375156-0.00011-4.

19. Slifka, M. K. & Amanna, I. How advances in immunology provide insight into improving vaccine efficacy. *Vaccine* **32**, 2948–2957 (2014).

20. Li, Y.-D. *et al.* Coronavirus vaccine development: from SARS and MERS to COVID-19. *J. Biomed. Sci.* **27**, 104 (2020).

21. Dumpa, N. *et al.* Stability of Vaccines. *AAPS PharmSciTech* **20**, 42 (2019).

22. Inactivated Vaccines Advantages & Disadvantages of Inactivated Vaccines. https://www.healthcentre.org.uk/vaccine/advantages-disadvantages-inactivated-vaccines.html.

23. Pinkbook | Principles of Vaccination | Epidemiology of VPDs | CDC. https://www.cdc.gov/vaccines/pubs/pinkbook/prinvac.html (2021).

24. Mehndiratta, M. M., Mehndiratta, P. & Pande, R. Poliomyelitis: historical facts, epidemiology, and current challenges in eradication. *The Neurohospitalist* **4**, 223–229 (2014).

25. André, F., Van Damme, P., Safary, A. & Banatvala, J. Inactivated hepatitis A vaccine: immunogenicity, efficacy, safety and review of official recommendations for use. *Expert Rev. Vaccines* **1**, 9–23 (2002).

26. Wong, S.-S. & Webby, R. J. Traditional and New Influenza Vaccines. *Clin. Microbiol. Rev.* **26**, 476–492 (2013).

27. Plitnick, L. M. Chapter 9 - Global Regulatory Guidelines for Vaccines. in *Nonclinical Development of Novel Biologics, Biosimilars, Vaccines and Specialty Biologics* (eds. Plitnick, L. M. & Herzyk, D. J.) 225–241 (Academic Press, 2013). doi:10.1016/B978-0-12-394810-6.00009-5.

28. Katz, S. L. *et al.* Studies on an Attenuated Measles-Virus Vaccine. *N. Engl. J. Med.* **263**, 180–184 (1960).

29. Hilleman, M. R., Buynak, E. B., Weibel, R. E. & Stokes, J. Live, Attenuated Mumps-Virus Vaccine. *N. Engl. J. Med.* **278**, 227–232 (1968).

30. Prinzie, A., Huygelen, C., Gold, J., Farquhar, J. & McKee, J. Experimental Live Attenuated Rubella Virus Vaccine: Clinical Evaluation of Cendehill Strain. *Am. J. Dis. Child.* **118**, 172–177 (1969).

31. Plotkin, S. A. & Plotkin, S. L. The development of vaccines: how the past led to the future. *Nat. Rev. Microbiol.* **9**, 889–893 (2011).

32. Chen, Y. *et al.* Immune memory at 17-years of follow-up of a single dose of live attenuated hepatitis A vaccine. *Vaccine* **36**, 114–121 (2018).

33. Chen, J. *et al.* A live attenuated virus-based intranasal COVID-19 vaccine provides rapid, prolonged, and broad protection against SARS-CoV-2. *Sci. Bull.* **67**, 1372–1387 (2022).

34. Wahid, R. *et al.* Genetic and phenotypic stability of poliovirus shed from infants who received novel type 2 or Sabin type 2 oral poliovirus vaccines in Panama: an analysis of two clinical trials. *Lancet Microbe* **3**, e912–e921 (2022).

35. Geier, D. A., Kern, J. K. & Geier, M. R. Childhood MMR vaccination and the incidence rate of measles infection: a ten year longitudinal cohort study of American children born in the 1990s. *BMC Pediatr.* **19**, 325 (2019).

36. Epidemiology of Varicella During the 2-Dose Varicella Vaccination Program — United States, 2005–2014 | MMWR. https://www.cdc.gov/mmwr/volumes/65/wr/mm6534a4.htm.

37. Burnett, E., Parashar, U. & Tate, J. Rotavirus Vaccines: Effectiveness, Safety and Future Directions. *Paediatr. Drugs* **20**, 223–233 (2018).

38. Kumru, O. S. *et al.* Vaccine instability in the cold chain: Mechanisms, analysis and formulation strategies. *Biologicals* **42**, 237–259 (2014).

39. Abd Albagi, S. O. *et al.* A multiple peptides vaccine against COVID-19 designed from the nucleocapsid phosphoprotein (N) and Spike Glycoprotein (S) via the immunoinformatics approach. *Inform. Med. Unlocked* **21**, 100476 (2020).

40. Corchero, J. L. *et al.* Unconventional microbial systems for the cost-efficient production of high-quality protein therapeutics. *Biotechnol. Adv.* **31**, 140–153 (2013).

41. Ferrer-Miralles, N., Domingo-Espín, J., Corchero, J. L., Vázquez, E. & Villaverde, A. Microbial factories for recombinant pharmaceuticals. *Microb. Cell Factories* **8**, 17 (2009).

42. Berlec, A. & Štrukelj, B. Current state and recent advances in biopharmaceutical production in Escherichia coli, yeasts and mammalian cells. *J. Ind. Microbiol. Biotechnol.* **40**, 257–274 (2013).

43. Taguchi, S., Ooi, T., Mizuno, K. & Matsusaki, H. Advances and needs for endotoxin-free production strains. *Appl. Microbiol. Biotechnol.* **99**, 9349–9360 (2015).

44. Gerngross, T. U. Advances in the production of human therapeutic proteins in yeasts and filamentous fungi. *Nat. Biotechnol.* **22**, 1409–1414 (2004).

45. Tan, E., Chin, C. S. H., Lim, Z. F. S. & Ng, S. K. HEK293 Cell Line as a Platform to Produce Recombinant Proteins and Viral Vectors. *Front. Bioeng. Biotechnol.* **9**, 796991 (2021).

46. Demain, A. L. & Vaishnav, P. Production of recombinant proteins by microbes and higher organisms. *Biotechnol. Adv.* **27**, 297–306 (2009).

47. Janson, J.-C. *Protein Purification: Principles, High Resolution Methods, and Applications.* (John Wiley & Sons, 2012).

48. Guide to Protein Purification - Google Books. https://books.google.com/books?hl=en&lr=&id=zTiRJHpKIQoC&oi=fnd&pg=PR11&dq =protein+purification+techniques&ots=Y2aM5DOpeK&sig=i0knN-xNUtE71Xqms0Z1OL7nUp0#v=onepage&q=protein%20purification%20techniques&f= false.

49. Roe, S. *Protein Purification Techniques: A Practical Approach.* (OUP Oxford, 2001).

50. Mahmoudi Gomari, M. *et al.* Opportunities and challenges of the tag-assisted protein purification techniques: Applications in the pharmaceutical industry. *Biotechnol. Adv.* **45**, 107653 (2020).

51. Vaccine Development, Testing, and Regulation. https://cpp-hov.netlify.app//vaccines-101/how-are-vaccines-made/vaccine-development-testing-and-regulation.

52. McAleer, W. J. *et al.* Human hepatitis B vaccine from recombinant yeast. *Nature* **307**, 178–180 (1984).

53. Pinkbook: Hepatitis B | CDC. https://www.cdc.gov/vaccines/pubs/pinkbook/hepb.html (2022).

54. Pattyn, J., Hendrickx, G., Vorsters, A. & Van Damme, P. Hepatitis B Vaccines. *J. Infect. Dis.* **224**, S343–S351 (2021).

55. CDC. Human Papillomavirus (HPV) Vaccine. *Centers for Disease Control and Prevention* https://www.cdc.gov/hpv/parents/vaccine-for-hpv.html (2019).

56. Frazer, I. & Zhou, J. Papillomavirus vaccines. (2009).

57. Schiller, J. & Lowy, D. Explanations for the high potency of HPV prophylactic vaccines. *Vaccine* **36**, 4768–4773 (2018).

58. De Vuyst, H., Clifford, G. M., Nascimento, M. C., Madeleine, M. M. & Franceschi, S. Prevalence and type distribution of human papillomavirus in carcinoma and intraepithelial

neoplasia of the vulva, vagina and anus: A meta-analysis. *Int. J. Cancer* **124**, 1626–1636 (2009).

59.   Kash, N. *et al.* Safety and Efficacy Data on Vaccines and Immunization to Human Papillomavirus. *J. Clin. Med.* **4**, 614–633 (2015).

60.   Thaxton, L. & Waxman, A. G. Cervical Cancer Prevention: Immunization and Screening 2015. *Med. Clin. North Am.* **99**, 469–477 (2015).

61.   HPV Vaccine | CDC. https://www.cdc.gov/vaccines/vpd/hpv/hcp/vaccines.html (2022).

62.   Bonanni, P. *et al.* Human papilloma virus vaccination: impact and recommendations across the world. *Ther. Adv. Vaccines* **3**, 3–12 (2015).

63.   Kamolratanakul, S. & Pitisuttithum, P. Human Papillomavirus Vaccine Efficacy and Effectiveness against Cancer. *Vaccines* **9**, 1413 (2021).

64.   Pinkbook: Pertussis | CDC. https://www.cdc.gov/vaccines/pubs/pinkbook/pert.html (2022).

65.   Burnette, W. N. *et al.* Direct Expression of Bordetelia pertussis Toxin Subunits to High Levels in Escherichia coli. *Bio/Technology* **6**, 699–706 (1988).

66.   Pizza, M. *et al.* Mutants of Pertussis Toxin Suitable for Vaccine Development. *Science* **246**, 497–500 (1989).

67.   Shapiro-Shapin, C. G. Pearl Kendrick, Grace Eldering, and the Pertussis Vaccine. *Emerg. Infect. Dis.* **16**, 1273–1278 (2010).

68.   Kuchar, E., Karlikowska-Skwarnik, M., Han, S. & Nitsch-Osuch, A. Pertussis: History of the Disease and Current Prevention Failure. *Adv. Exp. Med. Biol.* **934**, 77–82 (2016).

69.   Pichichero, M. E. *et al.* Combined Tetanus, Diphtheria, and 5-Component Pertussis Vaccine for Use in Adolescents and Adults. *JAMA* **293**, 3003–3011 (2005).

70.   D'Amico, C., Fontana, F., Cheng, R. & Santos, H. A. Development of vaccine formulations: past, present, and future. *Drug Deliv. Transl. Res.* **11**, 353–372 (2021).

71.   Baxter, D. Active and passive immunity, vaccine types, excipients and licensing. *Occup. Med.* **57**, 552–556 (2007).

72.   Subunit Vaccines Advantages & Disadvantages of Subunit Vaccines. https://www.healthcentre.org.uk/vaccine/advantages-disadvantages-subunit-vaccines.html.

73.   Pulendran, B., S. Arunachalam, P. & O'Hagan, D. T. Emerging concepts in the science of vaccine adjuvants. *Nat. Rev. Drug Discov.* **20**, 454–475 (2021).

74.   Facciolà, A., Visalli, G., Laganà, A. & Di Pietro, A. An Overview of Vaccine Adjuvants: Current Evidence and Future Perspectives. *Vaccines* **10**, 819 (2022).

75.   Travieso, T., Li, J., Mahesh, S., Mello, J. D. F. R. E. & Blasi, M. The use of viral vectors in vaccine development. *Npj Vaccines* **7**, 1–10 (2022).

76.   Afkhami, S., Yao, Y. & Xing, Z. Methods and clinical development of adenovirus-vectored vaccines against mucosal pathogens. *Mol. Ther. - Methods Clin. Dev.* **3**, 16030 (2016).

77.   Ura, T., Okuda, K. & Shimada, M. Developments in Viral Vector-Based Vaccines. *Vaccines* **2**, 624–641 (2014).

78.   Delany, I., Rappuoli, R. & De Gregorio, E. Vaccines for the 21st century. *EMBO Mol. Med.* **6**, 708–720 (2014).

79.   Adenovirus receptors and their implications in gene delivery - PMC. https://www.ncbi.nlm.nih.gov/pmc/articles/PMC2903974/.

80.   Shabram, P., Vellekamp, G., Ruan, Q. & Scandella, C. 8 - Purification of Adenovirus. in *Adenoviral Vectors for Gene Therapy (Second Edition)* (ed. Curiel, D. T.) 197–230 (Academic Press, 2016). doi:10.1016/B978-0-12-800276-6.00008-5.

81.   Duffy, A. M., O'Doherty, A. M., O'Brien, T. & Strappe, P. M. Purification of adenovirus and adeno-associated virus: comparison of novel membrane-based technology to conventional techniques. *Gene Ther.* **12**, S62–S72 (2005).

82.   Zolotukhin, S. *et al.* Recombinant adeno-associated virus purification using novel methods improves infectious titer and yield. *Gene Ther.* **6**, 973–985 (1999).

83.   Potter, M. *et al.* A simplified purification protocol for recombinant adeno-associated virus vectors. *Mol. Ther. - Methods Clin. Dev.* **1**, (2014).

84.   Woolsey, C. & Geisbert, T. W. Current state of Ebola virus vaccines: A snapshot. *PLoS Pathog.* **17**, e1010078 (2021).

85.   Pavot, V. Ebola virus vaccines: Where do we stand? *Clin. Immunol.* **173**, 44–49 (2016).

86.   First Ebola vaccine approved. *Nat. Biotechnol.* **38**, 6–6 (2020).

87.   Four countries in the African region license vaccine in milestone for Ebola prevention. https://www.who.int/news/item/14-02-2020-four-countries-in-the-african-region-license-vaccine-in-milestone-for-ebola-prevention.

88.   EMA. First vaccine to protect against Ebola. *European Medicines Agency* https://www.ema.europa.eu/en/news/first-vaccine-protect-against-ebola (2019).

89.   EMA. Ervebo. *European Medicines Agency* https://www.ema.europa.eu/en/medicines/human/EPAR/ervebo (2019).

90.   Research, C. for B. E. and. ERVEBO. *FDA* (2022).

91.   Henao-Restrepo, A. M. *et al.* Efficacy and effectiveness of an rVSV-vectored vaccine in preventing Ebola virus disease: final results from the Guinea ring vaccination, open-label, cluster-randomised trial (Ebola Ça Suffit!). *The Lancet* **389**, 505–518 (2017).

92.   Marzi, A. *et al.* Single low-dose VSV-EBOV vaccination protects cynomolgus macaques from lethal Ebola challenge. *eBioMedicine* **49**, 223–231 (2019).

93.   Ewer, K. *et al.* A Monovalent Chimpanzee Adenovirus Ebola Vaccine Boosted with MVA. *N. Engl. J. Med.* **374**, 1635–1646 (2016).

94.   Manno, D. *et al.* Safety and immunogenicity of an Ad26.ZEBOV booster dose in children previously vaccinated with the two-dose heterologous Ad26.ZEBOV and MVA-BN-Filo Ebola vaccine regimen: an open-label, non-randomised, phase 2 trial. *Lancet Infect. Dis.* **23**, 352–360 (2023).

95.   Janssen Vaccines & Prevention B.V. *A Staged Phase 3 Study, Including a Double-Blinded Controlled Stage to Evaluate the Safety and Immunogenicity of Ad26.ZEBOV and MVA-BN-Filo as Candidate Prophylactic Vaccines for Ebola.* https://clinicaltrials.gov/ct2/show/NCT02509494 (2022).

96.   EMA. New vaccine for prevention of Ebola virus disease recommended approval in the European Union. *European Medicines Agency* https://www.ema.europa.eu/en/news/new-vaccine-prevention-ebola-virus-disease-recommended-approval-european-union (2020).

97.   Watson-Jones, D. *et al.* Protocol for a phase 3 trial to evaluate the effectiveness and safety of a heterologous, two-dose vaccine for Ebola virus disease in the Democratic Republic of the Congo. *BMJ Open* **12**, e055596 (2022).

98.   Johnson & Johnson Announces European Commission Approval for Janssen's Preventive Ebola Vaccine | Johnson & Johnson. *Content Lab U.S.* https://www.jnj.com/johnson-johnson-announces-european-commission-approval-for-janssens-preventive-ebola-vaccine.

99.   Kerstetter, L. J., Buckley, S., Bliss, C. M. & Coughlan, L. Adenoviral Vectors as Vaccines for Emerging Avian Influenza Viruses. *Front. Immunol.* **11**, (2021).

100.   Matsuda, K. *et al.* A replication-competent adenovirus-vectored influenza vaccine induces durable systemic and mucosal immunity. *J. Clin. Invest.* **131**, (2021).

101.   Xiang, K. *et al.* Progress on adenovirus-vectored universal influenza vaccines. *Hum. Vaccines Immunother.* **11**, 1209–1222 (2015).

102.   Lingel, A., Bullard, B. L. & Weaver, E. A. Efficacy of an Adenoviral Vectored Multivalent Centralized Influenza Vaccine. *Sci. Rep.* **7**, 14912 (2017).

103. Gao, W. *et al.* Protection of Mice and Poultry from Lethal H5N1 Avian Influenza Virus through Adenovirus-Based Immunization. *J. Virol.* **80**, 1959–1964 (2006).

104. Bliss, C. M. *et al.* A single-shot adenoviral vaccine provides hemagglutinin stalk-mediated protection against heterosubtypic influenza challenge in mice. *Mol. Ther.* **30**, 2024–2047 (2022).

105. Hrycak, C. P., Windmann, S. & Bayer, W. Comparative Evaluation of the Vaccine Efficacies of Three Adenovirus-Based Vector Types in the Friend Retrovirus Infection Model. *J. Virol.* **93**, e01155-19 (2019).

106. Tatsis, N. *et al.* Multiple Immunizations with Adenovirus and MVA vectors improve CD8+ T cell functionality and mucosal homing. *Virology* **367**, 156–167 (2007).

107. Kreijtz, J. H. C. M. *et al.* MVA-Based H5N1 Vaccine Affords Cross-Clade Protection in Mice against Influenza A/H5N1 Viruses at Low Doses and after Single Immunization. *PLOS ONE* **4**, e7790 (2009).

108. Ao, Z. *et al.* A Recombinant VSV-Based Bivalent Vaccine Effectively Protects against Both SARS-CoV-2 and Influenza A Virus Infection. *J. Virol.* **96**, e01337-22 (2022).

109. Furuyama, W. *et al.* A single dose of a vesicular stomatitis virus-based influenza vaccine confers rapid protection against H5 viruses from different clades. *Npj Vaccines* **5**, 1–10 (2020).

110. Schwartz, J. A. *et al.* Vesicular Stomatitis Virus-Based H5N1 Avian Influenza Vaccines Induce Potent Cross-Clade Neutralizing Antibodies in Rhesus Macaques ▽. *J. Virol.* **85**, 4602–4605 (2011).

111. Roberts, A. *et al.* Vaccination with a Recombinant Vesicular Stomatitis Virus Expressing an Influenza Virus Hemagglutinin Provides Complete Protection from Influenza Virus Challenge. *J. Virol.* **72**, 4704–4711 (1998).

112. Sebastian, S. & Lambe, T. Clinical Advances in Viral-Vectored Influenza Vaccines. *Vaccines* **6**, 29 (2018).

113. de Vries, R. D. & Rimmelzwaan, G. F. Viral vector-based influenza vaccines. *Hum. Vaccines Immunother.* **12**, 2881–2901 (2016).

114. Vaxart. *Phase 2 Randomized, Controlled, Human Influenza A (H1N1) Challenge Study Following Administration of an Oral H1N1 HA Adenoviral-Vector Based Seasonal Influenza Vaccine and dsRNA Adjuvant to Healthy Adult Volunteers.* https://clinicaltrials.gov/ct2/show/NCT02918006 (2022).

115. Bekker, L.-G. *et al.* Effectiveness of the Ad26.COV2.S vaccine in health-care workers in South Africa (the Sisonke study): results from a single-arm, open-label, phase 3B, implementation study. *The Lancet* **399**, 1141–1153 (2022).

116. Elkashif, A., Alhashimi, M., Sayedahmed, E. E., Sambhara, S. & Mittal, S. K. Adenoviral vector-based platforms for developing effective vaccines to combat respiratory viral infections. *Clin. Transl. Immunol.* **10**, e1345 (2021).

117. Fausther-Bovendo, H. & Kobinger, G. P. Pre-existing immunity against Ad vectors. *Hum. Vaccines Immunother.* **10**, 2875–2884 (2014).

118. Le Gars, M. *et al.* Impact of Preexisting Anti–Adenovirus 26 Humoral Immunity on Immunogenicity of the Ad26.COV2.S Coronavirus Disease 2019 Vaccine. *J. Infect. Dis.* **226**, 979–982 (2022).

119. Li, J.-X. *et al.* Immunity duration of a recombinant adenovirus type-5 vector-based Ebola vaccine and a homologous prime-boost immunisation in healthy adults in China: final report of a randomised, double-blind, placebo-controlled, phase 1 trial. *Lancet Glob. Health* **5**, e324–e334 (2017).

120. Lin, J., Calcedo, R., Vandenberghe, L. H., Figueredo, J. M. & Wilson, J. M. Impact of Preexisting Vector Immunity on the Efficacy of Adeno-Associated Virus-Based HIV-1 Gag Vaccines. *Hum. Gene Ther.* **19**, 663–669 (2008).

121. See, I. *et al.* US Case Reports of Cerebral Venous Sinus Thrombosis With Thrombocytopenia After Ad26.COV2.S Vaccination, March 2 to April 21, 2021. *JAMA* **325**, 2448–2456 (2021).

122. Uczkowski, D. & Sekhri, A. COVID-19 vaccine (Ad26.COV2.S), an unlikely culprit of portal vein thrombosis in a middle-aged man. *Thromb. Update* **8**, 100119 (2022).

123. Muir, K.-L., Kallam, A., Koepsell, S. A. & Gundabolu, K. Thrombotic Thrombocytopenia after Ad26.COV2.S Vaccination. *N. Engl. J. Med.* **384**, 1964–1965 (2021).

124. Sadoff, J., Davis, K. & Douoguih, M. Thrombotic Thrombocytopenia after Ad26.COV2.S Vaccination — Response from the Manufacturer. *N. Engl. J. Med.* **384**, 1965–1966 (2021).

125. Salmon, D. A. *et al.* Impact of vaccine pause due to Thrombosis with thrombocytopenia syndrome (TTS) following vaccination with the Ad26.COV2.S vaccine manufactured by Janssen/Johnson & Johnson on vaccine hesitancy and acceptance among the unvaccinated population. *PLOS ONE* **17**, e0274443 (2022).

126. Commissioner, O. of the. Coronavirus (COVID-19) Update: FDA Limits Use of Janssen COVID-19 Vaccine to Certain Individuals. *FDA* https://www.fda.gov/news-events/press-announcements/coronavirus-covid-19-update-fda-limits-use-janssen-covid-19-vaccine-certain-individuals (2022).

127. Pardi, N., Hogan, M. J., Porter, F. W. & Weissman, D. mRNA vaccines — a new era in vaccinology. *Nat. Rev. Drug Discov.* **17**, 261–279 (2018).

128. Non-viral COVID-19 vaccine delivery systems - PMC. https://www.ncbi.nlm.nih.gov/pmc/articles/PMC7744276/.

129. Schlake, T., Thess, A., Fotin-Mleczek, M. & Kallen, K.-J. Developing mRNA-vaccine technologies. *RNA Biol.* **9**, 1319–1330 (2012).

130. Wolff, J. A. *et al.* Direct Gene Transfer into Mouse Muscle in Vivo. *Science* **247**, 1465–1468 (1990).

131. Reichmuth, A. M., Oberli, M. A., Jaklenec, A., Langer, R. & Blankschtein, D. mRNA vaccine delivery using lipid nanoparticles. *Ther. Deliv.* **7**, 319–334 (2016).

132. Karikó, K., Buckstein, M., Ni, H. & Weissman, D. Suppression of RNA recognition by Toll-like receptors: the impact of nucleoside modification and the evolutionary origin of RNA. *Immunity* **23**, 165–175 (2005).

133. Corbett, K. S. *et al.* Evaluation of the mRNA-1273 Vaccine against SARS-CoV-2 in Nonhuman Primates. *N. Engl. J. Med.* **383**, 1544–1555 (2020).

134. Jackson, L. A. *et al.* An mRNA Vaccine against SARS-CoV-2 — Preliminary Report. *N. Engl. J. Med.* **383**, 1920–1931 (2020).

135. Tang, J. *et al.* Respiratory mucosal immunity against SARS-CoV-2 after mRNA vaccination. *Sci. Immunol.* **7**, eadd4853 (2022).

136. Nagata, S. *et al.* Synthesis and biological activity of artificial mRNA prepared with novel phosphorylating reagents. *Nucleic Acids Res.* **38**, 7845–7857 (2010).

137. Safety and Efficacy of the BNT162b2 mRNA Covid-19 Vaccine | NEJM. https://www.nejm.org/doi/full/10.1056/nejmoa2034577.

138. Baden, L. R. *et al.* Efficacy and Safety of the mRNA-1273 SARS-CoV-2 Vaccine. *N. Engl. J. Med.* **384**, 403–416 (2021).

139. Bahl, K. *et al.* Preclinical and Clinical Demonstration of Immunogenicity by mRNA Vaccines against H10N8 and H7N9 Influenza Viruses. *Mol. Ther.* **25**, 1316–1327 (2017).

140. Chahal, J. S. *et al.* Dendrimer-RNA nanoparticles generate protective immunity against lethal Ebola, H1N1 influenza, and Toxoplasma gondii challenges with a single dose. *Proc. Natl. Acad. Sci.* **113**, E4133–E4142 (2016).

141. Moderna Announces Interim Phase 3 Safety and Immunogenicity Results for mRNA-1010, a Seasonal Influenza Vaccine Candidate. https://investors.modernatx.com/news/news-details/2023/Moderna-Announces-Interim-Phase-3-Safety-and-Immunogenicity-Results-for-mRNA-1010-a-Seasonal-Influenza-Vaccine-Candidate/default.aspx.

142. Pardi, N. *et al.* Zika virus protection by a single low-dose nucleoside-modified mRNA vaccination. *Nature* **543**, 248–251 (2017).

143. Richner, J. M. *et al.* Modified mRNA Vaccines Protect against Zika Virus Infection. *Cell* **168**, 1114-1125.e10 (2017).

144. Wollner, C. J. *et al.* A Dengue Virus Serotype 1 mRNA-LNP Vaccine Elicits Protective Immune Responses. *J. Virol.* **95**, e02482-20 (2021).

145. He, L., Sun, W., Yang, L., Liu, W. & Li, J. A multiple-target mRNA-LNP vaccine induces protective immunity against experimental multi-serotype DENV in mice. *Virol. Sin.* **37**, 746–757 (2022).

146. Ovchinnikov, S. & Huang, P.-S. Structure-based protein design with deep learning. *Curr. Opin. Chem. Biol.* **65**, 136–144 (2021).

147. Mazur, N. I. *et al.* The respiratory syncytial virus vaccine landscape: lessons from the graveyard and promising candidates. *Lancet Infect. Dis.* **18**, e295–e311 (2018).

148. Scheltema, N. M. *et al.* Global respiratory syncytial virus-associated mortality in young children (RSV GOLD): a retrospective case series. *Lancet Glob. Health* **5**, e984–e991 (2017).

149. Zhou, H. *et al.* Hospitalizations Associated With Influenza and Respiratory Syncytial Virus in the United States, 1993–2008. *Clin. Infect. Dis.* **54**, 1427–1436 (2012).

150. Shi, T. *et al.* Global, regional, and national disease burden estimates of acute lower respiratory infections due to respiratory syncytial virus in young children in 2015: a systematic review and modelling study. *The Lancet* **390**, 946–958 (2017).

151. McLellan, J. S., Ray, W. C. & Peeples, M. E. Structure and Function of RSV Surface Glycoproteins. *Curr. Top. Microbiol. Immunol.* **372**, 83–104 (2013).

152. KIM, H. W. *et al.* RESPIRATORY SYNCYTIAL VIRUS DISEASE IN INFANTS DESPITE PRIOR ADMINISTRATION OF ANTIGENIC INACTIVATED VACCINE12. *Am. J. Epidemiol.* **89**, 422–434 (1969).

153. Wright, P. F. *et al.* Evaluation of a Live, Cold-Passaged, Temperature-Sensitive, Respiratory Syncytial Virus Vaccine Candidate in Infancy. *J. Infect. Dis.* **182**, 1331–1342 (2000).

154. Structure of RSV Fusion Glycoprotein Trimer Bound to a Prefusion-Specific Neutralizing Antibody | Science. https://www.science.org/doi/full/10.1126/science.1234914?casa_token=c22iKamH7SkA AAAA%3AtkpaB9lG7Ojd1SqV7iye16l82nszNCMAbC7zTzmpmoGTGiDd248ZLfG5o OL8-89-ocQbIYot7WeQ3WY.

155. Krarup, A. *et al.* A highly stable prefusion RSV F vaccine derived from structural analysis of the fusion mechanism. *Nat. Commun.* **6**, 8143 (2015).

156. Falsey, A. R. *et al.* Efficacy and Safety of an Ad26.RSV.preF–RSV preF Protein Vaccine in Older Adults. *N. Engl. J. Med.* **388**, 609–620 (2023).

157. Pfizer Announces Positive Top-Line Data from Phase 3 Trial of Older Adults for its Bivalent Respiratory Syncytial Virus (RSV) Vaccine Candidate | Pfizer. https://www.pfizer.com/news/press-release/press-release-detail/pfizer-announces-positive-top-line-data-phase-3-trial-older.

158. Walsh, E. E. *et al.* Efficacy and Safety of a Bivalent RSV Prefusion F Vaccine in Older Adults. *N. Engl. J. Med.* **0**, null (2023).

159. Schmoele-Thoma, B. *et al.* Vaccine Efficacy in Adults in a Respiratory Syncytial Virus Challenge Study. *N. Engl. J. Med.* **386**, 2377–2386 (2022).

160. Walsh, E. E. *et al.* A Randomized Phase 1/2 Study of a Respiratory Syncytial Virus Prefusion F Vaccine. *J. Infect. Dis.* **225**, 1357–1366 (2022).

161. Simões, E. A. F. *et al.* Prefusion F Protein–Based Respiratory Syncytial Virus Immunization in Pregnancy. *N. Engl. J. Med.* **386**, 1615–1626 (2022).

162. Kampmann, B. *et al.* Bivalent Prefusion F Vaccine in Pregnancy to Prevent RSV Illness in Infants. *N. Engl. J. Med.* **0**, null (2023).

163. Pallesen, J. *et al.* Immunogenicity and structures of a rationally designed prefusion MERS-CoV spike antigen. *Proc. Natl. Acad. Sci.* **114**, E7348–E7357 (2017).

164. Wrapp, D. *et al.* Cryo-EM structure of the 2019-nCoV spike in the prefusion conformation. *Science* **367**, 1260–1263 (2020).

165. Hsieh, C.-L. *et al.* Structure-based design of prefusion-stabilized SARS-CoV-2 spikes. *Science* **369**, 1501–1505 (2020).

166. Seephetdee, C. *et al.* Mice Immunized with the Vaccine Candidate HexaPro Spike Produce Neutralizing Antibodies against SARS-CoV-2. *Vaccines* **9**, 498 (2021).

167. Accurate prediction of protein structures and interactions using a three-track neural network | Science. https://www.science.org/doi/10.1126/science.abj8754.

168. Highly accurate protein structure prediction with AlphaFold | Nature. https://www.nature.com/articles/s41586-021-03819-2.

169. Yu, M. *et al.* Design of a Recombinant Multivalent Epitope Vaccine Based on SARS-CoV-2 and Its Variants in Immunoinformatics Approaches. *Front. Immunol.* **13**, 884433 (2022).

170. Ross, T. M. *et al.* A computationally designed H5 antigen shows immunological breadth of coverage and protects against drifting avian strains. *Vaccine* **37**, 2369–2376 (2019).

171. Hederman, A. P. & Ackerman, M. E. Leveraging deep learning to improve vaccine design. *Trends Immunol.* **0**, (2023).

172. Dreaming up new proteins, AI churns out possible medicines and vaccines | Science | AAAS. https://www.science.org/content/article/dreaming-new-proteins-ai-churns-out-possible-medicines-and-vaccines.

173. Callaway, E. Scientists are using AI to dream up revolutionary new proteins. *Nature* **609**, 661–662 (2022).

174. Higgins, M. K. Can We AlphaFold Our Way Out of the Next Pandemic? *J. Mol. Biol.* **433**, 167093 (2021).

175. Birkhoff, M., Leitz, M. & Marx, D. Advantages of Intranasal Vaccination and Considerations on Device Selection. *Indian J. Pharm. Sci.* **71**, 729–731 (2009).

176. Topol, E. J. & Iwasaki, A. Operation Nasal Vaccine—Lightning speed to counter COVID-19. *Sci. Immunol.* **7**, eadd9947 (2022).

177. Chavda, V. P., Vora, L. K., Pandya, A. K. & Patravale, V. B. Intranasal vaccines for SARS-CoV-2: From challenges to potential in COVID-19 management. *Drug Discov. Today* **26**, 2619–2636 (2021).

178. Jahnsen, F. L., Gran, E., Haye, R. & Brandtzaeg, P. Human nasal mucosa contains antigen-presenting cells of strikingly different functional phenotypes. *Am. J. Respir. Cell Mol. Biol.* **30**, 31–37 (2004).

179. Goetsch, L. *et al.* Targeting of Nasal Mucosa-Associated Antigen-Presenting Cells In Vivo with an Outer Membrane Protein A Derived from Klebsiella pneumoniae. *Infect. Immun.* **69**, 6434–6444 (2001).

180. Oh, J. E. *et al.* Intranasal priming induces local lung-resident B cell populations that secrete protective mucosal antiviral IgA. *Sci. Immunol.* **6**, eabj5129 (2021).

181. Almeida, A. J. & Alpar, H. O. Nasal delivery of vaccines. *J. Drug Target.* **3**, 455–467 (1996).

182. Hartwell, B. L. *et al.* Intranasal vaccination with lipid-conjugated immunogens promotes antigen transmucosal uptake to drive mucosal and systemic immunity. *Sci. Transl. Med.* **14**, eabn1413 (2022).

183. Li, L. *et al.* Mucosal IgA response elicited by intranasal immunization of Lactobacillus plantarum expressing surface-displayed RBD protein of SARS-CoV-2. *Int. J. Biol. Macromol.* **190**, 409–416 (2021).

184. Sterlin, D. *et al.* IgA dominates the early neutralizing antibody response to SARS-CoV-2. *Sci. Transl. Med.* **13**, eabd2223 (2021).

185. Brown, T. A., Russell, M. W., Kulhavy, R. & Mestecky, J. IgA-mediated elimination of antigens by the hepatobiliary route. *Fed. Proc.* **42**, 3218–3221 (1983).

186. Lamm, M. E. Interaction of antigens and antibodies at mucosal surfaces. *Annu. Rev. Microbiol.* **51**, 311–340 (1997).

187. Corthesy, B. Multi-Faceted Functions of Secretory IgA at Mucosal Surfaces. *Front. Immunol.* **4**, (2013).

188. Uddbäck, I. *et al.* Long-term maintenance of lung resident memory T cells is mediated by persistent antigen. *Mucosal Immunol.* **14**, 92–99 (2021).

189. Kim, E. *et al.* A single subcutaneous or intranasal immunization with adenovirus-based SARS-CoV-2 vaccine induces robust humoral and cellular immune responses in mice. *Eur J Immunol* **51**, 1774–1784 (2021).

190. Lemiale, F. *et al.* Enhanced Mucosal Immunoglobulin A Response of Intranasal Adenoviral Vector Human Immunodeficiency Virus Vaccine and Localization in the Central Nervous System. *J. Virol.* **77**, 10078–10087 (2003).

191. Live Intranasal Influenza Vaccine Information Statement | CDC. https://www.cdc.gov/vaccines/hcp/vis/vis-statements/flulive.html (2022).

192. Barría, M. I. *et al.* Localized Mucosal Response to Intranasal Live Attenuated Influenza Vaccine in Adults. *J. Infect. Dis.* **207**, 115–124 (2013).

193. Mohn, K. G.-I., Smith, I., Sjursen, H. & Cox, R. J. Immune responses after live attenuated influenza vaccination. *Hum. Vaccines Immunother.* **14**, 571–578 (2018).

194. Nichol, K. L. *et al.* Effectiveness of Live, Attenuated Intranasal Influenza Virus Vaccine in Healthy, Working Adults: A Randomized Controlled Trial. *JAMA* **282**, 137–144 (1999).

195. Andersohn, F. *et al.* Vaccination of children with a live-attenuated, intranasal influenza vaccine – analysis and evaluation through a Health Technology Assessment. *GMS Health Technol. Assess.* **10**, Doc03 (2014).

196. Trombetta, C. M., Gianchecchi, E. & Montomoli, E. Influenza vaccines: Evaluation of the safety profile. *Hum. Vaccines Immunother.* **14**, 657–670 (2018).

197. Vaca, G. B. *et al.* Intranasal mRNA-LNP vaccination protects hamsters from SARS-CoV-2 infection. 2023.01.11.523616 Preprint at https://doi.org/10.1101/2023.01.11.523616 (2023).

198. Boley, P. A. *et al.* Enhanced mucosal immune responses and reduced viral load in the respiratory tract of ferrets to intranasal lipid nanoparticle-based SARS-CoV-2 proteins and mRNA vaccines. *J. Nanobiotechnology* **21**, 60 (2023).

199. Schultz, M. D. *et al.* A single intranasal administration of AdCOVID protects against SARS-CoV-2 infection in the upper and lower respiratory tracts. *Hum. Vaccines Immunother.* **18**, 2127292 (2022).

200. Liu, S. *et al.* Intranasal delivery of a rationally attenuated SARS-CoV-2 is immunogenic and protective in Syrian hamsters. *Nat. Commun.* **13**, 6792 (2022).

201. Wong, T. Y. *et al.* Intranasal administration of BReC-CoV-2 COVID-19 vaccine protects K18-hACE2 mice against lethal SARS-CoV-2 challenge. *Npj Vaccines* **7**, 1–15 (2022).

202. Zhou, R. *et al.* Nasal prevention of SARS-CoV-2 infection by intranasal influenza-based boost vaccination in mouse models. *eBioMedicine* **75**, (2022).

203. Jakobsen, H. *et al.* Intranasal Immunization with Pneumococcal Conjugate Vaccines with LT-K63, a Nontoxic Mutant of Heat-Labile Enterotoxin, as Adjuvant Rapidly Induces Protective Immunity against Lethal Pneumococcal Infections in Neonatal Mice. *Infect. Immun.* **70**, 1443–1452 (2002).

204. Ivanov, V. *et al.* Intranasal and intrapulmonary vaccination with an M protein-deficient respiratory syncytial virus (RSV) vaccine improves clinical signs and reduces viral replication in infant baboons after an RSV challenge infection. *Vaccine* **39**, 4063–4071 (2021).

205. Rigter, A. *et al.* A Protective and Safe Intranasal RSV Vaccine Based on a Recombinant Prefusion-Like Form of the F Protein Bound to Bacterium-Like Particles. *PLOS ONE* **8**, e71072 (2013).

206. Vlachantoni, I. *et al.* S68 Phase 1 trial of an intranasal respiratory syncytial virus (rsv) subunit candidate vaccine: safety results from the muc-syngem study. *Thorax* **72**, A43–A44 (2017).

207. Klechevsky, E. *et al.* Functional Specializations of Human Epidermal Langerhans Cells and CD14+ Dermal Dendritic Cells. *Immunity* **29**, 497–510 (2008).

208. Rahman, F. *et al.* Cellular and humoral immune responses induced by intradermal or intramuscular vaccination with the major hepatitis B surface antigen. *Hepatology* **31**, 521–7 (2000).

209. Kenney, R. T., Frech, S. A., Muenz, L. R., Villar, C. P. & Glenn, G. M. Dose Sparing with Intradermal Injection of Influenza Vaccine. *N. Engl. J. Med.* **351**, 2295–2301 (2004).

210. Schnyder, J. L., de Jong, H. K. & Grobusch, M. P. Intradermal immunization—a dose-sparing strategy to combat global shortages of severe acute respiratory syndrome coronavirus 2 vaccines? *Clin. Microbiol. Infect.* **28**, 6–8 (2022).

211. Zuo, W. *et al.* Dose-Sparing Intradermal DTaP-sIPV Immunization With a Hollow Microneedle Leads to Superior Immune Responses. *Front. Microbiol.* **12**, 757375 (2021).

212. Iwata, H. *et al.* Safety and dose-sparing effect of Japanese encephalitis vaccine administered by microneedle patch in uninfected, healthy adults (MNA-J): a randomised, partly blinded, active-controlled, phase 1 trial. *Lancet Microbe* **3**, e96–e104 (2022).

213. Halder, J., Gupta, S., Kumari, R., Gupta, G. D. & Rai, V. K. Microneedle Array: Applications, Recent Advances, and Clinical Pertinence in Transdermal Drug Delivery. *J. Pharm. Innov.* **16**, 558–565 (2021).

214. Mdanda, S., Ubanako, P., Kondiah, P. P. D., Kumar, P. & Choonara, Y. E. Recent Advances in Microneedle Platforms for Transdermal Drug Delivery Technologies. *Polymers* **13**, 2405 (2021).

215. Sartawi, Z., Blackshields, C. & Faisal, W. Dissolving microneedles: Applications and growing therapeutic potential. *J. Controlled Release* **348**, 186–205 (2022).

216. Faraji Rad, Z., Prewett, P. D. & Davies, G. J. An overview of microneedle applications, materials, and fabrication methods. *Beilstein J. Nanotechnol.* **12**, 1034–1046 (2021).

217. Kim, E. *et al.* Microneedle array delivered recombinant coronavirus vaccines: Immunogenicity and rapid translational development. *EBioMedicine* **55**, 102743 (2020).

218. Shim, W. S., Hwang, Y. M., Park, S. G., Lee, C. K. & Kang, N. G. Role of Polyvinylpyrrolidone in Dissolving Microneedle for Efficient Transdermal Drug Delivery: In vitro and Clinical Studies. *Bull. Korean Chem. Soc.* **39**, 789–793 (2018).

219. Crothers, J. W. *et al.* Intradermal fractional-dose inactivated polio vaccine (fIPV) adjuvanted with double mutant Enterotoxigenic Escherichia coli heat labile toxin (dmLT) is well-tolerated and augments a systemic immune response to all three poliovirus serotypes in a randomized placebo-controlled trial. *Vaccine* **40**, 2705–2713 (2022).

220. Kouiavskaia, D. *et al.* Intradermal Inactivated Poliovirus Vaccine: A Preclinical Dose-Finding Study. *J. Infect. Dis.* **211**, 1447–1450 (2015).

221. Llanes, A. *et al.* Betacoronavirus Genomes: How Genomic Information has been Used to Deal with Past Outbreaks and the COVID-19 Pandemic. *Int. J. Mol. Sci.* **21**, 4546 (2020).

222. Li, X. *et al.* Genomic Feature Analysis of Betacoronavirus Provides Insights Into SARS and COVID-19 Pandemics. *Front. Microbiol.* **12**, (2021).

223. Mackay, I. M. & Arden, K. E. MERS coronavirus: diagnostics, epidemiology and transmission. *Virol. J.* **12**, 222 (2015).

224. WHO Coronavirus (COVID-19) Dashboard. https://covid19.who.int.

225. Benton, D. J. *et al.* Receptor binding and priming of the spike protein of SARS-CoV-2 for membrane fusion. *Nature* **588**, 327–330 (2020).

226. Bosch, B. J., van der Zee, R., de Haan, C. A. M. & Rottier, P. J. M. The coronavirus spike protein is a class I virus fusion protein: structural and functional characterization of the fusion core complex. *J. Virol.* **77**, 8801–8811 (2003).

227. Huang, Y., Yang, C., Xu, X., Xu, W. & Liu, S. Structural and functional properties of SARS-CoV-2 spike protein: potential antivirus drug development for COVID-19. *Acta Pharmacol. Sin.* **41**, 1141–1149 (2020).

228. Watanabe, Y., Allen, J. D., Wrapp, D., McLellan, J. S. & Crispin, M. Site-specific glycan analysis of the SARS-CoV-2 spike. *Science* **369**, 330–333 (2020).

229. Gong, Y., Qin, S., Dai, L. & Tian, Z. The glycosylation in SARS-CoV-2 and its receptor ACE2. *Signal Transduct. Target. Ther.* **6**, 1–24 (2021).

230. Peacock, T. P. *et al.* The furin cleavage site in the SARS-CoV-2 spike protein is required for transmission in ferrets. *Nat. Microbiol.* **6**, 899–909 (2021).

231. Distinctive Roles of Furin and TMPRSS2 in SARS-CoV-2 Infectivity | Journal of Virology. https://journals.asm.org/doi/10.1128/jvi.00128-22.

232. Lan, J. *et al.* Structure of the SARS-CoV-2 spike receptor-binding domain bound to the ACE2 receptor. *Nature* **581**, 215–220 (2020).

233. Shang, J. *et al.* Structural basis of receptor recognition by SARS-CoV-2. *Nature* **581**, 221–224 (2020).

234. Piccoli, L. *et al.* Mapping Neutralizing and Immunodominant Sites on the SARS-CoV-2 Spike Receptor-Binding Domain by Structure-Guided High-Resolution Serology. *Cell* **183**, 1024-1042.e21 (2020).

235. Greaney, A. J. *et al.* Comprehensive mapping of mutations in the SARS-CoV-2 receptor-binding domain that affect recognition by polyclonal human plasma antibodies. *Cell Host Microbe* **29**, 463-476.e6 (2021).

236. Garcia-Beltran, W. F. *et al.* COVID-19-neutralizing antibodies predict disease severity and survival. *Cell* **184**, 476-488.e11 (2021).

237. Bai, Z., Cao, Y., Liu, W. & Li, J. The SARS-CoV-2 Nucleocapsid Protein and Its Role in Viral Structure, Biological Functions, and a Potential Target for Drug or Vaccine Mitigation. *Viruses* **13**, (2021).

238. Bessa, L. M. *et al.* The intrinsically disordered SARS-CoV-2 nucleoprotein in dynamic complex with its viral partner nsp3a. *Sci. Adv.* **8**, eabm4034 (2022).

239. Craig Fenwick *et al.* Changes in SARS-CoV-2 Spike versus Nucleoprotein Antibody Responses Impact the Estimates of Infections in Population-Based Seroprevalence Studies. *J. Virol.* **95**, e01828-20 (2021).

240. Mishra, T. *et al.* SARS CoV-2 Nucleoprotein Enhances the Infectivity of Lentiviral Spike Particles. *Front. Cell. Infect. Microbiol.* **11**, (2021).

241. Marra, M. A. *et al.* The Genome sequence of the SARS-associated coronavirus. *Science* **300**, 1399–404 (2003).

242. Oliveira, S. C., de Magalhães, M. T. Q. & Homan, E. J. Immunoinformatic Analysis of SARS-CoV-2 Nucleocapsid Protein and Identification of COVID-19 Vaccine Targets. *Front. Immunol.* **11**, (2020).

243. Le Bert, N. *et al.* SARS-CoV-2-specific T cell immunity in cases of COVID-19 and SARS, and uninfected controls. *Nature* **584**, 457–462 (2020).

244. Lineburg, K. E. *et al.* CD8(+) T cells specific for an immunodominant SARS-CoV-2 nucleocapsid epitope cross-react with selective seasonal coronaviruses. *Immunity* **54**, 1055-1065.e5 (2021).

245. Lee, E. *et al.* Identification of SARS-CoV-2 Nucleocapsid and Spike T-Cell Epitopes for Assessing T-Cell Immunity. *J. Virol.* **95**, (2021).

246. Zhang, Z. *et al.* Structure of SARS-CoV-2 membrane protein essential for virus assembly. *Nat. Commun.* **13**, 4399 (2022).

247. Schoeman, D. & Fielding, B. C. Coronavirus envelope protein: current knowledge. *Virol. J.* **16**, 69 (2019).

248. Lamers, M. M. & Haagmans, B. L. SARS-CoV-2 pathogenesis. *Nat. Rev. Microbiol.* **20**, 270–284 (2022).

249. Tatar, M., Shoorekchali, J. M., Faraji, M. R. & Wilson, F. A. International COVID-19 vaccine inequality amid the pandemic: Perpetuating a global crisis? *J. Glob. Health* **11**, 03086–03086 (2021).

250. Krause, P. R. *et al.* SARS-CoV-2 Variants and Vaccines. *N. Engl. J. Med.* **385**, 179–186 (2021).

251. Harvey, W. T. *et al.* SARS-CoV-2 variants, spike mutations and immune escape. *Nat Rev Microbiol* **19**, 409–424 (2021).

252. CSR. MERS outbreaks. *World Health Organization - Regional Office for the Eastern Mediterranean* http://www.emro.who.int/health-topics/mers-cov/mers-outbreaks.html.

253. Zhang, A.-R. *et al.* Epidemiology and evolution of Middle East respiratory syndrome coronavirus, 2012–2020. *Infect. Dis. Poverty* **10**, 66 (2021).

254. Du, L. *et al.* MERS-CoV spike protein: a key target for antivirals. *Expert Opin. Ther. Targets* **21**, 131–143 (2017).

255. Watanabe, Y. *et al.* Vulnerabilities in coronavirus glycan shields despite extensive glycosylation. *Nat. Commun.* **11**, 2688 (2020).

256. Barlan, A. *et al.* Receptor Variation and Susceptibility to Middle East Respiratory Syndrome Coronavirus Infection. *J. Virol.* **88**, 4953–4961 (2014).

257. Alharbi, S. N. & Alrefaei, A. F. Comparison of the SARS-CoV-2 (2019-nCoV) M protein with its counterparts of SARS-CoV and MERS-CoV species. *J. King Saud Univ. Sci.* **33**, 101335 (2021).

258. Aldaais, E. A., Yegnaswamy, S., Albahrani, F., Alsowaiket, F. & Alramadan, S. Sequence and structural analysis of COVID-19 E and M proteins with MERS virus E and M proteins—A comparative study. *Biochem. Biophys. Rep.* **26**, 101023 (2021).

259. Pormohammad, A. *et al.* Comparison of confirmed COVID-19 with SARS and MERS cases - Clinical characteristics, laboratory findings, radiographic signs and outcomes: A systematic review and meta-analysis. *Rev. Med. Virol.* **30**, e2112 (2020).

260. Zhou, H. *et al.* A Review of SARS-CoV2: Compared With SARS-CoV and MERS-CoV. *Front. Med.* **8**, (2021).

261. Rockx, B. *et al.* Comparative pathogenesis of COVID-19, MERS, and SARS in a nonhuman primate model. *Science* **368**, 1012–1015 (2020).

262. Why no MERS vaccine? Lack of foresight frustrates scientists. *Reuters* (2015).

263. Tai, W., Zhang, X., Yang, Y., Zhu, J. & Du, L. Advances in mRNA and other vaccines against MERS-CoV. *Transl. Res.* **242**, 20–37 (2022).

264. Cross-Protection against MERS-CoV by Prime-Boost Vaccination Using Viral Spike DNA and Protein | Journal of Virology. https://journals.asm.org/doi/10.1128/JVI.01176-20.

265. Al-amri, S. S. *et al.* Immunogenicity of Candidate MERS-CoV DNA Vaccines Based on the Spike Protein. *Sci. Rep.* **7**, 44875 (2017).

266. Fathi, A. *et al.* Increased neutralization and IgG epitope identification after MVA-MERS-S booster vaccination against Middle East respiratory syndrome. *Nat. Commun.* **13**, 4182 (2022).

267. Koch, T. *et al.* Safety and immunogenicity of a modified vaccinia virus Ankara vector vaccine candidate for Middle East respiratory syndrome: an open-label, phase 1 trial. *Lancet Infect. Dis.* **20**, 827–838 (2020).

268. Weskamm, L. M. *et al.* Persistence of MERS-CoV-spike-specific B cells and antibodies after late third immunization with the MVA-MERS-S vaccine. *Cell Rep. Med.* **3**, 100685 (2022).

269. Bosaeed, M. *et al.* Safety and immunogenicity of ChAdOx1 MERS vaccine candidate in healthy Middle Eastern adults (MERS002): an open-label, non-randomised, dose-escalation, phase 1b trial. *Lancet Microbe* **3**, e11–e20 (2022).

270. Folegatti, P. M. *et al.* Safety and immunogenicity of the ChAdOx1 nCoV-19 vaccine against SARS-CoV-2: a preliminary report of a phase 1/2, single-blind, randomised controlled trial. *The Lancet* **396**, 467–478 (2020).

271. COVID-19 vaccine tracker and landscape. https://www.who.int/publications/m/item/draft-landscape-of-covid-19-candidate-vaccines.

272. Vaccines – COVID19 Vaccine Tracker. https://covid19.trackvaccines.org/vaccines/approved/#vaccine-list.

273. Kurup, D. & Schnell, M. J. SARS-CoV-2 vaccines — the biggest medical research project of the 21st century. *Curr. Opin. Virol.* **49**, 52–57 (2021).

274. Bos, R. *et al.* Ad26 vector-based COVID-19 vaccine encoding a prefusion-stabilized SARS-CoV-2 Spike immunogen induces potent humoral and cellular immune responses. *Npj Vaccines* **5**, 91 (2020).

275. Voysey, M. *et al.* Safety and efficacy of the ChAdOx1 nCoV-19 vaccine (AZD1222) against SARS-CoV-2: an interim analysis of four randomised controlled trials in Brazil, South Africa, and the UK. *Lancet Lond. Engl.* **397**, 99–111 (2021).

276. The Sinopharm COVID-19 vaccine: What you need to know. https://www.who.int/news-room/feature-stories/detail/the-sinopharm-covid-19-vaccine-what-you-need-to-know.

277. The Sinovac-CoronaVac COVID-19 vaccine: What you need to know. https://www.who.int/news-room/feature-stories/detail/the-sinovac-covid-19-vaccine-what-you-need-to-know.

278. Pramod, S., Govindan, D., Ramasubramani, P., Kar, S. S. & Aggarwal, R. Effectiveness of Covishield vaccine in preventing Covid-19 – A test-negative case-control study. *Vaccine* **40**, 3294–3297 (2022).

279. The Bharat Biotech BBV152 COVAXIN vaccine against COVID-19: What you need to know. https://www.who.int/news-room/feature-stories/detail/the-bharat-biotech-bbv152-covaxin-vaccine-against-covid-19-what-you-need-to-know.

280. The Novavax vaccine against COVID-19: What you need to know. https://www.who.int/news-room/feature-stories/detail/the-novavax-vaccine-against-covid-19-what-you-need-to-know.

281. Fukushima, A. *et al.* Genetic background determines susceptibility to experimental immune-mediated blepharoconjunctivitis: comparison of Balb/c and C57BL/6 mice. *Exp. Eye Res.* **82**, 210–218 (2006).

282. Schulte, S., Sukhova, G. K. & Libby, P. Genetically Programmed Biases in Th1 and Th2 Immune Responses Modulate Atherogenesis. *Am. J. Pathol.* **172**, 1500–1508 (2008).

283. Chen, X., Oppenheim, J. J. & Howard, O. M. BALB/c mice have more CD4+CD25+ T regulatory cells and show greater susceptibility to suppression of their CD4+CD25- responder T cells than C57BL/6 mice. *J Leukoc Biol* **78**, 114–21 (2005).

284. Jia, W. *et al.* The Mechanisms and Animal Models of SARS-CoV-2 Infection. *Front. Cell Dev. Biol.* **9**, (2021).

285. Dinnon, K. H. *et al.* A mouse-adapted model of SARS-CoV-2 to test COVID-19 countermeasures. *Nature* **586**, 560–566 (2020).

286. Winkler, E. S. *et al.* SARS-CoV-2 infection of human ACE2-transgenic mice causes severe lung inflammation and impaired function. *Nat. Immunol.* **21**, 1327–1335 (2020).

287. Montagutelli, X. *et al.* Variants with the N501Y mutation extend SARS-CoV-2 host range to mice, with contact transmission. 2021.03.18.436013 Preprint at https://doi.org/10.1101/2021.03.18.436013 (2021).

288. Niu, Z. *et al.* N501Y mutation imparts cross-species transmission of SARS-CoV-2 to mice by enhancing receptor binding. *Signal Transduct. Target. Ther.* **6**, 1–3 (2021).

289. Pan, T. *et al.* Infection of wild-type mice by SARS-CoV-2 B.1.351 variant indicates a possible novel cross-species transmission route. *Signal Transduct. Target. Ther.* **6**, 1–12 (2021).

290. Hansen, S. G. *et al.* Prevention of tuberculosis in rhesus macaques by a cytomegalovirus-based vaccine. *Nat. Med.* **24**, 130–143 (2018).

291. Shedlock, D. J., Silvestri, G. & Weiner, D. B. Monkeying around with HIV vaccines: using rhesus macaques to define 'gatekeepers' for clinical trials. *Nat. Rev. Immunol.* **9**, 717–728 (2009).

292. Vogel, A. B. *et al.* BNT162b vaccines protect rhesus macaques from SARS-CoV-2. *Nature* **592**, 283–289 (2021).

293. Milligan, E. C. *et al.* Infant rhesus macaques immunized against SARS-CoV-2 are protected against heterologous virus challenge 1 year later. *Sci. Transl. Med.* **15**, eadd6383 (2022).

294. Chu, H., Chan, J. F.-W. & Yuen, K.-Y. Animal models in SARS-CoV-2 research. *Nat. Methods* **19**, 392–394 (2022).

295. Shou, S. *et al.* Animal Models for COVID-19: Hamsters, Mouse, Ferret, Mink, Tree Shrew, and Non-human Primates. *Front. Microbiol.* **12**, (2021).

296. Woolsey, C. *et al.* Establishment of an African green monkey model for COVID-19 and protection against re-infection. *Nat. Immunol.* **22**, 86–98 (2021).

297. Chen, H. *et al.* Immunological evaluation of an inactivated SARS-CoV-2 vaccine in rhesus macaques. *Mol. Ther. - Methods Clin. Dev.* **23**, 108–118 (2021).

298. Sui, Y. *et al.* Protection against SARS-CoV-2 infection by a mucosal vaccine in rhesus macaques. *JCI Insight* **6**, (2021).

299. Volkmann, A. *et al.* A Capsid Virus-Like Particle-Based SARS-CoV-2 Vaccine Induces High Levels of Antibodies and Protects Rhesus Macaques. *Front. Immunol.* **13**, (2022).

300. Yu, J. *et al.* DNA vaccine protection against SARS-CoV-2 in rhesus macaques. *Science* **369**, 806–811 (2020).

301. Charles A Janeway, J., Travers, P., Walport, M. & Shlomchik, M. J. The distribution and functions of immunoglobulin isotypes. *Immunobiol. Immune Syst. Health Dis. 5th Ed.* (2001).

302. Bolles, M. *et al.* A Double-Inactivated Severe Acute Respiratory Syndrome Coronavirus Vaccine Provides Incomplete Protection in Mice and Induces Increased Eosinophilic Proinflammatory Pulmonary Response upon Challenge. *J. Virol.* (2011) doi:10.1128/JVI.06048-11.

303. Tseng, C.-T. *et al.* Immunization with SARS coronavirus vaccines leads to pulmonary immunopathology on challenge with the SARS virus. *PloS One* **7**, e35421 (2012).

304. Lai, C.-Y. *et al.* Recombinant protein subunit SARS-CoV-2 vaccines formulated with CoVaccine HT^{TM} adjuvant induce broad, Th1 biased, humoral and cellular immune responses in mice. *Vaccine X* **9**, 100126 (2021).

305. Lynch, K. L., Zhou, S., Kaul, R., Walker, R. & Wu, A. H. Evaluation of neutralizing antibodies against SARS-CoV-2 variants after infection and vaccination using a multiplexed surrogate virus neutralization test. *Clin. Chem.* hvab283 (2022) doi:10.1093/clinchem/hvab283.

306. Sancilio, A. E. *et al.* A surrogate virus neutralization test to quantify antibody-mediated inhibition of SARS-CoV-2 in finger stick dried blood spot samples. *Sci. Rep.* **11**, 15321 (2021).

307. Amin Addetia *et al.* Neutralizing Antibodies Correlate with Protection from SARS-CoV-2 in Humans during a Fishery Vessel Outbreak with a High Attack Rate. *J. Clin. Microbiol.* **58**, e02107-20 (2020).

308. Khoury, D. S. *et al.* Correlates of protection, thresholds of protection, and immunobridging in SARS-CoV-2 infection. 2022.06.05.22275943 Preprint at https://doi.org/10.1101/2022.06.05.22275943 (2022).

309. Earle, K. A. *et al.* Evidence for antibody as a protective correlate for COVID-19 vaccines. *Vaccine* **39**, 4423–4428 (2021).

310.	Goldblatt, D., Alter, G., Crotty, S. & Plotkin, S. A. Correlates of protection against SARS-CoV-2 infection and COVID-19 disease. *Immunol. Rev.* 10.1111/imr.13091 (2022) doi:10.1111/imr.13091.

311.	Bange, E. M. *et al.* CD8+ T cells contribute to survival in patients with COVID-19 and hematologic cancer. *Nat. Med.* **27**, 1280–1289 (2021).

312.	Rha, M.-S. & Shin, E.-C. Activation or exhaustion of CD8+ T cells in patients with COVID-19. *Cell. Mol. Immunol.* **18**, 2325–2333 (2021).

313.	Bertoletti, A., Le Bert, N. & Tan, A. T. SARS-CoV-2-specific T cells in the changing landscape of the COVID-19 pandemic. *Immunity* **55**, 1764–1778 (2022).

314.	Grifoni, A. *et al.* SARS-CoV-2 Human T cell Epitopes: adaptive immune response against COVID-19. *Cell Host Microbe* (2021) doi:https://doi.org/10.1016/j.chom.2021.05.010.

315.	Guo, L. *et al.* SARS-CoV-2-specific antibody and T-cell responses 1 year after infection in people recovered from COVID-19: a longitudinal cohort study. *Lancet Microbe* **3**, e348–e356 (2022).

316.	Lu, X. & Yamasaki, S. Current understanding of T cell immunity against SARS-CoV-2. *Inflamm. Regen.* **42**, 51 (2022).

317.	Moss, P. The T cell immune response against SARS-CoV-2. *Nat. Immunol.* **23**, 186–193 (2022).

318.	T cells found in COVID-19 patients 'bode well' for long-term immunity | Science | AAAS. https://www.science.org/content/article/t-cells-found-covid-19-patients-bode-well-long-term-immunity.

319.	Visvabharathy, L. *et al.* Neuro-COVID long-haulers exhibit broad dysfunction in T cell memory generation and responses to vaccination. *MedRxiv Prepr. Serv. Health Sci.* 2021.08.08.21261763 (2021) doi:10.1101/2021.08.08.21261763.

320.	Glynne, P., Tahmasebi, N., Gant, V. & Gupta, R. Long COVID following mild SARS-CoV-2 infection: characteristic T cell alterations and response to antihistamines. *J. Investig. Med.* **70**, 61 (2022).

321.	Jaana Westmeier *et al.* Impaired Cytotoxic CD8^{+} T Cell Response in Elderly COVID-19 Patients. *mBio* **11**, e02243-20 (2020).

322.	Raoult, D., Zumla, A., Locatelli, F., Ippolito, G. & Kroemer, G. Coronavirus infections: Epidemiological, clinical and immunological features and hypotheses. *Cell Stress* **4**, 66–75 (2020).

323.	de Wit, E., van Doremalen, N., Falzarano, D. & Munster, V. J. SARS and MERS: recent insights into emerging coronaviruses. *Nat. Rev. Microbiol.* **14**, 523–534 (2016).

324. Hilgenfeld, R. & Peiris, M. From SARS to MERS: 10 years of research on highly pathogenic human coronaviruses. *Antivir. Res* **100**, 286–95 (2013).

325. Acter, T. *et al.* Evolution of severe acute respiratory syndrome coronavirus 2 (SARS-CoV-2) as coronavirus disease 2019 (COVID-19) pandemic: A global health emergency. *Sci. Total Environ.* **730**, 138996 (2020).

326. Lai, C. C., Shih, T. P., Ko, W. C., Tang, H. J. & Hsueh, P. R. Severe acute respiratory syndrome coronavirus 2 (SARS-CoV-2) and coronavirus disease-2019 (COVID-19): The epidemic and the challenges. *Int J Antimicrob Agents* **55**, 105924 (2020).

327. Chakraborty, I. & Maity, P. COVID-19 outbreak: Migration, effects on society, global environment and prevention. *Sci Total Env.* **728**, 138882 (2020).

328. Bandyopadhyay, S. Coronavirus Disease 2019 (COVID-19): we shall overcome. *Clean Technol. Environ. Policy* **22**, 545–546 (2020).

329. Lurie, N., Saville, M., Hatchett, R. & Halton, J. Developing Covid-19 Vaccines at Pandemic Speed. *N. Engl. J. Med.* **382**, 1969–1973 (2020).

330. Chen, W.-H., Strych, U., Hotez, P. J. & Bottazzi, M. E. The SARS-CoV-2 Vaccine Pipeline: an Overview. *Curr. Trop. Med. Rep.* **7**, 61–64 (2020).

331. Amanat, F. & Krammer, F. SARS-CoV-2 Vaccines: Status Report. *Immunity* **52**, 583–589 (2020).

332. Lu, S. Timely development of vaccines against SARS-CoV-2. *Emerg. Microbes Infect.* **9**, 542–544 (2020).

333. Khan, S. *et al.* Emergence of a Novel Coronavirus, Severe Acute Respiratory Syndrome Coronavirus 2: Biology and Therapeutic Options. *J Clin Microbiol* **58**, (2020).

334. Tang, T., Bidon, M., Jaimes, J. A., Whittaker, G. R. & Daniel, S. Coronavirus membrane fusion mechanism offers a potential target for antiviral development. *Antivir. Res* **178**, 104792 (2020).

335. Li, X., Luk, H. K. H., Lau, S. K. P. & Woo, P. C. Y. Human Coronaviruses: General Features. *Ref. Module Biomed. Sci.* B978-0-12-801238-3.95704–0 (2019) doi:10.1016/B978-0-12-801238-3.95704-0.

336. Walls, A. C. *et al.* Structure, Function, and Antigenicity of the SARS-CoV-2 Spike Glycoprotein. *Cell* **181**, 281-292.e6 (2020).

337. Wang, Q. *et al.* Structural and Functional Basis of SARS-CoV-2 Entry by Using Human ACE2. *Cell* **181**, 894-904.e9 (2020).

338. Yan, R. *et al.* Structural basis for the recognition of SARS-CoV-2 by full-length human ACE2. *Science* **367**, 1444–1448 (2020).

339. Jiang, S., Hillyer, C. & Du, L. Neutralizing Antibodies against SARS-CoV-2 and Other Human Coronaviruses. *Trends Immunol* **41**, 355–359 (2020).

340. Song, F. *et al.* Middle East respiratory syndrome coronavirus spike protein delivered by modified vaccinia virus Ankara efficiently induces virus-neutralizing antibodies. *J. Virol.* **87**, 11950–11954 (2013).

341. Coleman, C. M. *et al.* Purified coronavirus spike protein nanoparticles induce coronavirus neutralizing antibodies in mice. *Vaccine* **32**, 3169–3174 (2014).

342. Yong, C. Y., Ong, H. K., Yeap, S. K., Ho, K. L. & Tan, W. S. Recent Advances in the Vaccine Development Against Middle East Respiratory Syndrome-Coronavirus. *Front. Microbiol.* **10**, (2019).

343. Kim, E. *et al.* Immunogenicity of an adenoviral-based Middle East Respiratory Syndrome coronavirus vaccine in BALB/c mice. *Vaccine* **32**, 5975–5982 (2014).

344. Gao, W. *et al.* Effects of a SARS-associated coronavirus vaccine in monkeys. *Lancet* **362**, 1895–6 (2003).

345. Zhang, C., Maruggi, G., Shan, H. & Li, J. Advances in mRNA Vaccines for Infectious Diseases. *Front. Immunol.* **10**, (2019).

346. DNA vaccines: prime time is now - PubMed. https://pubmed.ncbi.nlm.nih.gov/32259744/.

347. Mascola, J. R. & Fauci, A. S. Novel vaccine technologies for the 21st century. *Nat. Rev. Immunol.* **20**, 87–88 (2020).

348. Lee, J., Arun Kumar, S., Jhan, Y. Y. & Bishop, C. J. Engineering DNA vaccines against infectious diseases. *Acta Biomater.* **80**, 31–47 (2018).

349. Ivory, C. & Chadee, K. DNA vaccines: designing strategies against parasitic infections. *Genet. Vaccines Ther.* **2**, 17 (2004).

350. Ghaffarifar, F. Plasmid DNA vaccines: where are we now? *Drugs Today Barc. Spain 1998* **54**, 315–333 (2018).

351. Condon, C., Watkins, S. C., Celluzzi, C. M., Thompson, K. & Falo, L. D. DNA-based immunization by in vivo transfection of dendritic cells. *Nat. Med.* **2**, 1122–1128 (1996).

352. Maslow, J. N. Vaccine development for emerging virulent infectious diseases. *Vaccine* **35**, 5437–5443 (2017).

353. Martin, J. E. *et al.* A SARS DNA vaccine induces neutralizing antibody and cellular immune responses in healthy adults in a Phase I clinical trial. *Vaccine* **26**, 6338–6343 (2008).

354. Liu, S., Wang, S. & Lu, S. DNA immunization as a technology platform for monoclonal antibody induction. *Emerg. Microbes Infect.* **5**, e33 (2016).

355. Smith, T. R. F. *et al.* Immunogenicity of a DNA vaccine candidate for COVID-19. *Nat. Commun.* **11**, 2601 (2020).

356. Poland, G. A., Ovsyannikova, I. G., Crooke, S. N. & Kennedy, R. B. SARS-CoV-2 Vaccine Development: Current Status. *Mayo Clin. Proc.* **95**, 2172–2188 (2020).

357. Ewer, K. J. *et al.* Viral vectors as vaccine platforms: from immunogenicity to impact. *Curr. Opin. Immunol.* **41**, 47–54 (2016).

358. Draper, S. J. & Heeney, J. L. Viruses as vaccine vectors for infectious diseases and cancer. *Nat. Rev. Microbiol.* **8**, 62–73 (2010).

359. He, Y., Zhang, J., Donahue, C. & Falo, L. D. Skin-derived dendritic cells induce potent CD8(+) T cell immunity in recombinant lentivector-mediated genetic immunization. *Immunity* **24**, 643–656 (2006).

360. Gilbert, S. C. & Warimwe, G. M. Rapid development of vaccines against emerging pathogens: The replication-deficient simian adenovirus platform technology. *Vaccine* **35**, 4461–4464 (2017).

361. Van Kampen, K. R. *et al.* Safety and immunogenicity of adenovirus-vectored nasal and epicutaneous influenza vaccines in humans. *Vaccine* **23**, 1029–36 (2005).

362. Stanley, D. A. *et al.* Chimpanzee adenovirus vaccine generates acute and durable protective immunity against ebolavirus challenge. *Nat Med* **20**, 1126–9 (2014).

363. Erdos, G. *et al.* Improved Cutaneous Genetic Immunization by Microneedle Array Delivery of an Adjuvanted Adenovirus Vaccine. *J. Invest. Dermatol.* **140**, 2528-2531.e2 (2020).

364. Ledgerwood, J. E. *et al.* Chimpanzee Adenovirus Vector Ebola Vaccine. *N. Engl. J. Med.* **376**, 928–938 (2017).

365. Santis, O. D. *et al.* Safety and immunogenicity of a chimpanzee adenovirus-vectored Ebola vaccine in healthy adults: a randomised, double-blind, placebo-controlled, dose-finding, phase 1/2a study. *Lancet Infect. Dis.* **16**, 311–320 (2016).

366. Lane, R. Sarah Gilbert: carving a path towards a COVID-19 vaccine. *Lancet Lond. Engl.* **395**, 1247 (2020).

367. Zhu, F. C. *et al.* Safety, tolerability, and immunogenicity of a recombinant adenovirus type-5 vectored COVID-19 vaccine: a dose-escalation, open-label, non-randomised, first-in-human trial. *Lancet* **395**, 1845–1854 (2020).

368. Zhu, F. C. *et al.* Immunogenicity and safety of a recombinant adenovirus type-5-vectored COVID-19 vaccine in healthy adults aged 18 years or older: a randomised, double-blind, placebo-controlled, phase 2 trial. *Lancet* **396**, 479–488 (2020).

369. Ramasamy, M. N. *et al.* Safety and immunogenicity of ChAdOx1 nCoV-19 vaccine administered in a prime-boost regimen in young and old adults (COV002): a single-blind, randomised, controlled, phase 2/3 trial. *Lancet Lond. Engl.* **396**, 1979–1993 (2021).

370. Sadoff, J. *et al.* Interim Results of a Phase 1-2a Trial of Ad26.COV2.S Covid-19 Vaccine. *N. Engl. J. Med.* **384**, 1824–1835 (2021).

371. Gao, W., Rzewski, A., Sun, H., Robbins, P. D. & Gambotto, A. UpGene: Application of a Web-Based DNA Codon Optimization Algorithm. *Biotechnol. Prog.* **20**, 443–448 (2004).

372. Kim, E. *et al.* Preventative Vaccines for Zika Virus Outbreak: Preliminary Evaluation. *EBioMedicine* **13**, 315–320 (2016).

373. Hardy, S., Kitamura, M., Harris-Stansil, T., Dai, Y. & Phipps, M. L. Construction of adenovirus vectors through Cre-lox recombination. *J. Virol.* **71**, 1842–9 (1997).

374. Cossarizza, A. *et al.* Guidelines for the use of flow cytometry and cell sorting in immunological studies (second edition). *Eur J Immunol* **49**, 1457–1973 (2019).

375. Weisel, F. J., Zuccarino-Catania, G. V., Chikina, M. & Shlomchik, M. J. A Temporal Switch in the Germinal Center Determines Differential Output of Memory B and Plasma Cells. *Immunity* **44**, 116–130 (2016).

376. Good-Jacobson, K. L. *et al.* PD-1 regulates germinal center B cell survival and the formation and affinity of long-lived plasma cells. *Nat Immunol* **11**, 535–42 (2010).

377. Rodrigues, E. G., Zavala, F., Eichinger, D., Wilson, J. M. & Tsuji, M. Single immunizing dose of recombinant adenovirus efficiently induces CD8+ T cell-mediated protective immunity against malaria. *J. Immunol. Baltim. Md 1950* **158**, 1268–1274 (1997).

378. Schirmbeck, R., Reimann, J., Kochanek, S. & Kreppel, F. The immunogenicity of adenovirus vectors limits the multispecificity of CD8 T-cell responses to vector-encoded transgenic antigens. *Mol. Ther. J. Am. Soc. Gene Ther.* **16**, 1609–1616 (2008).

379. Percivalle, E. *et al.* West Nile or Usutu Virus? A Three-Year Follow-Up of Humoral and Cellular Response in a Group of Asymptomatic Blood Donors. *Viruses* **12**, 157 (2020).

380. Percivalle, E. *et al.* Prevalence of SARS-CoV-2 specific neutralising antibodies in blood donors from the Lodi Red Zone in Lombardy, Italy, as at 06 April 2020. *Euro Surveill. Bull. Eur. Sur Mal. Transm. Eur. Commun. Dis. Bull.* **25**, 2001031 (2020).

381. Kardani, K., Bolhassani, A. & Shahbazi, S. Prime-boost vaccine strategy against viral infections: Mechanisms and benefits. *Vaccine* **34**, 413–423 (2016).

382. Jung, S.-Y. *et al.* Heterologous prime-boost vaccination with adenoviral vector and protein nanoparticles induces both Th1 and Th2 responses against Middle East respiratory syndrome coronavirus. *Vaccine* **36**, 3468–3476 (2018).

383. Lu, S. Heterologous prime-boost vaccination. *Curr. Opin. Immunol.* **21**, 346–351 (2009).

384. Balmert, S. C. *et al.* Dissolving undercut microneedle arrays for multicomponent cutaneous vaccination. *J Control Release* **317**, 336–346 (2020).

385. Bachy, V. *et al.* Langerin negative dendritic cells promote potent CD8+ T-cell priming by skin delivery of live adenovirus vaccine microneedle arrays. *Proc Natl Acad Sci U A* **110**, 3041–6 (2013).

386. Korkmaz, E. *et al.* Microarray patches enable the development of skin-targeted vaccines against COVID-19. *Adv. Drug Deliv. Rev.* **171**, 164–186 (2021).

387. DeMuth, P. C. *et al.* Vaccine delivery with microneedle skin patches in nonhuman primates. *Nat. Biotechnol.* **31**, 1082–1085 (2013).

388. Shlomchik, M. J. & Weisel, F. Germinal center selection and the development of memory B and plasma cells. *Immunol. Rev.* **247**, 52–63 (2012).

389. Hoegh-Petersen, M., Thomsen, A. R., Christensen, J. P. & Holst, P. J. Mucosal immunization with recombinant adenoviral vectors expressing murine gammaherpesvirus-68 genes M2 and M3 can reduce latent viral load. *Vaccine* **27**, 6723–6730 (2009).

390. Thacker, E. E., Timares, L. & Matthews, Q. L. Strategies to overcome host immunity to adenovirus vectors in vaccine development. *Expert Rev. Vaccines* **8**, 761–777 (2009).

391. Haleem, A., Javaid, M. & Vaishya, R. Effects of COVID-19 pandemic in daily life. *Curr. Med. Res. Pract.* **10**, 78–79 (2020).

392. Milken Institute. COVID-19 treatment and vaccine tracker. (2020).

393. Kim, J. H. SARS-CoV-2 vaccine development, access, and equity. *J. Exp. Med.* **217**, (2020).

394. Moghadas, S. M. *et al.* The Impact of Vaccination on Coronavirus Disease 2019 (COVID-19) Outbreaks in the United States. *Clin Infect Dis* **73**, 2257–2264 (2021).

395. National Academies of Sciences, E. & Medicine. *Framework for Equitable Allocation of COVID-19 Vaccine*. (The National Academies Press, 2020).

396. Juno, J. A. & Wheatley, A. K. Boosting immunity to COVID-19 vaccines. *Nat. Med.* (2021) doi:10.1038/s41591-021-01560-x.

397. Shroff, R. T. *et al.* Immune responses to two and three doses of the BNT162b2 mRNA vaccine in adults with solid tumors. *Nat. Med.* (2021) doi:10.1038/s41591-021-01542-z.

398. Choi, A. *et al.* Safety and immunogenicity of SARS-CoV-2 variant mRNA vaccine boosters in healthy adults: an interim analysis. *Nat. Med.* (2021) doi:10.1038/s41591-021-01527-y.

399. Dyer, O. Covid-19: Rich countries' booster plans will impede global vaccination, experts say. *BMJ* **374**, n2353 (2021).

400. Tao, K. *et al.* The biological and clinical significance of emerging SARS-CoV-2 variants. *Nat. Rev. Genet.* **22**, 757–773 (2021).

401. Pulliam, J. R. C. *et al.* Increased risk of SARS-CoV-2 reinfection associated with emergence of the Omicron variant in South Africa. *MedRxiv Prepr. Serv. Health Sci.* 2021.11.11.21266068 (2021) doi:10.1101/2021.11.11.21266068.

402. He, X., Hong, W., Pan, X., Lu, G. & Wei, X. SARS-CoV-2 Omicron variant: Characteristics and prevention. *MedComm* **2**, 838–845 (2021).

403. Khoury, D. S. *et al.* Neutralizing antibody levels are highly predictive of immune protection from symptomatic SARS-CoV-2 infection. *Nat Med* **27**, 1205–1211 (2021).

404. Mendonça, S. A., Lorincz, R., Boucher, P. & Curiel, D. T. Adenoviral vector vaccine platforms in the SARS-CoV-2 pandemic. *Npj Vaccines* **6**, 97 (2021).

405. Hernández-Bello, J. *et al.* Neutralizing Antibodies against SARS-CoV-2, Anti-Ad5 Antibodies, and Reactogenicity in Response to Ad5-nCoV (CanSino Biologics) Vaccine in Individuals with and without Prior SARS-CoV-2. *Vaccines* **9**, (2021).

406. Palgen, J.-L. *et al.* Optimize Prime/Boost Vaccine Strategies: Trained Immunity as a New Player in the Game. *Front. Immunol.* **12**, (2021).

407. McCoy, K. *et al.* Effect of Preexisting Immunity to Adenovirus Human Serotype 5 Antigens on the Immune Responses of Nonhuman Primates to Vaccine Regimens Based on Human- or Chimpanzee-Derived Adenovirus Vectors. *J. Virol.* **81**, 6594–6604 (2007).

408. Sapkota, B. *et al.* Heterologous prime-boost strategies for COVID-19 vaccines. *J. Travel Med.* **29**, taab191 (2022).

409. Shaw, R. H. *et al.* Heterologous prime-boost COVID-19 vaccination: initial reactogenicity data. *Lancet Lond. Engl.* **397**, 2043–2046 (2021).

410. Tenbusch, M. *et al.* Heterologous prime-boost vaccination with ChAdOx1 nCoV-19 and BNT162b2. *Lancet Infect. Dis.* **21**, 1212–1213 (2021).

411. Jenna J. Guthmiller *et al.* SARS-CoV-2 Infection Severity Is Linked to Superior Humoral Immunity against the Spike. *mBio* **12**, e02940-20 (2021).

412. Carrillo, J. *et al.* Humoral immune responses and neutralizing antibodies against SARS-CoV-2; implications in pathogenesis and protective immunity. *Biochem. Biophys. Res. Commun.* **538**, 187–191 (2021).

413. Levin, E. G. *et al.* Waning Immune Humoral Response to BNT162b2 Covid-19 Vaccine over 6 Months. *N. Engl. J. Med.* **385**, e84 (2021).

414. Anand, S. *et al.* SARS-CoV-2 Vaccine Antibody Response and Breakthrough Infection in Patients Receiving Dialysis. *Ann. Intern. Med.* (2021) doi:10.7326/M21-4176.

415. Huang, J., Nagy, S. S., Koide, A., Rock, R. S. & Koide, S. A peptide tag system for facile purification and single-molecule immobilization. *Biochemistry* **48**, 11834–11836 (2009).

416. Moyle, P. M. & Toth, I. Modern Subunit Vaccines: Development, Components, and Research Opportunities. *ChemMedChem* **8**, 360–376 (2013).

417. Joag, V. *et al.* Cutting Edge: Mouse SARS-CoV-2 Epitope Reveals Infection and Vaccine-Elicited CD8 T Cell Responses. *J. Immunol.* **206**, 931–935 (2021).

418. Russell, M. W., Moldoveanu, Z., Ogra, P. L. & Mestecky, J. Mucosal Immunity in COVID-19: A Neglected but Critical Aspect of SARS-CoV-2 Infection. *Front. Immunol.* **11**, (2020).

419. Biancolella, M. *et al.* COVID-19 2022 update: transition of the pandemic to the endemic phase. *Hum. Genomics* **16**, 19 (2022).

420. Aleem, A., Akbar Samad, A. B. & Slenker, A. K. Emerging Variants of SARS-CoV-2 And Novel Therapeutics Against Coronavirus (COVID-19). in *StatPearls* (StatPearls Publishing, 2022).

421. Kimura, I. *et al.* Virological characteristics of the SARS-CoV-2 Omicron BA.2 subvariants including BA.4 and BA.5. *Cell* **0**, (2022).

422. Shrestha, L. B., Foster, C., Rawlinson, W., Tedla, N. & Bull, R. A. Evolution of the SARS-CoV-2 omicron variants BA.1 to BA.5: Implications for immune escape and transmission. *Rev. Med. Virol.* **32**, e2381 (2022).

423. Ng, K. T., Mohd-Ismail, N. K. & Tan, Y.-J. Spike S2 Subunit: The Dark Horse in the Race for Prophylactic and Therapeutic Interventions against SARS-CoV-2. *Vaccines* **9**, 178 (2021).

424. Earle, K. A. *et al.* Evidence for antibody as a protective correlate for COVID-19 vaccines. *Vaccine* **39**, 4423–4428 (2021).

425. Triccas, J. A., Kint, J. & Wurm, F. M. Affordable SARS-CoV-2 protein vaccines for the pandemic endgame. *Npj Vaccines* **7**, 1–2 (2022).

426. Khan, M. S. *et al.* Adenovirus-vectored SARS-CoV-2 vaccine expressing S1-N fusion protein. *Antib. Ther.* **5**, 177–191 (2022).

427. Kim, E. *et al.* SARS-CoV-2 S1 Subunit Booster Vaccination Elicits Robust Humoral Immune Responses in Aged Mice. 2022.10.25.513090 Preprint at https://doi.org/10.1101/2022.10.25.513090 (2022).

428. Guest, P. C. Multivalent Vaccine Strategies in Battling the Emergence of COVID-19 Variants. in *Multiplex Biomarker Techniques: Methods and Applications for COVID-19 Disease Diagnosis and Risk Stratification* (ed. Guest, P. C.) 21–36 (Springer US, 2022). doi:10.1007/978-1-0716-2395-4_2.

429. He, X. *et al.* From Monovalent to Multivalent Vaccines, the Exploration for Potential Preventive Strategies Against Hand, Foot, and Mouth Disease (HFMD). *Virol. Sin.* **36**, 167–175 (2021).

430. Hernandez-Davies, J. E. *et al.* Administration of Multivalent Influenza Virus Recombinant Hemagglutinin Vaccine in Combination-Adjuvant Elicits Broad Reactivity Beyond the Vaccine Components. *Front. Immunol.* **12**, (2021).

431. Chalkias, S. *et al.* A Bivalent Omicron-Containing Booster Vaccine against Covid-19. *N. Engl. J. Med.* **387**, 1279–1291 (2022).

432. Pelton, S. I. *et al.* Evaluating the Relative Vaccine Effectiveness of Adjuvanted Trivalent Influenza Vaccine Compared to High-Dose Trivalent and Other Egg-Based Influenza Vaccines among Older Adults in the US during the 2017–2018 Influenza Season. *Vaccines* **8**, 446 (2020).

433. Myers, M. L. *et al.* Impact of adjuvant: Trivalent vaccine with quadrivalent-like protection against heterologous Yamagata-lineage influenza B virus. *Front. Immunol.* **13**, (2022).

434. Ortega-Rivera, O. A. *et al.* Trivalent Subunit Vaccine Candidates for COVID-19 and Their Delivery Devices. *J. Am. Chem. Soc.* **143**, 14748–14765 (2021).

435. González-Domínguez, I. *et al.* Trivalent NDV-HXP-S Vaccine Protects against Phylogenetically Distant SARS-CoV-2 Variants of Concern in Mice. *Microbiol. Spectr.* **10**, e01538-22.

436. From trivalent to quadrivalent influenza vaccines: Public health and economic burden for different immunization strategies in Spain | PLOS ONE. https://journals.plos.org/plosone/article?id=10.1371/journal.pone.0233526.

437. Frey, A., Di Canzio, J. & Zurakowski, D. A statistically defined endpoint titer determination method for immunoassays. *J. Immunol. Methods* **221**, 35–41 (1998).

438. Pegu, A. *et al.* Durability of mRNA-1273 vaccine-induced antibodies against SARS-CoV-2 variants. *Science* **373**, 1372–1377 (2021).

439. Joyce, M. G. *et al.* Efficacy of a Broadly Neutralizing SARS-CoV-2 Ferritin Nanoparticle Vaccine in Nonhuman Primates. *BioRxiv Prepr. Serv. Biol.* 2021.03.24.436523 (2021) doi:10.1101/2021.03.24.436523.

440. Kumar, S., Karuppanan, K. & Subramaniam, G. Omicron (BA.1) and sub-variants (BA.1.1, BA.2, and BA.3) of SARS-CoV-2 spike infectivity and pathogenicity: A comparative sequence and structural-based computational assessment. *J. Med. Virol.* **94**, 4780–4791 (2022).

441. Christensen, D. *et al.* Protection against SARS-CoV-2 transmission by a parenteral prime—Intranasal boost vaccine strategy. *eBioMedicine* **0**, (2022).

442. Saito, A. *et al.* Enhanced fusogenicity and pathogenicity of SARS-CoV-2 Delta P681R mutation. *Nature* **602**, 300–306 (2022).

443. Moghaddar, M., Radman, R. & Macreadie, I. Severity, Pathogenicity and Transmissibility of Delta and Lambda Variants of SARS-CoV-2, Toxicity of Spike Protein and Possibilities for Future Prevention of COVID-19. *Microorganisms* **9**, 2167 (2021).

444. Akache, B. *et al.* Immunogenicity of SARS-CoV-2 spike antigens derived from Beta & Delta variants of concern. *Npj Vaccines* **7**, 1–7 (2022).

445. Hoffmann, M., Zhang, L. & Pöhlmann, S. Omicron: Master of immune evasion maintains robust ACE2 binding. *Signal Transduct. Target. Ther.* **7**, 1–3 (2022).

446. Motozono, C. *et al.* The SARS-CoV-2 Omicron BA.1 spike G446S mutation potentiates antiviral T-cell recognition. *Nat. Commun.* **13**, 5440 (2022).

447. Lai, C.-Y. *et al.* Recombinant protein subunit SARS-CoV-2 vaccines formulated with CoVaccine HT adjuvant induce broad, Th1 biased, humoral and cellular immune responses in mice. *BioRxiv Prepr. Serv. Biol.* 2021.03.02.433614 (2021) doi:10.1101/2021.03.02.433614.

448. Kim, K.-H. *et al.* Immunogenicity and Neutralizing Activity Comparison of SARS-CoV-2 Spike Full-Length and Subunit Domain Proteins in Young Adult and Old-Aged Mice. *Vaccines* **9**, 316 (2021).

449. Sablerolles, R. S. G. *et al.* Immunogenicity and Reactogenicity of Vaccine Boosters after Ad26.COV2.S Priming. *N. Engl. J. Med.* **386**, 951–963 (2022).

450. Shuai, H. *et al.* Emerging SARS-CoV-2 variants expand species tropism to murines. *EBioMedicine* **73**, 103643 (2021).

451. WHO. Status of COVID-19 Vaccines within WHO EUL/PQ evaluation process;

452. Tracking SARS-CoV-2 variants. https://www.who.int/activities/tracking-SARS-CoV-2-variants.

453. Santesmasses, D. *et al.* COVID-19 is an emergent disease of aging. *Aging Cell* **19**, e13230 (2020).

454. Farshbafnadi, M., Kamali Zonouzi, S., Sabahi, M., Dolatshahi, M. & Aarabi, M. H. Aging & COVID-19 susceptibility, disease severity, and clinical outcomes: The role of entangled risk factors. *Exp. Gerontol.* **154**, 111507 (2021).

455. Williamson, E. J. *et al.* Factors associated with COVID-19-related death using OpenSAFELY. *Nature* **584**, 430–436 (2020).

456. Mueller, A. L., McNamara, M. S. & Sinclair, D. A. Why does COVID-19 disproportionately affect older people? *Aging* **12**, 9959–9981 (2020).

457. O'Driscoll, M. *et al.* Age-specific mortality and immunity patterns of SARS-CoV-2. *Nature* **590**, 140–145 (2021).

458. Li, J. *et al.* Safety and immunogenicity of the SARS-CoV-2 BNT162b1 mRNA vaccine in younger and older Chinese adults: a randomized, placebo-controlled, double-blind phase 1 study. *Nat. Med.* **27**, 1062–1070 (2021).

459. Docherty, A. B. *et al.* Features of 20 133 UK patients in hospital with covid-19 using the ISARIC WHO Clinical Characterisation Protocol: prospective observational cohort study. *BMJ* **369**, m1985 (2020).

460. Collier, D. A. *et al.* Age-related immune response heterogeneity to SARS-CoV-2 vaccine BNT162b2. *Nature* **596**, 417–422 (2021).

461. Silva-Cayetano, A. *et al.* A booster dose enhances immunogenicity of the COVID-19 vaccine candidate ChAdOx1 nCoV-19 in aged mice. *Med N. Y. N* **2**, 243-262.e8 (2021).

462. Letko, M., Marzi, A. & Munster, V. Functional assessment of cell entry and receptor usage for SARS-CoV-2 and other lineage B betacoronaviruses. *Nat. Microbiol.* **5**, 562–569 (2020).

463. JCI Insight - A simple protein-based surrogate neutralization assay for SARS-CoV-2. https://insight.jci.org/articles/view/142362.

464. Hoffmann, M. *et al.* SARS-CoV-2 Cell Entry Depends on ACE2 and TMPRSS2 and Is Blocked by a Clinically Proven Protease Inhibitor. *Cell* **181**, 271-280.e8 (2020).

465. Atmar, R. L. *et al.* Homologous and Heterologous Covid-19 Booster Vaccinations. *N. Engl. J. Med.* **386**, 1046–1057 (2022).

466. Pavot, V. *et al.* Protein-based SARS-CoV-2 spike vaccine booster increases cross-neutralization against SARS-CoV-2 variants of concern in non-human primates. *Nat. Commun.* **13**, 1699 (2022).

467. Feng, S. *et al.* Correlates of protection against symptomatic and asymptomatic SARS-CoV-2 infection. *Nat. Med.* **27**, 2032–2040 (2021).

468. Gilbert, P. B. *et al.* Immune correlates analysis of the mRNA-1273 COVID-19 vaccine efficacy clinical trial. *Science* **375**, 43–50 (2022).

469. Cromer, D. *et al.* Neutralising antibody titres as predictors of protection against SARS-CoV-2 variants and the impact of boosting: a meta-analysis. *Lancet Microbe* **3**, e52–e61 (2022).

470. Barros-Martins, J. *et al.* Immune responses against SARS-CoV-2 variants after heterologous and homologous ChAdOx1 nCoV-19/BNT162b2 vaccination. *Nat. Med.* **27**, 1525–1529 (2021).

471. Schmidt, T. *et al.* Immunogenicity and reactogenicity of heterologous ChAdOx1 nCoV-19/mRNA vaccination. *Nat. Med.* **27**, 1530–1535 (2021).

472. Liu, X. *et al.* Safety and immunogenicity of heterologous versus homologous prime-boost schedules with an adenoviral vectored and mRNA COVID-19 vaccine (Com-COV): a single-blind, randomised, non-inferiority trial. *The Lancet* **398**, 856–869 (2021).

473. Shinde, V. *et al.* Efficacy of NVX-CoV2373 Covid-19 Vaccine against the B.1.351 Variant. *N. Engl. J. Med.* **384**, 1899–1909 (2021).

474. Abu-Raddad, L. J., Chemaitelly, H., Butt, A. A., & National Study Group for COVID-19 Vaccination. Effectiveness of the BNT162b2 Covid-19 Vaccine against the B.1.1.7 and B.1.351 Variants. *N. Engl. J. Med.* **385**, 187–189 (2021).

475. Chen, Y. *et al.* Age-associated SARS-CoV-2 breakthrough infection and changes in immune response in a mouse model. *Emerg. Microbes Infect.* **11**, 368–383 (2022).

476. Nanishi, E. *et al.* mRNA booster vaccination protects aged mice against the SARS-CoV-2 Omicron variant. *Commun. Biol.* **5**, 1–8 (2022).

477. Bi, X. *et al.* Longer Intervals before Vaccination Increase Spike Antibody Titers in Individuals Previously Infected with SARS-CoV-2. *Microbiol. Spectr.* **10**, e0023822 (2022).

478. Wang, Z. *et al.* Naturally enhanced neutralizing breadth against SARS-CoV-2 one year after infection. *Nature* **595**, 426–431 (2021).

479. Dan, J. M. *et al.* Immunological memory to SARS-CoV-2 assessed for up to 8 months after infection. *Science* **371**, eabf4063 (2021).

480. Cokarić Brdovčak, M. *et al.* ChAdOx1-S adenoviral vector vaccine applied intranasally elicits superior mucosal immunity compared to the intramuscular route of vaccination. *Eur. J. Immunol.* **52**, 936–945 (2022).

481. Langel, S. N. *et al.* Adenovirus type 5 SARS-CoV-2 vaccines delivered orally or intranasally reduced disease severity and transmission in a hamster model. *Sci. Transl. Med.* **14**, eabn6868 (2022).

482. Barouch, D. H. *et al.* Durable Humoral and Cellular Immune Responses 8 Months after Ad26.COV2.S Vaccination. *N. Engl. J. Med.* **385**, 951–953 (2021).

483. Hall, V. *et al.* Protection against SARS-CoV-2 after Covid-19 Vaccination and Previous Infection. *N. Engl. J. Med.* **386**, 1207–1220 (2022).

484. Israelow, B. *et al.* Adaptive immune determinants of viral clearance and protection in mouse models of SARS-CoV-2. *Sci. Immunol.* **6**, eabl4509 (2021).

485. Li, X. *et al.* Combining intramuscular and intranasal homologous prime-boost with a chimpanzee adenovirus-based COVID-19 vaccine elicits potent humoral and cellular immune responses in mice. *Emerg. Microbes Infect.* **11**, 1890–1899 (2022).

486. Lapuente, D. *et al.* Protective mucosal immunity against SARS-CoV-2 after heterologous systemic prime-mucosal boost immunization. *Nat. Commun.* **12**, 6871 (2021).

487. Nanishi, E. *et al.* An aluminum hydroxide:CpG adjuvant enhances protection elicited by a SARS-CoV-2 receptor binding domain vaccine in aged mice. *Sci. Transl. Med.* **14**, eabj5305 (2022).

488. Ahmad, L. Implication of SARS-CoV-2 Immune Escape Spike Variants on Secondary and Vaccine Breakthrough Infections. *Front. Immunol.* **12**, (2021).

489. Hoffmann, M. *et al.* SARS-CoV-2 variants B.1.351 and P.1 escape from neutralizing antibodies. *Cell* **184**, 2384-2393.e12 (2021).

490. Khan, M. S., Kim, E., Huang, S., Kenniston, T. W. & Gambotto, A. Trivalent SARS-CoV-2 S1 Subunit Protein Vaccination Induces Broad Humoral Responses in BALB/c Mice. *Vaccines* **11**, 314 (2023).

491. Spinelli, M. A. *et al.* Differences in Post-mRNA Vaccination Severe Acute Respiratory Syndrome Coronavirus 2 (SARS-CoV-2) Immunoglobulin G (IgG) Concentrations and Surrogate Virus Neutralization Test Response by Human Immunodeficiency Virus (HIV) Status and Type of Vaccine: A Matched Case-Control Observational Study. *Clin. Infect. Dis. Off. Publ. Infect. Dis. Soc. Am.* **75**, e916–e919 (2022).

492. Hensley, K. S. *et al.* Immunogenicity and reactogenicity of SARS-CoV-2 vaccines in people living with HIV in the Netherlands: A nationwide prospective cohort study. *PLOS Med.* **19**, e1003979 (2022).

493. Pandrea, I. *et al.* Simian immunodeficiency virus SIVagm.sab infection of Caribbean African green monkeys: a new model for the study of SIV pathogenesis in natural hosts. *J. Virol.* **80**, 4858–4867 (2006).

494. Pandrea, I. *et al.* Functional Cure of SIVagm Infection in Rhesus Macaques Results in Complete Recovery of CD4+ T Cells and Is Reverted by CD8+ Cell Depletion. *PLOS Pathog.* **7**, e1002170 (2011).

495. Ma, D. *et al.* Simian Immunodeficiency Virus SIVsab Infection of Rhesus Macaques as a Model of Complete Immunological Suppression with Persistent Reservoirs of Replication-Competent Virus: Implications for Cure Research. *J. Virol.* **89**, 6155–6160 (2015).

496. Viallard, J.-F. *et al.* CD8+HLA-DR+ T lymphocytes are increased in common variable immunodeficiency patients with impaired memory B-cell differentiation. *Clin. Immunol.* **119**, 51–58 (2006).

497. Sandoval-Montes, C. & Santos-Argumedo, L. CD38 is expressed selectively during the activation of a subset of mature T cells with reduced proliferation but improved potential to produce cytokines. *J. Leukoc. Biol.* **77**, 513–521 (2005).

498. Quarona, V. *et al.* CD38 and CD157: a long journey from activation markers to multifunctional molecules. *Cytometry B Clin. Cytom.* **84**, 207–217 (2013).

499. Willcox, A. C. *et al.* Macaque-human differences in SARS-CoV-2 Spike antibody response elicited by vaccination or infection. *bioRxiv* 2021.12.01.470697 (2021) doi:10.1101/2021.12.01.470697.

500. Arunachalam, P. S. *et al.* Adjuvanting a subunit COVID-19 vaccine to induce protective immunity. *Nature* **594**, 253–258 (2021).

501. Grimaldi Jr, G. The utility of rhesus monkey (Macaca mulatta) and other non-human primate models for preclinical testing of Leishmania candidate vaccines. *Mem. Inst. Oswaldo Cruz* **103**, 629–644 (2008).

502. Bukh, I. *et al.* Increased mucosal CD4+ T cell activation in rhesus macaques following vaccination with an adenoviral vector. *J. Virol.* **88**, 8468–8478 (2014).

503. Phares, T. W. *et al.* Rhesus macaque and mouse models for down-selecting circumsporozoite protein based malaria vaccines differ significantly in immunogenicity and functional outcomes. *Malar. J.* **16**, 115 (2017).

504. Martins, M. A. & Watkins, D. I. What Is the Predictive Value of Animal Models for Vaccine Efficacy in Humans? *Cold Spring Harb. Perspect. Biol.* **10**, a029504 (2018).

505. Juliet R. C. Pulliam *et al.* Increased risk of SARS-CoV-2 reinfection associated with emergence of Omicron in South Africa. *Science* **376**, eabn4947 (2022).

506. Kim, S. *et al.* Binding of human ACE2 and RBD of Omicron enhanced by unique interaction patterns among SARS-CoV-2 variants of concern. *J. Comput. Chem.* **44**, 594–601 (2023).

507.   Kumar, S., Karuppanan, K. & Subramaniam, G. Omicron (BA.1) and sub-variants (BA.1.1, BA.2, and BA.3) of SARS-CoV-2 spike infectivity and pathogenicity: A comparative sequence and structural-based computational assessment. *J. Med. Virol.* **94**, 4780–4791 (2022).

508.   Heidary, M. *et al.* A Comprehensive Review of the Protein Subunit Vaccines Against COVID-19. *Front. Microbiol.* **13**, 927306 (2022).

509.   Vaccine Types | NIH: National Institute of Allergy and Infectious Diseases. https://www.niaid.nih.gov/research/vaccine-types.

510.   Forni, G. *et al.* COVID-19 vaccines: where we stand and challenges ahead. *Cell Death Differ.* **28**, 626–639 (2021).

511.   Migliore, A., Gigliucci, G., Di Marzo, R., Russo, D. & Mammucari, M. Intradermal Vaccination: A Potential Tool in the Battle Against the COVID-19 Pandemic? *Risk Manag. Healthc. Policy* **14**, 2079–2087 (2021).

512.   Zhao, J.-H. *et al.* Enhanced immunization via dissolving microneedle array-based delivery system incorporating subunit vaccine and saponin adjuvant. *Int. J. Nanomedicine* **12**, 4763–4772 (2017).

513.   Goldberg, Y. *et al.* Waning Immunity after the BNT162b2 Vaccine in Israel. *N. Engl. J. Med.* (2021) doi:10.1056/NEJMoa2114228.

514.   Peng, Q. *et al.* Waning immune responses against SARS-CoV-2 variants of concern among vaccinees in Hong Kong. *eBioMedicine* **77**, (2022).

515.   Tut, G. *et al.* Strong peak immunogenicity but rapid antibody waning following third vaccine dose in older residents of care homes. *Nat. Aging* **3**, 93–104 (2023).

516.   Modeling of waning immunity after SARS-CoV-2 vaccination and influencing factors | Nature Communications. https://www.nature.com/articles/s41467-022-29225-4.

517.   Waning Immune Humoral Response to BNT162b2 Covid-19 Vaccine over 6 Months | NEJM. https://www.nejm.org/doi/full/10.1056/nejmoa2114583.

518.   Havervall, S. *et al.* Anti-Spike Mucosal IgA Protection against SARS-CoV-2 Omicron Infection. *N. Engl. J. Med.* (2022) doi:10.1056/NEJMc2209651.

519.   Wellford, S. A. *et al.* Mucosal plasma cells are required to protect the upper airway and brain from infection. *Immunity* **55**, 2118-2134.e6 (2022).

520.   Zhao, Z. *et al.* Omicron SARS-CoV-2 mutations stabilize spike up-RBD conformation and lead to a non-RBM-binding monoclonal antibody escape. *Nat. Commun.* **13**, 4958 (2022).

521.   Walsh, E. E. *et al.* Safety and Immunogenicity of Two RNA-Based Covid-19 Vaccine Candidates. *N. Engl. J. Med.* **383**, 2439–2450 (2020).

522. Oehler, R. L. & Vega, V. R. Conquering COVID: How Global Vaccine Inequality Risks Prolonging the Pandemic. *Open Forum Infect. Dis.* **8**, (2021).